The New Swiss Glacier Inventory 2000

Application of Remote Sensing and GIS

Dissertation

zur

Erlangung der naturwissenschaftlichen Doktorwürde
(Dr. sc. nat.)

vorgelegt der

Mathematisch-naturwissenschaftlichen Fakultät

der

Universität Zürich

von

Frank Paul

aus

Deutschland

Promotionskomitee

Prof. Dr. Wilfried Haeberli

Dr. Andreas Kääb

Prof. Dr. Klaus Itten

Zürich 2003

The New Swiss Glacier Inventory 2000

Application of Remote Sensing and GIS

For my mother

Summary

Glacier changes are considered to be the best natural indicators of ongoing climate changes. Since glaciers are able to integrate atmospheric conditions (temperature and precipitation) over a time period of climatic relevance (decades), their investigation is of great value to the discussion of an anthropogenically-influenced increase in the natural greenhouse effect. Fluctuations of Swiss glaciers have been documented in great detail for more than 100 years on topographic maps and by taking annual measurements of length changes. The latest assessment of glacier areas and topographic parameters is compiled in the 1973 Swiss glacier inventory, which is based on cartographic-planimetric analysis of specially-acquired aerial photographs. The new Swiss glacier inventory 2000 (SGI 2000) shows the possibilities and limitations of a glacier inventory from satellite data using GIS (Geographic Information System) technology in combination with a digital elevation model (DEM).

There are a number of reasons for compiling a new glacier inventory: From about 1970 to 1985 Alpine glaciers experienced a well-documented phase of intermittent advance, which included for a certain time 75% of all measured glaciers. Thereafter a strong decrease in glacier length and size was observed. The consequences of this fluctuation have not been assessed yet in full, as the sample of glaciers within the length measurement network is not representative with respect to its size distribution, and only five percent of all Swiss glaciers are included.

With the advent of the Landsat era in 1972, multi-spectral satellite imagery became available, initially with a spatial resolution of 80 m (Multi-Spectral Scanner - MSS), and since 1982 also with 30 m (Thematic Mapper - TM). These globally-available data sets document glacier change quite well, thereby facilitating automatic assessments for large areas. In parallel, there have been rapid advances in computer capacity during the 1980s, improving the efficiency and capabilities of GIS and DEM-related calculations.

In the late 1990s, the USGS initiated the GLIMS (Global Land Ice Measurements from Space) project to conduct a global glacier inventory from space using the ETM+ and ASTER sensors. The SGI 2000 also acts as a pilot study for GLIMS, by investigating the required methods and applying them to TM data from 1998/9 in order to create a new Swiss glacier inventory. Intermediate glacier fluctuations are investigated with TM data from 1985 and 1992.

In the pre-processing stage, selection of the most suitable satellite scenes (with respect to cloud cover and snow conditions), as well as their exact orthorectification, are the most important tasks. Both issues are described in detail. The methods used in the literature for glacier classification with TM are discussed and illustrated for a test region. The accuracy of the most appropriate method (a thresholded ratio image from TM4 and TM5 raw data) is assessed by means of comparison with higher-resolution satellite imagery. The influence of the various pre- and post-processing steps on the derived glacier areas are also examined.

A geographic information system (GIS) enables the automatic processing, integration, analysis and display of spatially-oriented data sets (e.g., raster, vector, image), as well as storage and management of object specific attributes, making it a preferred tool for conducting glacier inventories. In order to facilitate GIS-based processing, the glacier inventories from 1973 and 1850 are digitized. Outlines from 1973 are also used to define glacier basins for intersection with the TM-derived glacier areas. 3D glacier parameters are obtained by fusion of glacier outlines with a DEM and DEM-derived products (such as slope or aspect).

The most costly work in technical terms is the accurate orthorectification of the satellite scenes used as well as the manual delineation of debris-covered glaciers. A semi-automatic method for classification of debris-covered ice as developed for the SGI 2000 supports this task. Methodological questions are encountered relating to glacier identification (basin delineation) and to the calculation of glacier parameters or length changes after a change in glacier geometry. For this purpose the definition of new and GIS-adapted standards is required in the future.

The main results of the glacier change analysis are:

- The relative loss in glacier size from 1973-1998/9 is about -20%, with small changes until 1985 (-1%) and a loss of about -10% from 1985-1992 and 1992-1998/9. Glaciers smaller than 1 km^2 contribute about 40% to the total loss although they cover only 15% of the area.
- The average decadal relative loss of area from 1985 to 1998/9 is about seven times higher than from 1850 to 1973 (the samples are not exactly identical).
- The relative changes in glacier size are highly individual with a fair dependence on glacier size (increasing scatter towards smaller glaciers) and no correlation to other investigated parameters. Only a large number of glaciers from all size classes will give a representative evaluation of ongoing changes.
- Loss of glacier area (valley and mountain glaciers) is due to separation from formerly connected tributaries and emerging rock outcrops. Shrinkage of small glaciers took place along the entire perimeter and is enhanced by disintegration.

Zusammenfassung

Gletscheränderungen gelten als die bedeutendsten natürlichen Indikatoren für Klimaänderungen. Da Gletscher die atmosphärischen Bedingungen (Temperatur und Niederschlag) über einen klimatisch relevanten Zeitraum (Dekaden) integrieren, ist die Untersuchung ihres Verhaltens im Zusammenhang mit der Diskussion um eine anthropogen bedingte Zunahme des natürlichen Treibhauseffektes besonders interessant. Die Schwankungen der Schweizer Gletscher sind seit über 100 Jahren auf topographischen Karten und durch jährliche Messungen von Längenänderungen dokumentiert. Letztmalig wurden die Flächen und topographischen Parameter aller Schweizer Gletscher im Inventar von 1973 erfasst, welches auf der kartographisch-planimetrischen Auswertung von speziell angefertigten Luftbildern basiert. Das Schweizer Gletscherinventar 2000 (SGI 2000) zeigt die Möglichkeiten und Grenzen eines GIS-basierten Inventars aus Satellitendaten und einem digitalen Höhenmodell (DHM) auf.

Die Gründe für ein neues Gletscherinventar sind vielfältig: Von etwa 1970 bis 1985 kam es zu einer gut dokumentierten Gletschervorstossphase, an der zeitweilig bis zu 75% aller vermessenen Alpengletscher beteiligt waren. Anschliessend kam es zu einem starken Gletscherschwund. Die Auswirkungen dieser Fluktuation auf die Gletscherflächen war bisher gesamthaft unbekannt, da z.B. die Stichprobe im Längenänderungsmessnetz bezüglich der Grössenklassen nicht repräsentativ ist und überdies nur etwa 5% aller Gletscher enthält.

Mit dem Beginn der Landsat Ära im Jahr 1972 stehen multispektrale Satellitenbilder mit zunächst 80 m (Multi Spectral Scanner - MSS), seit 1982 auch mit 30 m (Thematic Mapper - TM) Bodenauflösung zur Verfügung, welche die Gletscherentwicklung sehr gut dokumentieren und sich bestens für eine grossflächige und automatisierte Auswertung eignen. Parallel dazu setzte in den 80er Jahren eine rasante Entwicklung bei der Rechenleistung von Computern ein, welche auch den effizienten Einsatz von GIS und Höhenmodellen beschleunigte.

Ende der 90er Jahre wurde vom USGS das Projekt GLIMS (Global Land Ice Measurements from Space) lanciert, welches die Erstellung eines globalen Gletscherinventars aus Daten der Sensoren ETM+ und ASTER zum Ziel hat. Das SGI 2000 stellt für dieses weltweite Projekt eine Pilotstudie dar, in der die erforderliche Methodik untersucht wird sowie durch Anwendung auf TM Szenen der Jahre 1998/9 ein neues Schweizer Gletscherinventar erstellt wird. Kurzfristigere Schwankungen werden durch Auswertung der Jahre 1985 und 1992 erfasst.

Bei der Vorverarbeitung ist die Auswahl der geeignetsten Satellitenszenen (Wolken, Schneeverhältnisse) wie auch die genaue Orthorektifizierung aller Szenen von grösster Wichtigkeit. Die in der Literatur diskutierten Methoden der Gletscherklassifikation mit TM Daten werden vorgestellt und für ein Testgebiet miteinander verglichen. Die Genauigkeit der besten Methode (segmentiertes Ratiobild aus TM4 / TM5 Rohdaten) wird durch Vergleich mit höher aufgelösten Satellitendaten ermittelt. Die Auswirkungen der verschiedenen Vor- und Nachverarbeitungsschritte auf die abgeleiteten Gletscherflächen werden ebenfalls untersucht.

Geographische Informationssysteme (GIS) erlauben unter anderem die automatisierte Verarbeitung, Integration und Visualisierung von raumbezogenen Datensätzen aller Art (Raster, Vektor, Bild) sowie die Verwaltung von objektspezifischen Attributen. Damit eignen sie sich besonders für ein digitales Gletscherinventar. Für die GIS-basierte Verarbeitung wurden die Gletscherinventare von 1973 und 1850 digitalisiert. Die digitalisierten Gletscherumrisse von 1973 definieren zugleich die Einzugsgebiete (Bassins), mit denen die aus TM Daten abgeleiteten Gletscherflächen verschnitten werden. 3D Gletscherparameter werden durch Verschneiden der Gletscherumrisse mit einem DHM sowie daraus abgeleiteten Produkten berechnet.

Technisch aufwendig ist die genaue Orthorektifizierung aller Satellitenszenen sowie die manuelle Abgrenzung schuttbedeckter Gletscher. Eine zur halbautomatischen Schuttklassierung entwickelte Methode war dabei sehr hilfreich. Methodische Probleme ergeben sich bei der Gletscheridentifikation (Bassinabgrenzung) sowie der Berechnung von Gletscherparametern und Längenänderungen nach einer Veränderung der Gletschergeometrie (Aufspaltung). Hierfür wäre zukünftig die Definition von verbindlichen und GIS-tauglichen Regeln nötig.

Die wesentlichen Ergebnisse der Gletscherdatenauswertung sind:

- Zwischen 1973 und 1998/9 haben die Schweizer Gletscher etwa 20% ihrer Fläche verloren, wobei der Verlust bis 1985 sehr gering ist (-1%) und etwa gleich gross (-10%) für die Perioden 1985 bis 1992 und 1992 bis 1998/9. Gletscher kleiner als 1 km^2 tragen etwa 40% zum totalen Verlust bei, obwohl sie nur 15% Anteil an der Gesamtfläche haben.
- Der mittlere Flächenverlust pro Dekade zwischen 1985 und 1998/9 ist etwa sieben mal grösser als zwischen 1850 und 1973 (die Stichproben sind jedoch nicht ganz identisch).
- Die relativen Flächenänderungen sind sehr individuell, hängen nur schwach von der Gletschergrösse ab (zunehmende Streuung mit kleineren Gletschern) und korrelieren nicht mit anderen untersuchten Parametern. Allgemeine Rückschlüsse über Gletscheränderungen sind deshalb nur für grosse und repräsentative Stichproben sinnvoll.
- Grosse Gletscher verlieren Fläche durch Abtrennung von Seitengletschern und Ausschmelzen von Felsinseln. Bei kleinen Gletschern tritt der Flächenverlust entlang des gesamten Perimeters auf oder beschleunigt sich durch Eiszerfall.

CONTENTS

C

C

C

8. CONCLUSIONS AND PERSPECTIVES

1. INTRODUCTION

1.1. Background

Changes in glaciers are among the best natural indicators of climatic change (Haeberli, 1990 and 1994; IPCC, 2001; Oerlemans, 1986 and 1994). Since the end of the Little Ice Age (LIA) around 1850, alpine glaciers worldwide have retreated up to several km (Grove, 1988). Such extreme changes in glacier length are much easier for the general public to discern than is the 0.7 °C increase since 1850 in the globally-averaged mean surface temperature. In a global context, glaciers play an important role in the production of energy (hydro-electric power), they have an effect on hydrologic regimes, agriculture, tourism and sea level rise and they are a source of natural hazards (UNEP, 1992). The recent drastic glacial retreat in the Himalayas is responsible for the considerable increase, in size and in number, of glacier lakes, endangering numerous settlements down the valley (UNEP, 2002). Also in the Alps, glacier fluctuations over the last few centuries have been linked with natural hazards such as ice avalanches or glacier lake outbursts (Glacierhazards, 2002). Historical catastrophes of this order provided the impetus for the initial scientific investigations of glaciers (Richter, 1892; Walcher, 1773).

Accurate topographic maps dating from the end of the 19th century, combined with the early beginning of annually repeated length measurements at selected glaciers (Forel, 1895), make the changes in Swiss glaciers since the LIA among the best documented in the world. Since 1850, glaciers in the Alps have retreated more or less continuously (depending on size), interrupted by advance periods from 1920-1930 and 1970-1985 (Gross, 1987). During the 1970s national glacier inventories from aerial photography were compiled around the world (IAHS, 1980 and 1989) following international standards and documenting strongly-reduced glacier extension since the LIA maximum extent in the Alps. Glacier changes since 1850 have been documented by Maisch et al. (2000) for Switzerland and by Gross (1987) for Austria. Since 1985 most glaciers have been retreating at accelerated rates and today's glacier size is, apart from a few cases, not known. Moreover, repeated compilation of regional inventories at time intervals of a few decades, the typical dynamic response time of mountain glaciers, is now part of the Global Climate Observing System (GCOS) and the time for compilation of a new glacier inventory including documentation of changes has come (Haeberli et al., 2002a).

With the launch of the first Landsat satellites in 1972, digital data from the Multi-Spectral Scanner (MSS) sensor at 80 m resolution became available for glacier studies. Since 1984 the Landsat radiometer Thematic Mapper (TM) has been acquiring calibrated data in seven spectral bands at 30 m resolution achieving almost global coverage today. Many studies have shown the potential of glacier classification with TM, based on differences in spectral reflectivity of ice and snow compared to other terrain (e.g., Hall et al., 1987 and 1992; Jacobs et al., 1997; Sidjak and Wheate, 1999; Williams et al., 1991 and 1997). Theses studies were mostly applied to small regions, because commercial distribution of raw digital data results in high prices, prohibiting large scale applications (Williams and Hall, 1993 and 1998).

With the launch of the satellites Landsat 7 and Terra, prices have decreased and international collaborations for worldwide glacier monitoring from satellites were initiated (GLIMS, see below). Within the framework of GCOS, a Global Hierarchical Observing Strategy (GHOST) of tiers has been defined, specifying satellite-derived glacier inventories as Tier 5 (Haeberli et al., 2000). In order to examine the required methods and address possible problems, Landsat 5 TM data from 1998 and 1999 are used for a new Swiss glacier inventory (SGI 2000). The large area covered on a single TM-scene (185 km on each side) combined with the high-spatial resolution (30 by 30 m per pixel), favours this sensor for glacier monitoring.

One drawback of most existing glacier inventories is that glacier outlines are given as analogue maps. This makes the quantitative tracking of changes in glacier geometry a laborious task. Nowadays, the management of digital geospatial data uses a Geographic Information System (GIS). A GIS also allows data capture, storage, retrieval, analysis and display (Walsh et al., 1998), making it a preferred tool for glacier inventorying. The integration of classified glacier maps (derived from satellite data or other sources) is possible by raster-vector conversion with glacier data stored in attribute tables. Furthermore, a GIS allows script-based automatic processing, enabling rapid and efficient application of established algorithms to new data sets. This is of great advantage for the operational monitoring of glaciers.

Apart from analyzing changes in glacier area, the combination with a digital elevation model (DEM) allows calculation of 3D glacier parameters. This includes parameters that could directly be inferred from the DEM (e.g., highest or lowest point of a glacier) as well as parameters obtained from DEM-derived products (e.g., slope, aspect). The spatial resolution and vertical accuracy of the DEM used should be appropriate for the size of the glaciers monitored. A DEM is also required for orthorectification in alpine terrain and is used in the SGI 2000 for visualization of glacier changes in 3D perspective views.

The SGI 2000 will also serve as a pilot study on methods and problems of glacier monitoring from space for the USGS-led GLIMS project (Global Land Ice Measurements from Space), which aims at a global inventory of all land-ice masses from satellite. According to Tier 5 of GHOST, a network of international collaboration is established within GLIMS, facilitating efficient (regional) data processing and global communication of problems and standards, in order to transfer ground-based to digital methods (see also Haeberli et al., 1998).

1.2. Objectives

The two central issues of the SGI 2000 are: (1) examination of methods for obtaining glacier inventories by combined use of remote sensing, GIS and DEMs, and (2) application of these methods to satellite imagery from Switzerland in order to obtain a new digital glacier inventory. Some of the investigations with respect to (1) are:

- A review of methods for multi-spectral glacier mapping as discussed in the literature;
- application of these methods to a test region and selection of the 'best' method;
- evaluation of the accuracy of this method by comparison with higher resolution data sets;
- assessment of errors due to image pre-processing and sensor resolution;
- development of a method for mapping of debris-covered glacier ice;

- digitizing of 1973 glacier outlines from the original topographic maps;
- GIS-based extraction of individual glaciers from the TM-derived maps;
- inferring 3D glacier parameters from DEM fusion for digitized and TM-derived glaciers;
- investigating the possibilities for GIS-based automatic data processing.

With respect to point (2) the new SGI 2000 should include:

- New digital outlines for most Swiss glaciers in 1998/9 (1985 and 1992 where available);
- DEM-derived glacier parameters for 1973 with an update for 1998/9;
- calculation of glacier area changes since 1973 for various time intervals;
- dependence of glacier changes on glacier parameters;
- calculation of length changes and application to mass balance parameterizations;
- visualization of glacier changes with 2D and 3D graphics.

1.3. General work flow

In order to achieve these objectives, they are integrated in a work-flow which is given in Fig. 1.1 and discussed below. The work-flow is non-linear and in practise many of the tasks are performed in parallel. The colours and symbols used in Fig. 1.1 were related to GIS-based processing and data (yellow ellipses), digital image processing (DIP) issues (blue rectangles), and combination of GIS and DIP (green rounded rectangles). Required additional input (data or methods) is shown in black boxes and dotted lines denote additional usage of data.

First (cf. top right of Fig. 1.1), suitable Landsat TM scenes must be selected. Apart from cloud-free conditions, scenes must be acquired at the end of the melting period in years with a minimum amount of snow remaining adjacent to glaciers. The corresponding internet-based analysis of quicklooks is not easy, as their resolution often gives no clear evidence of snow conditions. The most time-consuming part is the geocoding of satellite imagery, which includes the collection and exact positioning of suitable ground control points (GCPs). The DEM should cover the entire region of the satellite scene, in order to avoid misregistration. Different methods of glacier classification are tested within a small sub-region of the entire scene and the accuracy of the most appropriate method is evaluated further. Methods for the mapping of debris cover and snow are examined in further test regions.

The separation of contiguous ice bodies in the classified satellite map (according to their 1973 divides) is accomplished by interactive digitizing of glacier basins using the digitized glacier outlines as a background. After glacier IDs (identification codes) are added, each glacier can be extracted within the GIS from the classified satellite map.

The digitized glacier outlines from 1973 are combined with a DEM to obtain 3D glacier parameters. Glacier change statistics are calculated from these data set and additional outlines derived from TM imagery for distinct years. Glacier outlines are also used in combination with a DEM for visualization of glacier changes. While the final SGI 2000 will contain all the data, the GLIMS or WGMS database will use only selected parts of it.

1.

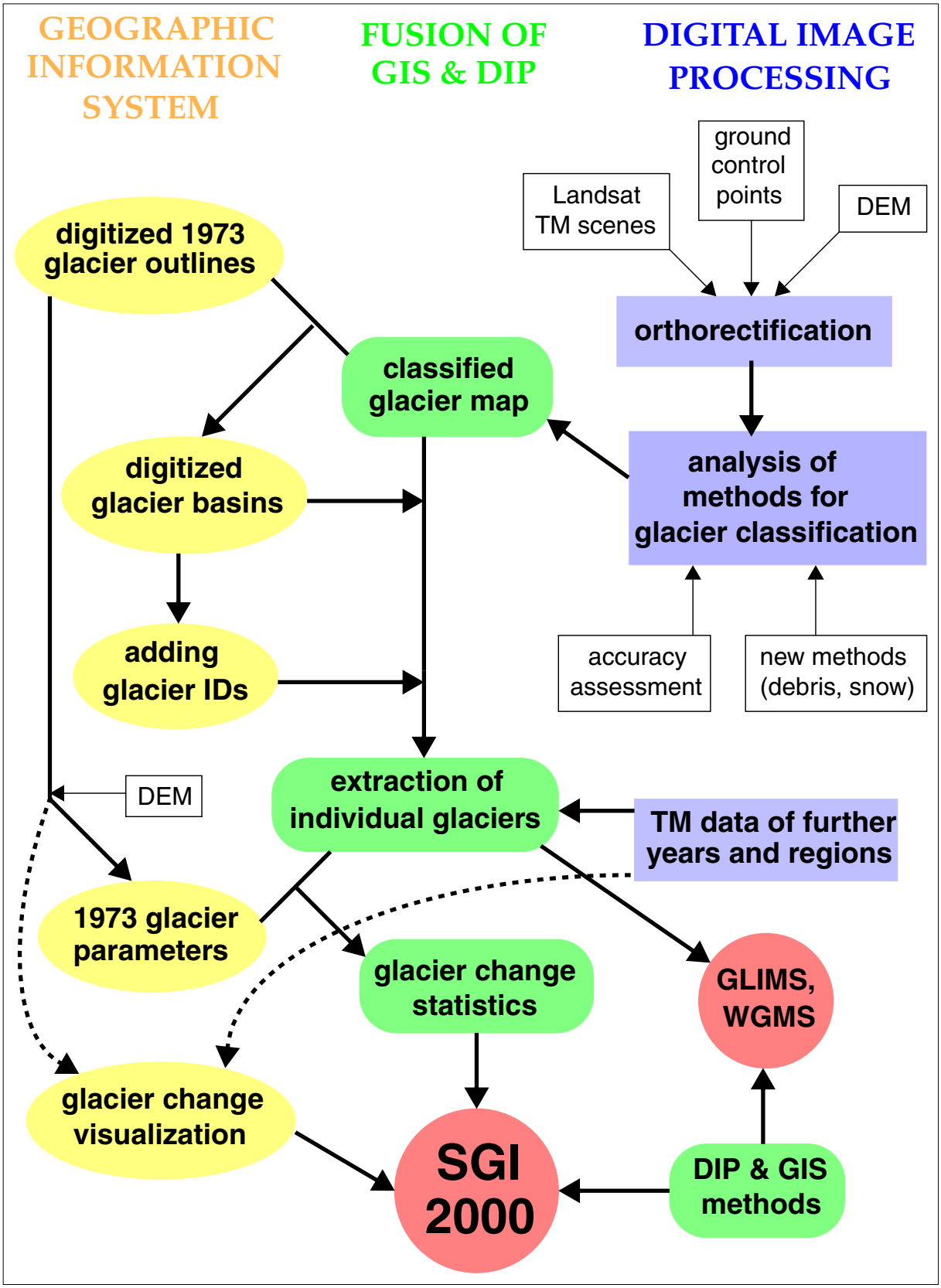

Figure 1.1: *Schematic overview of individual steps towards the new Swiss glacier inventory (SGI 2000). While some parts are performed solely in the GIS or DIP environment, the integration of both data sets is performed by raster-vector conversion and vice versa.*

1.4. Structure of the thesis

Discussion of the objectives mentioned before is organized in the following way: Theoretical background on glaciers, DEMs, remote sensing and digital image processing is given in Chapters 2 to 4, applications in Chapter 5 (glacier classification) and 6 (GIS related processing), and results (glacier change statistics) in Chapter 7. At the end conclusions and perspectives, references and an appendix are given. A short summary for each chapter is given below.

Chapter 2 (Glaciers) gives background on glacier formation, occurrence, types and properties. Glacier monitoring is presented with respect to traditional methods, the use of remote sensing techniques and GIS applications. The significance of glacier monitoring in various fields (climate change detection, natural hazards, hydrology) is discussed in the last paragraph of the chapter.

Chapter 3 (Digital elevation models) gives information on DEMs in general and the DEM25 used, in particular. The accuracy of the DEM25 is investigated with respect to glacier parameters and previous glacier-related studies with DEMs are discussed. DEM applications within the SGI 2000 (orthorectification, glacier parameters, digital terrain modelling, visualization) are summarized in this chapter.

In Chapter 4 (Remote sensing) characteristics of the satellite sensors used are explained, an overview of the processed scenes is given, and geometric errors of Landsat raw data are described. The process of orthorectification and atmospheric correction is explained in theory and by application to a test region. Afterwards, the spectral properties of ice and snow are described with respect to TM and the digital image processing techniques as used in the SGI 2000 for mapping of snow and ice are presented. The chapter closes with a description of image fusion as used in the SGI 2000.

In Chapter 5 (Methods for glacier mapping) a review of methods for glacier mapping from Landsat data is given and the application of these methods to a test area is shown, including a compilation of error sources. A new method for mapping debris-covered glacier ice is presented and the method used for mapping of snow on glaciers is discussed thereafter. The chapter finishes with an accuracy assessment of the TM-derived glacier outlines by comparison with higher-resolution satellite data.

Chapter 6 (GIS) starts with a description of GIS definitions and commands used. Next, the digitizing of the Swiss glacier inventory and the GIS-integration of TM-derived glacier maps is explained. Deriving glacier parameters by DEM fusion is described and at the end the processing, work-flow and its application is discussed.

Chapter 7 (Results) gives results from the application of the developed methods to Swiss glaciers. Starting with a description of the digitized data sets and their usage for visualization, the next paragraph gives basic data from the digitized 1973 inventory (e.g., histograms and scatter plots). Glacier change since 1973 for various samples and time intervals is presented and a parameterization scheme to obtain further glacier parameters is applied to the digital glacier data. A general discussion of the results concludes the chapter.

The main conclusions and perspectives for future work are summarized in Chapter 8 (Conclusions and perspectives). The work concludes with references and an appendix, which gives additional data (tables, programs, visualizations).

All figures with TM-images or vector outlines are oriented north, if not indicated otherwise. Special fonts (capital letters, plain, HELVETICA) are used for programs of the digital image processing software (PCI, 1998) and Arc/Info commands (small letters, italic, *helvetica*) or products/names (*italic*). The software applied is described in App. 4. The last page gives a list of used acronyms and abbreviations and a short index to the chapters. The use of names which are protected by a copyright without explicit notification within this thesis does not indicate that they can be used free of charge.

1.

For the following Figures the DEM25 (level1 or level2) from Swisstopo (former Swiss Federal Office of Topography) is used:

3.1, 3.2, 3.5, 3.6, 3.7, 4.11, 5.7, 5.8, 6.7, 7.1, 7.4, 7.5, 7.15, 7.16 and App. 3.3-1 to 3.3-5.

The DEM25 is reproduced by permission of the Swiss Federal Office of Topography (BA024887).

2. GLACIERS

2.1. Background

2.1.1. Formation of glacier ice

Glaciers can be defined as visibly moving bodies of perennial surface ice that have been formed by recrystallization (or metamorphism) of snow. The snow crystals are transformed to rounded grains by evaporation and mechanical destruction (wind, compression), as well as by cycles of melting and refreezing, if temperature permits. After one year of metamorphism the material is called firn. Further compression under subsequent layers of snow will finally turn the firn to ice which is by definition not permeable for air. The time needed for the transformation of snow to ice depends on the present climatic regime and the availability of percolating meltwater, as it strongly facilitates metamorphosis (e.g., Paterson, 1994; UNEP, 1992; Wilhelm, 1975).

Mean annual air temperature and precipitation control global distribution of glaciers as well as their climatic regime. Their occurrence depends on the elevation of the equilibrium line (see 2.1.2) and a given topography, which must be above the equilibrium line and allow snow accumulation. The climate type can range from maritime (high precipitation and temperatures) to continental (low precipitation and temperatures), with a transitional type in-between (cf. Fig. 2.1). While mean temperature on earth is decreasing from low to high latitudes and altitudes, the precipitation pattern is very complex and dominated by the global circulation pattern with a strong influence of topography. These two parameters cause the observed discontinuous global glacier distribution, as documented for the northern hemisphere by Field (1975), for the southern hemisphere by Mercer (1967) and in the first status report of the world glacier inventory (IAHS, 1980 and 1989).

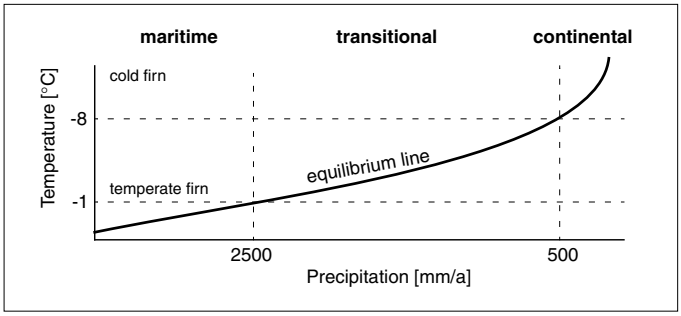

Figure 2.1: *The climate type of a glacier is governed by the annual precipitation and the average annual air temperature at the equilibrium line (after UNEP, 1992).*

2.1.2. Glacier zones

In the upper parts of a glacier, gain of snow (accumulation) is greater than its loss (ablation), in the lower parts it is vice versa. The transient snow line (TSL) defines the position of the ice/ snow boundary during the year. At the end of the melting period or balance year, the TSL is often near to the equilibrium line (EL), where accumulation equals ablation. A possible zone with refrozen meltwater and soaked firn (superimposed ice zone, SIZ) is located below the TSL and belongs to the accumulation area. Firn layers from previous years appear below this zone and are part of the ablation area (Fig. 2.2). Thus, the ablation area contains the bare ice and firn zone and the accumulation area covers the SIZ and the snow zone (Gross et al., 1976; Paterson, 1994). The latter is divided into a dry snow, percolation and wet snow zone for Arctic glaciers (Müller, 1962). In the Alps nearly all glaciers below 3500-4000 m a.s.l. have a wet upper snow layer at the end of the ablation period (absent dry snow and percolation zone), but some regions with cold firn and ice exists (Haeberli and Alean, 1985; Suter et al., 2001). Impurities (dust, soot, debris) and meltwater are visible on the glacier surface in the ablation area, diminishing reflection compared to the accumulation area (e.g., Koelemeijer et al., 1993).

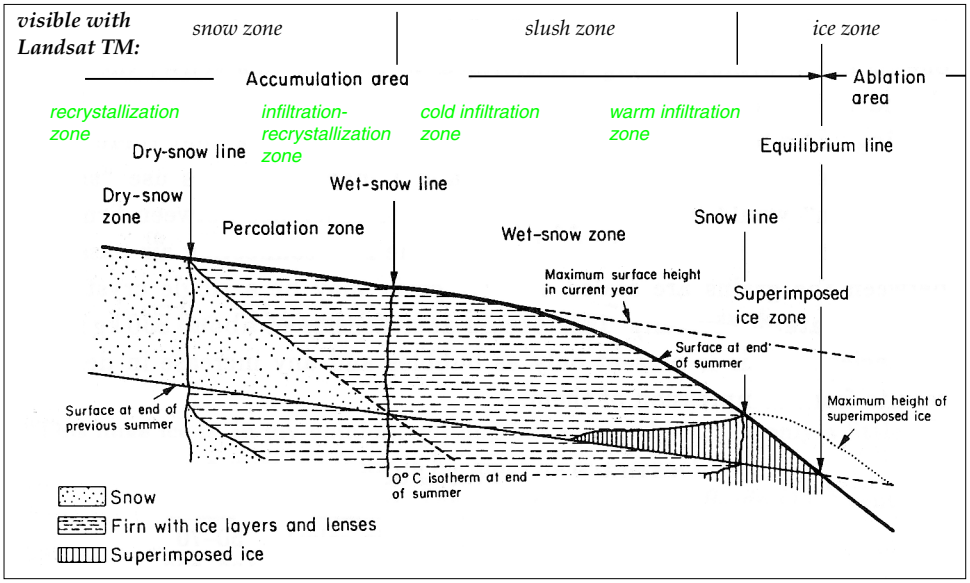

Figure 2.2: *Schematic profile of the different ice and snow zones on a glacier (after Paterson, 1994; Williams and Hall, 1993), including zones for mid-latitude glaciers in green (after Shumskii, 1964).*

Since spectral properties of snow change with grain size and liquid water content (e.g., Warren, 1982; Winther, 1993), some of the zones mentioned above can be distinguished from space. Williams et al. (1991) and König et al. (2001) have investigated the visibility of each zone by means of optical and SAR (Synthetic Aperture Radar) data, respectively. For alpine glaciers, the separation of firn from snow and between the SIZ and the bare ice zone is of interest, for the purpose of distinguishing the accumulation area from the ablation area. According to König et al. (2001), a possible SIZ cannot be detected from optical satellite data (same reflectance as ice) or SAR data (same material as bare ice). Possible firn layers cannot be distinguished from snow in the case of clean firn or from ice in the case of polluted firn (Gross et al., 1976). Assuming a comparatively small SIZ and generally dirty firn layers on Alpine glaciers, it may be possible to distinguish the accumulation (snow) from the ablation (ice, firn) area. Moreover, Hall et al. (1987 and 1988) and Williams et al. (1991) were able to distinguish slush (soaked snow) from fresh snow with TM data (see top of Fig. 2.2).

The classification of the snow zone from space is of interest with respect to a glacier's mass balance. Definitions of mass balance terms were given by Meier (1962), were discussed by Hoinkes (1970) and reviewed by Dyurgerov (2002). For many glaciers with a measured mass balance series, a near-linear relationship between the equilibrium line altitude (ELA) and mean specific net mass balance $<b_n>$ (in mm water equivalent per unit area) of a certain year was established (e.g., Braithwaite, 1984; Kulkarni, 1992; MBB, 2001). Such a relationship can be used to determine an ELA corresponding to a $<b_n>$ of 0, the steady state ELA or ELA_0. Strictly speaking, the ELA concept is only valid for glaciers, where $<b_n>$ is a linear function of elevation, excluding most glaciers with debris-covered tongues, nourished by avalanches or with an irregular hypsography (Braithwaite and Müller, 1980). Assuming an EL that corresponds to the TSL at the end of a balance year, the accumulation area ratio (AAR) can be calculated from the snow-covered glacier area divided by the entire glacier area (e.g., Paterson, 1994). The AAR also correlates with $<b_n>$ (e.g., MBB, 2001), for some glaciers the correlation is even higher than with ELA (Reinwarth and Escher-Vetter, 1999). Analogue to the ELA_0 calculation, an AAR_0 can be obtained for each glacier measured.

While Gross et al. (1976) determined an average AAR_0 of 0.67 (or 2/3) for six Alpine glaciers, a more recent investigation by Bader (1990) with nine glaciers suggests 0.6 for AAR_0. He also pointed out that the AAR_0 depends on the climate type of a glacier (smaller for maritime type, higher for continental type) and that topographic and morphologic conditions influence its value. As a result of the many exceptions, there is some debate if the AAR_0 concept is of any use for global comparisons, for instance for Quaternary ELA reconstructions (Benn and Lehmkuhl, 2000; Klein et al., 1999). However, the AAR of a certain year can be derived from satellite data (taken near the end of the ablation period) for a large number of glaciers at the same time (Aniya et al., 1996; Østrem, 1975; Rott, 1976) and a comparison with a measured AAR_0 for that region can be used to indicate mass balance qualitatively.

For each glacier measured, ELA_0 and AAR_0 values were also reported in the bi-annually published mass balance bulletin (e.g., MBB, 2001). All mass balance measurements available so far were recently published by Dyurgerov (2002) and reviewed by Braithwaite (2002). This allows selection of appropriate AAR_0 values for nearly every mountain region in the world, if satellite derived AAR measurements were analyzed. However, the more serious issue is to find appropriate satellite scenes from the end of the ablation period to allow AAR calculations. In most cases, just the best available scene for glacier classification is used and derived AAR values only indicate regional snow distribution and not glacier mass balance.

2.1.3. Glacier fluctuations and climate change

In general, the advance or retreat of a glacier tongue is a complex dynamic reaction to a change in local climate, at least for larger alpine glaciers (cf. Fig. 2.3). As a glacier flows to lower elevations, temperature is increasing and the melting of ice dominates. In the case of a stationary glacier front, this melting balances the ice flux, which is determined by the cross section of a glacier and its flow velocity. If a glacier tongue is advancing (or receding), the flow velocity must be above (or below) its balanced value. This change in flow velocity will result after several years with mainly positive or negative mass balances. The response time of a glacier to a change in climate (e.g., more precipitation / higher temperatures) depends on many factors, such as its climate sensitivity (determined by its mass balance gradient), mean slope, length and hypsography. However, the change in glacier length as a result of climate change is a strongly smoothed and delayed, but also an enhanced signal, while mass balance is the direct and undelayed reaction to the local weather conditions during a year (Haeberli, 1995).

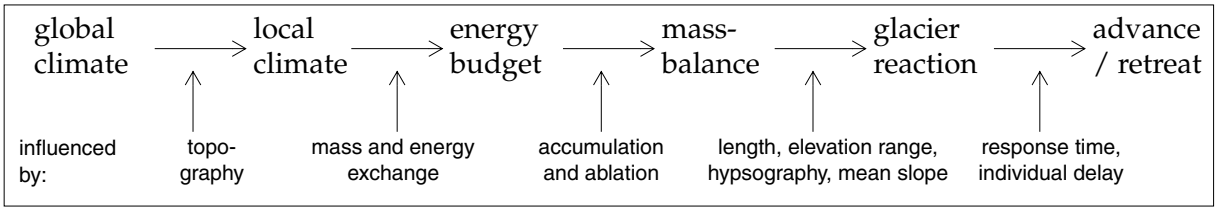

Figure 2.3: *Change in glacier length as delayed reaction to a climatic change (after Haeberli, 1995).*

2.

2.1.4. Distribution of glaciers

According to the status report of the world glacier inventory (IAHS, 1989), 549056 km^2 of the earth's surface is covered by glaciers and ice caps, which is 3.5% of the entire glacierized area (15.86×10^6 km^2) if the continental ice sheets Antarctica (13.586×10^6 km^2) and Greenland (1.726×10^6 km^2) are included. Taking this 3.5% as 100%, European glaciers (including Iceland and Svalbard) account for 53967 km^2 or 9.8%, Alpine glaciers for 2909 km^2 or 0.5% (see App. 1-1), and glaciers in Switzerland for 1342 km^2 or 0.24%. A more detailed discussion of the global glacier distribution with respect to their area is given by Zuo and Oerlemans (1997).

In the Alps (and also in Switzerland) the size distribution of glaciers is strongly biased. In the 1973 Swiss glacier inventory (Müller et al., 1976) glaciers smaller than 1 km^2 cover 24.1% of the area, but they account for 78.7% of the number (Fig. 2.4a and App. 1-2). Annual observation of changes in glacier length are mainly performed for glaciers larger than 1 km^2, in the Swiss network they account for 76.2% by number and 98.2% by area (Fig. 2.4b and App. 1-2). Thus, little is known from the length measurements about the changes in glaciers smaller than 1 km^2. In the Alps these small glaciers account for 1/3 of the entire glacierized area (1/4 in Switzerland) and thus they play an important role in hydrology.

From the estimated 160000 glaciers worldwide (Meier and Bahr, 1996), about 800 have annual length measurements (e.g., IAHS, 1998) and about 50 glaciers experience mass balance measurements (e.g., Dyurgerov and Meier, 1997a; MBB, 2001), mostly concentrated in the Alps and Scandinavia. Although glaciers with length change measurements in the Alps are rather small compared to other regions in the world, the historical record of measurements is the longest and most complete, revealing in great detail the dynamic reactions of glacier tongues to climatic changes.

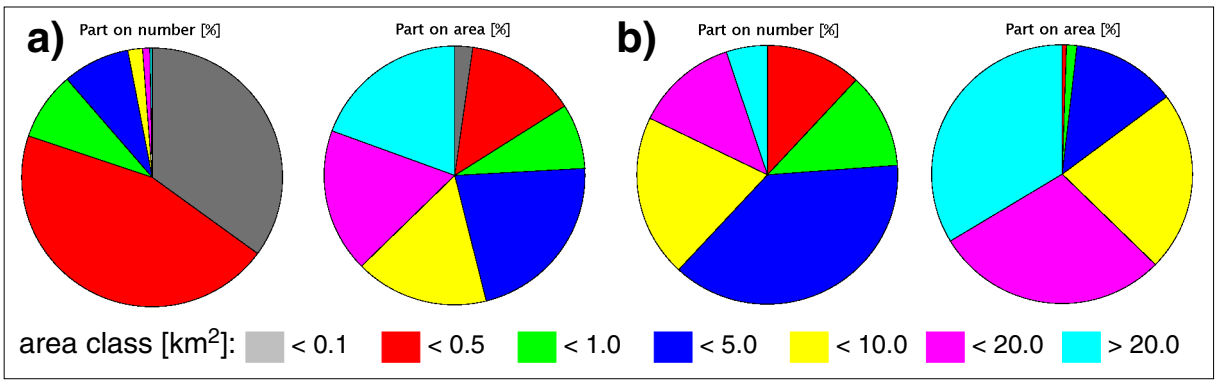

Figure 2.4: *Percentage of number (left circle) and area (right circle) for seven area classes (data from 1973): (a) within the Swiss glacier inventory and (b) within the Swiss length measurement network.*

2.1.5. Glacier types

Apart from climatological parameters, topography determines the size of a glacier as well as its general shape, form and profile. UNESCO (1970) has published a scheme for glacier characterization based on these categories. With respect to the glacier type (first digit of the code) the following categories were used: ice sheet, ice field, ice cap, outlet-, valley- and mountain glacier, glacierete, ice shelf and rock glacier. While the term ice sheet is only used for Antarctica and Greenland, ice fields can be found in numerous regions of the world (e.g., Patagonia, Alaska, Norway). They are composed of a large ice mass (with nunataks) from which several 'outlet glaciers' originate, divided by mountain ridges. An ice cap is a compact mass of ice, which is not divided by topography, but also with numerous 'outlet glaciers' possible (e.g., top of many volcanoes, Vatnajøkul, Barnes Icecap). In the Alps the types valley and mountain glacier predominate with respect to the area covered, and glaciereteses account for most of the glaciers by number. Also some small ice caps (or corniches) exist.

For illustration and reference, a few examples of Alpine glaciers are shown in Fig. 2.5 (see Bachmann (1978) for detailed descriptions with hundreds of pictures). The 'Oberaargletscher' in Fig. 2.5a illustrates the single basin type with a regular hypsography. The brighter snow-covered area is clearly distinguishable from the darker bare ice zone (ablation area). The TSL shows a quite complex structure in this picture from late August 1993, but its highest position is not reached. The glacier terminus has contact to a lake by the end of summer (used for hydro-power generation), resulting in an ice-cliff shaped terminus with calving characteristics. While the glacier perimeter is well-defined to the right (although debris cover is present), it is hardly recognizable to the left.

In Fig. 2.5b the lower part of the Trientglacier tongue in August 1992 is shown, still in an advanced position with a convex terminus shape, but already showing some depressions. Although free of larger debris (stones, pebbles), the very end of the tongue appears quite dark, due to debris of a much smaller size (sand, silt). The glacier is located at the outer western rim of the Alps and has a large accumulation area with a comparable short and steep tongue, resulting in a high climate sensitivity (e.g., Oerlemans and Hoogendorn, 1989).

The debris cover detail presented in Fig. 2.5c illustrates differences in ablation due to debris cover of varying thickness (e.g., Nakawo and Rana, 1999). While most of the small pebbles melt themselves a few cm into the ice (resulting in a porous surface), the large stone visible (about 5 cm thick) protects the ice underneath from melting and rests on a pedestal. As some ice shines through everywhere, multi-spectral ice classification may still be possible here.

The disintegrating tongue of the comparably large Triftglacier (size 17.1 km^2) as seen in August 2002 is shown in Fig. 2.5d. The hypsography is similar to the Trientglacier, but the end of the glacier tongue rests in a closed basin. Due to a reduced ice flux over a ridge, surface lowering leads finally to formation of a lake at the terminus. This lake has grown drastically during the last 3 years and a collapse of the tongue by floating is expected (cf. App. 3.3-3b). Automatic determination of glacier terminus position from satellite imagery is quite difficult in such cases with mixed pixels of turbid water / floating ice / glacier ice.

Liquid water may occupy a large part of a glacier surface in the ablation area, as visible from Fig. 2.5e (bright lines), showing a part of the 'Pasterzenkees' tongue (Austria) in back light. Due to this water, spectral properties of the bare ice zone are significantly altered. In the last spot, Fig. 2.5f a totally debris-covered glacier tongue is depicted ('Ödenwinkelkees', Austria), indicating the problems in glacier classification from spectral properties alone. In such cases, DEM information may also be useless and even manual delineation may fail.

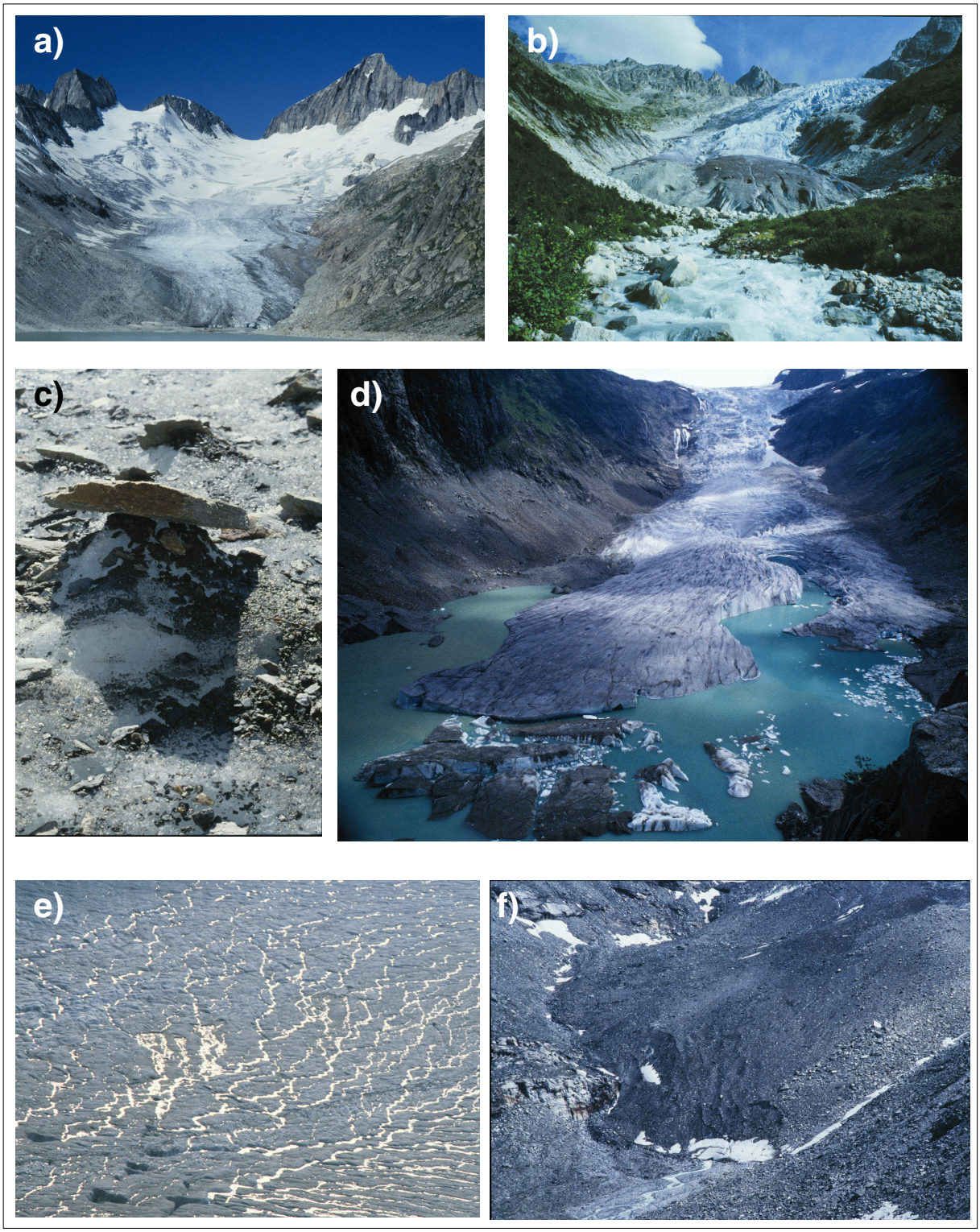

Figure 2.5: *A few examples of Alpine glaciers. a) Single basin 'Oberaargletscher' (5.2 km^2, Bernese Alps), terminating periodically in a lake. b) Advanced tongue of Trientglacier (6.6 km^2, Mont Blanc region), free of a thicker debris cover. c) Differences in ablation due to debris cover with varying size. d) Disintegrating tongue of Triftglacier (17.1 km^2). The lower, flat part of the tongue is about 2 km long. e) Meltwater channels in back light (bright lines) at the surface of 'Pasterzenkees' (Austria), swallowed by moulins. f) Totally debris-covered glacier snout of 'Ödenwinkelkess' (Austria), illustrating the problems of glacier delineation in such cases. All photos by the author.*

2.2. Glacier monitoring

2.2.1. Traditional data compilation

The historical evolution of worldwide glacier monitoring - from measuring length changes to mass balance studies to compilation of glacier inventories - is well documented (e.g., Haeberli et al., 1989; Haeberli, 1998). In recent years glacier monitoring has had its main focus on climate change detection (Haeberli, 1995; Hoelzle et al., 2000), as glaciers are considered to be prime indicators for ongoing climate changes (e.g., IPCC, 2001; Oerlemans, 1986 and 1994). The continuation of the established measurement network in the future is, thus a major challenge for this millennium and integration of glacier monitoring in the Global Climate Observation System (GCOS) is strongly encouraged (Haeberli et al., 2000 and 2002a).

History of glacier observation

Globally-coordinated observation of glacier changes was initiated in 1894 during the 6th International Geological Congress in Zurich, to answer the following central glaciological questions of that time (Forel, 1895):

1. What are the mechanisms of glacier fluctuations, and are they globally uniform and synchronous with extraterrestrial cause or not?
2. What were the causes for the ice ages?

According to Haeberli (1998), annual measurements of glacier length changes were initiated to answer these questions. The collected data have been published annually from 1896 to 1913, covering mainly the Alps and Scandinavia and rare information from the southern hemisphere. Between 1914 and 1961 the reports became thinner and were issued at longer time intervals. During the International Hydrological Decade between 1965 and 1974, many mass balance measurements were started and published in the 'Fluctuations of Glaciers' series at 5-year intervals since. In the present mass balance data from the USSR, USA and Canada have also been included. In the 1970s and 1980s, data from the southern hemisphere as well could be integrated regularly and a major step towards standardization and computer processing was accomplished. A World Glacier Inventory (WGI) was planned for the second half of the 20th century and instructions and guidelines for compilation were developed (UNESCO, 1970). Detailed and preliminary inventories were collected all over the world in a form compatible with computer processing. In 1986 the World Glacier Monitoring Service (WGMS) was founded to:

1. complete and upgrade the global glacier inventory;
2. continue collection and publication of glacier fluctuation data (5-year interval);
3. publish mass balance measurements of selected glaciers (2-years interval);
4. include satellite observations of remote glaciers to reach global coverage;
5. assess ongoing changes.

The status report of the world glacier inventory (IAHS, 1989) summarizes the available data in text, tabulated and graphical form. The latter includes location (area dependent circles) and aspect maps (area dependent sectors) as well as visualization of mean elevation and size distribution for selected regions.

Mountain glaciers and climate networks

Recently a Global Hierarchical Observing STrategy (GHOST) at five tier levels was developed within the framework of the Global Terrestrial Observing System (GTOS). The characteristic regional to global distribution of glaciers in space and measurements of glacier mass and area in time, should be assessed by more numerous observations in accordance to this tier strategy. This includes compilation of regional glacier inventories at time intervals of a few decades (the typical dynamic response time of mountain glaciers, see 2.3.1). The Global Terrestrial Network for Glaciers (GTN-G) represents the global network of glacier sites. Its structure will allow global to regional analyses of glacier change with differing measurement intensities at various sites. Using the tier strategy as defined above, the following sites and measurements are anticipated (Haeberli et al., 2002a):

Tier 1:
These major, intensive experimental sites should be arranged along large transects in order to facilitate process understanding across environmental gradients. Locations should show large spatial diversity, and covering the entire range of glacier types should be a critical priority. A transect with glaciers from Svalbard via Scandinavia and the Alps to the Pyrenees may form a tier 1 observation site in the future. The transition from initial intensive field studies to uninterrupted and long-term monitoring needs careful preparation.

Tier 2:
These sites should cover extensive and process-oriented glacier mass balance studies within major climatic zones. Ideally, they are located near the centre of the range of climatic conditions of the zone they are representing. Although the actual location will depend on accessibility, a broad range of climatic zones should be covered from tier 2 sites.

Tier 3:
At tier 3 sites, glacier samples should represent the environmental conditions within climatic zones or regions. Today's sample (about 50 glaciers with annual mass balance studies) reflects regional patterns of glacier change quite well, but they are somewhat concentrated at certain sites (Alps, Scandinavia). Within GCOS/GTOS a more balanced network of observing sites/ glacier types must be encouraged.

Tier 4:
At the tier 4 level, the spatial representativeness of the data sets has highest priority. The roughly 800 glaciers with length change measurements belong in this level. Due to the wide range of glacier types, typical selection criteria for all countries are difficult. Long-term observations at about 10 sites within each mountain range should be selected according to glacier size and dynamic response time from the existing network.

Tier 5:
The tier 5 level is compatible with glacier inventories repeated at time intervals of a few decades by satellite remote sensing. International collaboration is mandatory to produce the required data sets and a long-term strategy for data acquisition, archiving and quality control has to be established. However, glacier monitoring on a regular basis from space-borne sensors (ASTER and ETM+, see below) has been initiated within the USGS-led GLIMS project and the National Snow and Ice Data Centre (NSIDC) will handle the database issues according to tier 5 goals.

The NSIDC in Boulder, Colorado, maintains the cryospheric data (e.g., snow, glacier, sea ice, permafrost) gathered from all over the world, including the World Glacier Inventory (WGI) and the future GLIMS data base.

Applications of the compiled data sets

The WGMS collects world-wide measurements of glacier length changes and mass balance data and maintains data from national glacier inventories. Table 2.1 summarizes some issues connected with these data sets. While cumulative length changes can be used to calculate corresponding changes in secular glacier mass balance (see 2.3.1), annual mass balance data was used in combination with scaling schemes for global glacier distribution (Bahr 1997a; Meier and Bahr, 1996) to calculate the contribution of glaciers and ice caps to global sea level rise (e.g., Zuo and Oerlemans, 1997). However, recent measurements for glaciers in Alaska by Arendt et al. (2002) have revealed an underestimation of the sea level rise contribution compared to the global scaling. Glacier inventory data from the European Alps have been applied to parameterization schemes for glacier modelling (Haeberli and Hoelzle, 1995) and calculation of future glacier behaviour (Maisch et al., 2000).

	Length changes	Mass balance	Glacier inventory
Sources	direct measurements (1895) indirect measurements: - photos (since 1850), - paintings (17th century), - model calculations (ELA reconstruction)	- glaciological method (ablation stakes, snow pits) since 1950s - geodetic / photogrammetric - combined hydrological / meteorological method - index method (AAR, ELA) - cumulative length changes	topographic maps, aerial photography and satellite imagery, glacier parameters from planimetry or GIS-based DEM-fusion
Application	- filtered and delayed reaction to climate forcing - glacier-related hazards - mass balance reconstruction - global representativeness	- unfiltered and direct reaction to annual conditions - worldwide comparison possible (conversion to mm weq) - climate reconstruction and sea level change	- water resources assessment - tabulated data and outlines on maps - parameter modelling
World data sets	about 800, mostly > 1 km^2, easy to access, usually valley glaciers	about 50, distributed worldwide, mostly on northern hemisphere, complex scaling schemes for global assessments	- about 160000 glaciers (estimated from scaling) - large gaps in remote areas - forthcoming satellite snapshot within GLIMS
Data publication	'Fluctuations of glaciers' (5-year interval)	'Mass balance bulletin' (2-year interval, online: annually)	status report WGI decadal update proposed

Table 2.1: *Some of the topics addressed by the WGMS data collection (compiled from Dyurgerov, 2002; Haeberli, 1998; Haeberli et al., 1989 and 2000; IAHS, 1989; Williams and Hall, 1993).*

Measuring length changes

In a global context, the main technique used for the measurement of glacier length changes is tape readings. For selected glaciers, geodetic or photogrammetric measurements are also used. All methods can be hampered by bad weather conditions at the end of the ablation period, resulting in a variable number of measured glaciers. The measurements were conducted mostly by volunteers (e.g., mountaineers, forest services) for many years. In order to compare their data with satellite observations, the location of the reference points used (e.g., rocks in the glacier forefield) should be measured by GPS and transferred to a GIS data base. Whereas the number of glaciers that can be observed is restricted by accessibility, satellite data can be used to monitor even very remote glaciers and changes in the accumulation area.

Measuring mass balance

There are ample descriptions available of measurements and calculation of glacier mass balance and it is beyond the scope of this thesis to explain them in detail here. Most recent reviews (with references) are given by Braithwaite (2002), Dyurgerov (2002) and Hoelzle et al. (2003). An analysis of current mass balance data is given by Cogley and Adams (1998) and Dyurgerov and Meier (1997a and b). The most accurate (and expensive) technique used for measurement of glacier mass balance is the direct glaciological method, based on a network of snow pits and ablation stakes (cf. MBB, 2001) from which winter and summer balance is calculated by integration over the entire glacier area. Careful calibration by repeated geodetic (Krimmel, 1999) or photogrammetric (e.g., Finsterwalder and Rentsch, 1980; Kääb and Funk, 1999) measurements was used to compensate for crevassed areas and internal movement (submergent/emergent) of snow/ice (Haeberli et al., 1999). Comparisons with volume changes derived from accurate topographic maps were also used to confirm direct measurements (e.g., Andreassen, 1999; Haakensen, 1986; Østrem and Haakensen, 1999).

Photogrammetric techniques have been applied to glacier change studies for many decades (e.g., Brecher and Thompson, 1993; Finsterwalder, 1954; Pillewitzer, 1938). In particular photogrammetrically-derived DEMs from repeated aerial stereo-photography were used for calculation of glacier volume change (e.g., Fox and Nuttall, 1997); for example, the new Austrian glacier inventory as well will apply this method by comparison with the DEM from 1969 (Würländer and Eder, 1998). A sufficient degree of accuracy for mass balance determination was revealed even with only one year between both images (Willis et al., 1998). Apart from AAR measurements, satellites are not able to provide mass balance data on a yearly basis. However, glacier flow fields derived from sequential ASTER or SPOT imagery may provide useful information for mass balance calculations (cf. Kääb and Funk, 1999). New techniques such as laser-scanning (e.g., Baltsavias et al., 2001) or laser-profiling (Echelmeyer et al., 1996; Arendt et al., 2002) have been applied successfully to volume change calculation of glaciers.

2.2.2. Use of optical remote sensing

Remote sensing (the measurement of physical properties of objects without direct contact) can be carried out with ground-based, air-borne or space-borne sensors. The latter have the capability to image large areas of the earth's surface at nearly the same time with high resolution and under steady conditions for many years (e.g., with a nominal pixel size). The constant sensor calibration enables global application of algorithms developed. A review of the use of remote sensing techniques for glaciological investigations (including microwaves) is given by Williams and Hall (1993 and 1998) and König et al. (2001). A description of glacier mapping with respect to digital image processing is given in Chapter 5 of this thesis. The focus of the SGI 2000 is the usage of optical satellite sensors for the study of mountain glaciers. For this reason, microwave sensors (often applied to ice-sheet and snow studies) are not considered.

With the launch of the first Landsat satellite in 1972, glaciologists had for the first time the opportunity to study glaciers and their changes from a global perspective. Since 1972 the Multi-Spectral Scanner (MSS) radiometer and since 1984 the Thematic Mapper (TM) radiometer have been acquiring calibrated data with high spatial resolution (56 by 79 m and 30 by 30 m, respectively) achieving almost global coverage today. Already in the first studies with MSS data some authors mentioned the global application of their method for mass balance evaluation from satellites by means of AAR or ELA mapping (Krimmel and Meier, 1975; Østrem, 1975), but did not enforce operational application.

With the advent of the better-calibrated TM data, many researchers have been focusing on calculation of reflections and albedos of snow and ice (Hall et al., 1988; Jacobsen et al., 1993), often in relation to ground-truth measurements (Bronge and Bronge, 1999; Hall et al., 1989b and 1990; Koelemeijer et al., 1993; Winther, 1993). In addition, detailed studies on snow and ice properties (Bourdelles and Fily, 1993; Dozier and Marks, 1987) as well as on the discrimination of various glacier surface features were conducted (Hall et al., 1987; Orheim and Lucchitta, 1987; Williams, 1987; Williams et al., 1991). Apart from the investigations on glacier terminus fluctuations (e.g., Hall et al., 1992 and 1995a; Jacobs et al., 1997; Williams et al., 1997), some were also devoted to measurements of changes in areal glacier extent from Landsat data by time-series analysis (Bayr et al., 1994; Paul, 1995, 2002a and b; Serandrei-Barbero et al., 1999). The possibility of obtaining glacier inventory data from space (with Landsat MSS) was already mentioned by Rundquist et al. (1980) and Howarth and Ommanney (1986). The USGS Professional Paper series 'Satellite image atlas of glaciers of the world' gave an overview of Landsat 1-3 scenes (mainly from MSS) useful for glaciological studies (Williams and Ferrigno, 2002). In the European part (Williams and Ferrigno, 1988), the region of the Swiss Alps was discussed by Rott et al. (1988). Bindschadler et al. (2001) reviewed initial glaciological applications of the new sensor ETM+ (Enhanced Thematic Mapper plus) from Landsat 7.

Nearly all of these studies were applied to small test regions only, although almost every author emphasized the possibility of global application. Apart from restrictions due to data availability, the reason for this discrepancy was the commercial distribution of Landsat data from EOSAT between Jan 1995 and June 2001, resulting in enormous costs for a larger number of TM full scenes (about $4000 each). Today Landsat 7 data is available for $600 and data from the ASTER radiometer on board the platform Terra are available at about $60 each (EDC, 2002). Besides other points the new pricing policy leads to the USGS-coordinated project GLIMS (Global Land Ice Measurements from Space), which aims at a global snapshot of all land ice masses (Kieffer et al., 2000) from ASTER and ETM+ data. An operational monitoring system for European glaciers will also be developed in a cooperative project between Scandinavia and Austria (OMEGA, 2002; Pellikka et al., 2001).

The main advantages of **space-borne** (Landsat TM) derived glacier data compared to airborne glacier inventories are:

- the large area covered at the same time (with a spatial resolution suitable for the target);
- automatic glacier classification by means of multi-spectral image classification;
- the global data set in the archives enables time series analysis and trend calculation;
- costs are considerably lower (data and manpower).

The main advantages of **airborne** compiled glacier inventory data are:

- much higher spatial resolution possible (about 30 cm compared to 30 m);
- DEM generation from stereo imagery enables calculation of volume changes;
- date of image acquisition (weather, snow conditions) can be chosen.

In both cases the main **requirements** for successful data analysis are:

- cloud-free conditions (at least over glaciers) near the end of the ablation period;
- minimum possible snow cover adjacent to glaciers;
- accurate geocoding/orthorectification of all data (for overlays/DEM generation);
- availability of appropriate image processing and GIS software.

In summary, the main advantages of TM data are the automatic multi-spectral glacier classification and the large area covered at the same time, while airborne data have much greater precision. Both methods suffer from shadowed and debris-covered glacier parts and can take advantage of GIS-based data processing and DEM fusion for glacier parameter calculation.

2.2.3. Use of a geographic information system (GIS)

After Walsh et al. (1998), a geographic information system (GIS) can be described as being capable of data capture, storage, management, retrieval, analysis and display. It integrates spatially-arranged thematic data by means of geocoded data layers and associated information stored in attribute tables (cf. 6.1). Since it is quite difficult to track changes in glacier geometry on printed maps, a GIS could be the primary tool for the dynamic aspects of glacier monitoring (Gao and Liu, 2001). However, only few attempts have been made to utilize a GIS for that purpose (e.g., Klein and Isacks, 1996; Mennis and Fountain, 2001; Wipf, 1999). A GIS allows digitizing of glacier outlines or elevation contour lines from maps with a digitizer tablet or by on-screen cursor tracking using scanned maps as background. Elevation contourlines enable DEM generation from which glacier parameters can be obtained.

Although proper integration of remote sensing and GIS software has not been achieved during the last decade (Davis et al., 1991; Ehlers et al., 1989; Lunetta et al., 1991), it is possible to use classified remote sensing imagery as a data layer in a GIS by means of raster-vector conversion. The programming capabilities of most GIS software packages (e.g., Arc/Info from ESRI, 2001) allow automatic processing and enable the use of further software (e.g., image processing, Fortran, graphical output) by running batch mode scripts. For calculation of 3D glacier parameters from a DEM, glacier outlines are converted back from vector to raster format, because processing of DEM data within Arc/Info is raster-based.

Previous studies that used a GIS for glaciological applications can be divided into: (1) stand alone applications with a GIS, (2) using a GIS together with a DEM and (3) using a GIS together with remote sensing data. The integrated use of a GIS, remote sensing data and a DEM for glacier mapping, inventorying and monitoring has not been investigated thus far. This is the key issue of the SGI 2000 with respect to Swiss glaciers (Kääb et al., 2002; Paul et al., 2002) and of the GLIMS project with respect to global application (Kieffer et al., 2000).

(1) A GIS was used for the digitizing of glacier outlines from topographic maps of different years and automatic calculation of glacier areas, lengths, ELAs and their changes (Benz, 1995; Wipf, 1999). In addition to these parameters, Mennis and Fountain (2001) calculated glacier volumes and their changes by DEM generation from digitized contour lines of different years. Li et al. (1998) used a GIS to display changes of the Moromaha Icefield (Tibet) between 1976, 1987 and 1994 by overlay of glacier outlines. Changes in glacier terminus position were obtained for two outlet glaciers as an average from three manually specified profiles across each tongue.

(2) Gao and Liu (2001) also suggests a combined use of a GIS with a DEM to derive topographic glacier indices automatically, but apart from Allen (1998) most studies used only the DEM and not the GIS (e.g., Copland, 1998; Turpin et al., 1998). A DEM was also used to facilitate glacier classification from remote sensing data (Gratton et al., 1990; Binaghi et al., 1997), but not to derive 3D glacier parameters in a systematic way. Other applications of a DEM in glacier research are summarized in 3.1.4.

(3) Klein and Isacks (1996) used a GIS and remote sensing data (Landsat TM, SPOT pan) to study glacier change of the past centuries in the central Andes. The automatic retrieval of glacier areas by application of a GIS to Landsat TM data was demonstrated by Paul (2002b).

2.3. Environmental relevance of glaciers

The importance of frequent glacier observation (monitoring) results from their impact in many different parts of the global environment. First of all, their changes are key indicators for ongoing global climate change (2.3.1). Moreover, they may cause or trigger natural hazards (2.3.2), influence hydrologic regimes (2.3.3) and their worldwide melting accounts for part of global sea level rise (2.3.4). In addition, they are unique sources of fresh water and an important economic factor for tourism (enriching the landscape, serving as a location for ski resorts) and hydro-power production (UNEP, 1992).

2.3.1. Glacier fluctuations and climate change

The worldwide retreat of mountain glaciers is one of the clearest signals of ongoing climate change (Haeberli, 1995; Hoelzle et al., 2000; IPCC, 2001; Oerlemans, 1986, 1994 and 2000). As reported by Haeberli et al. (2000), glaciers are now part of the Global Climate Observing System (GCOS) and their monitoring from ground, air and space is integrated into the global hierarchical observing strategy (GHOST) described in 2.2.1.

It is important to distinguish between the mass balance of a glacier as the direct and undelayed reaction to yearly weather conditions and the change in glacier length as an indirect and delayed but also enhanced reaction to a longer climate forcing. There are many investigations on the correlation of mass balance and weather elements for mountain glaciers (e.g., Günther and Widlewski, 1986; Kuhn, 1980b; Schönher et al., 2000; Wakonigg, 1971). They show that summer weather conditions (temperature, precipitation) have the greatest influence on Alpine glaciers mass balance and that the amount of winter snow is of less importance. For maritime-type glaciers it is different and the advance period of Norwegian glaciers indicate a greater amount of winter precipitation in previous years (Reichert et al., 2001).

Although the change in glacier length is a complex reaction to a change in local climate, some assumptions are possible for steady state conditions (cf. Fig. 2.6): A given change in mass balance δb (Fig. 2.6a, top) will be followed by a change in glacier length δL after a glacier-specific reaction time (t_r). A new steady state is reached after the response time t_a (Fig. 2.6a, bottom), which is calculated from the maximum thickness h_m and the yearly ablation at the glacier tongue (a_z): $t_a = h_m / a_z$ (Johannesson et al., 1989a and b). According to Nye (1960) the change in glacier length is a function of δb and the original glacier length L_0, divided by a_z (Fig. 2.6b, top): $\delta L = (L_0 \times \delta b) / a_z$ (Haeberli and Hoelzle, 1995; Hoelzle et al., 2000).

The method was applied to measured cumulative changes in glacier length from 1850 to 1970 (near steady states), achieving a good correspondence of calculated and measured changes in mass balance (Hoelzle et al., 2003). The energy required for melting the corresponding ice mass can be computed from known correlations of climate and mass balance (e.g., Kuhn, 1980a and 1989; Oerlemans, 1989), yielding about 2-3 W/m^2 (Haeberli, 1995) and is in correspondence with independently calculated climate forcing (e.g., Oerlemans, 1994). Historic glacier fluctuations were reconstructed from climate models (Oerlemans, 1988), glacier fluctuations were used for verification of climate models (Beniston et al., 1997), and climate changes were derived from observed glacier changes (Smith and Budd, 1981). Furthermore, mass balance series were reconstructed from tree rings (Nicolussi and Patzelt, 1996) or nearby measured climate records for the Hintereisferner, Austria (Greuell, 1992).

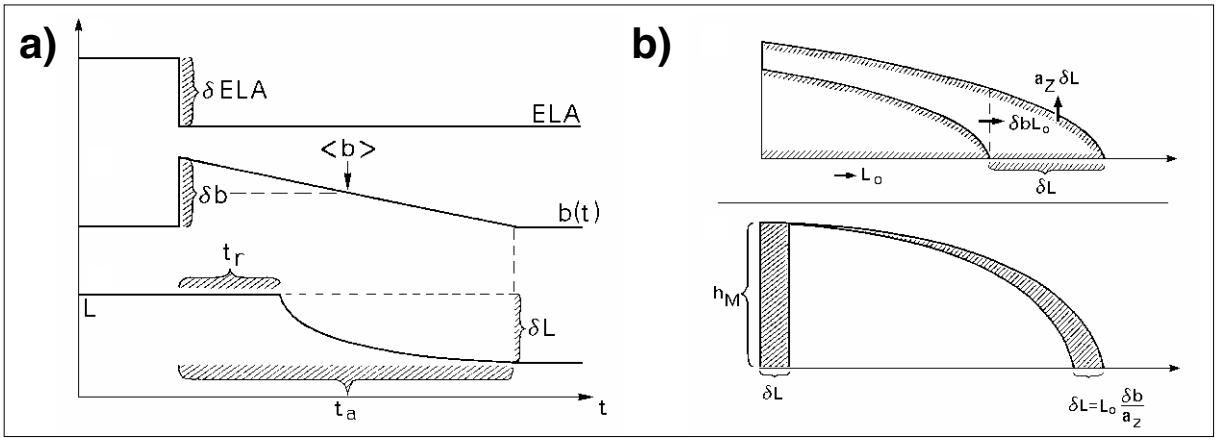

Figure 2.6: *Reaction of a glacier tongue after a step-wise displacement of the equilibrium line (δ ELA) and the resulting change in mass balance δb (after Haeberli, 1991and Hoelzle et al., 2000). See text for discussion.*

However, the change in glacier length can be seen as a delayed and enhanced signal to a change in local climate, and the size of a glacier determines smoothing and amplitude of the signal (see Fig. 2.7). While the largest glacier ('Grosser Aletsch') shows no advance during the last 150 years, medium-sized glaciers exhibit decadal variations ('Trient') and small glaciers display year-to-year fluctuations ('Pizol'). The latter are somewhat decoupled from climatic control and their behaviour seems much more influenced by topography (see 7.3). A world-wide comparison of glacier length changes also has to consider the glacier type (see Fig. 2.1), which determines a glaciers mass balance gradient and thus, its climatic sensitivity. The last decade has been the hottest since temperature measurements begun (IPCC, 2001), hence Alpine glaciers will retreat further. They are not in balance with the present day's climate (e.g., Haeberli et al., 1999; MBB, 2001).

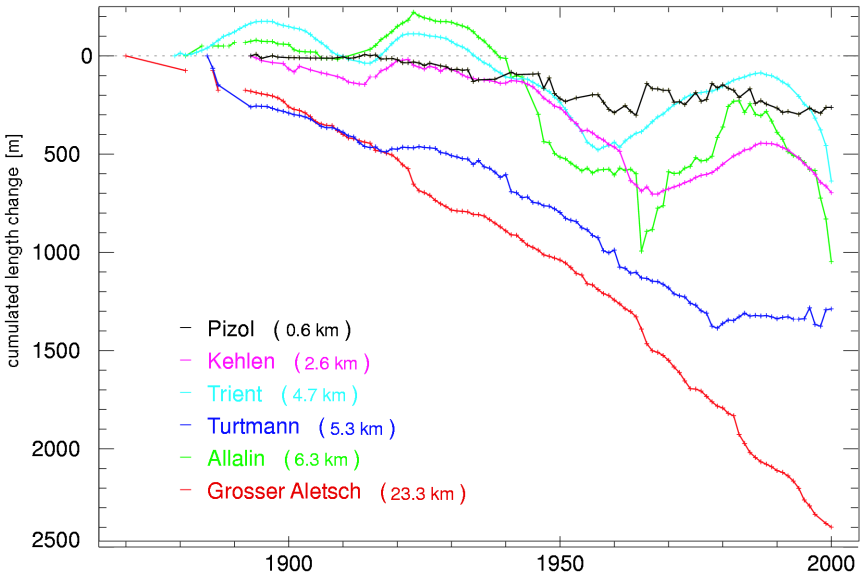

Figure 2.7: *Cumulative glacier length changes since the start of yearly measurements for selected Swiss glaciers of different sizes. The larger the glacier the greater the amplitude and the stronger the smoothing of climate disturbances (data with kind permission from WGMS).*

2.3.2. Glaciers and natural hazards

According to Richardson and Reynolds (2000), glacial hazards attract attention due to the risk of loss of life and their serious threat to infrastructure. Such hazards have been reported from all over the world, for example from China (Ding and Liu, 1992), Canada (Clague and Evans, 2000), Switzerland (Haeberli, 1983), Peru (Lliboutry et al., 1977) and Nepal (Mool, 1995; Vuichard and Zimmermann, 1987; Watanabe and Rothacher, 1996). The most prominent glacial hazards are (1) glacier floods, (2) ice avalanches and (3) glacier fluctuations / surges.

Glacier floods (1) can be the result of outbursts from (a) internal water pockets, (b) ice-dammed or (c) moraine-dammed lakes. While (a) refers to a sudden flood with rapid discharge of water under pressure, the development of pro-glacial lakes (b) and (c) requires some time and is thus visible prior to a possible glacier flood, for example, on satellite imagery (Huggel et al., 2002; Wessels et al., 2002). However, sudden ice and rock fall or calving events can result in displacement waves, which may overtop the freeboard of the dam (composed of ice and/or moraine) and trigger glacier lake outburst floods (GLOF). Such floods are often associated with debris flows, as large amounts of unconsolidated debris is available from the dam, the glacier forefield and along the river bed. Hence, a full understanding of a potentially dangerous situation requires an integrative assessment (Clague and Evans, 2000; Kääb et al., 2000b; Richardson and Reynolds, 2000). Detailed investigations of the technical aspects of dam failure were given by Clague and Evans (1994), Costa and Schuster (1988), and Walder and Costa (1996).

Apart from any direct effects of ice avalanches (2) on human lives or infrastructure, they are more dangerous for their indirect effects, i.e. triggering snow avalanches (Margreth and Funk, 1999) or GLOFs, which have much longer runout distances. Also glacier advance or retreat (3) and glacier surges are more dangerous for the indirect effects, i.e. damming of river discharge from a tributary valley or build-up of a morainic dam in the glacier forefield, both triggering formation of glacial lakes (Clague and Evans, 2000; Richardson and Reynolds, 2000).

As a result of the recognized damage potential of glacial hazards, a number of assessment and mitigation studies were carried out, for example by Haeberli et al. (1989 and 2001), Kääb and Haeberli (2001), Reynolds (1998), Reynolds et al. (1998), Röthlisberger (1981) and Vallon (1989). For the required integrated analysis of potentially dangerous lakes, satellite imagery have proven to be very valuable. They were used for Buthan and Nepal for compilation of an inventory of glaciers, glacial lakes and GLOFs (Mool et al., 2001a and b). In this region, enhanced glacier retreat with rapidly growing lakes during the last decades has amplified the problem (UNEP, 2002). Techniques for early recognition of such hazards by aerial photography (Kääb, 2000) and multi-spectral satellite imagery (Kääb et al., 2000a and b) have been developed, also utilizing automatic detection of glacier lakes (Huggel, 1998; Huggel et al., 2002). Future calculations may include GIS-based hydrologic modelling of debris flow paths to reveal endangered regions (e.g., Gamma, 2000).

2.3.3. Glaciers influence on hydrology

All glaciers together (without the ice sheets of Antarctica and Greenland) account only for 0.7% of the worlds liquid supply of fresh water (Williams and Hall, 1993). However, this small part is very important due to its multi-purpose usage. Glaciers supply most water during the hot summer months, thereby filling the lakes of hydro-electric power plants (especially in the Alps) or feeding rivers used for agriculture and as a source of drinking water (e.g., Himalayas, India, Andes).

In regions with glacier coverage, snowmelt in springtime was prolonged (reducing flood risk) and discharge after precipitation peaks from summer thunderstorms was moderated. However, rising temperature will increase glacier melt and higher flood peaks will result in combination with heavy summer precipitation in the future, until glacier area has diminished under a specific level and peak discharge is dominated by precipitation (Braun et al., 1999).

2.3.4. Glacier melt and sea level rise

There is growing concern about a rising sea level due to the predicted increase in global air temperature. Thermal expansion of ocean water will contribute about a half of this rise and melting glacier ice will contribute to the rest (IPCC, 2001). The role that the ice sheets Antarctica and Greenland will play is still under debate, as determination of their mass balance is extremely difficult (Zuo and Oerlemans, 1997). The assessment for small glaciers (other than ice sheets) is also difficult, as the global distribution of glacier areas with elevation is insufficiently known (Bahr, 1997a; Meier and Bahr, 1996), and the extrapolation from mass balance measurements of small glaciers to large glaciers is not straight forward. However, the initial estimation from Meier (1984) yielded a contribution of about 25 cm in total until the 1970s.

Based on the availability of global circulation models (GCMs) and relations for mass balance and climate (e.g., Kuhn, 1989), future glacier contributions were calculated (e.g., Kuhn, 1993). Global mass balance measurements for small glaciers have been compiled by Dyurgerov and Meier (1997b) and detailed regional assessments based on these mass balance data was discussed by Gregory and Oerlemans (1998). According to their study, the influence of glacier melt on rising sea level is slighter than predicted earlier (about 6 cm since 1865, with Greenland), but they use regionally-differentiated temperature estimates instead of global means.

However, the contribution from the Alaskan glaciers has probably been underestimated, as Arendt et al. (2002) have shown recently. These authors have used laser profiling to measure thickness changes during the last decade along selected profiles of about 30 glaciers (from small to large). Extrapolation to all Alaskan glaciers (covering 90000 km^2) and comparison with data collected 30 years earlier, reveal that the rate of thickness decrease is more than three times faster than before. Alaskan glaciers alone should have contributed 13 cm to the total rise, which is half of the total contribution from all glaciers, assuming the first guess by Meier (1984) is correct.

In a global context, Alpine glaciers (covering about 3000 km^2) will not contribute significantly to sea level rise, but they could provide important information for the development of scaling methods that can be used in other regions. This includes the large number and quality of mass balance measurements, the long length change and climate record, as well as the detailed inventories available (cf. Haeberli and Hoelzle, 1995).

3. DIGITAL ELEVATION MODEL (DEM)

3.1. Overview

3.1.1. Definitions

A digital elevation model (DEM) is a discrete and quantitative description of terrain elevation on earth from a set of x, y, z points. This DEM defines an idealized surface without vegetation and man-made structures (e.g., buildings, bridges). The 'real' earth surface (lower boundary of the atmosphere) can be described by a digital surface model (DSM), which may also include objects with temporal changes (e.g., vegetation). A digital terrain model (DTM) can be described as an interpolated DEM, either resulting in a triangular irregular network (TIN) or a gridded (equidistant spacing) representation of the elevation values (Prechtel, 2001). While the TIN form of a DTM can reproduce high-frequency topographic variations from a higher number of mesh points, a gridded DTM is better suited for raster-based applications (e.g., surface derivatives, digital image processing), but requires a constant cell size for the entire DTM perimeter (Mark, 1975). The DEM25 used in the SGI 2000 is actually a DTM and the term DEM is used for a DTM in the remote sensing community as well, while in photogrammetry and GIS science both terms are distinguished more precisely. In order to avoid confusion, DEM is used in this thesis for both terms. Wilson and Gallant (2000), Burrough and McDonnell (1998) and Wise (1998) gave a more detailed discussion of DEMs and Heitziger and Kager (1999) and Hutchinson (1989) of DEM interpolation techniques.

3.1.2. DEM Sources

Terrain elevations can be obtained by photogrammetric analysis of stereo images, which show the same area from different perspectives. In the case of stereo images obtained from aircraft, the change in viewing direction is due to motion, whereas satellites utilize additional (ASTER) or steerable (SPOT) sensors or overlapping regions from adjacent paths (Landsat). Interferometric techniques are applied to radar imagery acquired from ascending/descending paths of the same satellite (e.g., ERS-1) or two sensors spaced at a certain distance (e.g., ERS-1/2 tandem mission, and Shuttle Radar Topography Mission, SRTM). Each sensor needs its own algorithm to correct for internal distortions and get stereo pairs for DEM generation. Moreover, each DEM has its own special advantages or disadvantages regarding price, spatial resolution, area coverage or accuracy, and thus its special field of application. Further aspects

on DEM generation and applications were given by Kääb (1996) for DEMs from aerial photography, Al-Rousan et al. (1997) for SPOT, Ehlers and Welch (1987) for Landsat 5, Toutin (2002b) for Landsat 7, Kääb (2002) and Toutin (2002a) for ASTER and Small et al. (1998) for ERS-1. Another technique for high-resolution DSM generation is laser scanning (Belitz et al., 1996). It is used for mass balance determination by volume change calculation (Baltsavias et al., 2001; Favey et al., 1999). Compared to airborne InSAR (Interfereometric Synthetic Aperture Radar) laser scanning reveals highest accuracy (Meier and Nüesch, 2001).

3.1.3. The DEM25 from Swisstopo

Technical notes

The level 1 DEM25 was interpolated from digitized contour lines (using 1:25000 topographic maps from the mid 1980s) and manually added geodetic points. Although digitizing errors were corrected by manual editing, the interpolation algorithm used reveals smoothed elevations (Rickenbacher, 1998). According to Swisstopo (2001), the new level 2 version (DEM25L2) has four major improvements: (1) integration of terrain crests and folds, (2) updated contourlines on glaciers, (3) topological improvements of vector elements, and (4) a new interpolation algorithm. These corrections result in elevation differences of up to 300 m between both DEMs at isolated points. The vertical accuracy in the DEM25L2 is reported to be better than 10 m in the central Alps and better than 5 m in the Prealps. Elevation data was compiled between 1992 and 1998, depending on the region (Swisstopo, 2001).

Apart from DEM artefacts at individual points, systematic errors as well can be found for DEMs interpolated from digitized contour lines (e.g., Brown and Bara, 1994; Guth, 1999). Both DEMs from Swisstopo are hampered from such contour line artefacts, but they are much less pronounced in the new DEM25L2. A quantitative assessment of the level 1 DEM25 accuracy with respect to a reference DEM is given in 3.3. The DEM25L2 accuracy is not evaluated explicitly, since time of data acquisition differs too much and artefacts are strongly reduced.

Compared to international standards the DEM25L2 (and also the level 1 version) has a very high vertical accuracy and spatial resolution. Such high-quality DEMs are very expensive and only available for small parts of the world from national agencies, due to the large number of commercial applications and the generalizing effort. DEMs derived from 10 m SPOT data reveal a higher precision than those from 15 m ASTER data (Toutin and Cheng, 2002), but they are much more expensive. The global 1 arc second DEM from the SRTM is still under construction (Rabus et al., 2003). Although the high accuracy of the DEM25L2 is not required for orthorectification of satellite imagery or 3D visualizations, it is used for the SGI 2000 to obtain the highest possible precision for the DEM-derived glacier parameters.

Comparison of the level 1 DEM25 with the DEM25L2

The calculation of glacier volume changes from elevation differences between the level 1 DEM25 and the new DEM25L2 is not possible, for at least three reasons: (1) the date of acquisition varies with respect to the (rectangular) perimeter of the corresponding 1:25000 map sheet, (2) contour lines are updated for larger glacier tongues only, not considering snow-covered parts, and (3) elevation differences caused by the new interpolation method cannot be separated from 'real' glacier surface elevation changes. For the purpose of illustration, the dif-

ferences in elevation between both DEMs are shown colour-coded for a part of the Aletsch region in Fig. 3.1.

Data handling

At first the level 1 DEM25 in the 25 m spatial resolution grid version ('Matrixmodell') is used for the entire perimeter of Switzerland. In June 2001 the DEM25L2 became available and is obtained for a smaller perimeter (covering only the glacierized regions) and used for all calculations afterwards. For orthorectification of satellite imagery the DEM25L2 is nested into the larger perimeter of the level 1 DEM25 and also into a larger perimeter including parts of Germany, France, Italy and Austria. For theses regions outside of Switzerland a DEM with a coarser resolution (about 100 m) provided by the Remote Sensing Laboratories (RSL) is used.

Some care is necessary with respect to the location of the elevation values within a grid cell and the interpretation of location coordinates with different software products. Since the elevations for the DEM25L2 are defined for the mesh points of the grid (and not as the average of a grid cell), coordinates are shifted by 12.5 m towards the centre of each pixel, in order to use the elevation value as a cell average within PCI (1998). Data export with PCIs NUMWRIT in a geocoded form uses the centre of each pixel as the coordinate, and Arc/Info will interpret these coordinates as upper left corner. Thus, some caution is required. Because Arc/Infos *asciigrid* command needs a special header for conversion of ASCII-files to grid format, only elevations are written by NUMWRIT and the header is appended manually.

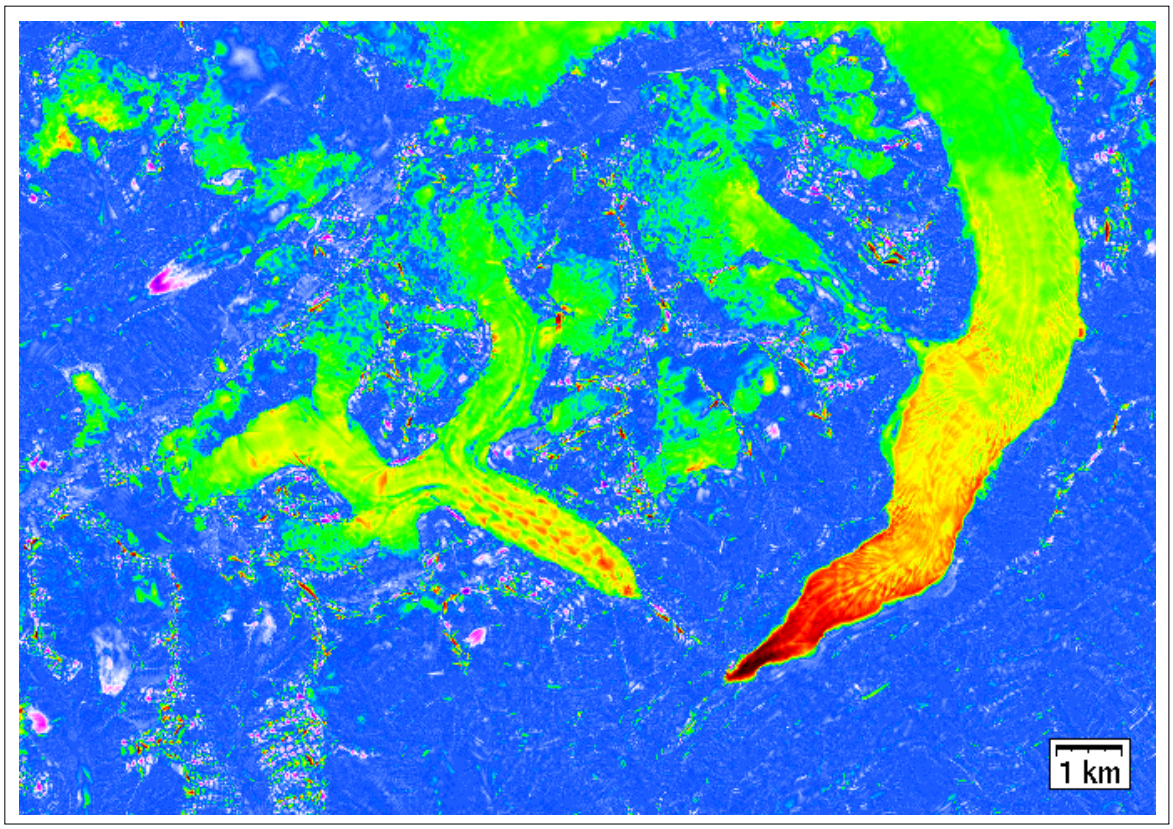

Figure 3.1: *Colour-coded elevation differences between the level 1 DEM25 and the DEM25L2 for a part of the Aletsch test region (cf. Fig. 7.1). Colours range from -110 m (dark red) to 0 m (blue) to +30 m (purple). The reduction of interpolation artefacts (coloured dots) and update of elevations on selected glacier tongues is evident (blue means no change). DEM25 © swisstopo.*

Accuracy of the level 1 DEM25

The vertical accuracy of the level 1 DEM25 is compared to a reference DEM which is inferred from stereo photogrammetry (Kääb, 2001). An illuminated version of the level 1 DEM25 is shown in Fig. 3.2a for a small sub-area (5.7 by 5.0 km) within the test region Weissmies (see Fig. 4.5 'A'), together with outlines from seven glaciers, analyzed below. Artefacts from the interpolation process of the original DTM are already visible in Fig. 3.2a (e.g., black and white streak across glacier 4). They are notably pronounced in gradient products like slope, as illustrated in Fig. 3.2b, which shows the difference in slope to the reference DEM. Fortunately, these artefacts are mostly located outside of glaciers and the influence on derived glacier parameters (apart from minimum and maximum slope) is rather small. Contour line ghosts have also been reported from Brown and Bara (1994) and Guth (1999) as a general problem of DEMs generated from digitized contour lines. Improvements to DEMs as necessary for geomorphological applications are discussed by Gruber and Kriz (1998).

The minimum (maximum) elevation differences are -96 (+74) m for the entire area as displayed in Fig. 4.5, with a standard deviation of 8.6 m. The corresponding values for the slope differences are -53° (+60°) and 6.6°. Such deviations are not acceptable for the SGI 2000, but they are mostly located at single spots or crests, usually not related to glacier coverage. In order to estimate the influence of the artefacts on the derived glacier parameters, some of them are calculated for the seven glaciers indicated in Figure 3.2a. The values for the individual glaciers are depicted in Fig. 3.3a (elevation) and 3.3b (slope). In both figures also the differences to a 50 m spatial resolution grid are shown (TYDAC, 1999). The average differences of minimum (maximum) elevation are -2.7 (-1.3) m, with a standard deviation of 7.6 (7.4) m. The corresponding values for slope are 1.2° (-2.5°) and 2.4° (3.3°). While these deviations are acceptable for glacier parameters, deviations for the 50 m DEM exceed 100 m for elevation and 20° for slope. Hence, the latter DEM will give excessively inaccurate glacier parameters for the comparable tiny Alpine glaciers.

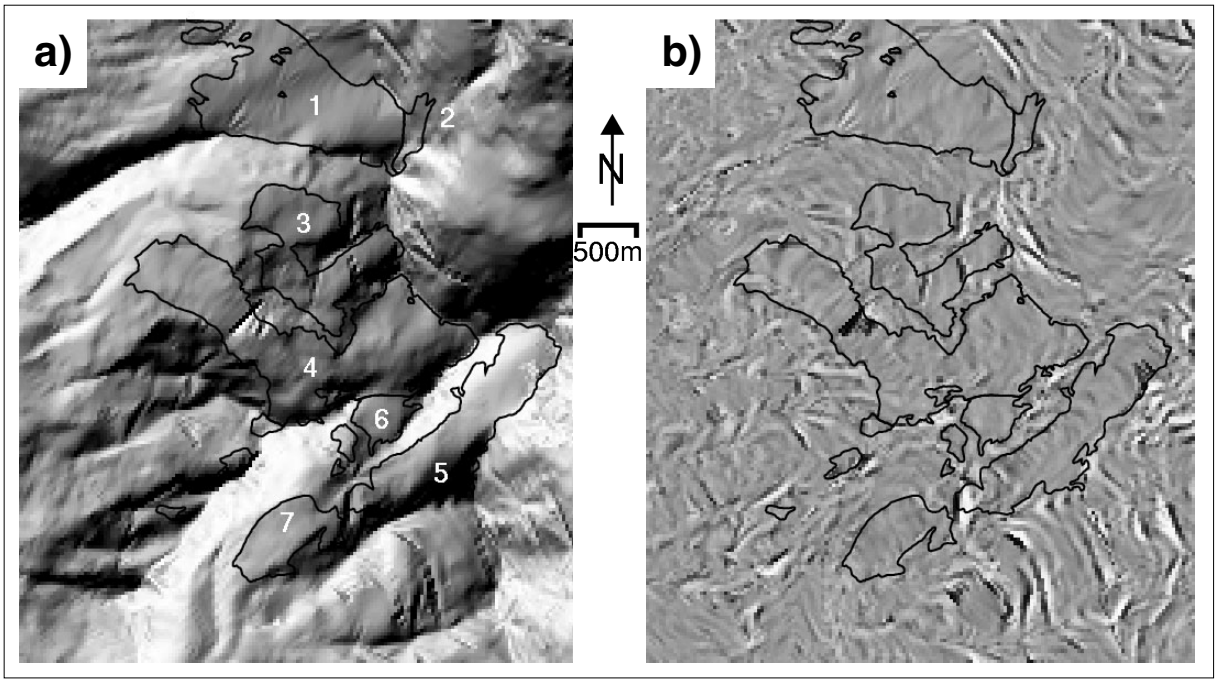

Figure 3.2: *a) Shaded level 1 DEM25 (subsection of the Weissmies test area) with outlines of seven glaciers (numbered). b) Differences in slope between the level 1 DEM25 and a reference DEM derived from stereo photogrammetry. Values range from -53° (black) to +65° (white). DEM25 © swisstopo.*

Although average values derived from the level 1 DEM25 are acceptable for this small region, it is possible that larger errors occur at other places, where interpolation artefacts are within a glacier. The DEM25L2 has much less interpolation artefacts and is, thus used to obtain the glacier parameters. A direct comparison between parameters derived from the level 1 DEM25 and the DEM25L2 is not possible, as glacier elevations are altered too much. Moreover, the latter is compiled about 10 years later (during the mid 1990s) than the level1 DEM25.

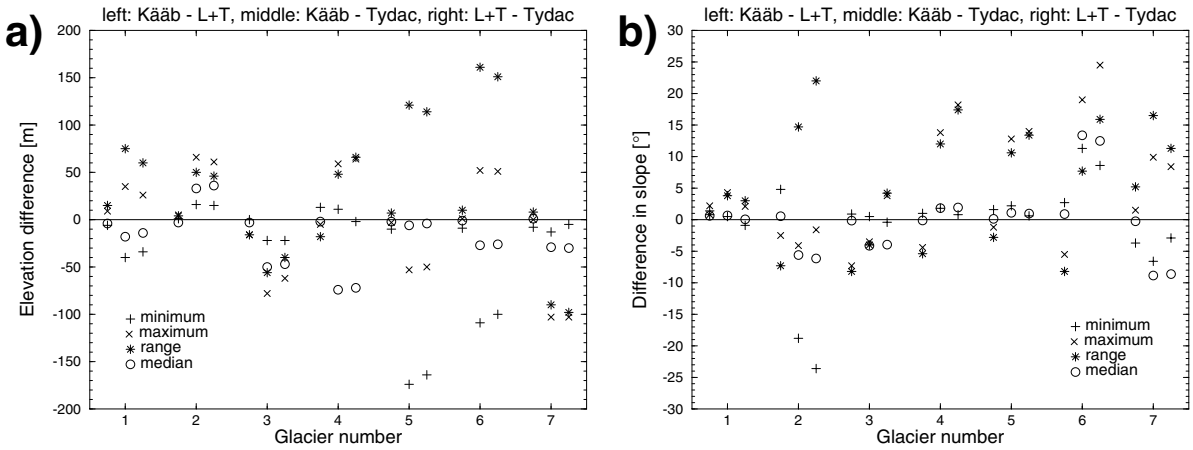

Figure 3.3: *Comparison of a) differences in elevation and b) in slope for each glacier numbered (cf. Fig. 3.2a) derived from the DEM25 (L+T) with a reference DEM (left part of each block) and a 50 m spatial resolution DEM with the reference DEM (middle part) and the DEM25 (right part).*

3.2. DEM applications

3.2.1. Previous studies

A gridded DEM allows calculation of various terrain properties, such as slope and aspect, plan and profile curvature, elevation-relief ratio or hydrological and radiation-related parameters (upstream area, flow length, direct potential solar radiation). An introduction to these geomorphometric modelling issues was given by Burrough and McDonnell (1998), Pike (1988) and Schmidt and Dikau (1999). For hydrologic applications (flow paths) of gridded DEMs refer to Jenson (1991), Quinn et al. (1991) and Tarboton et al. (1991). Radiation-based DEM modelling was described by Dozier and Frew (1990) and Dubayah and Rich (1995) and geomorphologic applications by Etzelmüller et al. (2001), Florinsky (1998) and Moore et al. (1991).

Interesting glaciological applications of a DEM were already mentioned by Peipe et al. (1978). They propose benefits for mass balance calculations and visualization. Reinhardt and Rentsch (1986) used DEMs for determination of volume and elevation changes of the 'Vernagtferner', Austria. Rentsch et al. (1990) mentioned a number of DEM-derived products (such as colour-coded maps of height, slope and aspect; shaded relief models and perspective views), in order

to give additional help in interpretation of glaciological phenomena. Etzelmüller and Sollid (1997) used DEMs of two different years (derived from aerial photgrammetry) for a geomorphometric characterization of five glaciers in Svalbard and calculation of their changes. They were able to correlate these DEM-derived changes with observed glacier evolution. Mennis and Fountain (2001) separated glaciers into an accumulation and ablation area according to their curvature and Kieffer et al. (2000) described the use of curvature information for delineation of debris-covered glacier tongues. Terrain modelling for the entire catchment area of a glacier is used by Copland (1998) to characterize snow cover distribution.

Allen (1998) has derived topographic glacier indices from a DEM (e.g., up-slope area, exposure index, terrain compactness) and searched for correlations with multi-variate regression and discriminant analysis. He also recommended the integration of satellite imagery and GIS-based DEM analysis for glacier characterization. In an earlier approach from Gratton et al. (1993) Landsat TM data was used in combination with a DEM to determine the net-radiation field of a mountain glacier, Jacobsen et al. (1993) used SPOT HRV data to calculate glacier surface albedo and Parrot et al. (1993) analyzed ice-snow fields on Arctic glaciers after atmospheric correction and DEM-derived reflectance calculation.

3.2.2. DEM usage in the SGI 2000

Orthorectification

Geocoding of satellite imagery in flat terrain only requires a set of ground control points (GCPs). In mountainous terrain a DEM is needed additionally for correction of panoramic distortion (see 4.2). The software used for geocoding with GCPs and DEM-based terrain correction (SORTHO) also corrects for the inner geometry of the sensor, resulting in geocoded and orthorectified images. Accurate orthorectification of satellite imagery in the SGI 2000 is mandatory for at least three different tasks: (1) overlay and spatial computations with independently geocoded vector layers (e.g., digitized glacier outlines), (2) combination with satellite imagery from other sensors (e.g., for image fusion) or from other years (e.g., change detection), and (3) fusion with the geocoded DEM itself (e.g., to obtain glacier parameters). As DEM grid spacing has to be constant (25 m), the nested grid used for orthorectification becomes very large. It is divided into an eastern and western part for this purpose. The technical aspects of orthorectification are discussed in more detail in 4.2.

Glacier parameters

The DEM25L2 is also used to obtain 3D glacier parameters. Some of them are shown in the schematic overview of Fig. 3.4a together with the 'Tschiervagletscher' (Fig. 3.4b) for comparison. While glacier area is provided within the GIS automatically for each polygon (glacier), other 3D glacier parameters are obtained from the co-registered DEM. The statistical GIS function *zonalstats* which is used interprets each glacier as a zone and gives minimum, maximum, range, mean, median and standard deviation (σ) from the underlaid DEM. The hypsography (distribution of area with height) as well as 2:1 elevation (ELA) and 1:1 elevation (median) are derived by further computation (cf. 6.4). Glacier length is obtained from digitized central flow lines and further 3D parameters (e.g., slope, aspect) are derived from DEM-derived products, which are obtained by digital terrain modelling (see 3.2.3).

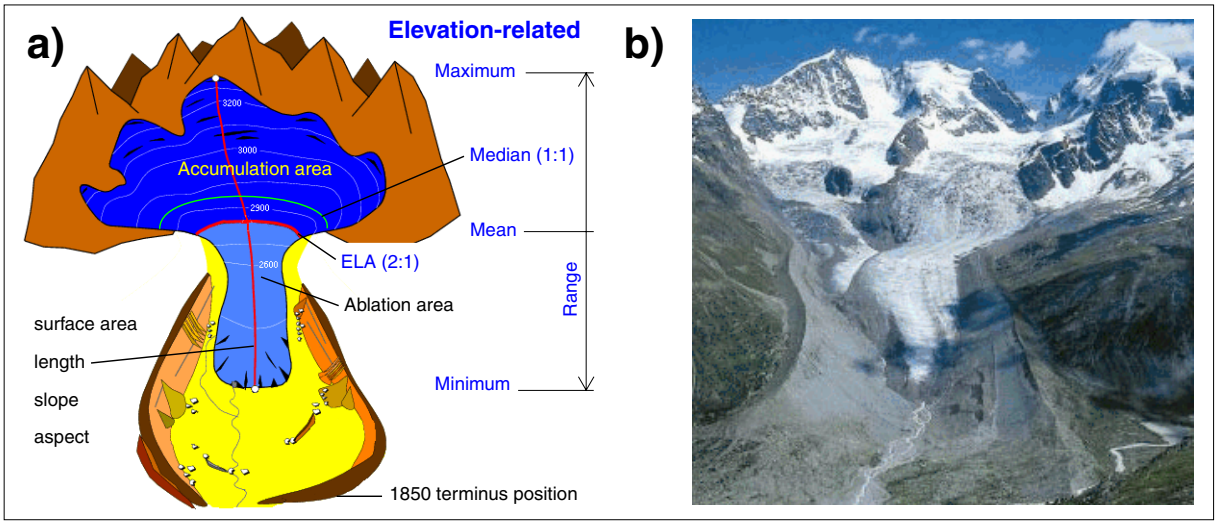

Figure 3.4: *a) Schematic overview of 3D glacier parameters (Cartoon: Max Maisch) and b) the 'Tschiervagletscher' with 'Piz Bernina' in the background for comparison (Foto: Andreas Wipf).*

3.

Digital terrain modelling

Geomorphometric analysis is used to derive further parameters from the DEM for glacier characterization. According to Burrough and McDonnell (1998) the gridded surface of a DEM is supposed to be mathematically continuous, so that it is possible to infer first- and higher-order derivatives. Slope and aspect are first order derivatives, while plan and profile curvature (or convexity) are of second order. Slope is defined by a plane tangent to the surface at any point of the DEM and its value is the maximum rate of change in altitude (from 0 to 100% or 0 to 90°), while aspect is the compass direction of this change (from 0 to 360°).

Since computation of slope with the simple 'maximum downward gradient' method is strongly susceptible to small deviations in elevation, other methods are used in commercial software packages (Bolstad and Stowe, 1994; Jones, 1998; Skidmore, 1989). The applied Arc/Info function *curvature* operates with 'second-order finite differences' for slope calculation as described by Zevenbergen and Thorne (1987). Plan and profile curvature are defined as the rate of change of slope and aspect, respectively, and are not used in the SGI 2000. See Evans (1998) for a more thorough discussion of the meaning of terrain statistical parameters.

The two parameters slope (0-90°) and aspect (0-360°) are used for glacier characterization and are calculated directly within Arc/Info in grid format (using *curvature*). The sky-view factor (0-100%) is obtained from VDVT (PCI, 1998) and defines the portion of sky (hemisphere) that is visible from each pixel of the DEM. It is also used for atmospheric correction (calculation of diffuse radiation) and calculated according to the local horizon algorithm by Dozier and Frew (1990). Four time independent 3D DEM parameters are displayed in Fig. 3.5 for the Weissmies test area (cf. Fig. 4.5, 'D'). In Fig. 3.5a grey shades from black to white denote slope from high to low values. The aspect values in Fig. 3.5b are coded by eight grey levels, representing eight aspect sectors. Curvature (plan and profile together) is visualized in Fig. 3.5c, while sky-view factor is depicted in Fig. 3.5d with values from 0% (black) to 100% (white). The artefacts clearly indicate that the level 1 DEM25 has been used for these images.

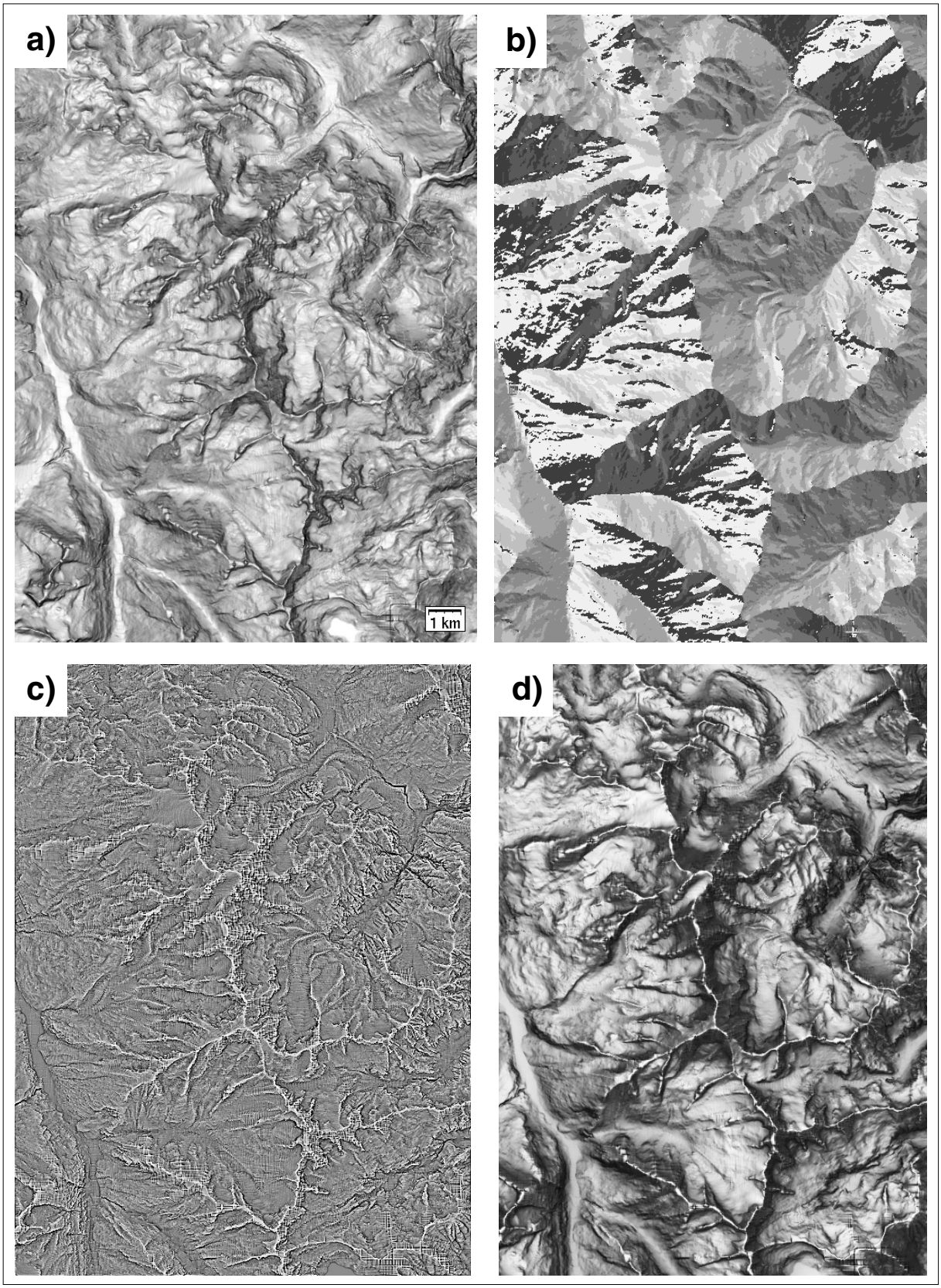

Figure 3.5: *Illustration of time-independent products from the level 1 DEM25 for the Weissmies test region (cf. Fig. 4.5 'A'). a) Slope, b) aspect, c) curvature and d) sky-view factor. All images are scaled to the range of 256 grey levels. DEM25 © swisstopo.*

Apart from the time-independent parameters slope, aspect and sky-view factor, also time-dependent (mostly radiation-related) parameters can be calculated from a DEM (e.g., Dubayah, 1992; Kumar et al., 1997), for example, direct potential short-wave radiation (psr) and cast shadow maps. Because their value depends on sun position, they vary with the time of a day and the day of the year. In order to use them as a glacier specific index, averages are computed for each parameter. The psr is calculated from SRAD-code (see Wilson and Gallant, 2000) as the mean for the summer months June to September (Gruber, 2002) and shown in Fig. 3.6a for the Weissmies test region. Cast shadow is calculated for the 21st August at one-hour intervals starting at 9:00 and ending at 18:00 UT. The ten derived maps are converted to grid format, multiplied by 10 and added within Arc/Info (colour-coded in Fig. 3.6b). Hence, regions located in cast shadow for all time slices receive a value of 100%.

Atmospheric and terrain correction

For the calculation of spectral reflection from each pixel, satellite imagery has to be corrected for atmospheric (height dependent scattering and absorption) and topographic (shadowing, direction of illumination) influences (see 4.3). The latter includes computation of illumination and cast shadow maps at the time of satellite overpass (to account for direct radiation) as well as sky-view and terrain-view factors (to account for diffuse radiation). The calculations are performed with the level 1 DEM25 and its artefacts. Improvements from the DEM25L2 are likely, but have not been investigated yet.

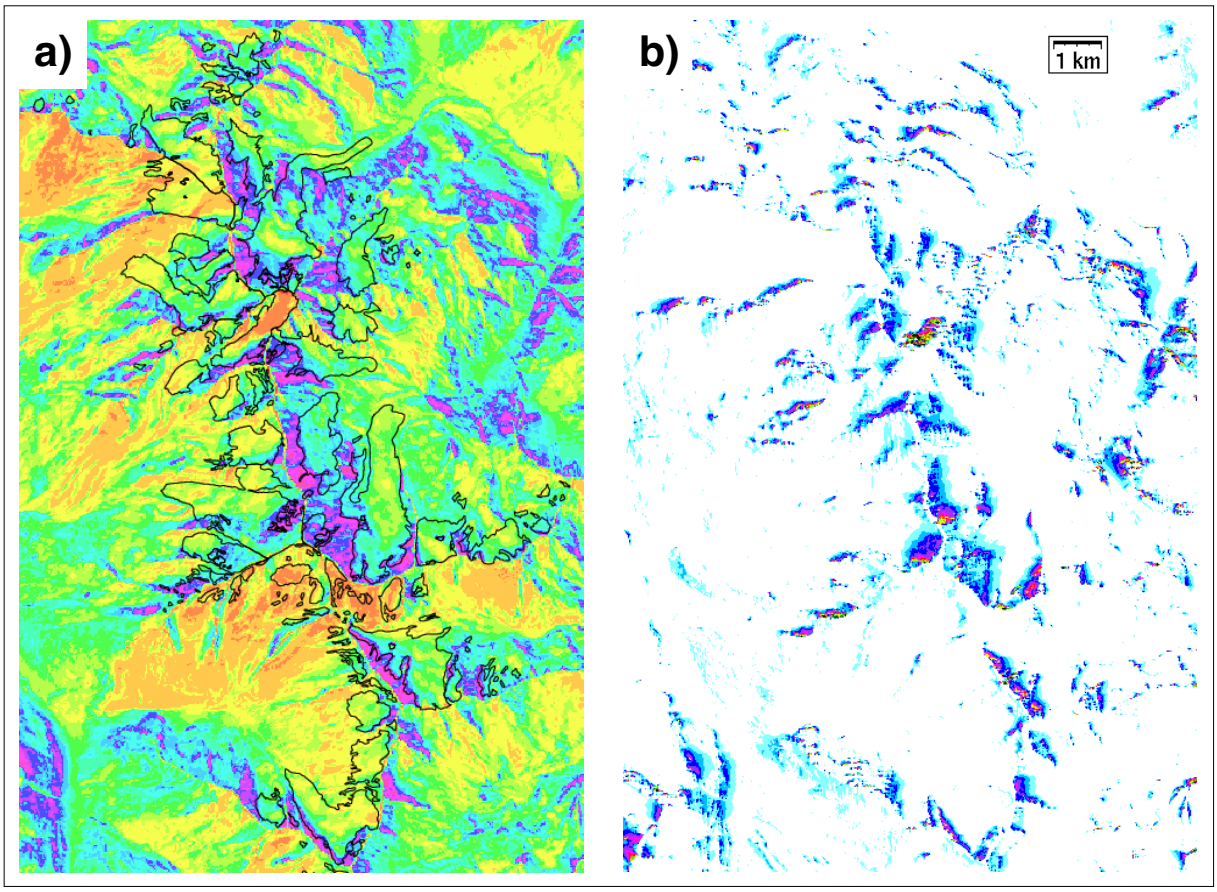

Figure 3.6: *Radiation-related parameters from DEM analysis for the Weissmies test region (cf. Fig. 4.5 'A'). a) Mean of potential solar radiation (psr) for the months June to September (from orange = highest to pink = lowest values). b) Digitally combined binary maps of cast shadow (10 slices) for the 21st of August. DEM25 © swisstopo.*

3D Visualization

The DEM is also used for visualization purposes. Especially oblique perspective views have the ability to exhibit the very steep topography around glaciers and can be used together with glacier outlines from distinct years to visualize glacier retreat as well. In combination with natural colour high-resolution satellite imagery, such maps satisfy a basic demand of the glaciological community (Haeberling, 1998; Hurni et al., 2000) and were already used for illustration of glacier change (Haeberli et al., 2002a and b). In Fig. 3.7 the Belvedereglacier below the Monta Rosa east face (Anzasca valley, Italy) is shown for example. Some more examples from the SGI 2000 are given in Fig. 7.1 and App. 3.3. In addition stereo images can be created from the DEM by calculation of two images with a small change in the observer's position. Combination to anaglyph pictures enables realistic 3D viewing with special glasses (KfG, 2002).

Furthermore, each other DEM product or modelling result can be draped over a DEM in order to show topography-influenced parameters more clearly (e.g., Copland, 1998; Etzelmüller et al., 2001). However, the viewing position and angles must be selected carefully, as the terrain may hide relevant features or a large scale view does not allow visualization of small-scale details. The overlay of various GIS layers (vector, raster, image) in the SGI 2000 is accomplished within the Arc/Info module *arcplot* using *surfacedrape* (see 6.1.2). If digitized contour lines from older glacier maps are available and proper geocoding is possible, DEMs can be obtained from the contour lines and 3D animations of glacier retreat can be computed by the use of specialized software (Kaufmann and Plösch, 2000).

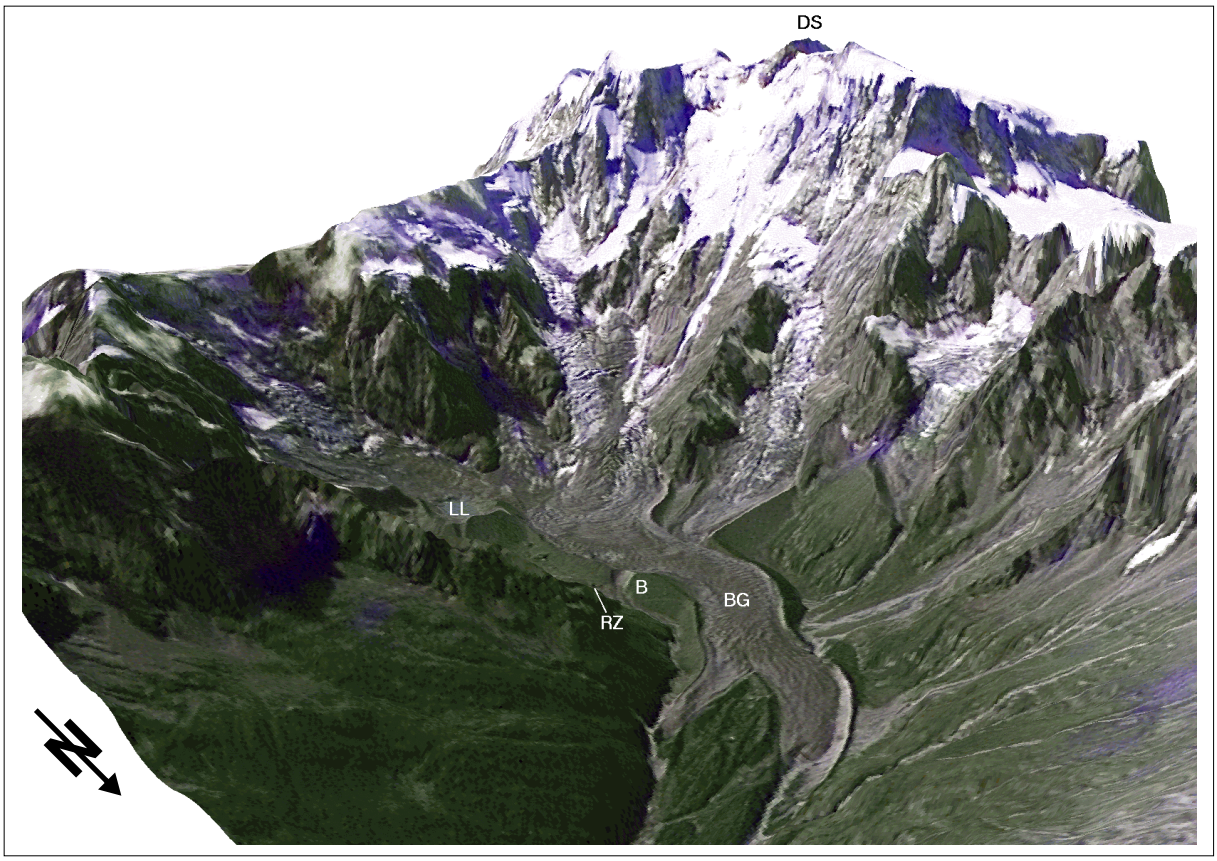

Figure 3.7: *Oblique perspective view of Monte Rosa east face above Belvedereglacier (BG). The debris-covered tongue is about 3 km long. The view is created from a fused IRS-1C / TM image acquired at 20 Sep 1997 / 31 Aug 1998 and draped over the DEM25L2. Additional abbreviations: DS=Dufourspitze (4634 m a.s.l.), LL=Lago Locce, RZ=Refugio Zamboni, B=Breach. DEM25 © swisstopo.*

4. REMOTE SENSING

4.1. Satellites and Sensors

4.1.1. Overview

The sensors used in the SGI 2000 are placed on board the satellites Landsat 5 and 7, SPOT 2 (Système Pour l'Observation de la Terre), IRS-1C (Indian Remote sensing Satellite), Terra and Ikonos. All these satellites revolve around the earth from north to south (at daytime) on a near-polar orbit with the earth rotating from west to east beneath them (Fig. 4.1a). This ensures acquisition of another swath (the area on earth covered by the sensor) during the next orbit. Their orbits are sun-synchronous, resulting in image acquisition at nearly the same local time for each area of the world. A summary of orbit characteristics (apart from Ikonos) is given in Table 4.1. For more technical details of satellites and sensors see Kramer (2002).

Satellite	**Landsat 5**	**Landsat 7**	**SPOT 2**	**IRS-1C**	**Terra**
Sensors	TM	ETM+	HRV (Pan)	LISS-III (Pan)	ASTER
Launch Date	1.3. 1985	15.4. 1999	22.1. 1990	28.12. 1996	18.12.1999
Earth distance [km]	705	705	830	817	705
Revisiting period [days]	16	16	26 (5)	24 (5)	16
Equator crossing [UT]	9.30	10:00	10.31	10:30	10:30
Image size [km × km]	185 × 170	185 × 170	60× 60	141×141 (70×70)	60 × 60
Spatial resolution [m]	30, 120 (T)	30 (15), 60 (T)	20 (10)	23.6 (5.8)	15 (V), 30 (M), 90 (T)

Table 4.1: *Some characteristics of the satellites used (V=visible, M=middle infrared, T=Thermal infrared). Values in brackets are valid for the Pan band. Taken from NASA (2002) and Kramer (2002).*

The sensors Thematic Mapper (TM) and Enhanced Thematic Mapper plus (ETM+) on board Landsat 5 and 7, respectively, are opto-mechanical multi-spectral scanners, which scan the surface line by line with an oscillating mirror perpendicular to the flight direction (across-track scanning). Each line represents a 185 km long and 480 m wide sweep (using 16 detector rows) on the surface (Fig. 4.1b). The incoming reflected or emitted radiation passes a telescope and is separated into seven spectral bands with 30 m (reflective bands 1-5 and 7) and 120 m (thermal band 6) spatial resolution (see Table 4.2). The received electromagnetic energy is converted into 256 discrete levels (digital numbers or DN). The ETM+ has an additional panchromatic band (Pan) with 15 m spatial resolution and the thermal bands has 60 m resolution and operates at two different sensitivities. The thermal band registers emitted radiation and is thus able to collect data from the night-side of the earth during the ascending part of the orbit. In contrast to SPOT or Terra, Landsat is not able to look at any position other than directly

downward (nadir-viewing), so the revisiting period (when the satellite reaches the same path) is fixed at 16 days (the orbit cycle period). Getting nearer to the pole, the overlap of adjacent orbit paths increases and the same point is acquired more often. Landsat 5 is still in operation and is flying in formation with Landsat 7 (8 days ahead). Furthermore, both Landsat satellites acquire data about the land surface all the time (as cloud cover permits), whereas SPOT, IRS-1C and Terras sensor ASTER (Advanced Spaceborne Thermal Emission and reflection Radiometer) do so only upon user request. The performance of ETM+ is improved compared to TM in terms of radiometric calibration, sensor response range (saturation), and band-to-band registration (NASA, 2002). From the multi-instrument platform Terra only its sensor ASTER is used. Terra uses also the Landsat orbit (30 minutes behind) and each scene is 60 by 60 km (same as for SPOT), which is about 1/9 of a TM full scene.

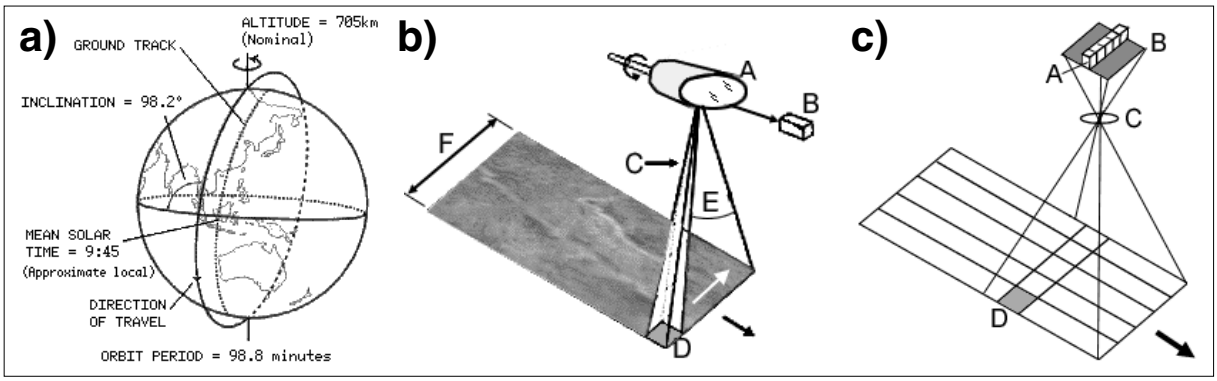

Figure 4.1: *a) Near-polar orbit of Landsat, b) working principle of across-track scanners (Landsat TM) and c) along-track scanners (SPOT HRV, IRS-1C). Taken from CCRS, 2002.*

Opposite to TM (or ETM+) the two sensors of SPOT and IRS-1C are opto-electronical multi-spectral scanners, which scan the earth's surface during satellite motion (along-track) with a complete array of detectors arranged in a line (Fig. 4.1c). This allows for smaller detectors (higher ground resolution) due to a longer measuring period for each detector and a pointing capability of the sensor with a steerable mirror (±27°). The latter leads also to a shortening of the revisiting period and allows the acquisition of stereo images. Both satellites operate with a multi-spectral mode (XS and LISS-III) with 20 and 23.5 m spatial resolution, and a pan mode with 10 and 5.8 m spatial resolution, respectively (Table 4.1). On SPOT 4 the multi-spectral sensor was renamed to XI and equipped with an additional MIR band.

TM Band	Landsat 5 TM	Landsat 7 ETM+	SPOT 1-3	SPOT 4	IRS-1C	ASTER	Ikonos
1 (blue)	0.45-0.52	0.45-0.515	-	-	-	-	0.45-0.52
2 (green)	0.52-0.60	0.53-0.61	0.50-0.59	0.50-0.59	0.52-0.59	0.52-0.60	0.52-0.60
3 (red)	0.63-0.69	0.63-0.69	0.61-0.68	0.61-0.68	0.62-0.68	0.63-0.69	0.63-0.69
4 (NIR)	0.76-0.90	0.75-0.90	0.79-0.89	0.79-0.89	0.77-0.86	0.76-0.86	0.76-0.90
5 (MIR)	1.55-1.75	1.55-1.75	-	1.55-1.75	1.55-1.70	1.60-1.70	-
7 (MIR)	2.08-2.35	2.09-2.35	-	-	-	2.15-2.43[1]	-
Pan	-	0.52-0.90	0.51-0.79	0.51-0.79	0.50-0.75	-	0.45-0.90

Table 4.2: *Spectral bandwidths of reflective bands from the different sensors in μm.* [1]*= summary of 5 individual bands. The IRS-1C MIR-band has 70 m spatial resolution. Data taken from Kramer (2002), NASA (2002), Spaceimaging (2002) and Spotimage (2002).*

The fixed revisiting period from Landsat causes a simple path and row pattern (Fig. 4.2a). For full coverage of the entire area of Switzerland eight Landsat scenes are needed (path 193 - 196, row 27 - 28). In order to cover all Swiss glaciers, only two scenes are required, as it is possible to order scenes which are shifted within the path. The 30% overlap between adjacent scenes extends the chance for a cloud-free scene of a specified region from the end of the ablation period (e.g., path 193 for the eastern part of Switzerland). The pointing capability of SPOT enables a free path and row pattern, however a nominal grid exists (Fig. 4.2b) to obtain scenes from the distributor SPOT Image. See Table 4.3 and Fig. 4.5 for a summary of scenes used.

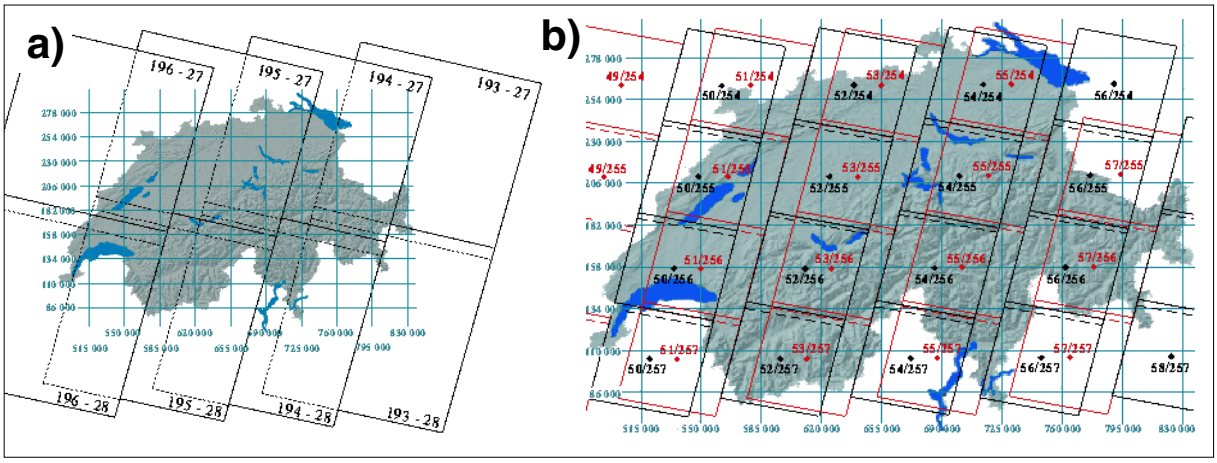

Figure 4.2: *Path and row pattern over Switzerland for a) Landsat and b) SPOT (NPOC, 2002).*

4.

Resolution

In remote sensing the term resolution can be used to describe: (1) spatial, (2) spectral, and (3) radiometric resolution (Darvishsefat, 1995):

(1) There are various definitions of spatial resolution (Joseph, 2000), as it is possible to distinguish a more technical term from a more user-defined term. In the first case, spatial resolution is the area on the ground over which the sensor integrates electromagnetic radiation and is equivalent to pixel size. In the second case, spatial resolution refers to the smallest identifiable object. In the latter case, resolution is highly variable and can be much smaller than the nominal pixel size, depending on image contrast. In Fig. 4.3 a comparison of three different spatial resolutions is shown, which are simulated from the IRS- 1C pan sensor with 5 m pixel size (Fig. 4.3a). While there is only little decline in the visibility of spatial details compared to 15 m resolution (Fig. 4.3b), the separation of details decreases notably at 30 m resolution (Fig. 4.3c).

(2) Spectral resolution is often referred to as the number of spectral channels. The original definition uses the bandwidth of each spectral channel (Simonett, 1983). While the possibility of spectral discrimination of certain objects increases with decreasing bandwidth, the signal to noise ratio decreases. The spectral range covered from each respective band of each sensor mentioned in Table 4.2 are very similar. The sensitivity of the Pan band from ETM+ is extended to the near infrared compared to SPOT and IRS-1C, resulting in higher grey levels upon vegetated terrain (stronger reflection from chlorophyll) and lower grey levels over water (stronger absorption).

Regarding the number of spectral channels, the MIR-band TM5 is essential for glacier mapping and not available from SPOT 1-3 (HRV sensor) and Ikonos (cf. Table 4.2).

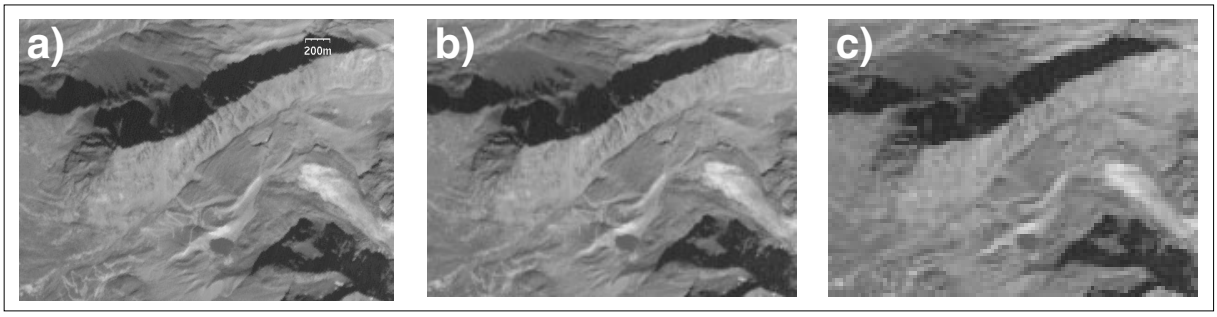

Figure 4.3: *Comparison of typical spatial resolutions for a sub-section ('Grubengletscher') of the Weissmies test region: a) 5 m, b) 15 m and c) 30 m. The coarser resolutions in b) and c) are down-sampled from a), the original IRS-1C image (cf. Fig. 4.8 for a true colour display with TM321).*

The emissive thermal band (TM6) is only available from Landsat and Terra sensors, and only Landsat (apart from Ikonos) is equipped with a blue channel (TM1). The thermal channel (especially the improved 60 m resolution from ETM+) is of interest for mapping of glaciers under thin debris cover (Taschner and Ranzi, 2002), and the blue channel from TM/ETM+ and Ikonos allows RGB composites in nearly real colours. This is advantageous for comparison of classification results by visual inspection (moraine, snow in cast shadow) and visualization of results in 3D perspective views (satellite image draped over a DEM).

(3): Radiometric resolution can be described as the number of grey levels to which the received electromagnetic radiation is converted. The higher this number is, the better the radiometric discrimination of objects will be. While Landsat and SPOT sensors (TM, ETM+, XS, pan) use an 8 bit quantization (256 grey levels), the LISS-III sensor has 128 grey levels (7 bit) and the IRS-1C pan channel (and also the former Multi-Spectral Scanner, MSS) uses 6 bit quantization (64 grey levels).

Radiation path

In summary, the path of the radiation through a sensor can be described with the sensor model from Cracknell (1998):

		Sensor specific part		
INPUT -—>	**OPTICS**	**DETECTOR**	**ELECTRONICS**	**—> OUTPUT**
radiance from surface	*spatial resolution*	*spectral resolution (number of channels)*	*quantization of signal (number of grey levels)*	*digital number (DN)*

Three comments are noteworthy: (1) the original information (radiance) about any object is altered during passage to the sensor, (2) the input radiance is also altered by atmospheric and topographic effects (described in 4.3.1) and (3) the final pixels with certain DNs have an analogy to real world objects only. In reality the latter have neither a quadratic shape, nor the exact size of a pixel (Fig. 4.4a). If they are smaller they are neither equally distributed within a pixel, nor placed in the centre of a pixel. Thus, mixed pixels with an unknown location of the object boundary within a pixel occur (Fig. 4.4b). Refer to Cracknell (1998) and Fisher (1987) for more details. However, spatial resolution of TM is appropriate for the monitoring of even small alpine glaciers (cf. 5.1.3), spectral resolution allows automatic glacier classification with TM5 (cf. 4.4.1 and 4.4.2) and radiometric resolution allows snow characterization (apart from the often-saturated band TM1).

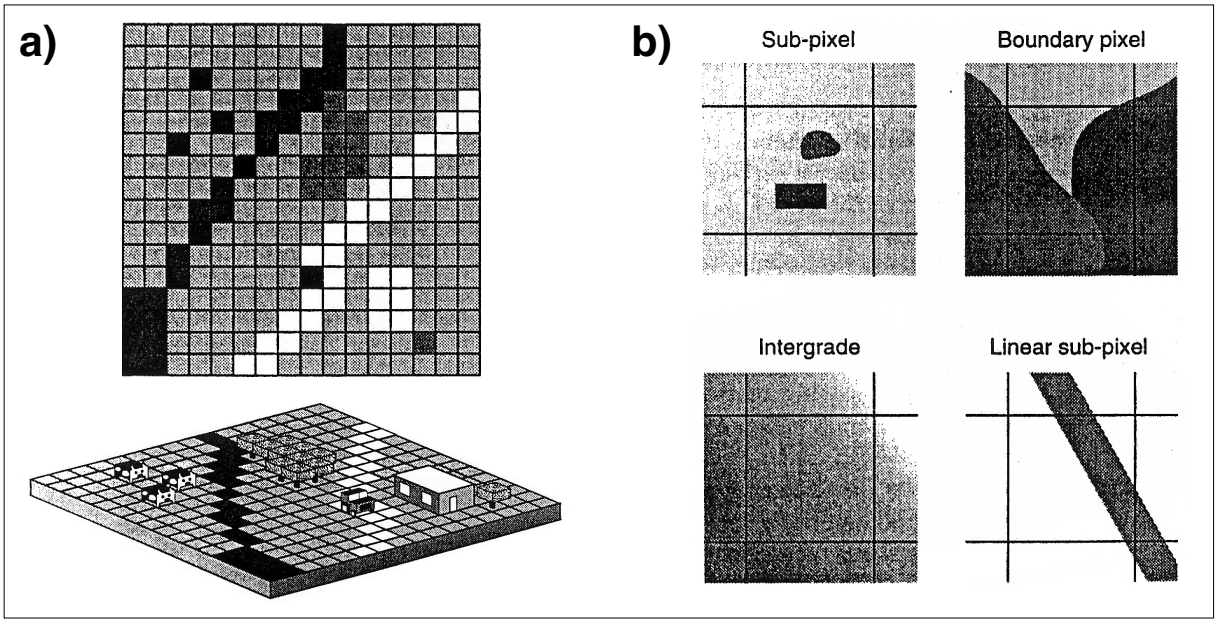

Figure 4.4: *a) Idealized objects exactly occupying whole pixels and having uniform horizontal top surfaces, b) examples of mixed pixels (after Fisher, 1997 and Cracknell, 1998).*

4.1.2. Scene selection

In the SGI 2000 glacier outlines are derived from 30 m Landsat 5 TM data and Pan bands from SPOT and IRS-1C are used for evaluation of glacier mapping accuracy as well as for visualization. The scenes obtained for the SGI 2000 are summarized in Table 4.3 together with a short description of snow and cloud conditions within each scene. In Fig. 4.5 the regions covered by each scene and sensor, as well as the location of the test regions used is indicated.

The selection of a TM scene is governed by at least three conditions: The scene has to be acquired (1) under cloud-free conditions (2) near the end of the ablation period (3) in a year without any snowfields connected to glaciers. The last point is most crucial, since location of snow cover shows high spatial and temporal variability. Because spatial variations of snow cover are hardly detectable from the small quicklooks available on-line for scene selection, weather report summaries should be used to determine possible late summer snowfall. Together with the 16-day revisiting period of Landsat 5, only a small number of scene acquisitions between 1984 and 2001 meet all three conditions.

The SGI 2000 should include new glacier outlines for the year '2000' (approx.) as well as satellite imagery from earlier years to assess possible acceleration trends in glacier retreat. With respect to the good glacier classification conditions found in previous studies for the years 1985 and 1992 in the Tyrolean Alps, Austria (Paul, 2002a and 2002b), both years were also investigated for the SGI 2000. Since autumn snow conditions at the end of the ablation period were very bad for glacier classification in 2000 and 2001, scenes from 1998 and 1999 are selected for the new '2000' glacier outlines. Hence, glacier changes from 1985 to 1992 (7-year period) and from 1992 to 1998/9 (6/7-year period) could be investigated with TM data alone, and the periods 1973 to 1985 (12 years) and 1985 to 1998/9 (13/14 years) could be compared in combination with the digitized 1973 glacier outlines. For the region between Landsat paths 193 and 195 (see Fig. 4.5) a satisfactory TM scene from 1992 (± 1 year) is not available.

Nr.	Sensor	Path-Row	Date	Description
1	TM	193-27 (+50%)	30.9. 1985	no clouds, some snow at gl. (increasing towards the west)
2	TM	193-27 (+50%)	17.9. 1992	no clouds, very little snow at gl., shifted scene from NPOC
3	ETM+	193-27 (+50%)	13.9. 1999	few clouds over glaciers (Bernina, Adamello), no snow south of Silvretta and Tyrolean Alps, too much snow to the north
4	TM	194-27 (+60%)	21.9. 1985	high clouds in the western part of the scene, some cumulus convection to the east, but not affecting glaciers, snow as in #1
5	TM	194-27 (+60%)	12.9. 1999	low clouds in the eastern part, no clouds over Bernina and Silvretta, snow conditions very bad in the northern part
6	TM	195-28	12.9. 1985	no clouds, but some snow at gl., especially to the north, scene used for algorithm comparison
7	TM	195-27 (+70%)	28.9. 1985	thin contrail over Mischabel group, some snow left at gl.
8	TM	195-27 (+70%)	15.9. 1992	cumulus to the north, but not over glaciers, sparse snow at gl.
9	TM	195-27	31.8. 1998	no snow at gl., best snow conditions for glacier mapping
10	TM	195-28	31.8. 1998	some cumulus (south east) and over 3 glaciers, snow as #9
11	SPOT Pan	55-256	17.9. 1992	no clouds, not much snow at gl.
12	SPOT Pan	55-257	17.9. 1992	no clouds, not much snow at gl.
13	IRS-1C Pan	25-36A	20.9. 1997	low clouds in the north but not affecting glaciers, increasing amount of snow at gl. to the north, but below average
14	IRS-1C Pan	25-36C	20.9. 1997	few cumulus clouds to the south-east, little snow at gl.
15	IRS-1C Pan	26-36C	25.9. 1997	few cumulus clouds in the south, little snow at gl.
16	Ikonos Pan	Trift / Rhonegl.	17.9. 2000	much snow around glaciers, but some usable for delineation

Table 4.3: *Overview of the satellite scenes used and description of image conditions. In the 'Path-Row' column (+xx%) means shifted scene, in the last column 'gl.' means 'glaciers'.*

Test regions

For comparison of glacier mapping methods and development of image processing techniques four test regions are selected. They are depicted in Fig. 4.5 by black rectangles and labelled from A to D. Most of the comparisons were performed for test region (A) Weissmies (or parts of it) covering 12.6 by 18 km on a side. In this region, elevation ranges from 1500 to 4000 m a.s.l. resulting in very steep topography, pronounced cast shadows and debris-covered glaciers: a worst-case region for glacier mapping. Test region (B) covers the area to the south of the 'Nufenenpass' and is mainly used for comparison between TM- and SPOT-derived glacier outlines. The test region 'Aletsch' (C) is chosen for development of a debris-cover mapping technique, as many glaciers in this area are heavily covered by debris. Examples of glacier change visualization are given for the Mischabel mountain range (D).

Landsat (#1-#10):

Scenes from path 193 (#1 - #3) are selected for their better snow conditions in 1985 (compared to path 194), the availability of a scene from 1992, and to assess the performance of the new Landsat ETM+ sensor for glacier mapping. Path 194 scenes (#4, #5) are used to cover the regions between path 193 and path 195. Only scene #6 from 1985 was available at first and is used for comparison of glacier mapping methods. Scenes #7 and #8 from path 195 (western part of Switzerland) experience good glacier classification conditions. Scenes #9 and #10 in particular meet superb conditions, as they were acquired near the end of the 1997/98 balance year with extremely negative mass balances (Herren et al., 2001). Larger data gaps for 1999 remain to the north of the Rivers Rhine and Inn, due to snow cover (cf. Fig. 5.14, App. 3.2-2).

SPOT (#11,#12), IRS-1C (#13-#15) and Ikonos (#16):

For comparison with Landsat TM-derived glacier outlines two SPOT Pan scenes were obtained (#11 and #12), which were acquired only two days after TM scene #8 and cover a small part of the same region. The three IRS-1C Pan scenes (#13 - #15) were acquired in September 1997 under quite good conditions. They are used to improve spatial resolution by fusion with TM scenes from 1998 (#9 and #10) and 1999 (#5), in order to illustrate glacier change. The Ikonos scene (#16) is used instead of aerial photography for manual glacier delineation at 1 m spatial resolution for five small glaciers with almost snow-free perimeters.

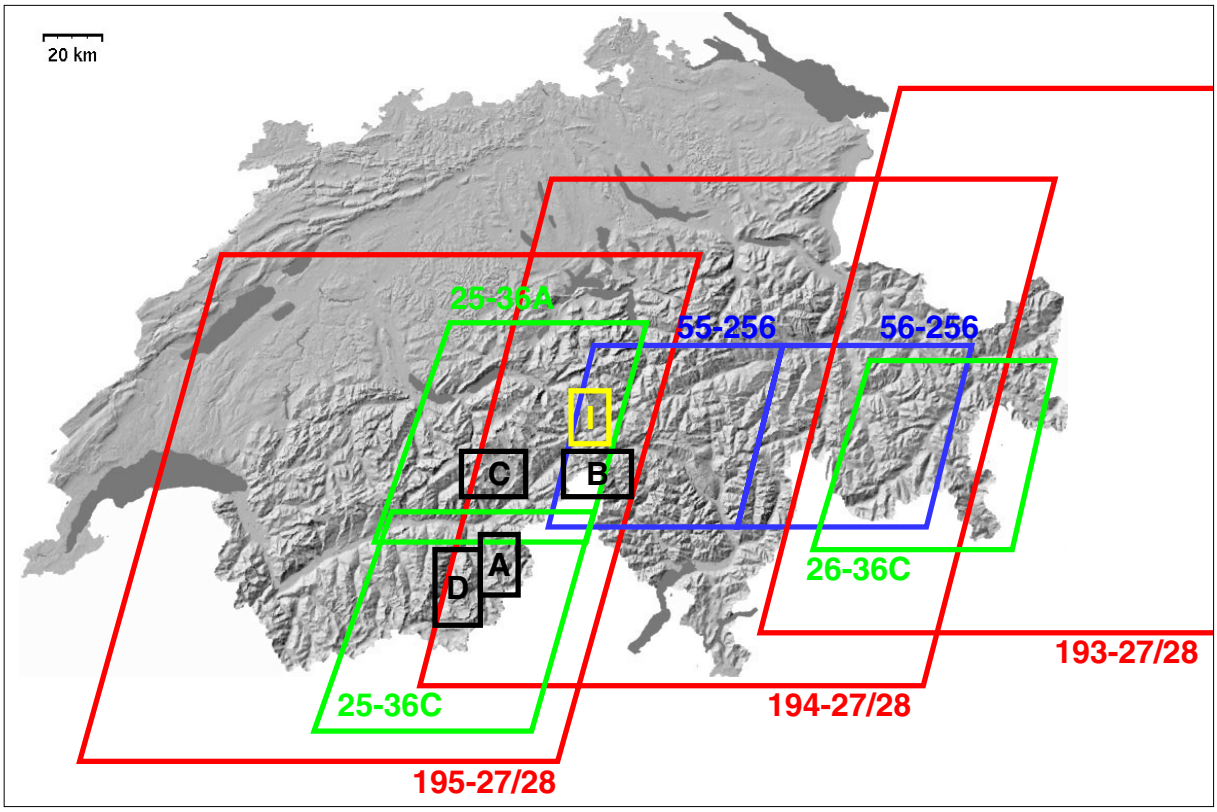

Figure 4.5: *Footprints of the satellite scenes used (red: Landsat (shifted), blue: SPOT, green: IRS-1C, yellow: Ikonos) and location of test regions: A=Weissmies, B=Nufenen, C=Aletsch and D=Mischabel.*

4.1.3. Geometric distortions of TM raw data

In the following sections, only distortions of Landsat scenes are considered, since they are mainly used for the SGI 2000. It is possible to obtain Landsat TM data from the distributor Eurimage at different levels of pre-processing. The selected 'system corrected' level 4 data includes radiometric corrections from level 2 (compensation of the different sensitivities of individual detectors) and geometric corrections from level 3, such as mirror rotation, earth rotation and - curvature, satellite elevation and - position (ESA, 1994). While the radiometric quality of Landsat data after ESA system correction is not evaluated here, some comments on the geometric quality must be given. The scenes suffer from (1) duplicated lines and (2) columns introduced by the geometric restoration algorithm used by ESA as well as from (3) an irregular column shift of 16 lines (a sweep) across all channels and (4) a shift of one column for TM bands 5 (TM5) and 7 and about 12 columns for TM6 (band-to-band misregistration).

(1): Duplicated lines are introduced by ESA to maintain the nominal pixel size of the scenes and are found in each channel at the same position through the entire width of the scene (blue lines in Fig. 4.6a). They show an irregular distance pattern and a variation of the average distance from scene to scene. For example, in one scene the values of minimum and maximum distance between duplicated lines are 30 and 33 lines, while in another scene these values are 34 and 48 lines.

For the SGI 2000 the duplicated lines were not deleted before orthorectification of the scenes (although they contain no additional information), because the main sample of ground control points (GCPs) used is collected on scenes with duplicated lines. Although some software has been written for semi-automatic correction of the resulting GCP-shift, the expected time required for correction of all scenes was not worth the effort.

(2): Duplicated columns (red lines in Fig. 4.6a) do not run across the entire scene, but are restricted to a sweep of 16 lines. With increasing distance from the nadir point their number increases also, since they are introduced for compensation of earth curvature and panoramic distortion. They can not be removed, because they are the result of more than one correction and, thus, are non-linear artefacts (Darvishsefat, 1995).

(3): The column shift of an entire sweep is notably visible along straight lines (streets, rivers). This artefact is also present in TM raw data and is not removed completely during ESA system corrections (instead of data delivered by EOSAT). Since manual correction will disturb the inner geometry of the image, this artefact cannot be eliminated (Darvishsefat, 1995).

(4): The offset of TM5 and TM7 is due to their shifted position in the sensor (cooled focal plane) and known as 'band-to-band misregistration'. It is visible in a false colour composite (FCC) with TM bands 5, 4 and 3 (TM543) as red, green and blue (RGB), respectively, around lakes with a red seam to the left and a blue-green seam to the right (Fig. 4.6b). Differences in glacier classification with TM4 and TM5 occur in the case of a correction before processing (see 5.1.3). The exact shift of the thermal band 6 is difficult to estimate as image resolution is four times lower. For most scenes the TM6 shift has been corrected before orthorectification.

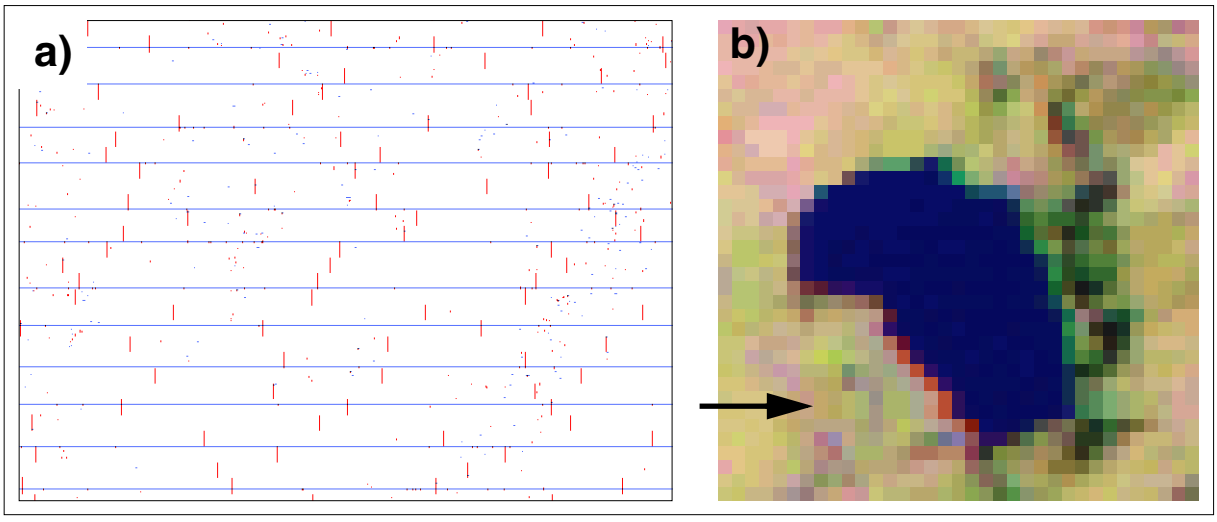

Figure 4.6: *Geometric errors in TM images after system correction from ESA. a) Duplicated lines (blue) and column segments (red) for a sub-section of 680 by 500 pixels. b) Band-to-band misregistration of TM5 compared to TM4 and TM3 produces a red seam to the left of a lake (and cyan to the right) in TM 543 composites. The arrow indicates a double line, pixel size is 30 m.*

4.2. Geometric correction

4.2.1. General remarks

For multi-sensoral and multi-temporal image fusion or overlay, as well as for all GIS-based applications, satellite imagery has to be in the same map projection. During geocoding or georeferencing the row/column coordinates are transformed to an earth-based map projection. In the high mountain environment of the Alps, terrain elevation has to be considered as well, in order to correct the panoramic distortion (Fig. 4.7a). In the case of Landsat TM, a pixel representing a point on earth with an elevation of 3000 m, located 70 km from the nadir point is shifted by 300 m from its real position. For other distances and terrain heights the shift is depicted in Fig. 4.7b. The inner geometry of the satellite images has partly been corrected during ESA pre-processing and orthorectification is used as a synonym for the combination of geocoding, correction of panoramic distortion and orthorectification.

Terrain elevations from the DEM25L2 (nested into the larger level 1 DEM25 perimeter) is used for orthorectification, as elevation differences of up to 300 m have been observed at crests (compared to the level 1 DEM25), resulting in a 30 m location shift on the ground. Geocoding is based on a set of 40 to 100 GCPs, which are collected from various sources (see 4.2.2).

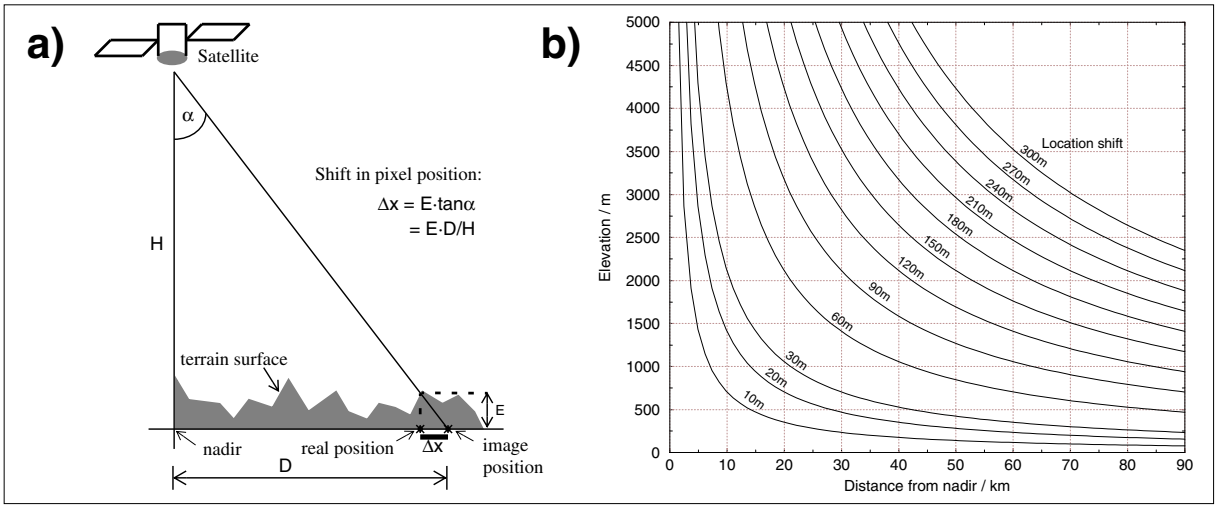

Figure 4.7: *a) Transformation of pixel row and column numbers to a geodetic map projection without considering elevation, results in a shift of pixel location (neglecting earth curvature). b) Shift of pixel location as a function of terrain elevation and nadir distance for Landsat TM.*

During the process of orthorectification, the spatial resolution of TM is resampled from 30 m to 25 m for better matching with map coordinates. The calculation of new pixel values (DNs) at positions different from the old ones is possible with different resampling methods named 'nearest neighbour' (NN), 'bilinear interpolation' (BI) and 'cubic convolution' (CC). While NN-resampling just takes the nearest pixel to fill the new location without altering the DN (Fig. 4.8a), BI uses four pixels (Fig. 4.8b) and CC 16 pixels (Fig. 4.8c) around the old position of a pixel, for calculation of the new DN (e.g., Richards, 1994; Schowengerdt, 1997). The influence of the resampling method on the derived glacier map is discussed in 5.1.3.

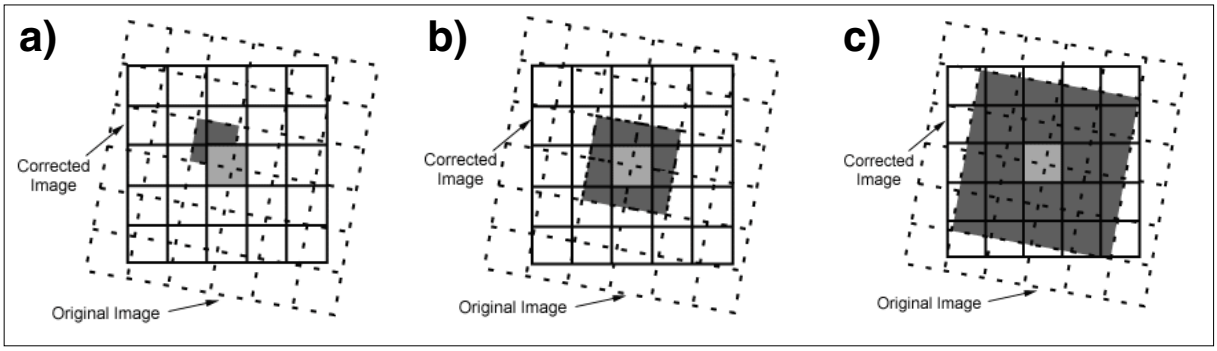

Figure 4.8: *Different resampling methods. a) nearest neighbour, b) bilinear interpolation, and c) cubic convolution (adapted from CCRS, 2002).*

The differences between the three methods and the raw data are illustrated with a TM321 image in Fig. 4.9 for a small sub-set of the Weissmies test region with the 'Grubengletscher'. The differences can be followed by the visibility of breaches (white arrow) formed by outbursts of the Gruben lake. The NN-resampling (Fig. 4.9b) does not alter the DN of the raw data and the breaches are still clearly visible. But the image appears rather 'blocky' and not very realistic. With BI (Fig. 4.9c) the DNs are changed, the image is smoothed and the breaches are barely visible. Resampling with CC (Fig. 4.9d) is a compromise with a much lesser smoothing and even the breaches are visible again, but not as good as in Fig. 4.9b. However, CC is used for resampling of all images during orthorectification.

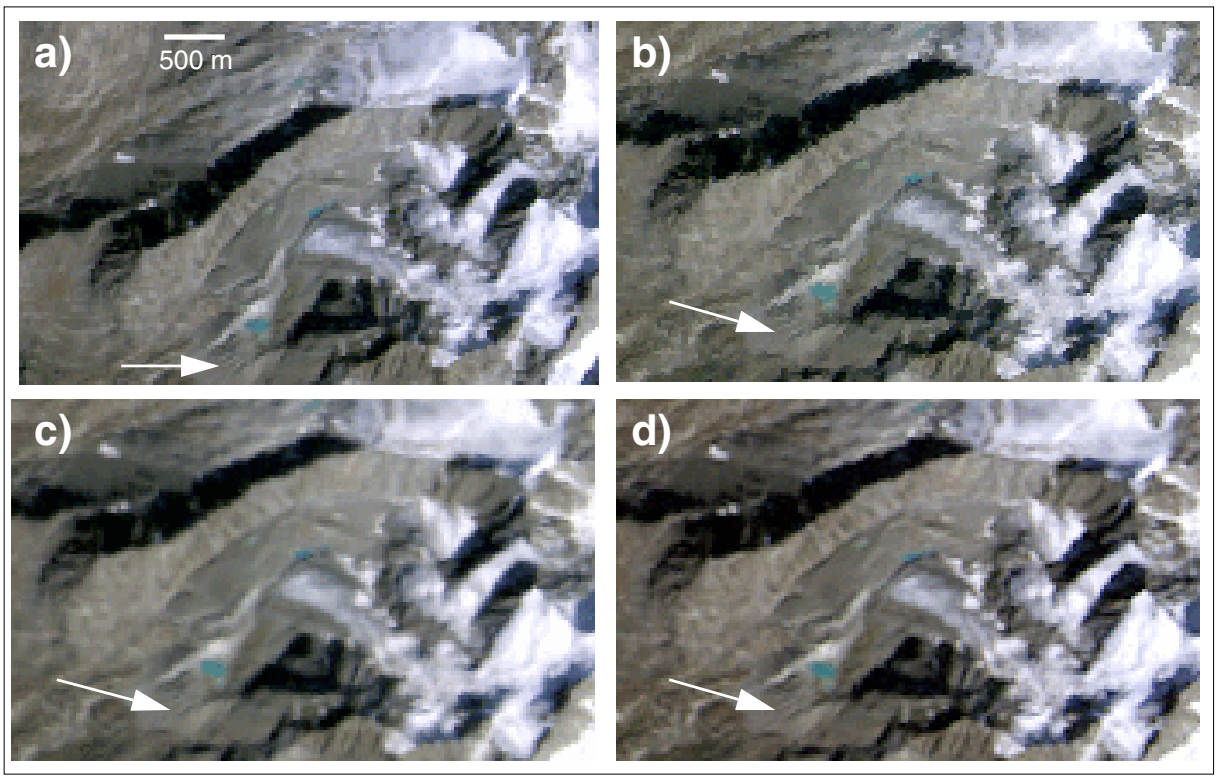

Figure 4.9: *Resampling of Landsat TM data with different methods shown for a subset (Grubenglacier) of the Weissmies test region: a) raw data (30 m resolution), b) nearest neighbour, c) bilinear interpolation, d) cubic convolution. Due to the orthorectification the view in a) slightly differs from b) to d). The arrows indicate the position of lake outburst breaches for comparison with a).*

4.2.2. Application in the SGI 2000

If the inner geometry of the image data is undisturbed, three GCPs are theoretically sufficient for an affine-transformation. However, there are many geometric artefacts in Landsat data (cf. 4.1.3), and a large number of GCPs are collected over Switzerland and neighbouring countries for geocoding. There are some selection criteria for good GCPs: They should be evenly distributed in space and elevation, they should stay unchanged for many years and also within a year (illumination), and they should be identifiable in all images (e.g., Richards, 1994). Thus, cross-streets and bridges over rivers, isolated buildings and the dams of hydroelectric power plants, road bends and tunnel gates, and also distinct mountain tops are all used as GCPs. The collection of GCPs and their correction is a very time-consuming task; nevertheless, in order to retain control over accuracy, all TM scenes are obtained without geocoding. In the case of GCP sampling from topographic maps, the work flow can be summarized as:

(1) selection of GCPs on the map with a cross-check for correspondence in the satellite image,
(2) storage in a text file (format: index, pixel x/y, map x/y, elevation),
(3) elimination of gross errors and correction of worst pixels as far as possible,
(4) selection of randomly-spaced check points for independent accuracy assessment,
(5) calculation of the transformation parameters and orthorectification of the image.

(1): The GCPs are collected from the official topographic map (scale 1:25000) with an accuracy of 1/2 mm (equivalent to 12.5 m in nature). Image-works from PCI (1998) is used for determination of the corresponding point in the satellite image at 8 to 16 times magnification (accuracy about 1/4 pixel). It should be noted that image x/y-coordinates in image-works are starting with 0/0 instead of 1/1 in gcp-works.

(2) All GCP data are entered into a text file with a text editor. The individual values are separated by a comma. While a basic GCP file remains unchanged, various excerpts were generated, since the covered area differs for the individual satellite images.

(3) With the ability to sort the GCPs for 'worst', gross errors can be eliminated rather quickly. The correction of all other GCPs (fine tuning) is rather tricky and time-consuming. Before eliminating the GCP, one should try to shift its location within the image. This is done for most GCPs with root mean square errors (RMSE) greater than about one pixel. Because of mixed pixels (Fig. 4.4) it is often quite difficult to locate a special point within - or even around a 30 m pixel. Nevertheless, this is the only way for accurate orthorectification of satellite imagery and the mean RMSE is reduced by the large number of GCPs used.

(4) With a print of the GCP number in a x/y plane (using XMGR) some GCPs are selected to act as a check point (CP). They are not considered for calculation of the transformation equations and have proven to be a more reliable and independent measure of the positional accuracy (e.g., Schowengerdt, 1997). RMSE of check points and GCPs are given in App. 1-3.

(5) The calculation of the transformation equations is carried out with SMODEL and the orthorectification itself with SORTHO from PCI.

In general it is possible to overlay TM scenes from different years by applying a constant shift to all pixels, if the regions are smaller than about 1000 by 1000 pixels (Paul, 2002a and b). Thus, it is also possible to use the same set of GCPs for scenes from different years if they have the same path and row. The relative displacement is calculated as an average of five to ten points in both images, and added to the entire set of GCPs with a short Fortran program.

Unfortunately, every GCP has to be controlled again, because for larger areas (TM full scene = 6920 by 5760 pixels), the relative displacement is not constant (due to the changing number of duplicated rows and columns). In general thenew position can be found within a two or three pixel neighbourhood of the calculated position. Some GCPs are rejected for scenes of the same path/row, as they are hidden by clouds or cannot be identified again. In general the RMSE of the GCPs and CPs are similar for each scene and in the order of a half to a full TM pixel (15 to 30 m). If the RMSE seems to be unrealistic, an inspection of the ephemerides data is appropriate. The row/column coordinates of the centre pixel in particular could be erroneous.

4.3. Atmosphere and terrain correction

4.3.1. Radiation paths in rugged terrain

The influence of atmospheric effects on spectral signatures is discussed by Kaufman (1988) and their correction for TM in Gilabert et al. (1994). Application of a DEM to correct satellite data over rugged terrain was examined by Justice et al. (1981) and Dozier and Frew (1981) and in more general terms by Proy et al. (1989). Conese et al. (1993), Itten and Meyer (1993) and Sandmeier and Itten (1997) debate case studies with comparison of classification results with and without atmospheric correction. The radiative transfer code 6S is described in Vermote et al. (1994 and 1997) and the PCI implementation of the components by Richter (1997).

Remote sensing is based on the measurement of reflected or emitted energy from long distances. For passive remote sensing sensors (such as TM), the sun is the source of the reflected radiation and the earth is the source of emitted thermal radiation (which can only be measured with the TIR channel TM6). The irradiance from the sun is strongly altered and weakened during atmospheric passage, mainly by gaseous absorption and by scattering from molecules and aerosols. Generally, absorption by aerosols is small and is treated in radiative transfer calculations as a correction factor (selection of urban -, maritime - or continental type aerosol distribution). Moreover, satellite sensor channels avoid molecular absorption bands and are located in the so-called atmospheric windows, where transmission is highest (Jia et al., 1999; Schowengerdt, 1997).

The paths of scattered photons through the atmosphere can be rather complex and are summarized in Fig. 4.10a (the following numbers refer to the figure): The target itself is illuminated directly (1) or after atmospheric scattering (2) from the sun or from adjacent terrain (3). A small part of the irradiance is scattered into space (4) without reaching the sensor, another part is scattered into the sensor without reaching the target, either coming directly from the sun (5) or from adjacent terrain (6). The strength of scattering is increasing with decreasing wavelength (e.g., Vermote et al., 1997). Considering all possible combinations and using 'Atm.' (atmosphere) as a synonym for atmospheric scattering processes, the path through the atmosphere can be summarized as:

SUN -> Atm. -> (Surface -> Atm.) -> Target -> Atm. -> SENSOR

The part in brackets can illuminate the target additionally but, with the exception of snow in rugged terrain, its contribution is rather negligible. This model can be seen as an extension to the sensor model described in 4.1.1 and as a substitution for the 'Input' part. For the SGI 2000, atmospheric correction is carried out for the Weissmies test region with the 6S radiative transfer code (see 4.3.2).

Besides the atmospheric conditions, the illumination conditions also have to be taken into account for calculation of target reflectance. They vary with the position of the sun (elevation and azimuth in degrees), which may be treated as constant for a distinct scene, and topographic conditions (e.g., slope, see top of Fig. 4.10b). In mountainous terrain also adjacency effects (additional illumination from direct and scattered radiation of adjacent slopes) have to be considered (bottom of Fig. 4.10b). A DEM of suitable spatial resolution and elevation accuracy (depending on the sensor) has to be used to consider topography and calculate local incidence angles of solar radiation on tilted surfaces (e.g., Sandmeier and Itten, 1997).

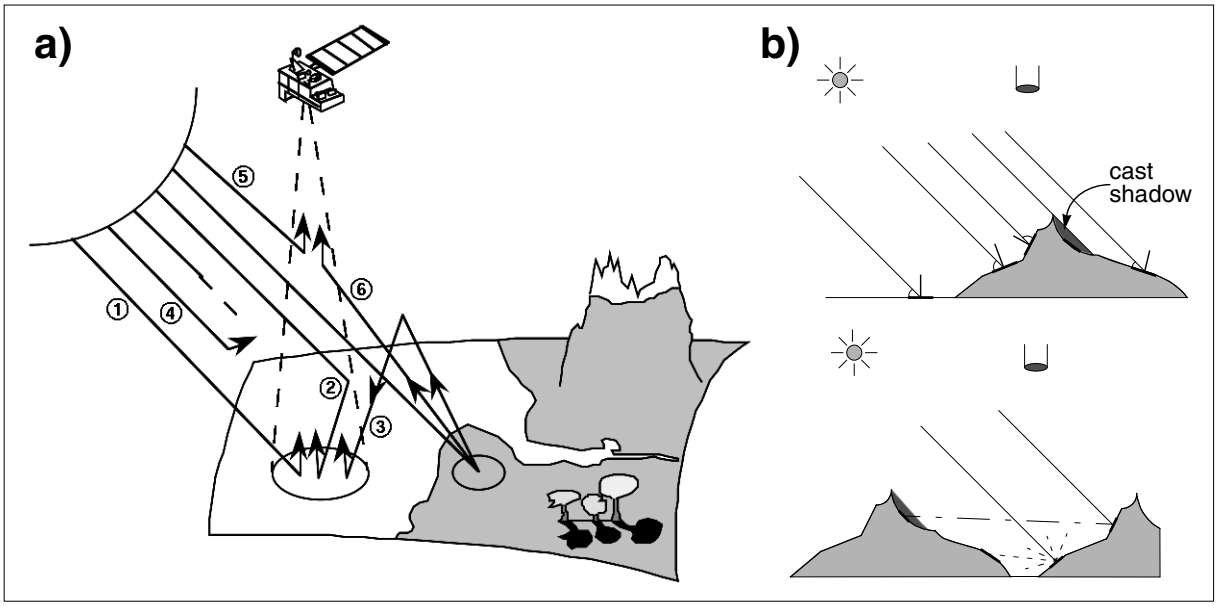

Figure 4.10: *a) Possible paths of radiation from the sun to the satellite sensor (after Vermote et al., 1994); numbers are explained in the text. b) Top: varying illumination conditions on tilted slopes, bottom: additional illumination from reflected direct and scattered radiation in mountainous terrain.*

In order to facilitate processing speed, a number of parameters are calculated from the DEM before the atmospheric correction: (1) illumination, (2) regions in cast shadow, and (3) sky view and terrain view factor. (1) The illumination is the cosine of the local incidence angel, which gives the direction to the sun with respect to the normal vector of the surface (Civco, 1989). Some illuminated regions may be placed in regions with shadow casted by the nearby terrain. (2) To avoid an over-correction here, regions in cast shadow are calculated in advance. For each pixel it is calculated, whether or not the path of the vector to the sun is obscured by the surrounding terrain. The illumination (in shades of grey) is shown in Fig. 4.11a for the time of satellite overpass (12 Sep 1985, 9:30 UT) together with the cast shadow map (black areas) in Fig. 4.11b. (3) Sky-view and terrain-view factors are needed for calculation of diffuse irradiance. The local horizon algorithm from Dozier and Frew (1990) is most often used for this calculation and also included in PCI. A grey scale representation for the test region Weissmies is shown in Fig. 3.5d.

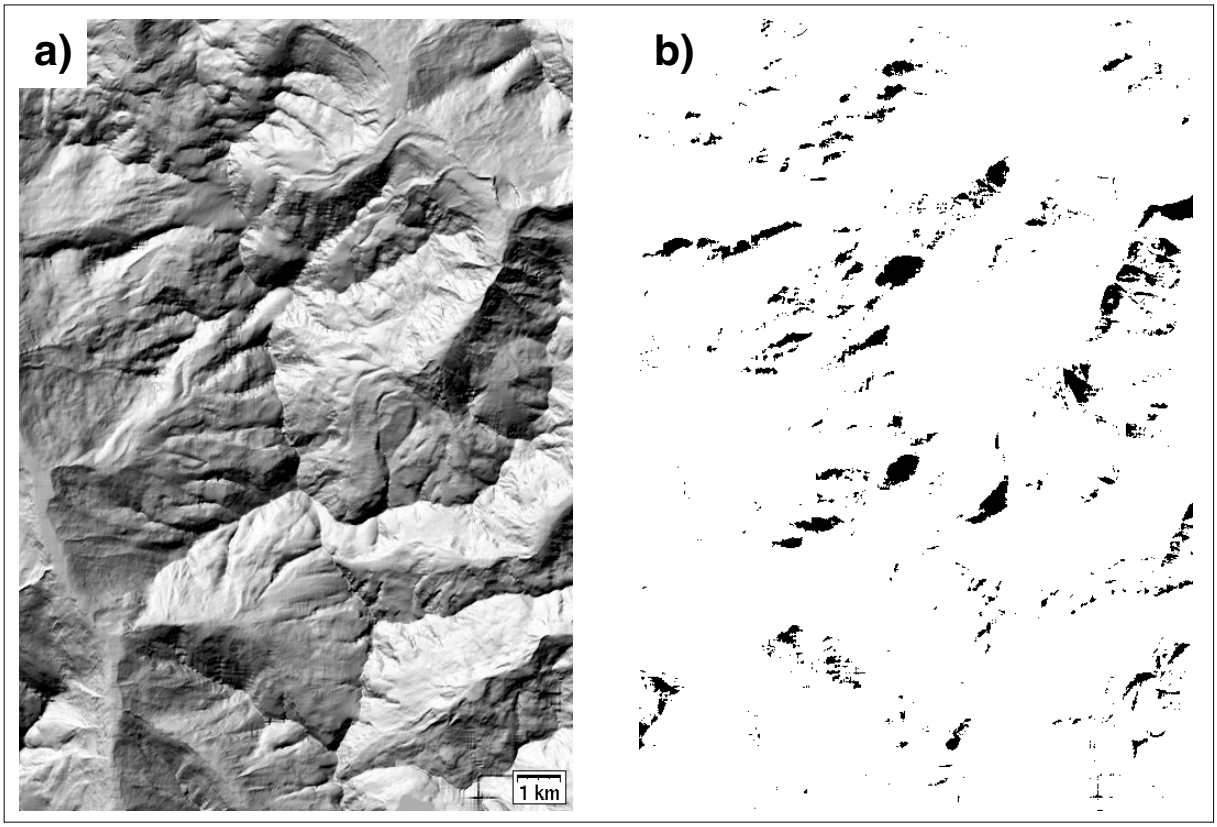

Figure 4.11: *Time-dependent DEM products as calculated for atmospheric and terrain correction of the Weissmies test region at the time of satellite overpass. a) Illumination (cosine of the local incidence angle) scaled to 256 grey levels. b) Regions located in cast shadow (black). DEM25 © swisstopo*

4.3.2. Usage in the SGI 2000

The ground reflectance of each pixel is computed within PCI using RCOR2 (a RSL implementation). This program calculates three different parts: (1) at sensor radiance, (2) altitude dependent solar irradiance for horizontal surfaces (atmospheric module), and (3) the same for tilted surfaces from a DEM (topography module).

(1): The DNs of the image are transformed into radiance at the sensor (L_λ) using the calibration coefficients gain (a_λ) and offset (b_λ) according to:

$$L_\lambda = a_\lambda + b_\lambda \cdot DN_\lambda$$

for each TM band λ. The calibration coefficients are given together with all other data for atmospheric correction in App. 1-4. The spectral radiance is needed for calculation of the unitless-effective-at-satellite planetary reflectance (R_λ) according to:

$$R_\lambda = (L_\lambda \cdot \pi \cdot d^2) \; / \; (S_\lambda \cdot \cos\theta_S)$$

with d=sun-earth distance in astronomical units, S_λ =solar exo-atmospheric spectral irradiance, and θ_S = solar zenith angle (Markham and Barker, 1986). R_λ is not computed within RCOR2, but needed for algorithm comparison and computed with MODEL (cf. App. 2.1-1).

(2): The atmospheric module uses an atmospheric catalogue file containing six different standard atmospheres and seven aerosol types for various sensors based on the atmospheric radiative transfer code 6S (Vermote et al., 1994). From this catalogue the mid-latitude summer atmosphere with continental type aerosol is used. While adjacency effects are not taken into account at this point, the horizontal visibility is used for altitude-dependent correction of optical thickness.

(3): The topography module is based on the Lambertian assumption (100% diffuse reflection) and computes direct, diffuse, and terrain irradiance for tilted surfaces. Direct irradiance (illumination) is calculated with REL2 using the cosine law of spherical geometry (e.g., Civco, 1989) and regions in cast shadow are computed by CAST. The diffuse irradiance is separated into an isotropic and a circum-solar component. The calculation of the irradiance reflected from the terrain and the isotropic diffuse sky irradiance is performed with VD (sky-view factor) and VT (terrain-view factor) using the method of Dozier and Frew (1990).

Thus, before correction with RCOR2, the following components are computed from the DEM using EASI from PCI: illumination (REL2), cast-shadow (CAST), sky-view (VD) and terrain view factor (VT). Moreover, data for satellite gain and offset, calibration coefficients and the elevation-dependent horizontal visibility (from meteorological observations at different heights) must be compiled. The latter are given in App. 1-4 and were obtained from the former SMA (Swiss Meteorological Office, now MeteoSwiss). The output is ground reflectance for each pixel with values from 0.0 to 1.0.

4.3.3. Consequences

In Fig. 4.12a the test region Weissmies is shown with TM321 after contrast stretching but without any other correction and in Fig. 4.12b after atmospheric and terrain correction using RCOR2. The terrain appears flat now and artefacts from the level 1 DEM25 used are clearly visible. Besides some under-correction in regions with cast shadow over snow, the over-corrections near the northern end of cast shadow regions caused by mountain crests are particularly conspicuous. The latter are also visible at the valley bottom in the upper right part of Fig. 4.12b, and may be the consequence of the very steep terrain to the south. Some other artefacts of the DEM are also visible in the image.

Regarding glaciers, their perimeter is barely visible in the corrected image, since illumination differences that shape the glacier tongues are strongly reduced. As a consequence, multi-spectral classification techniques of debris cover on glaciers based on reflectance values will also fail, as the only source of information (texture) is removed. Moreover, classification of glaciers based on spectral reflectance values is somewhat restricted, since artefacts from the DEM introduce a large number of new object classes. Although the artefacts are greatly reduced in the new DEM25L2, a test of glacier mapping methods based on atmospheric/terrain corrected reflectance is not carried out, as such high quality DEMs are not available worldwide.

Hence, all image processing techniques and glacier mapping methods described in the following are based on digital numbers, except where noted.

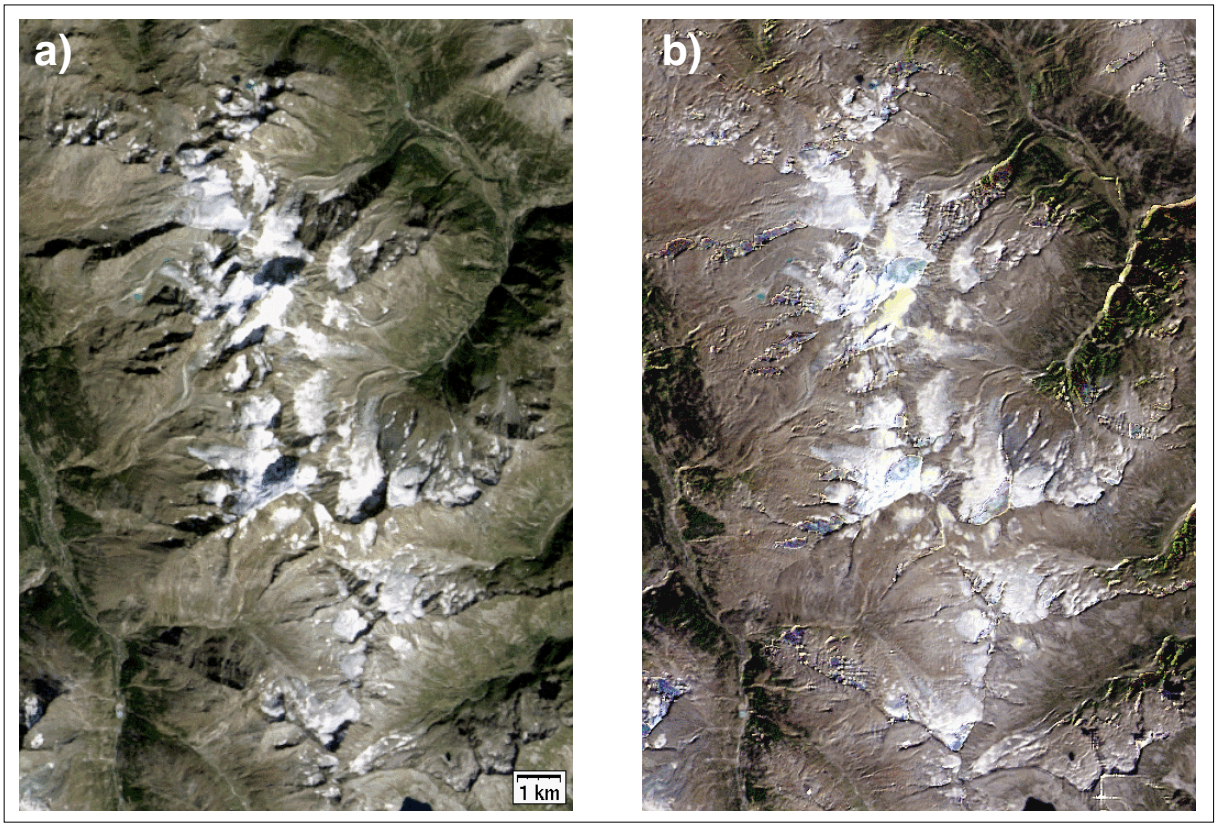

Figure 4.12: *The Weissmies test region with TM321 (contrast stretched) using raw data (a) and after atmospheric and terrain correction (b). The DEM artefacts and over-correction in shadow are visible.*

4.4. Digital image processing techniques

4.4.1. Spectral properties of ice and snow

The surface of alpine glaciers is comprised of snow and ice (i.e., metamorphosed snow), apart from regions covered by debris or water. Thus the spectral properties of glaciers are similar to those of snow (Hall and Martinec, 1985). The spectral properties of snow were studied in-situ (e.g., Grenfell et al., 1981) and modelled numerically (e.g., Dozier, 1984 and 1989; Warren, 1982). A result for three different snow grain sizes is shown in Fig. 4.13a with model results from 0.3 to 2.08 µm and measured values thereafter. The reflection of fresh snow reaches 95% in the visible part of the spectrum and resembles a Lambertian reflector closely. According to Hall et al. (1989b), the reflection in this spectral range is virtually independent of grain size, but depends strongly on contamination by soot and dust. In the near-infrared (between 0.7 and 1.5 µm), however, reflection decreases strongly with increasing wavelength and dependence of reflection from grain size increases. On the other hand, dependence of reflection on contamination decreases. Between 1.5 and 2.2 µm, the reflection of snow is very low, whereas it is high for water clouds and ice clouds. There is only minor dependence of reflection on contamination, but a strong one on grain size around 1.8 and 2.2 µm (Dozier, 1989).

Spectral reflectance curves from in-situ measurements for fresh snow, firn, glacier ice and dirty glacier ice are compiled in Fig. 4.13b. In this figure, measurements from TM for different glaciers as well as positions of TM bands 1-4 are also indicated (after Hall et al., 1989b). In terms of the spectral properties of snow (and also of glacier ice, assuming very large grain sizes) the consequences for the TM reflective bands are (cf. Orheim and Lucchitta, 1987):

TM1, TM2, TM3 (0.45-0.7 µm): Very high reflection over snow with possible detector saturation (DN=255) in TM1 and also TM2 and TM3, if the surface is tilted towards the sensor (Dozier, 1984; Gangkofner, 1989). The reflection decreases strongly, if contamination with small amounts of soot, dust or pollen occur (Warren, 1982). Also clean (debris-free) bare glacier ice is always polluted and, hence, much darker in the visible bands (no detector saturation).

TM4 (0.76-0.9 µm): The reflection over snow is lower (about 90%) and detector saturation seldom. The dependence of reflection from contamination is much lower and the dependence from snow grain size increases. Clean glacier ice has a much lower reflectance in the near infrared (about 40%), maybe due to the presence of liquid water on the surface, which strongly absorbs radiation in this part of the spectrum.

TM5 (1.55-1.75 µm): Very low reflection of snow and even lower reflection of ice with a strong dependence on grain size (cf. 4.13a). As a result, snow appears somewhat brighter than ice in TM5, due to the smaller grain sizes. TM5 and TM7 have also been used successfully for calculation of snow grain sizes (Bourdelles and Fily, 1993). In regions with snow or ice in cast shadow, considerable noise is present (DNs less than 5), which makes glacier mapping somewhat difficult in those areas. In TM7 noise is even stronger (also over glacier ice in sunlight) and, hence, this band is not used for glacier mapping.

The comparison of TM-derived glacier reflectance with in-situ measurements is discussed in 5.1.1, but should already be mentioned here (Fig. 4.13b) to show the drop in reflectance from snow to firn in TM1 to TM3 (due to impurities) and from firn to glacier ice in TM4 (due to the presence of liquid water).

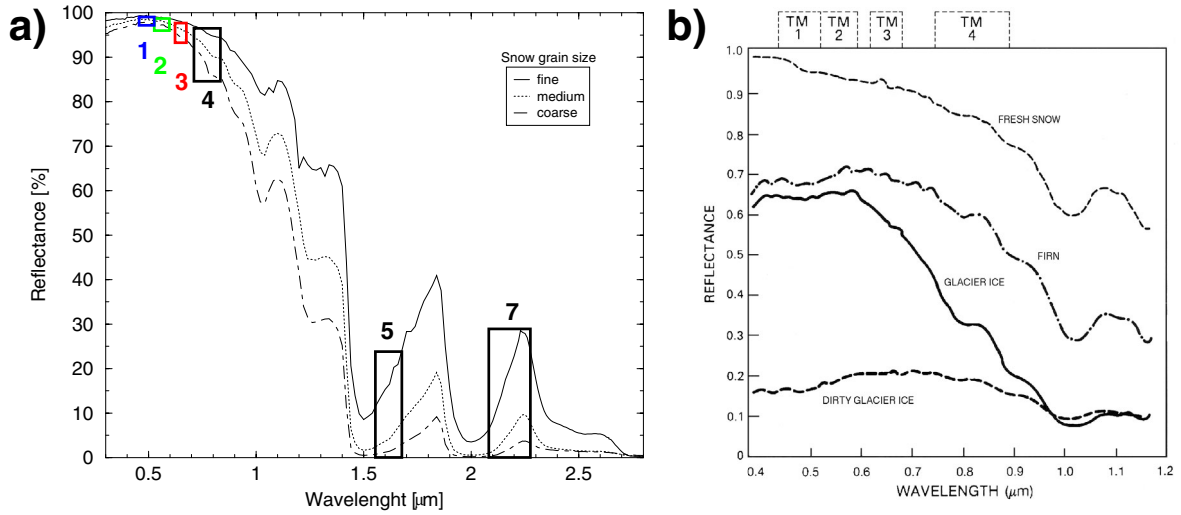

Figure 4.13: *a) Spectral properties of snow for different grain sizes from numerical models with data taken from the ASTER spectral library (JPL, 2002). Position and reflectance range for TM-spectral bands are indicated. b) Spectral reflectance curves for different glacier facies after in-situ measurements (modified from Hall et al., 1989b; based on Zeng et al., 1983).*

4.4.2. Glacier classification methods

In this section the digital image processing techniques as mentioned in previous studies about glacier classification with TM (see 5.1.1) or as used for the SGI 2000 are described. They are applied to the same test region Weissmies (or the northern part of it) to allow a comparison of results. While the methods (1) - (4) discussed below are used for creation of glacier maps, (5) is used for mapping of debris cover on glaciers or for fusion of Landsat TM with SPOT or IRS-1C pan bands (see 4.5), and method (6) is discussed for the sake of completeness only. For a more detailed description of image processing techniques refer to Jia et al. (1999), Lillesand and Kieffer (1999), Mather (1999) and Schowengerdt (1987).

(1) Ratio images

Ratio images were used to enhance the spectral properties of certain objects while reducing the bias in illumination caused by rugged terrain (e.g., Holben and Justice, 1981). Spectral separation was improved if the raw data was corrected for atmospheric scattering before ratioing (Crippen, 1988). This is possible by subtracting the lowest DN within a scene for each channel from each DN (also called dark object subtraction or DOS). Otherwise illumination differences (cast shadow areas) are strongly enhanced, especially if TM bands 1 to 3 are used. In Fig. 4.14 the creation of a glacier map from a TM4 / TM5 ratio image is presented. As discussed before, glacier ice is light grey (snow is white) in TM4 (Fig. 4.14a), while it is nearly black (snow is dark grey) in TM5 (Fig. 4.14b). Shaded areas have low reflection and appear black in both channels. Figure 4.14c gives the result of the division of TM4 by TM5 (without DOS), yielding high grey levels over ice and snow, and very low grey levels over other terrain. As a consequence of the higher reflection of turbid water in TM4 (compared to TM5), pro-glacial lakes are partly included in the glacier map after thresholding. They were deleted by another technique which is described in 4.4.2 (4).

Thresholding of the ratio image reveals Fig. 4.14d where the grey levels darker or brighter than the threshold are colour-coded. The blue and green pixels are removed (turned to white together with the other, even darker pixels), the red and yellow pixels are brighter than the threshold value and are not removed (turned to black). This thresholding is to some degree subjective, and in the course of removing pixels enclosing other terrain, some mixed pixels also disappear. However, the errors introduced by this procedure are small, because the number of terrain pixels assigned to the glacier class is nearly the same as the number of glacier pixels assigned to the terrain class (cf. 5.1.3). Because of spectral similarities with the surrounding terrain, it is not possible to include the debris-covered parts of a glacier with this technique. A semi-automatic method for debris-cover mapping is presented in 5.2.

After applying a 3 by 3 median filter to the black and white glacier mask, isolated pixels are removed (red in Fig. 4.14e) and isolated gaps are filled (blue). If glaciers are not too small (larger than 0.1 km^2), the change in glacier area remains small and a better glacier map is the result. The number of pixels added and subtracted to a single glacier by the median filter lies in a similar range (cf. 5.1.3). The delineation of the glacier perimeter is performed by a raster - vector conversion and the resulting outline is shown in white on a TM543 FCC in Fig. 4.14f.

Since this method is used for glacier mapping with TM within the SGI 2000, the algorithm is implemented in a PCI-script (using MODEL), which is given in App. 2.1-2, together with the method for debris mapping. The threshold values used for each scene are summarized in App. 1-3.

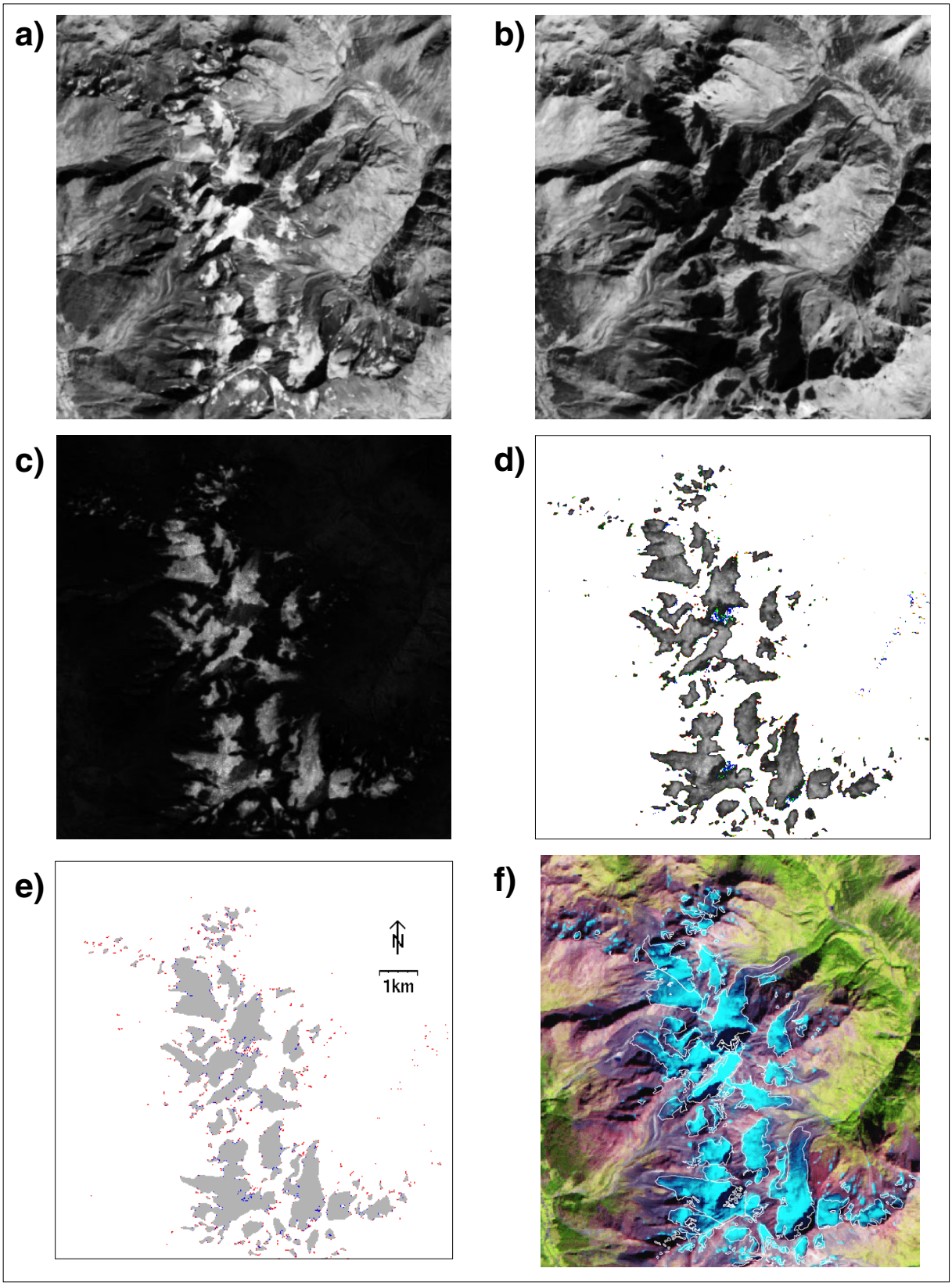

Figure 4.14: *Creation of a glacier map with segmentation of a TM4 / TM 5 ratio image illustrated for the northern part of the Weissmies test region. a) TM4, b) TM5, c) ratio image, d) different threshold values colour-coded (see text), e) deleted (red) and added (blue) pixels by median filtering, and f) overlay of digitized 1973 outlines (white) on a TM543 composite. Scale for all images is given in e).*

(2) Unsupervised classification: ISODATA clustering

Unsupervised image classification offers the advantage of little user interaction while producing comparably good results. However, results are scene-dependent and work according to trial and error. Since ISODATA clustering is used by Aniya et al. (1996) for glacier classification, the method is also investigated for the SGI 2000 and a short description of the method follows. For a more detailed discussion of the algorithm refer to the PCI help (ISOCLUS).

The ISODATA (Iterative Self Organizing DATa Analysis) method searches iteratively for centres of clusters in the n-dimensional image space (set up by the n image bands). The user has to assign the number of clusters (with an upper and lower limit), the maximum number of iterations, and a threshold below which the movement of cluster centres is neglected, so that the iteration can stop. A seed file (with the starting centres of clusters) is generated diagonally along the n-dimensional histogram.

The results for 20 and 31 classes using TM bands 1-5 within the test region 'Weissmies' are depicted in Fig. 4.15a and 4.15b, respectively. Conversion to a glacier map is carried out interactively by visual comparison with a TM543 FCC. While the conversion of most of the classes to 'glacier' or 'other' is rather easy, there are perhaps one or two classes where the decision takes a longer time. The resulting glacier boundaries appear somewhat randomly (see comparison in 5.1.2) and a different number of initial clusters will alter their shape to some degree. Thus, this method may reveal better results in other regions or with different parameters, but it is not very practical for worldwide application.

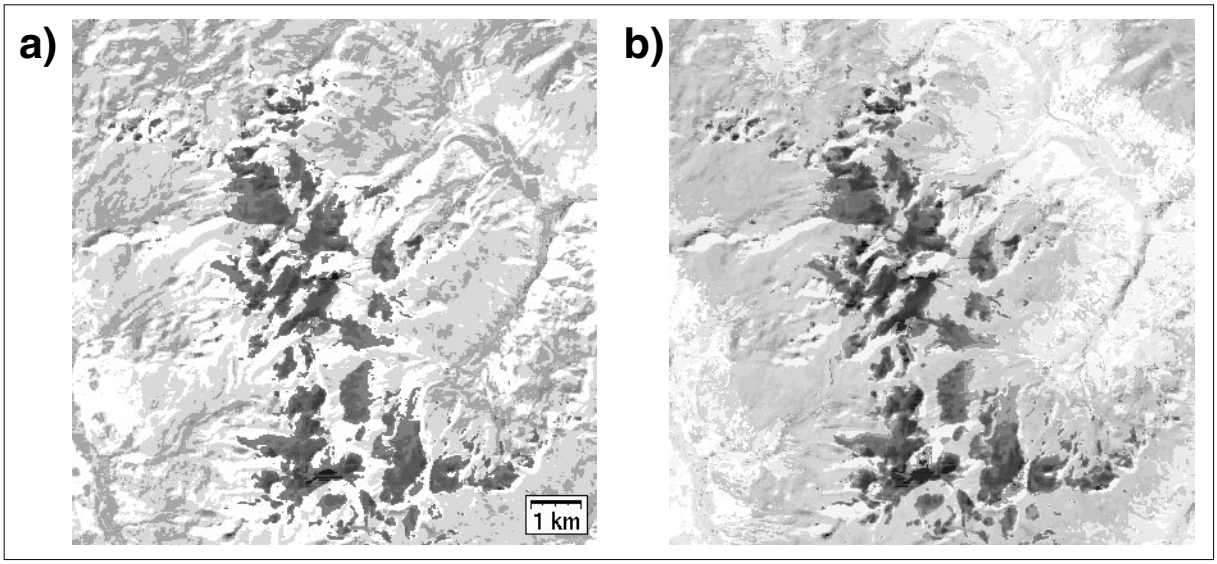

Figure 4.15: *Result of the unsupervised ISODATA clustering with a) 20 and b) 31 classes.*

The reduction of the number of colours in a FCC is also a kind of unsupervised classification. Normally a combination of three different TM bands (with 256 grey levels) will reveal a maximum of 256^3 (or about 16.78 million) colours. A reduction to 64 or 32 colours is, thus, a form of image classification. Especially the TM543 FCC have proven to be very useful for separation of (for example) snow/glaciers (light blue), bedrock without vegetation (purple), meadows (yellow) and forest (green) at first glance. Nevertheless, these colours give no clear indication of the spectral properties of distinct objects, since they are altered by topography-induced bias in illumination.

(3) Supervised classification: Maximum-Likelihood

Supervised classification is a two-step process: selection of probable training areas and classification of the data. The training areas provide class signatures for the classifier and should have a Gaussian distribution; careful selection is necessary, as they should include all visible objects and their spectral variation. Moreover, sample sizes should be large enough (Richards, 1994; Schowengerdt, 1997).

In Fig. 4.16a the location and area covered by the training areas used is depicted, while Fig. 4.16b shows the result of a Maximum-Likelihood classification (MLC) from these training areas. The nine classes used are: ice, ice at steep slopes, snow in sunlight, snow in shadow, terrain, cast shadow, forest, meadow and water. The classes 'water', 'frame' and 'zero' are not shown, but are listed together with all other classes in the confusion matrix of the classification (App. 1-5). The internal overall accuracy reaches 95.7%, and the confusion matrix reveals that misclassifications occur mainly between the forest and shadow class as well as between ice at steep slopes and ice or snow. But the latter has no consequences for the resulting glacier map, which is generated from both ice and snow classes. In the end the method is not applied, as expert knowledge is required and the spectral signatures are changing with the scene used.

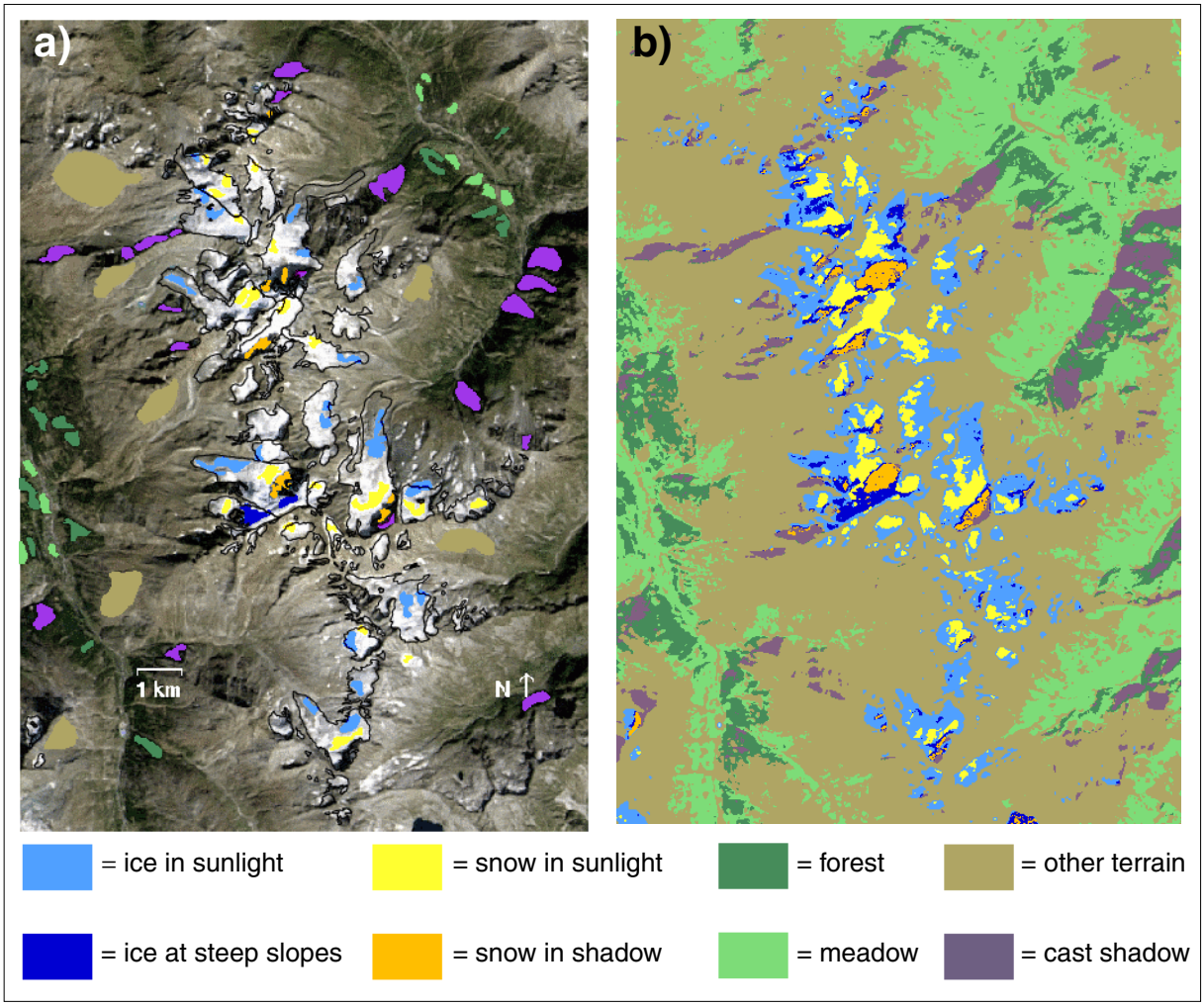

Figure 4.16: *Maximum-Likelihood classification for the Weissmies test region. a) Location and size of training areas used, b) result of the MLC. The glacier map is created from the two ice and snow classes.*

(4) Normalized Difference Indices: NDVI, NDSI and NDWI

The detection of snow and ice with Landsat TM can also be achieved by enhancing differences in spectral reflectance. While snow and ice have very low reflectance in the middle infrared, the reflection is very high in the visible part of the spectrum (see 4.4.1). Thus, the maximum reflectance difference can be used for a normalized difference index with TM2 and TM5, analogue to the Normalized Difference Vegetation Index (NDVI). The latter is widely used for vegetation monitoring from satellite data (e.g., Hardy and Burgan, 1999) and is calculated as (TM4-TM3)/(TM4+TM3).

The Normalized Difference Snow Index (NDSI) is used by Hall et al. (1995b) for snow mapping or Sidjak and Wheate (1999) for glacier mapping and calculated as (TM2-TM5)/(TM2+TM5). In Fig. 4.17a a grey scale representation of the NDSI is displayed, showing the great contrast between ice and snow (nearly white) and other terrain (grey to black). Data adjustments (removal of scattering by DOS) have been applied to TM2 before the calculation. A glacier map is obtained from thresholding of this image (see Fig. 5.1d).

As already mentioned (see 4.4.2 (1)), turbid lakes are classified in large parts as glacier ice with the TM4 / TM5 method. Thus, they are problematic in glacier mapping with this method, because they are often in direct contact with glacier ice. Huggel (1998) developed a method for detecting lakes from Landsat spectral bands using a Normalized Difference Water Index (NDWI), similar to the NDSI or NDVI. While water strongly absorbs radiation in the near- and middle infrared part of the spectrum, it is much more reflective in the visible part, especially in the case of turbid lakes. Most other surface types (such as vegetation or soil) have higher (or equal) reflection in the near infrared than in the visible part (Pietroniro and Leconte, 2000). Hence, the NDWI is calculated as (TM1-TM4)/(TM1+TM4), with lakes having typical values > 0.45. TM5 or TM7 could be used instead of TM4, but the NDWI with TM4 has proven to be more capable of discerning water from ice and snow, which is the reason for its application here (Huggel et al., 2002).

By subtracting the darkest grey level from TM1 (normally about 30 DN) before calculation of the NDWI, most of the turbid lakes (sediment from glacial erosion) can be classified by a simple segmentation of the NDWI image. In Fig. 4.17b a grey scale representation is shown, ranging from NDWI=-1 (white) to NDWI=+1 (black). Lakes appear as small white spots and regions in cast shadow have clearly lower grey values. Without applying DOS to TM1, also some of the clear lakes (within the glacier map from TM4 / TM5) can be classified from the NDWI, using a different threshold. Other techniques (e.g., using a DEM and slope values less than 1°) can be applied to classify remaining lakes. Although this is not necessary for the SGI 2000 (vectorized glacier basins are also used for separation of wrong classification), detection of lakes without DEM information has strong advantages in regions with potentially hazardous (pro-)glacial lakes and poor DEM information (Huggel et al., 2002; Kääb et al., 2000a and b). The NDWI and the classified lake map is shown for a larger region (southwestern part of Switzerland) in App. 3.2-5.

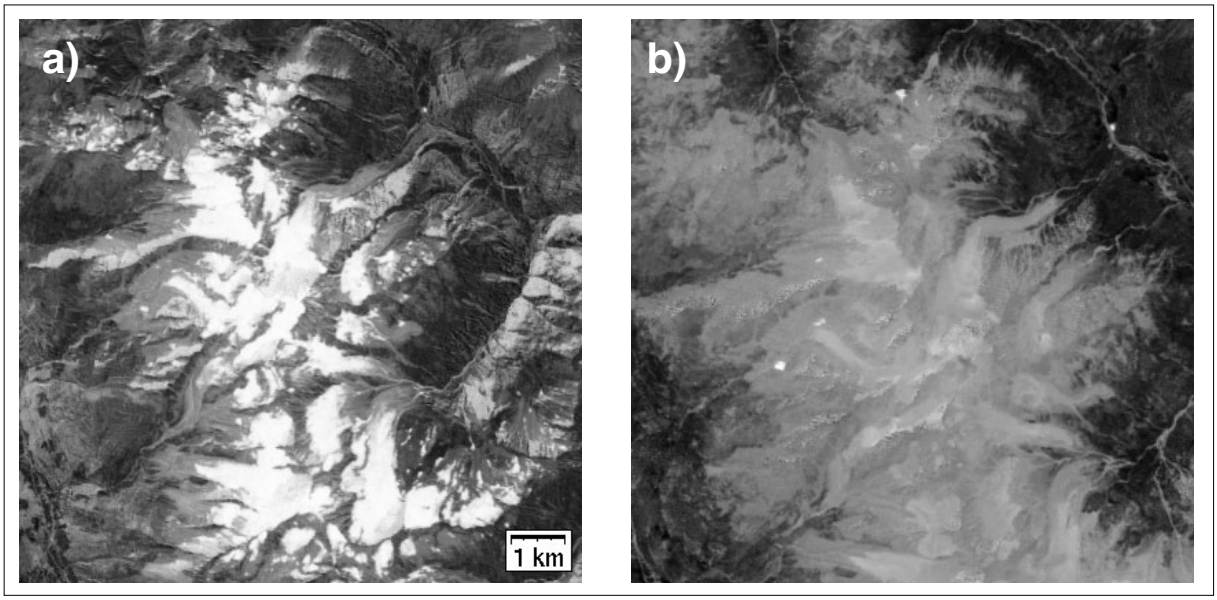

Figure 4.17: *Grey scale representation of the NDSI (a) and the NDWI (b).*

(5) The IHS colour-space transformation

The Intensity-Hue-Saturation (I-H-S) colour-space transformation separates the spatial (I) from the spectral (H, S) information in an RGB image (e.g., Pohl and van Genderen, 1998). The replacement of the I-component by an image band with higher spatial resolution before back transformation to RGB colour-space is widely used for image fusion (e.g., Carper et al., 1990). Image fusion itself is discussed in more detail in paragraph 4.5.1. Another application is colour enhancement of highly correlated image bands, using a contrast stretched H-component for back transformation (Gillespie et al., 1986). The IHS transformation is only possible with three bands at a time, but any band combination is possible.

In Fig. 4.18 the H and S components from TM bands 2, 3 and 4 (left column) and 3, 4 and 5 (right column) is shown. While the I-components represent just the average intensity of all three input bands, the H- and S-components show some remarkable features. The H-component of TM bands 2, 3 and 4 (H234) is composed mainly of white, black and grey, maybe representing forest, vegetated and non-vegetated terrain, respectively (Fig. 4.18a). The H-component of TM bands 3, 4 and 5 (H345) is comprised mainly of brighter and darker grey levels (Fig. 4.18b). Grey values > 126 correspond to the grey areas in Fig. 4.18a and separate non-vegetated from vegetated terrain (comparable to NDVI values > 0). A map of vegetation-free areas derived from H345 is also used to reduce misclassification with TM4 / TM5 over vegetated terrain and for mapping of debris cover on glaciers (see 5.2.2 and App. 2.1-2A). The H345 component and the classified map of vegetation-free areas is shown for a larger region (southwestern part of Switzerland) in App. 3.2-4. The S234 image (Fig. 4.18c) shows a great variety of grey values, which are difficult to assign to characteristic surface features. In the S345 image (Fig. 4.18d) all snow and glacier ice is surrounded by a black line and the contrast between debris-cover on glaciers and the surrounding terrain is enhanced.

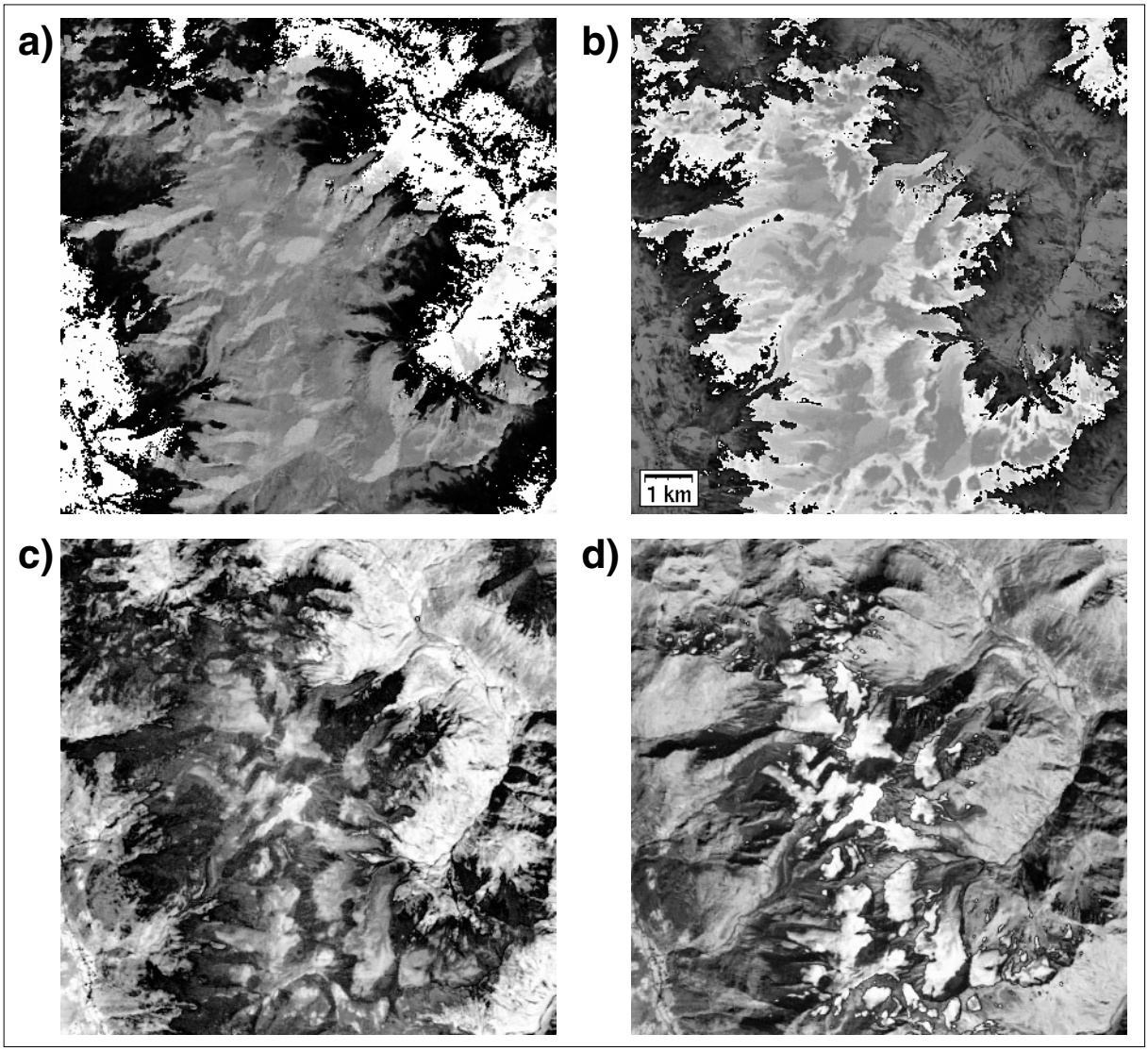

Figure 4.18: *Results of a RGB-IHS transformation with TM234 (a and c) and TM345 (b and d) after contrast stretching. The hue-components are at top (a and b), saturation is at bottom (c and d).*

(6) Principal Component Analysis: PCA

In general, PCA is a statistical technique that transforms a multi-variate data set of intercorrelated variables into a data set of new uncorrelated linear combinations of the original variables. In remote sensing the PCA is used in particular for image data compression and enhancement, digital change detection and image fusion (Pohl and van Genderen, 1998). Since the grey values (DNs) between the TM bands (in the visible part) are more or less correlated, PCA reduces the image dimension (number of bands), by putting as much spectral variance as possible in the least number of principal components (Canas, 1985).

The computation of the PCs can be separated into three steps: (1) The calculation of a covariance matrix (App. 1-6) from the multi-band image will give the correlation of bands between one another. (2) The calculation of the corresponding eigenvectors and their eigenvalues (App. 1-7 and 1-8) will give the orientation of the axes in the n dimensional image space and the variance along the axes, respectively. (3) Each PC (j) is calculated as the sum of the eigen-

vector (E_{ji}) - weighted DNs over each band (i). Hence, the equation for the calculation of the first PC is formulated as:

$$\text{PC } 1 = \sum_{i=1}^{5} DN_1 \cdot E_{1i}$$

The PCs 1-4 from TM bands 1-5 for the test region 'Weissmies' are displayed in Fig. 4.19a-d, respectively. While the first principal component (PC1) explains 65.4% of the variance and represents most of the intensity variations from TM bands 1-4 (Fig. 4.19a), PC2 explains 29.6% of the variance and represents most of the differences introduced by the MIR band TM5 (Fig. 4.19b). The interpretation of PC3 (Fig. 4.19c with 4.5% variance) and PC4 (Fig. 4.19d with 0.5% variance) is rather difficult and not discussed here, since no correspondence with glacial features can be seen. However, PCA is used for snow cover mapping under a glacier mask obtained from PC 2 by Sidjak and Wheate (1999). PCA is not used in the SGI 2000 as principal components vary with scene content.

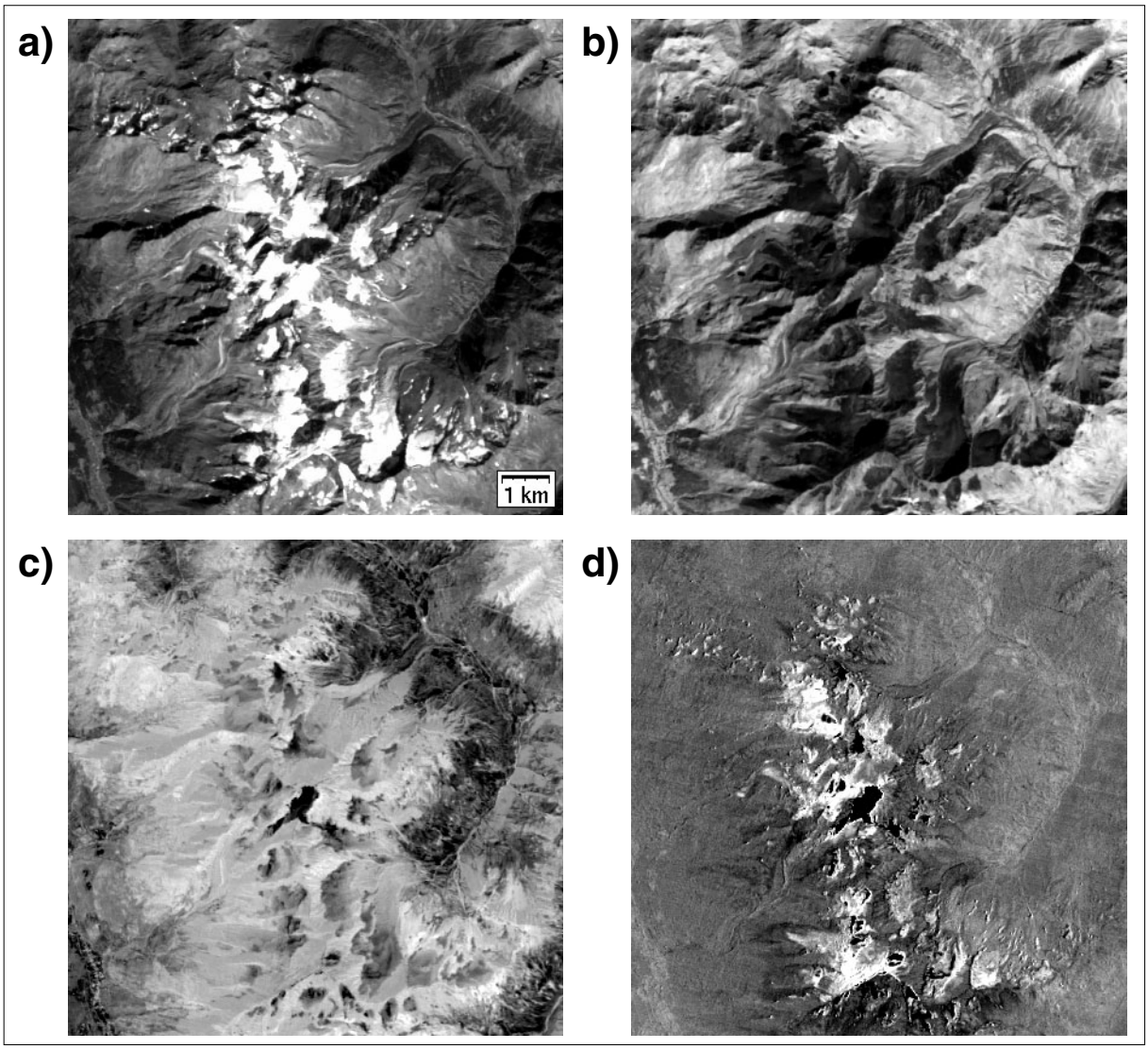

Figure 4.19: *Principal components 1-4 (a-d) from TM bands 1-5. Especially in PC 3 and 4 various surface properties are enhanced, but with a difficult interpretation.*

4.5. Image fusion

4.5.1. Background

Image fusion is a way to combine multi-source imagery with advanced image processing techniques. An overview of concepts in multi-source image fusion in remote sensing is given by Ehlers (1991), Pohl and Genderen (1998) and Schowengerdt (1997). Regarding image fusion in the spatial domain (see Yocky (1996) for the frequency domain), it is possible to distinguish between (a) fusion at pixel level, (b) feature level (classified images) or (c) decision level (GIS applications). While (b) and (c) are also used for the SGI 2000, the discussion here focuses on image fusion at pixel level. A huge number of different sensors acquire data from the earth's surface (Kramer, 2002) and possible methods include fusion of data from different time, sensors and spatial resolutions. Some objectives of image fusion are summarized in Table 4.4 together with the methods used, fused sensors and some references. The table is obviously not exhaustive, since fusion at the scale of airborne sensors (about 10 cm resolution) or weather satellites (about 1 km resolution) are neglected.

Method	Sensor	Objectives	References
sensor (temporal)	TM / SAR	improved classification	Welch and Ehlers (1988)
temporal	TM / TM	change detection, missing information	Singh (1989)
spatial	SPOT XS / Pan	image sharpening, improved interpretation and classification	Cliche et al. (1985), Carper et al. (1990), Pellemans et al. (1993)
sensor & spatial	TM / Spot Pan	scenes from same date: see 'spatial', different dates: image display	Chavez et al. (1991), Shettigara (1992), Sunar and Musaoglu (1998), Munechika et al. (1993)

Table 4.4: *Summary of methods for image fusion (see Schowengerdt, 1997; Pohl and Genderen, 1998).*

Accurate orthorectification is an essential prerequisite for all fusion techniques. With respect to spatial fusion of multi-spectral with panchromatic bands, the main problem is keeping of spectral characteristics from the multi-spectral bands in the fused images. This problem is pronounced if the spectral range of the low resolution band (like TM5) differ from the pan band. Thus, fusion of TM with SPOT and IRS-1C pan is used in the SGI 2000 only for visualization purposes and comparison of TM-derived results with higher resolution data sets.

4.5.2. Applications

From the various image fusion techniques described in Table 4.4, only the widely-used IHS-fusion is applied in the SGI 2000 and described here for TM / SPOT pan fusion. The processing steps are: (1) proper orthorectification of both images, (2) selection of corresponding subscenes, (3) scaling of TM bands to the spatial resolution of SPOT pan (25 m to 10 m), (4) colour-space transformation with TM bands 3, 2 and 1 from RGB to IHS, (5) contrast enhancement of the SPOT Pan channel similar to the contrast of the I-component, and (6) back transformation from IHS to RGB after replacement of the I-component with the contrast stretched SPOT pan band. The SPOT pan scene #14 (cf. Table 4.3) is used for fusion with TM scene #10. The good temporal coincidence (2 days apart) allows a genuine evaluation of the TM glacier mapping

accuracy, but both scenes share only a small region. From this region another test area ('Nufenen') is chosen for comparison, which is located to the south of the 'Nufenenpass' and is 19 by 12 km in size (see Fig. 4.5 'B' for location). In Fig. 4.20a-c the I-, H-, and S-component from TM bands 1-3 are shown after contrast enhancement, respectively. While the I-component represents more or less the average intensity values of all three bands, the H-component shows a strong contrast enhancement between snow and ice and also between lakes and the surrounding terrain. The S-component exhibits some interesting details of the snow surface.

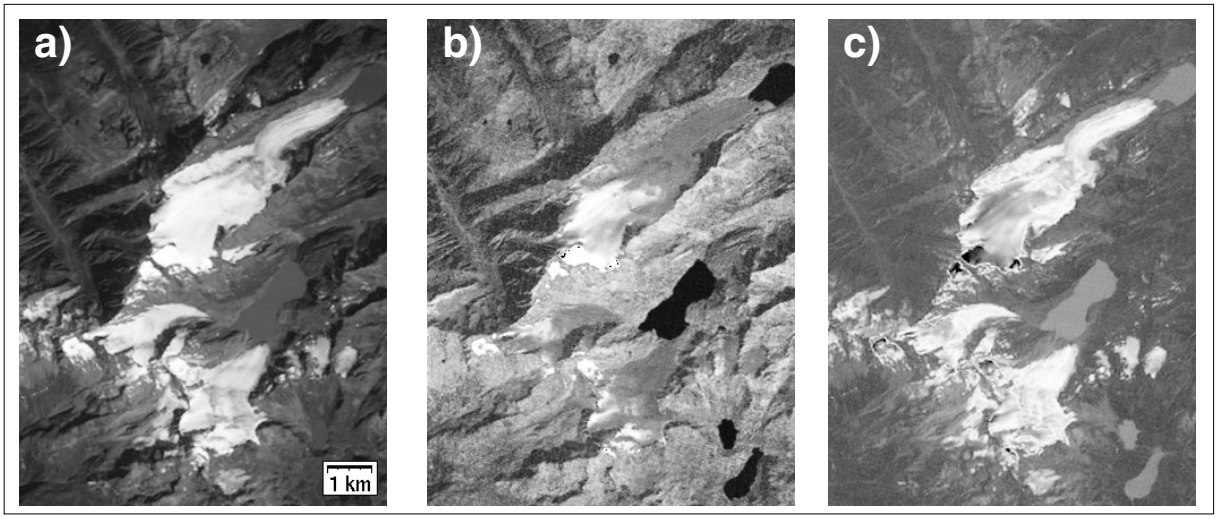

Figure 4.20: *A subset of the Nufenen test region with the Gries- and Hohsandglacier. a) Intensity-, b) hue-, and c) saturation component of TM bands 1, 2 and 3.*

In the fused image (Fig. 4.21b) all spatial details are greatly enhanced (crevasses, topographic features) and colour (spectral characteristics) is altered very little (cf. Fig. 4.21a). There is a purple seam around snow fields, as a result of the high reflectivity in TM bands 1-3 for mixed pixels, which are only partly covered by snow. The comparison with TM-derived glacier outlines is discussed in Chapter 5.4.

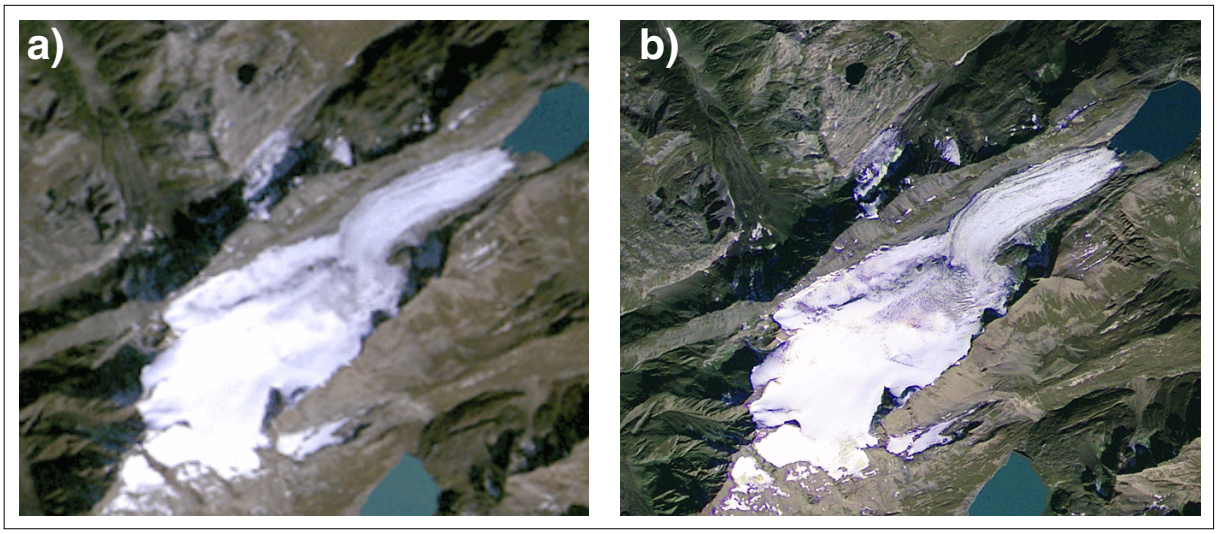

Figure 4.21: *a) TM image of Griesglacier (15 Sep 1992) before and b) after IHS-fusion with SPOT pan (17 Sep 1992). All spatial details are greatly enhanced. SPOT data: © SPOTimage.*

4.

5. METHODS OF GLACIER MAPPING

5.1. Glacier ice

5.1.1. Previous work

In this chapter studies about optical remote sensing of alpine glaciers are discussed, snow and ice properties are not considered. General overviews were given by Gao and Liu (2001), Williams (1983) and Williams and Hall (1993 and 1998). The glacier studies include: (1) analysis of false colour composites, (2) manual delineation of glacier outlines by on-screen tracking, (3) segmentation of ratio images from different input bands, (4) supervised or unsupervised classification, and (5) comparison of TM-derived reflection with in-situ measurements.

(1) False colour composites

A first description of the possibilities for glacier studies with Landsat MSS data (such as topography, velocities, surge type) was given by Krimmel and Meier (1975). Østrem (1975) used prints of FCCs to identify the position of the transient snow line (TSL) on numerous glaciers in Norway and Canada. He already mentioned the possibility of glacier mass balance determination from space. Rott (1976) used contrast enhanced prints from MSS data to estimate the height of the TSL of about 50 glaciers in the Tyrolean Alps (Austria) and calculated their AAR. Williams (1987) used a MSS winter image with low solar elevation for morphological mapping of the Vatnajøkull ice cap and a MSS late summer image with a special contrast enhancement for delineation of different ice and snow facies in a FCC.

(2) Manual delineation

This method is widely used for glacier boundary mapping with MSS and TM. For example, MSS-derived glacier outlines were combined with co-registered FCCs from Landsat TM of a later year (Hall et al., 1992 and 1995a; Williams et al., 1997; Williams and Hall, 1993) in order to derive changes in glacier length. In general a good agreement with in-situ measurements was obtained. Larger errors result if the glacier terminus was covered by debris and barely visible with TM or MSS. Rott and Markl (1989) used manual delineation for assessment of snow and glacier areas with TM. They had also shown that interactive cursor tracking of glacier boundary by an expert revealed more accurate results than an automatic algorithm. For mono-spectral bands (SPOT or IRS-1C pan) this is the only method to obtain glacier outlines.

(3) Segmentation of ratio images

A first attempt at using the different spectral properties of glacier ice in TM4 and TM5 for characterization of snow and ice zones on glaciers was presented by Hall et al. (1987). Later Rott and Markl (1989) explained that ratio images with TM3 / TM5 revealed better results in shadow zones than TM4 / TM5, whereas the latter showed better performance in mapping glacier areas facing towards the sun. Also Rott (1994) used a TM3 / TM5 ratio image, but with spectral reflectances (R) from both channels instead of DNs. He assigned values of [R(TM3) / R(TM5)] > 1.3 to the snow and ice class and separated this class into snow for R(TM3) > 0.48, firn (0.32 < R(TM3) < 0.48) and ice (R(TM3) < 0.32). Bayr et al. (1994) have used ratios of the digital numbers from TM4 and TM5 to delineate the glacier boundary of two different glaciers in Austria. Furthermore, Jacobs et al. (1997) used a segmentation threshold of R(TM4) / R(TM5) > 1.0 to delineate the perimeter of the Barnes Icecap. They had to apply manual corrections for debris-covered glacier areas. It is interesting to note that the TM4 / TM5 ratio was originally developed to facilitate ice/snow discrimination (Hall et al., 1987). The fact that there is also some contrast enhancement between glaciers and terrain was already mentioned, but not used for glacier mapping.

(4) Various classification methods

Della Ventura et al. (1983) developed a technique for automatic glacier classification (ice, snow, other) with MSS data for a small region in the Italian Alps. Later, Della Ventura et al. (1987) used a decision tree classifier and achieved more accurate results.
Gratton et al. (1990) used a GIS to improve the classification accuracy of Landsat MSS and TM data for mountain glacier mapping. Within the GIS environment they performed automated selection of training areas for a Maximum-Likelihood classification. Although high accuracy was achieved for most classes (snow, clean ice, vegetation, rock, water), regions with debris had to be classified by visual inspection. The DEM was not used to obtain glacier parameters.
Binaghi et al. (1993) used also a GIS to improve glacier mapping with TM data and for an update of glacier parameters. For classification they used fuzzy set theory and Dempster-Shafer theory to attribute probability distributions to sets of classes. They combined them with additional data to calculate the final classification (snow, ice, other).
Fuzzy set theory was also used more recently by Binaghi et al. (1997) for glacier classification in the Ortles-Cevedale Group and south Pusteresi Alps (Italy). Although a high accuracy was achieved, the presented method is quite complex and only hardly applicable for worldwide glacier monitoring. Moreover, debris cover on glaciers was not mapped.
An inventory of the entire Southern Patagonian Icefield (SPI) based on TM data from 1986 was performed by Aniya et al. (1996). They used cluster analysis (ISODATA) with TM bands 1, 4 and 5 on Morenoglacier and grouped the 20 clusters into three classes (snow, ice and rock). For the whole SPI a parallelepiped (or Maximum-Likelihood in cases of ambiguity) classification was performed. In case of misclassification (ice in shade, supraglacial till) manual correction was applied.
Li et al. (1998) used a supervised classification for delineation of the Moromaha Icefield in Tibet. They improved their classification by interactive manual correction. Changes in glacier area or length were derived within a GIS (see also 2.2.4).
A detailed evaluation of different glacier mapping algorithms was carried out by Sidjak and Wheate (1999). They applied supervised Maximum-Likelihood classification to different combinations of input bands. These bands were made of principal components (PC) 1-4 or 2-4, partly under a glacier mask derived from PC2 by thresholding, a NDSI, a TM4 / TM5 ratio image or a TM543 composite image. The best classification was revealed with a combination of PC 2-4, TM4/TM5 and the NDSI as the input bands. Even nunataks and medial or dispersed supraglacial debris were correctly mapped.

Spectral mixture analysis was applied to TM data for ice / snow discrimination on tropical Andean glaciers by Klein and Isacks (1999). The spectral endmembers that they used also allowed glacier classification, but problems occur for ice in shadow and under debris cover.

(5) Reflection calculations

In many glacier studies with TM, surface reflectance was calculated and assigned to different ice and snow zones. Moreover, assumptions about the general 'health' of a glacier were derived, although only yearly conditions were investigated (Hall et al., 1989a).
Hall et al. (1988) calculated the planetary reflectance at the satellite sensor for delineation of three different zones (bare ice, wet snow and fresh snow) on glaciers in Austria and Alaska. A comparison of TM-derived snow and ice reflectance with field measurements at the same time was carried out by Hall et al. (1990). By applying an atmospheric correction (accounting for scattering and absorption), reflectance increased by 5-17% and corresponds within 6% to field measurements. During snow metamorphism and with decreasing viewing angle the anisotropy of snow reflectance increased, so that TM-derived reflectances can only be used for nadir viewing conditions.
Koelemeijer et al. (1993) compared TM-derived reflectance (from the tongue of the Hintereisferner, Austria) with in-situ measurements obtained in a different year. They also corrected for atmospheric scattering and absorption yielding a good agreement with the measurements. They pointed out that the decrease in reflection towards the glaciers terminus depends on crevasses, dust, debris and concentration of air bubbles in the ice.
Winther (1993) compared TM-derived reflectance from August 1987 and 1988 with field measurements from August 1992 and 1993 over two glaciers in Svalbard. He discovered large variations in albedo within 5 days, both investigated years and also spatially on both glaciers. The calculated albedos were influenced by atmospheric scattering and absorption, topography (slope and aspect), adjacent pixels, and the anisotropy of snow reflectance.
A different approach was followed by Gratton et al. (1993). The authors determined the net radiation balance of the Athabascaglacier basin from TM data, a DEM and the radiative transfer code Lowtran 6. They produced a surface cover map from supervised classification and calculated albedo from TM band reflectances, using different weighting schemes for different cover types. Furthermore, they computed TM6 brightness temperatures to derive terrain emitted radiation.
An extensive comparison between ground-based and TM-derived albedo measurements of glaciers is given by Knap (1997) and Knap et al. (1999). The measurements agree quite well, apart from a large scatter over bare glacier ice, due to a high spatial variability of the albedo.

5.1.2. Comparison within one test region

Most of the methods discussed above within points (3) and (4) are applied to the test region Weissmies, in order to obtain the best glacier mapping method for the SGI 2000. Due to steep relief (altitudinal range 1500 - 4500 m a.s.l.) there is shadow and debris-cover present on some glaciers. Together with abundant small snow fields, there are three influences on glacier mapping accuracy, known to be critical from previous studies, which can be examined in this region (cf. Paul, 2001). The following methods are investigated for the SGI 2000:

(a) Ratio images from TM3 / TM5 and TM4 / TM5 with the DNs, planetary reflectance and atmosphere/terrain corrected reflectance for each channel, (b) an unsupervised ISODATA clustering with different input channels and number of clusters, (c) a supervised Maximum-

Likelihood classification (MLC), (d) the NDSI and (e) PCA. The individual glacier maps (black = 'glacier', white = 'other') are created as follows: For method (a) interactive thresholding of the ratio images is applied, the classes of (b) are separated into 'glacier' and 'other' by visual interpretation. For the MLC (c) the two ice and snow classes are assigned to 'glacier' and all other classes to 'other'. The threshold for the NDSI (d) is also selected by visual interpretation. The PCA (e) is not used for glacier mapping, as distinct glacial features could not be identified from any component.

In Fig. 5.1 a-f two glacier maps are compared at a time in each figure. The following colour scheme is used: 'glacier' on both maps: grey, 'other' on both maps: white and 'glacier' only on the first or second map: red or blue, respectively. In order to reduce noise a 3 by 3 median filter is applied to all glacier maps before combination (see 5.1.3). The used glacier maps in Fig. 5.1a-f are: (a) a ratio image from TM3 / TM5 versus TM4 / TM5 using DN, (b) same as (a), but using the planetary reflectance, (c) as (a) but using atmosphere and terrain corrected reflectance, (d) the NDSI versus TM4 / TM5 from DN, (e) the unsupervised ISODATA clustering with 20 classes versus TM4 / TM5 from DN, and (f) the supervised Maximum-Likelihood classification versus TM4 / TM5 from DN.

All methods other than TM4 / TM5 with DN reveal problems with regions in cast shadow (indicated by arrows in Fig. 5.1a), where they map too much (Figs. 5.1a, b, d, f) or too little (Fig. 5.1c and e) glacier area. Additional regions within cast shadow are mapped from both methods displayed in Fig. 5.1b and d. Small snow fields were especially mapped with the methods depicted in Fig. 5.1c, e and f. The accuracy of all investigated methods could be improved partly by changing the relevant parameters (thresholds, training areas, number of clusters) but at the cost of more incorrect results at other places. All methods fail in detection of debris-covered ice because of the spectral similarity to the surrounding terrain. The glacier classification with segmentation of a TM4 / TM5 ratio image using the raw DN proved to be the best method with respect to glacier areas in cast shadow or assignment of snow fields to 'other'. In paragraph 5.3 a comparison with results (manual delineation) from higher-resolution imagery is given.

The threshold value for the ratio image lies in general near 2.0 and no dark object subtraction is applied to TM4 before ratioing. Wrong classification occur for vegetation in shadow and for lakes. These areas are classified separately by a thresholded NDWI image (lakes, 4.4.2. (4)) and the hue-component from an RGB-IHS colour-space transformation with TM543 (vegetation, 4.4.2. (5)). The mapping algorithm is given in 5.4.3 (work-flow) and App. 2.1-2 (program). See 5.2 for a method of semi-automatic mapping of debris-covered glacier ice.

5.1.3. Possible error sources

Median filter and threshold

A median filter with a 3 by 3 kernel size is used for smoothing of the classified (black and white) glacier maps. This non-linear filter improves classification accuracy by filling/deleting small isolated gaps/noise pixels, respectively. While filling and deleting helps to correct glacier classification in cast shadow, the latter deletes also small snow fields. The 'fill' function of the filter has two opposite effects: While the inclusion of a medial moraine of one pixel width and arbitrary length is wanted, the filling of rock outcrops (nunataks) is not. However, the filter has more advantages than disadvantages, at least for larger glaciers.

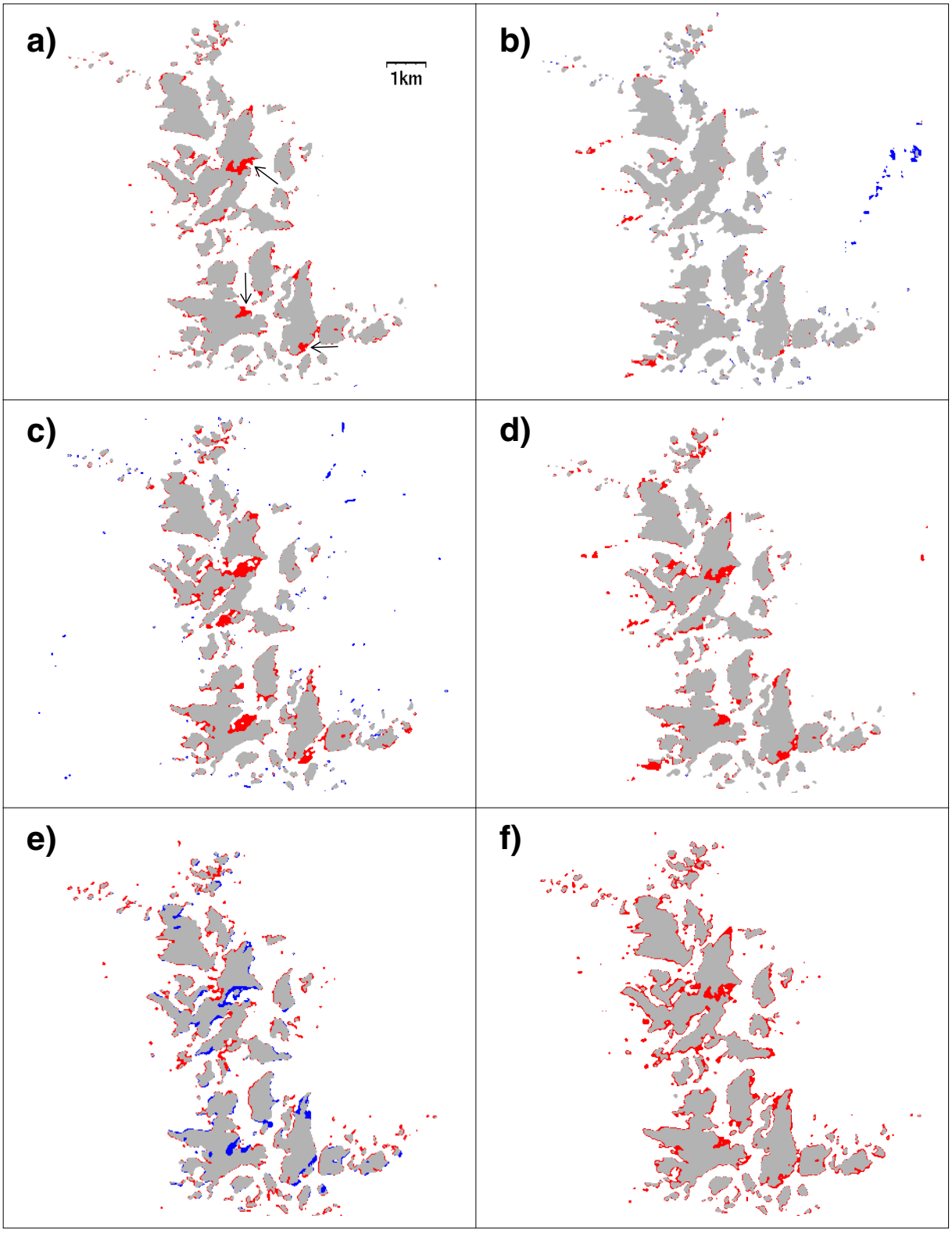

Figure 5.1: *Glacier maps comparing two methods at a time. Areas in grey were identified by both methods as being a glacier, red areas only by the first method, and blue areas only by the second method. The compared methods are: a) TM3 / TM5 and TM4 / TM5 from DN, b) as a) but all TM bands from at satellite planetary reflectance, c) as a) but all TM bands from atmospheric corrected reflectance, d) NDSI and TM4 / TM5 with DN, e) unsupervised ISODATA clustering (20 clusters) and TM4 / TM5 from DN, and f) supervised Maximum-Likelihood classification (8 classes) and TM4 / TM5 from DN.*

A more detailed analysis of 99 glaciers within the test regions Weissmies and Mischabel reveals an average change in glacier area by the median filter of -1.3± 2.86% for all glaciers and +0.3±1.00% if glaciers smaller than 0.1 km^2 are not considered. Thus, area is reduced by the filter for very small glaciers (the smaller, the stronger) and somewhat enlarged for larger glaciers (see Fig. 5.2). This has to be recognized during interpretation of glacier changes (see Chapter 7). If un-rectified TM data are used (without any resampling) the median filter should also be applied to TM5 before the division (not necessary for ETM+). This will reduce much of the noise over snow and ice in regions with cast shadow.

While a shift of the threshold for segmentation of the ratio image towards higher values reduces noise, glaciers became thinner due to removal of mixed ice/terrain pixels along the glacier perimeter. Lower values will result in larger glacier areas but more noise. In Fig. 5.2b the relative change in glacier area (same 99 glaciers as above) for 4 distinct values (1.7, 1.8, 2.0 and 2.1) of the threshold are shown. Glacier areas derived with a threshold value of 1.9 are used as the reference. Apart from the general increase of scatter and larger differences towards smaller glaciers, change in glacier area is mostly below ±2% for a ±0.1 variation of the threshold (i.e., 1.8 and 2.0) and glaciers larger 0.1 km^2. Thus, the threshold is quite robust and every attention could be paid to glacier parts in cast shadow, as these regions are most sensitive to noise (see example in App. 3.2-1. For the SGI 2000, the lowest possible threshold is used (compiled in App. 1-3), resulting in more remaining noise but somewhat larger glaciers.

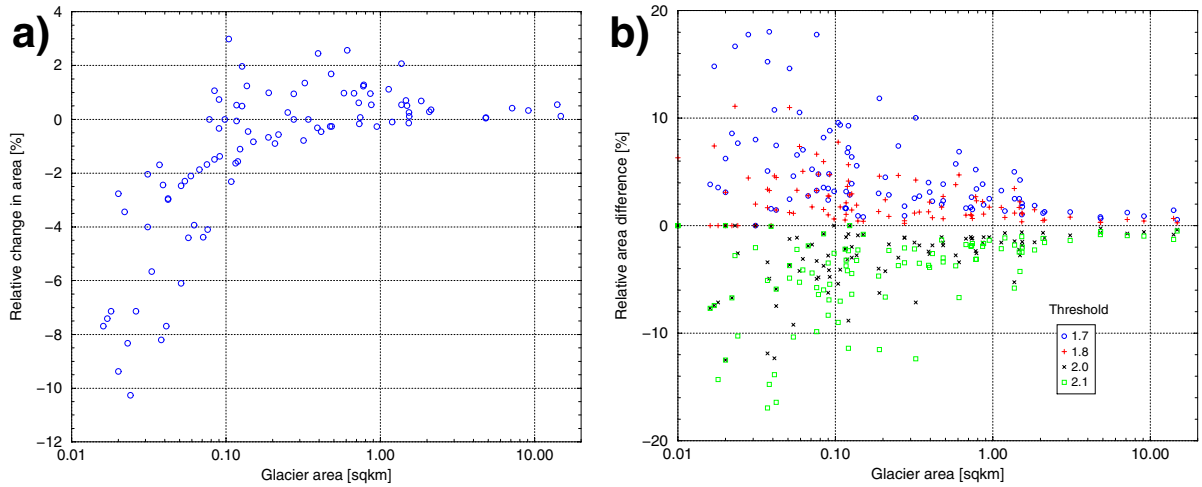

Figure 5.2: *a) Relative change in glacier area caused by the median filter (unfiltered values as the reference). A sub-sample of 99 glaciers from the test areas Weissmies and Mischabel is used. b) Relative change in glacier area as a result of a different threshold (see legend) for the same subsample. The reference glacier area for each glacier is obtained with a threshold value of 1.9.*

TM5 column shift

The correction of the 'band-to-band misregistration' (see 4.1.3) causes differences in glacier classification with TM4 / TM5. This can be seen in Fig. 5.3 for the Nufenen test region by combining both glacier maps with correction of the column shift (grey and red areas) and without correction (grey and blue areas). Apart from the general shift of both maps (red pixels to the right, blue to the left), there are some more changes: most of the additional red pixels are snow fields and additional blue pixels correspond to regions in cast shadow or to water. Since rejection of snow pixels outside of glaciers and a larger glacier area in regions with cast shadow is welcome, the 'band-to-band misregistration' was not corrected.

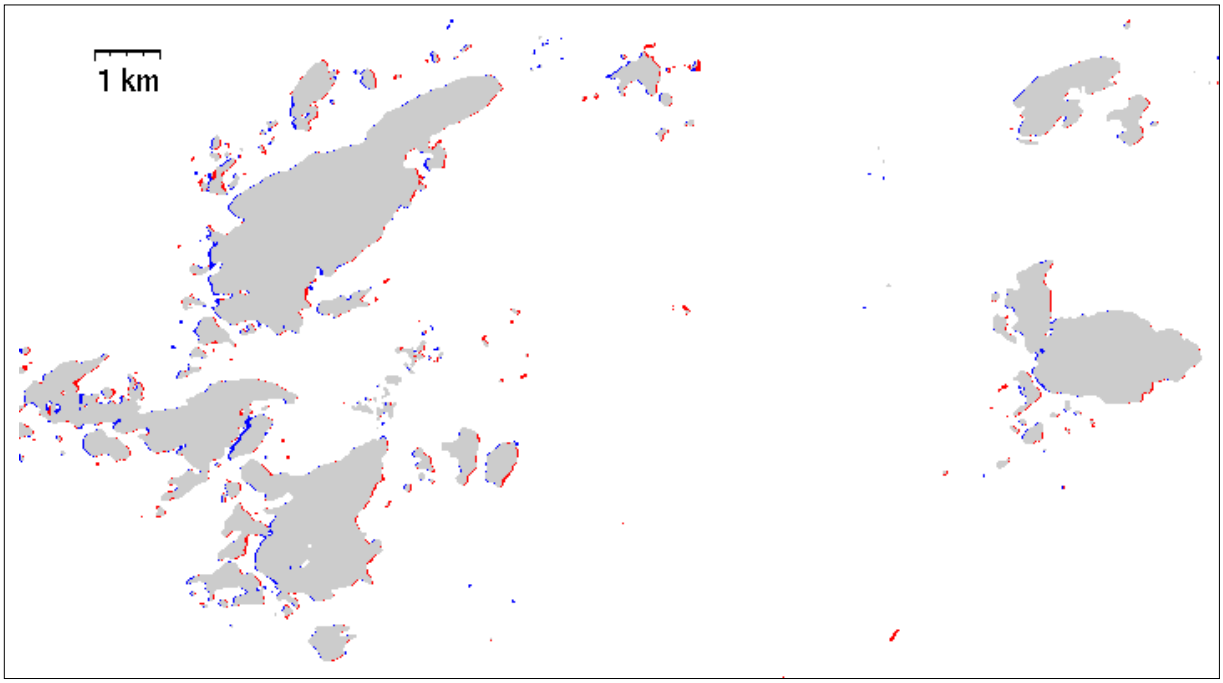

Figure 5.3: *Glacier classification with TM4 / TM5 in the Nufenen test region with correction of the 'band-to-band misregistration' (grey and red areas) and without (grey and blue areas).*

Resampling

The different methods of resampling during orthorectification (see Fig. 4.8) produces slightly different glacier maps. In Fig. 5.4 two glacier maps are compared at a time for a part of the test region 'Weissmies' (see Figure caption for used colours) and three resampling methods (cf. 4.2.1): nearest neighbour (NN), bilinear interpolation (BI) and cubic convolution (CC).

Since there are only small deviations between all of the methods, no quantitative measurement of glacier areas is carried out. Visual inspection reveals that the number of red and blue pixels along a glacier perimeter are similar and that the overall number of red and blue pixels is somewhat smaller in Fig. 5.4b than in 5.4a or 5.4c. Thus, BI and CC produces rather similar glacier maps, while there are some larger differences to nearest neighbour resampling.

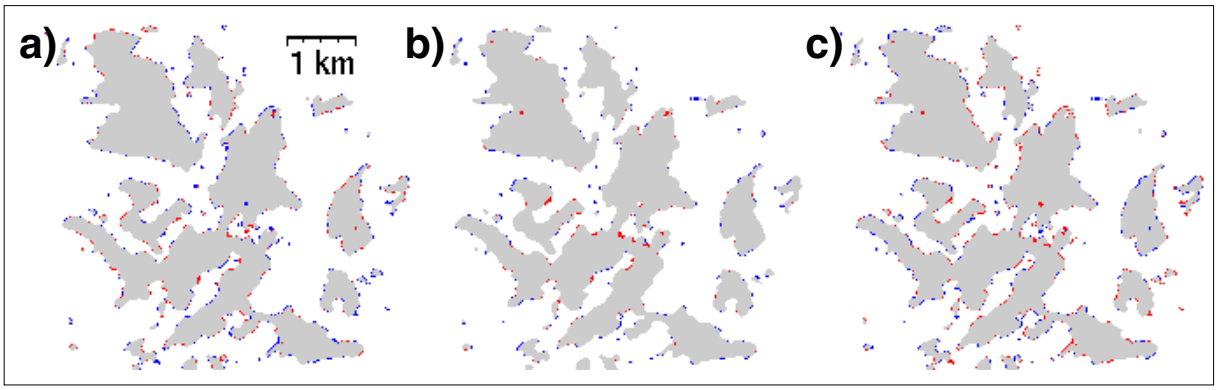

Figure 5.4: *Comparison of glacier maps from TM4 / TM5 and different resampling methods. Two glacier maps are compared at a time (first method: grey and red, second: grey and blue). a) bilinear interpolation (BI) with nearest neighbour (NN), b) cubic convolution (CC) with BI, and c) CC with NN.*

Pixel size

In the SGI 2000, glacier areas derived from digitized glacier outlines (~2 m resolution) are compared with TM-derived outlines (~ 25 m). Additionally, manually-derived glacier areas from SPOT pan (10 m), IRS-1C (5 m) and Ikonos (1 m) are used for comparison. As glaciers are natural objects, their dimension is fractal and their area or perimeter depends on the size of the yardstick used (e.g., Cao and Lam, 1997; Woodcock and Strahler, 1987). Thus, it is important to estimate the influence of spatial resolution on glacier areas (cf. Paul et al., in press) This is done by scaling the digitized glacier outlines to the following simulated cell sizes: 5 m, 10 m, 15 m, 20 m, 25 m, 30 m, and 60 m. The scaling is performed by vector-raster conversion using the *polygrid* command from Arc/Info and the cell sizes mentioned above.

In Fig. 5.5 two glaciers are shown as seen with TM (25 m resolution, grey area) and other cell sizes as colour-coded overlays (see legend). The black line indicates the original digitized outline. The glacier in Fig. 5.5a is 0.1 km^2 in size and there are only small area differences for all resolutions (ranging from 0.1002 to 0.1026 km^2). This indicates that even large pixels can give good results for area estimates of small glaciers, if mixed pixels cover the real glacier perimeter half in and half out. The glacier depicted in Fig. 5.5b is somewhat larger (0.3 km^2) and gives similar results.

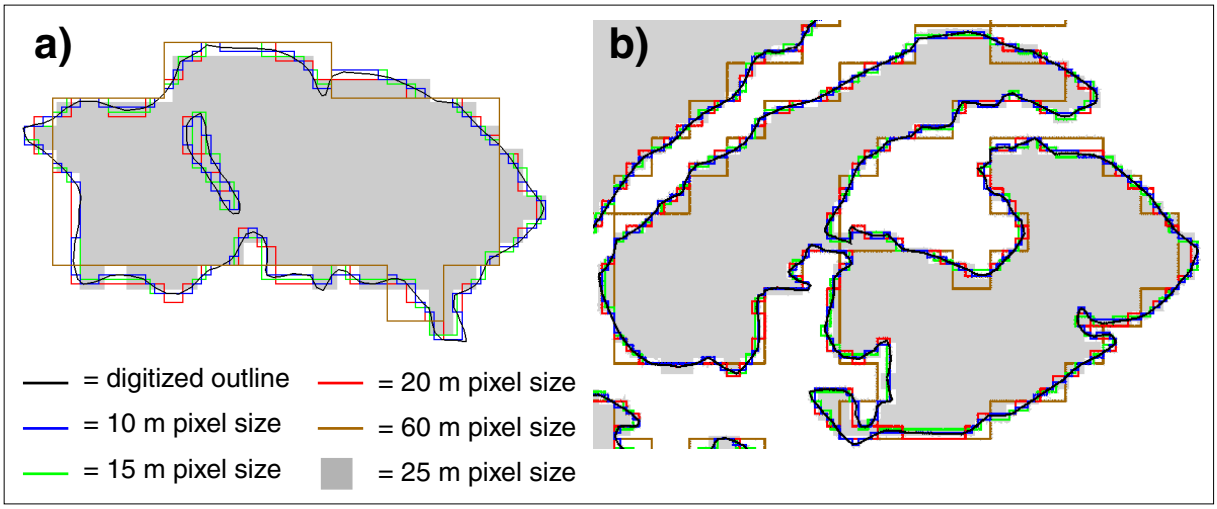

Figure 5.5: *Comparison of glacier outlines with different spatial resolutions (Mischabel test region). a) A glacier with a size of 0.01 km^2 and b) two glaciers with a size of 0.3 km^2 (together).*

In order to obtain a statistical measure for the change in glacier area due to sensor resolution, about 100 glaciers in the Mischabel test region are investigated in detail. In Fig. 5.6a the relative differences in glacier area are plotted against glacier size for seven different resolutions. Down to a glacier size of 0.05 km^2, the relative change is below 3 to 5% (with the exception of the 60 m pixels). For glaciers even smaller, the differences increase rather quickly. This can also be seen in Fig. 5.6b, where the standard deviation (σ) of the area differences (compared to the digitized areas) for seven area classes and all seven resolutions are given. Figure 5.6b exhibits that glacier size should be greater than 0.1 km^2 to keep σ below 3% if TM-derived glacier areas are compared with the digitized inventory data. The use of real data instead of simulated pixel sizes will increase the deviations, due to mixed pixels and debris cover. Hence, careful interpretation of area changes between higher-resolution and TM-derived areas for glaciers smaller than 0.1 km^2 is required (cf. Chapter 7). However, only standard deviation will increase, and specific glaciers will show similar deviations in both directions.

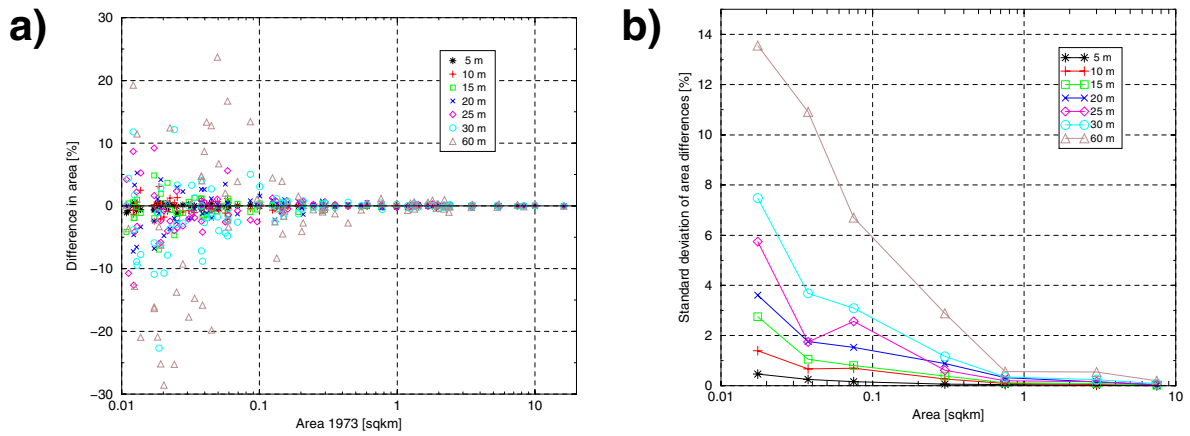

Figure 5.6: *a) Relative differences in glacier area between the digitized inventory and 7 simulated pixel sizes versus glacier area. b) Standard deviations of the area differences for the same data set (99 glaciers of the Mischabel test region) and 7 area classes (symbol location marks centre of each class).*

5.2. Debris cover on glaciers

5.2.1. Background and previous studies

5.

Characteristics of debris-covered glaciers

Debris is a typical feature at the surface of a glacier in the ablation area and is widely recognized as the main obstacle to glacier mapping. Distribution and particle sizes are highly variable, ranging from dust to house-sized blocks and from a rare occurrence to complete coverage (cf. Fig. 2.5f). Very small particles (dust, soot) are usually distributed evenly over the ablation area, but then enough ice shines through for classification (cf. Fig. 2.5b). The characteristic decrease of surface reflectance of the bare ice facies (compared to snow, see Fig. 4.13b) may be attributed to these particles (Hall et al., 1987; Williams et al., 1991). The larger sized till (stones, rocks) is often arranged to medial moraines, which originate where two glacier basins join. With the down-slope flow of a glacier the debris is transported to the terminus and deposited in the glacier forefield. Further aspects of debris-covered glaciers (e.g., hydrology, energy balance, supraglacial lakes) were discussed by Nakawo et al. (2000).

Glaciers with several accumulation basins and/or situated in steep topography commonly have completely debris-covered tongues. The 'Oberaletschgletscher' tongue is shown for example in Fig. 5.7a (synthetic oblique perspective view created from IRS-1C pan image (#13) and the DEM25L2). If the fraction of debris cover exceeds a certain limit within a pixel, the spectral signal is dominated by debris and the ice underneath cannot be detected by optical sensors. Sometimes geophysical field investigations are required to detect buried glacier ice (Haeberli and Epifani, 1986; Whalley and Martin, 1986). Hence, glaciers are mapped by TM4 / TM5 without the debris-covered parts, resulting in difficult time-series analysis, as the part with exposed debris cover depends on snow conditions which vary from year to year.

Mapping of debris-covered glaciers

Bishop et al. (1995 and 1999) were able to characterize the debris cover itself by spectral classification, but they used pre-defined glacier outlines for their approach. Geomorphometric DEM analysis was used by Kieffer et al. (2000) to obtain slope and curvature information for section-wise delineation of a glacier tongue, while Bishop et al. (2000) used flow paths generated by hydrologic modelling from seed points and a V-shaped operator. As flow lines from the left and right lateral moraines converge at the glacier snout, these flow lines resemble the glacier perimeter very closely. The DEMs used were derived photogrammetrically from SPOT pan stereo imagery of a test region in the Himalayas. Both methods require intense user interaction from experts, and the task of deriving the glacier areas involved from the generated outlines is not a trivial one. Another method proposed by Lougeay (1974), utilizes the lower emissivity in the thermal infrared from debris cover with ice underneath. Taschner and Ranzi (2002) indeed found a lower emissivity with TM6, at least for partly debris-covered ice.

Based on the observation that debris-covered glacier tongues are rather flat, transects of slope values are generated for several glaciers. A typical example for 'Oberaletschgletscher' (Fig. 5.7a) is presented in Fig. 5.7b. This Figure shows profiles of all slope values for the lower 2 km of the glacier tongue, sampled at 30 equidistant transects perpendicular to the flow direction. Slope values below 20° are indicative of the debris-covered glacier tongue. For other glaciers tested, slope values are at least below 25° and the selected 24° threshold (see below) is valid only for this sample, but a good starting point nevertheless. For mapping of debris-covered areas, the slope facet is combined with the glacier map and a map of vegetation-free areas.

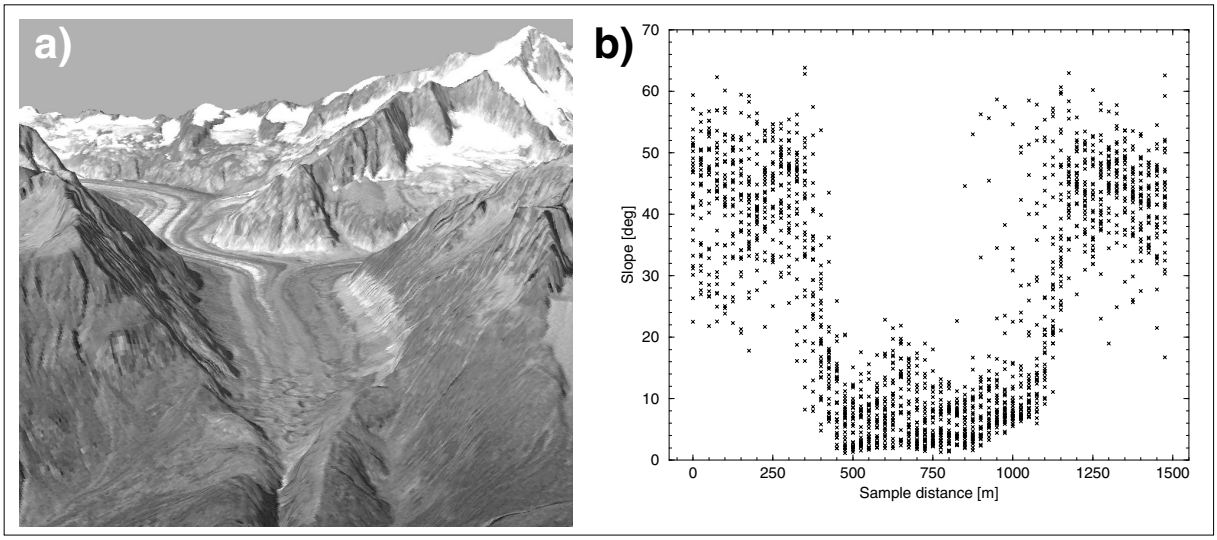

Figure 5.7: *a) Synthetic oblique perspective view of 'Oberaletschgletscher' for comparison with Fig. 5.8-5.10 (IRS-1C image draped over the DEM25L2). b) Slope profiles from 30 transects perpendicular to the flow direction sampled at the lower 2 km of the glacier tongue. DEM25 © swisstopo.*

5.2.2. The debris-cover mapping algorithm

Individual steps for debris-cover mapping with this combined method are illustrated in Fig. 5.8 to 5.10 for a subset of the Aletsch test region. The processing flow is drawn schematically in Fig. 5.12 (see App. 2.1-2 and 2.3-1 for the EASI and Fortran script). The steps are as follows:

(1) The TM4 / TM5 ratio image (Fig. 5.8a) is segmented into a binary glacier map (Fig. 5.8b) with a threshold value of 2.0 into the classes 'glacier' (black) and 'other' (white).

(2) The hue-component of the IHS-colour-space transformation from TM bands 3, 4 and 5 (Fig. 5.8c) is used to map the vegetation-free areas. In Fig. 5.8d a threshold value of 126 is used to map vegetated areas (white), and vegetation free areas (black). The vegetation free zones are also combined with the glacier map to reduce misclassification in regions with vegetation. In pseudo code the glacier classification is (pix=0 means 'glacier'):

```
IF ((TM4/TM5)>2.0) AND (hue345>126) THEN pix=0 else pix=255.
```

(3) Slope is calculated from the DEM25L2 (Fig. 5.8e) and all slope values less than 24° are assigned to be possibly debris covered. In Fig. 5.8f this slope facet is depicted in black, while all slope angles > 24° are white.

(4) The overlay of all three black and white maps is presented in Fig. 5.9a. The legend for the different grey shades is given in Table 5.1 (coloured version in App. 3.2-6). The class 'debris' is produced from the pseudo code (pix=255 means 'no glacier', pix=127 means 'debris'):

```
IF (pix=255) AND (hue345>126) AND (slope>24) THEN pix=127.
```

In order to reduce wrong classification and remove speckles, a 3 by 3 median filter is applied afterwards. The result is shown in Fig. 5.9b ('glacier' = black, 'debris' = grey), depicting also areas with 'debris' that are not connected with a glacier (in light grey). These areas are removed in the next step using the 'image polygon growing' (IPG) module from PCI.

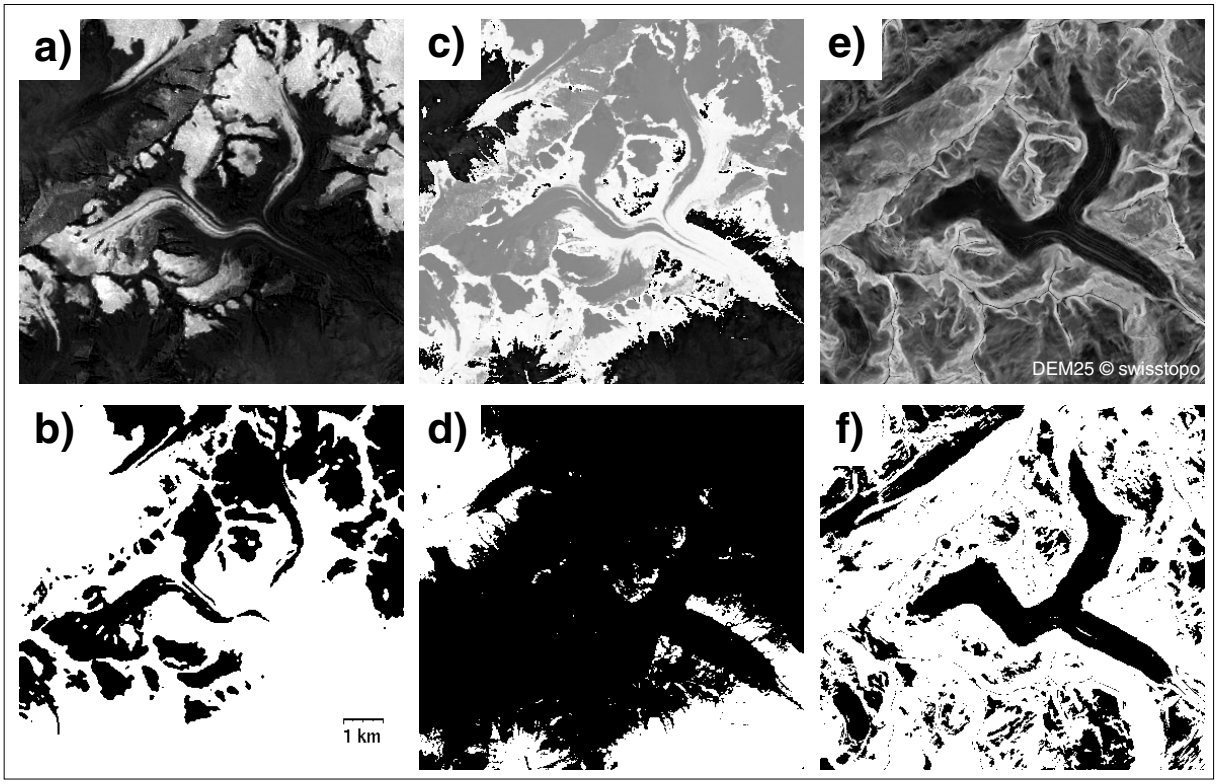

Figure 5.8: *Illustration of the debris-cover mapping algorithm. a) TM4 / TM5 ratio image, b) glacier map after thresholding, c) hue-component from IHS-colour-space transformation, d) map of vegetation free areas (black), e) slope as derived from the DEM25L2 and f) slope angles less than 24° (black).*

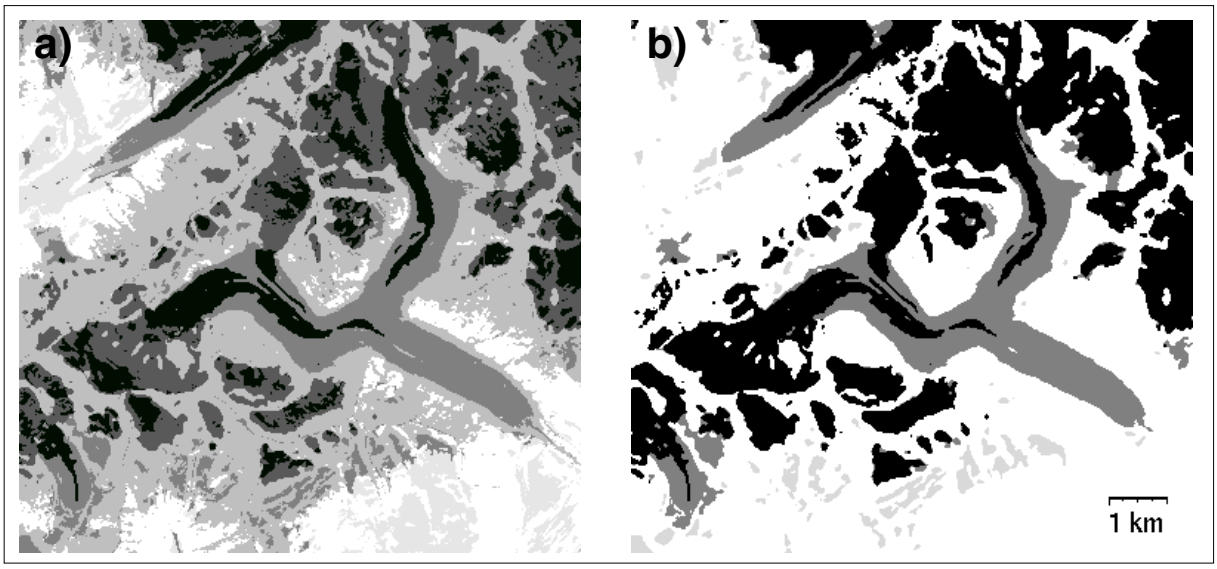

Figure 5.9: *a) Overlay of glacier, vegetation and slope map (Fig. 5.8b, d and f, see table 5.1 for grey shades). b) The resulting classes glacier (black) and debris (grey) with isolated debris areas in light grey.*

	white	light grey	grey	dark grey	very dark grey	black
slope < 23° ?	-	x	-	x	-	x
vegetation ?	x	x	-	-	-	-
glacier ?	-	-	-	-	x	x
classification	other			debris	glacier	

Table 5.1: *Colour scheme used for Fig. 5.9a ('-' = no, 'x' = yes) and final classification.*

(5) With IPG all areas connected to the class 'glacier' (grey level 0) or 'debris' (127) are assigned to an individual number (ID). These numbers are written to a text file for each pixel together with the data from the classified glacier map and read by a Fortran program, which seeks debris IDs without corresponding glacier IDs (App. 2.3-1). In this way each isolated 'debris' region was removed from the map. The general improvements are evident from Fig. 5.9b but some artefacts still remain, namely two errors with respect to the slope: (1) slope exceeds 24° (steep glacier snouts, local DEM artefacts and thin debris cover on steeper glacier parts) and (2) slope is less than 24° (forefield debris is connected to a glacier). While for (1) manual corrections have to be applied, the errors of (2) can be reduced by multi-temporal change detection analysis.

If glacier fluctuations are greater than a few TM pixels, this change can be used for an update of the glacier outline and a separation from the connected forefield 'debris'. For the multi-temporal analysis the raw data from TM5 of 1998 are subtracted from 1985 (Fig. 5.10a). TM5 is used because shadows are as black as glaciers and differences due to changed illumination conditions are less visible. The difference between the two scenes is superior to the ratio, since small differences in digital numbers over glaciers are less pronounced. A black seam is visible in Fig. 5.10a where a change from 'dark' glacier pixels to 'bright' debris pixels took place. This map is reduced to a binary map by segmentation (Fig. 5.10b) and combined with Fig. 5.9b to indicate regions where glacier change took place. Manual editing by changing colours to 'background' is applied at this final stage. Complete manual delineation of debris-covered glaciers also profits from the automatic pre-processing, as visual inspection can be quite difficult.

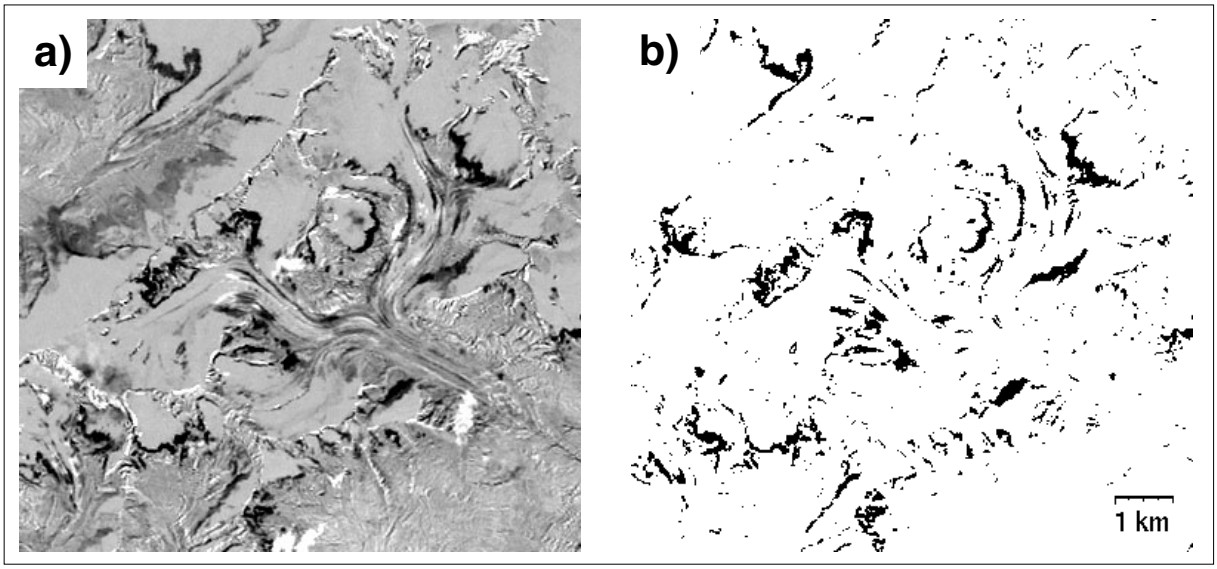

Figure 5.10: *Multi-temporal analysis: a) TM5 (1985) -TM5 (1998) after contrast stretching. Regions which are subject to change appear in black or white. b) After segmentation most of the black pixels indicate change due to glacier fluctuations.*

5.2.3. Accuracy of the method

The integration of DEM data and multi-temporal change detection analysis requires accurate orthorectification of the satellite images. Apart from that, DEM artefacts and the time of DEM acquisition has to be taken into account. Manual corrections are required for most glaciers without movement (less than one pixel) and flat glacier forefields.

A comparison with manually-delineated glacier outlines is not carried out, since manual corrections are also applied to the automatically-classified debris-cover map. However, in Fig. 5.11 an overlay with an independent vector data set from 1993 is shown (provided by Swisstopo). Glacier outlines are depicted in black and 'debris on glaciers' outlines in red. The arrows indicate regions where: (a) slope exceeds 24°, (b) glacier recession since 1993 occurs, and (c) misclassification with TM4 / TM5 for steep glaciers in cast shadow took place.

In all of these cases manual inspection can be used to correct the errors. A TM543 composite combined with the automatically-derived glacier areas (overlay) is used for this, using the public domain software tool XPAINT. The outline polygons are just 'filled' with the 'debris colour' after removal of the background image. Comparison with the digitized 1973 glacier outlines exhibits few cases (glaciers without movement and invisible margin) where even the combined method fails. Such glaciers (about 10) are excluded from further analysis. In App. 3.2-7 the comparison is shown for the entire test region Aletsch.

For a part of the same region, a DEM is derived from ASTER stereo data. The method discussed above is also applied to this ASTER DEM and compared with results derived from the DEM25L2 (see App. 3.2-7). A first assessment reveals encouraging results, but DEM artefacts enlarge the number of erroneously-classified regions with debris-cover, especially in rather steep topography. A more detailed analysis of ASTER-derived DEMs was given by Kääb (2002).

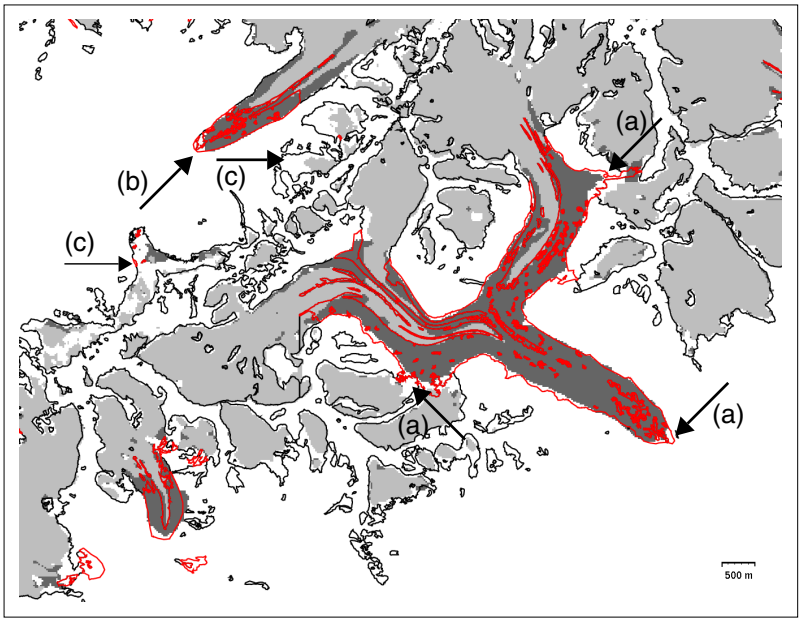

Figure 5.11: *Comparison of the classified and corrected image (light grey = 'glacier', dark grey = 'debris') with outlines from the Vector25 data set as an overlay (black = 'glacier', red = 'debris on glaciers'). Arrows indicate differences that are discussed in the text.*

The workflow for debris-cover mapping as given in Fig. 5.12 is described in detail in Chapter 5.2.2. The first row in the Figure displays the input data (TM bands or DEM) required for calculation of the parameters of the second row (calculation). The NDVI is added as an alternative to the hue component (from TM bands 3, 4 and 5). The third row gives the threshold parameter used for classification of ice (from hue > 126 and TM4 / TM5 ratio > 2.0) and debris (hue > 126, TM4 / TM5 ratio < 2.0 and slope < 24°). The median filter is applied to the glacier / debris map and isolated debris regions are detected from the image polygon growing (IPG) command in PCI in combination with a Fortran program (cf. App. 2.3-1). Finally, the multitemporal change map from TM5 is used to dissect debris in glacier forefields or adjust the DEM-derived outline to its present location (if the glacier has moved).

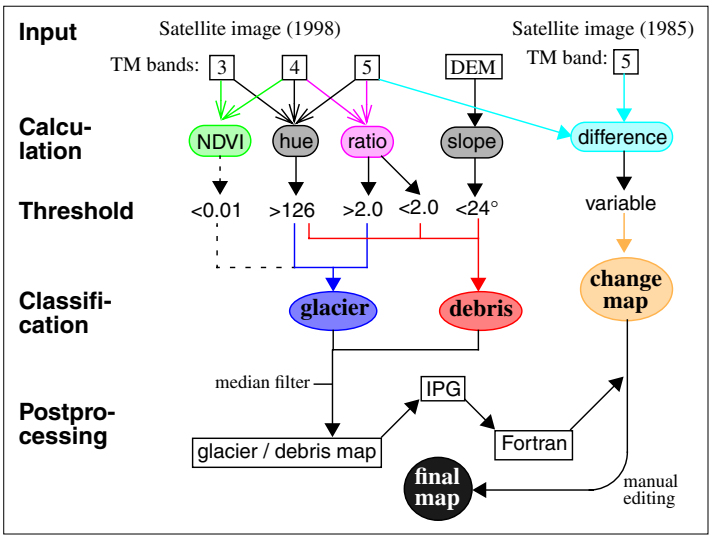

Figure 5.12: *Work flow for mapping of debris-covered glaciers in a schematic form.*

5.3. Mapping of snow cover on glaciers

5.3.1. Background and previous studies

Knowledge of the spatial distribution of snow cover is important at various levels of scale. On a global scale, the snow-albedo feedback strongly influences the earth's radiation budget. Numerical weather forecasts can be improved if hemispheric snow extent is known (Murphy, 1993). Thus, space-borne remote sensing is a primary tool to obtain hemispheric snow cover by means of multi-spectral classification. In particular, the daily images of the polar-orbiting NOAA satellites (about 1 km spatial resolution) were used to derive snow cover maps on an operational base (e.g., Voigt et al., 1999). Today the MODerate Imaging Spectro-radiometer (MODIS) on board Terra is also used for operational hemispheric snow cover mapping. With its high spectral (36 bands) and spatial resolution (up to 250 m) accurate snow cover maps were provided on a 2-day basis (NOAA, 2002). The algorithm uses the NDSI in combination with the NDVI to improve classification in areas with vegetation (Hall et al., 1995b).

On a regional scale, the snow-covered area (SCA) is the primary input parameter for hydrologic modelling (e.g., Martinec, 1975). In the Alps, prediction of snowmelt runoff plays an important role in calculation of river discharge (flood waves) or hydro-power production. In drier parts of the world (e.g., India, USA), the water from springtime snowmelt is also used for agriculture. As a consequence, sophisticated models have been developed to map SCA with high precision from Landsat TM (Rosenthal and Dozier, 1996; Schaper et al., 1999).

On a local scale, snow cover influences a glacier's mass balance. Although for Alpine glaciers winter snow accumulation is of a less importance for mass balance than summer temperature, summer snowfall is able to reduce glacier melt considerably due to the increase in albedo (e.g., Fliri, 1964). The mass balance can roughly be estimated from the AAR at the end of the ablation season (cf. 2.1.3). Differences in spectral reflectance between ice and snow (cf. Fig. 4.13b) allow their discernment in satellite imagery. This has been used for AAR calculation from the beginning of Landsat imagery, using the 80 m resolution MSS data (Østrem, 1975; Rott, 1976). More recently (and with TM) glacier facies have been separated by their spectral reflectance (Hall et al., 1988; Williams et al., 1991) and many field studies have been conducted to validate reflectance data from Landsat TM (Hall et al., 1989b and 1990; Koeljemeier et al., 1993; Knap et al., 1999). The non-Lambertian reflectance of snow at different viewing angles (forward scattering) in particular had caused deviations from measured values.

The NDSI has proven to be very efficient in snow cover mapping from MODIS and with TM (Dozier, 1989). Unfortunately, this method is not able to distinguish between snow and ice. The TM4 / TM5 ratio image method was originally developed to enhance the contrast between snow and ice on glaciers (Hall et al., 1987). In the SGI 2000, the method is used to map glaciers instead. Snow classification based on reflectance values has to use a high-precision DEM in the steep topography of the Alps, as a strong bias in illumination is caused by the varying local incidence angle of the sun. Moreover, sun-lit glacier ice may have nearly the same reflectance as snow in shadow, and inadequate DEMs (artefacts) cause additional noise. The high-precision snow cover mapping method used by Schaper et al. (1999) is too complex for application within the SGI 2000. Using PCA under a glacier mask, as proposed by Sidjak and Wheate (1999), seems to generate non-reproducable results, as principal components may change with image content (i.e., lakes, clouds, vegetation, etc.). Manual delineation of SCA is

highly accurate (Rott, 1976; Rott and Markl, 1989), but very laborious for a large number of glaciers. Thus, a simple, fast and robust method for mapping of snow on glaciers in steep topography without using DEM information does not exist today.

5.3.2. Mapping of snow in the SGI 2000

An approach for snow cover mapping without using a DEM is presented in Fig. 5.13 for a sub-region around Rhoneglacier (R). Spectral differences between snow and ice are enhanced by multiplication of TM2 with TM3 (Fig. 5.13a), where snow has highest reflectance (cf. Fig. 4.13a). In this enhanced image sun-lit snow is much brighter than ice and can be classified by a certain threshold (depicted yellow in Fig. 5.13c). Since snow in shadow is much brighter in TM1 than all other surfaces in shadow (Dozier, 1989), snow has a characteristic bluish colour in TM321 composites. In order to utilize this for snow mapping, a ratio image from TM1 / TM2 (Fig. 5.13b) is used with a threshold around 3 to map snow in shadow (red in Fig. 5.13c). In Fig. 5.13d the region is displayed in a TM321 composite image for comparison.

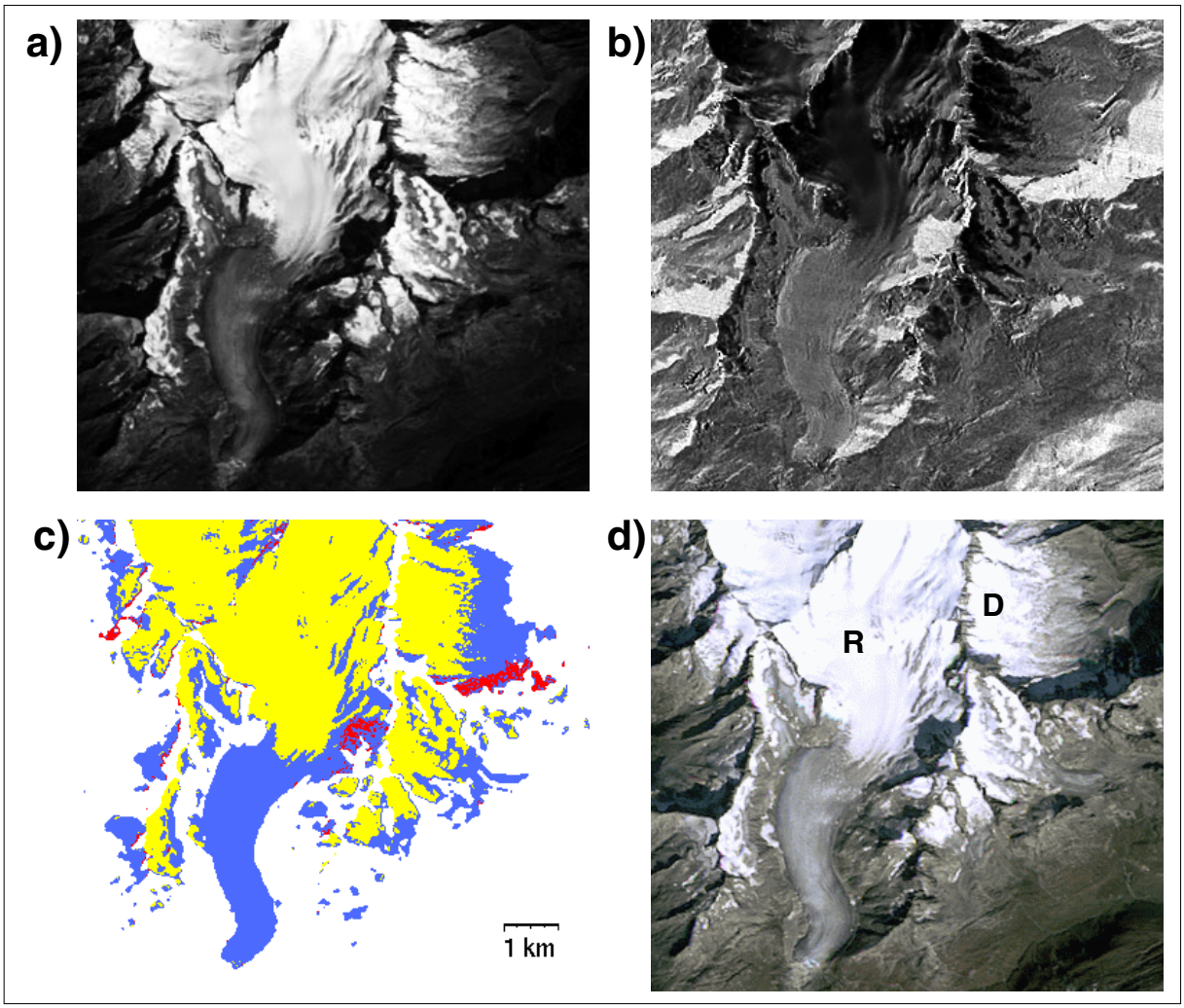

Figure 5.13: *Snow cover mapping with a) a TM2 * TM3 image (sunlight) and b) a TM1 / TM2 image (shadow) reveals c) snow in sunlight (yellow) and shadow (red), d) shows TM321 for comparison. The region is 9.2 by 8.5 km in size and shows Rhoneglacier (R) and Dammaglacier (D).*

Both methods are applied only within regions classified as glacier. While most of the fine spatial snow details are mapped, regions tilted away from the sun are completely missed. The regions in shadow are only small in this example, but may be larger elsewhere (see Fig. 5.15a). It must be noted that even manual delineation is sometimes not able to distinguish between snow and ice (e.g., Dammaglacier, 'D' in Fig. 5.13d). For these regions the method proposed here is at least consistent. For calculation of AAR statistics, only glaciers with an appropriate snow classification should be considered.

As mentioned previously, the major problem of glacier classification is to find satellite scenes without snowfields connected to glaciers. While Internet-based analysis of quicklooks from FCCs gives some hints on snow conditions, the quicklooks are too small for a clear decision in doubtful cases. Moreover, distribution of snow at the end of the ablation season (or at the time of the best available image) can exhibit a strong spatial heterogeneity, as its amount is influenced by the prevailing wind direction during winter. As a consequence, two TM scenes from Sep 1999 (#3 and #5) were hampered by bad conditions to the north of the rivers Rhine and Inn, but have much better (Rheinwald) to even favourable (Upper Engadin) conditions for glacier classification to the south of both rivers (see example in App. 3.2-2).

In order to remove snowfields outside of glaciers which are only present in a single year, two methods are applied. For Landsat path 193 the three classified scenes from 1999, 1992 and 1985 were used to form a RGB composite. In this composite the 1999 extra snow has a distinct colour (cyan) and can be removed from the 1999 map (Fig. 5.14). This method was firstly tested in a part of the southern Tyrolean Alps (Paul, 2002b) and applied here to another part of the same TM scenes. For path 194 only two scenes from 1985 and 1999 are available. Isolated snow patches in 1999 (not connected to 1985 snow/ice) are removed with the same method as used for the isolated debris areas (see 5.2.2). However, many glaciers have to be excluded from further analysis, as snow cover hides larger parts of the glacier perimeter.

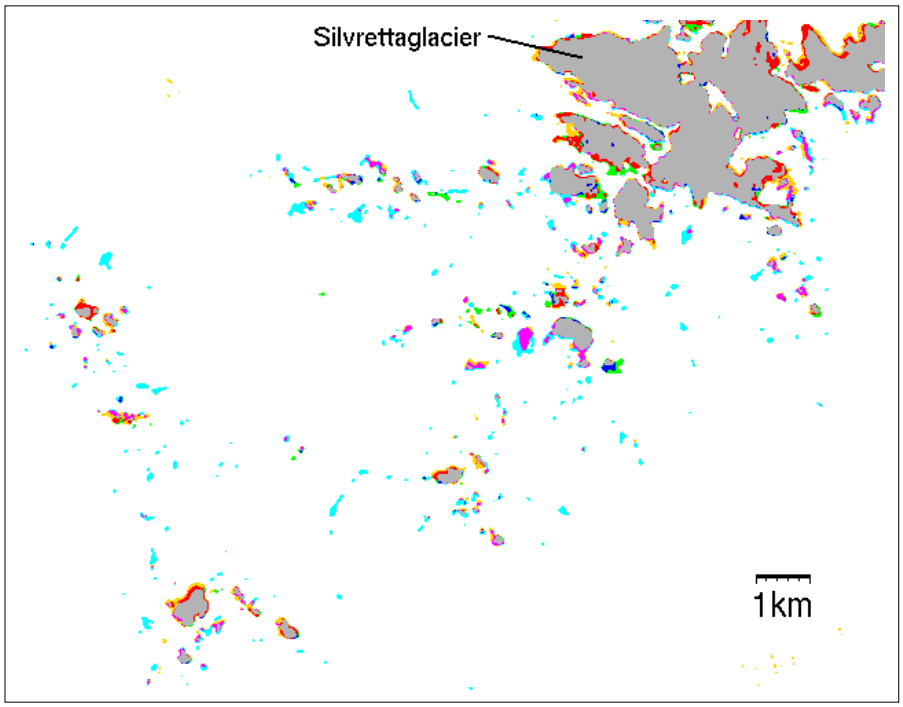

Figure 5.14: *Classifying snow patches in the 1999 scene (cyan) by multi-temporal overlay of glacier maps (1999, 1992 and 1985 as RGB) in a region to the southwest of the Silvretta group (cf. App. 3.2-2). Yellow is changed to orange for better visibility. See text for discussion.*

In the case of summer snowfall, the snow will melt away on glacier-free terrain rather quickly, while new snow persists much longer on glaciers. Due to the 'whitening' effect of the snow the visibility of the TSL can be very bad. Moreover, nine days of snowmelt can change bad into good glacier classification conditions, for example in the Bernina group from 21 to 30 Sep 1985 (cf. App. 3.2-3). During that period classification conditions were favourable in the south-eastern part of the Austrian Alps (Carinthia), as the 'photo glacier inventory' from Lang and Lieb (1993) clearly demonstrates, but became more difficult to the west.

5.3.3. Accuracy of snow-cover maps

The method described above is not able to map snow covered areas tilted away from the direction of solar illumination. Snow areas facing towards the sun are somewhat too large. The 'snow in shadow' method often maps the entire region in cast shadow and also crevassed areas. While the former are restricted to the glacier perimeter by the glacier map, there is no real correction for the latter. A median filter may remove these erroneous pixels, but all fine spatial details (characteristic for snow-cover) are also removed. An illumination dependent threshold may improve classification of sun-lit snow, but incorporation of a DEM is necessary. Two more examples of snow classification are given in Fig. 5.15, showing the upper part of 'Grosser Aletschgletscher' to the left and the Keesjen- / Kaltwasserglacier to the right.

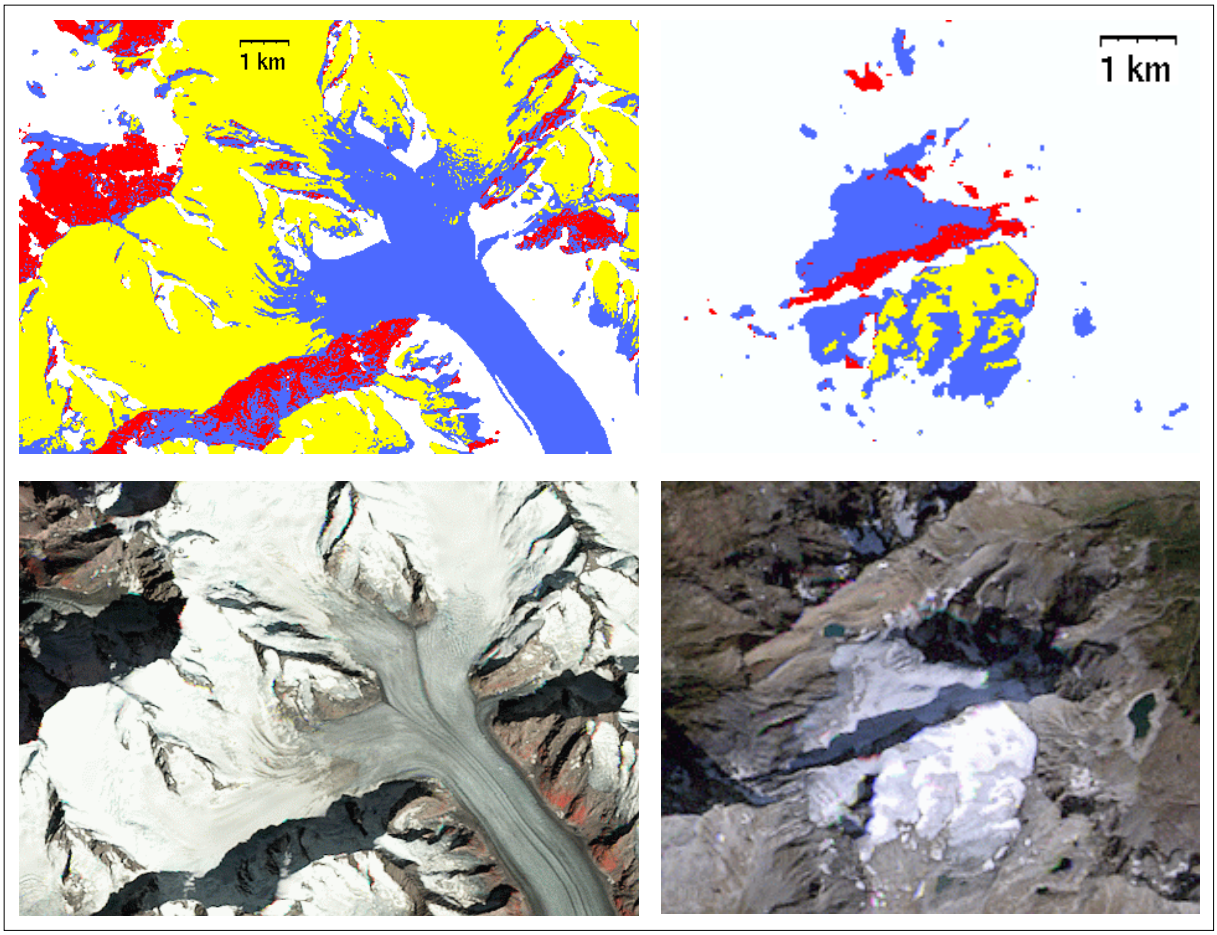

Figure 5.15: *Top row: Snow classification (see Fig. 5.13c for colours) for 'Grosser Aletschgletscher' (left) and Keesjen- / Kaltwasserglacier (right). Bottom row: RGB-composites for comparison.*

5.4. General assessment of accuracy

5.4.1. Comparison with higher resolution data

The accuracy of the TM-derived glacier outlines is assessed by means of a comparison with manually-derived outlines from higher-resolution satellite imagery (pan bands from SPOT: 10 m, IRS-1C: 5 m and Ikonos: 1 m). In order to obtain useful results, snow conditions should be similar in both images. Interpretation of pan bands from SPOT and IRS-1C is enhanced by IHS fusion with TM bands 1, 2 and 3. In the case of debris-covered glaciers, the two outlines obtained are not independent, as the manually-derived outline needs to be adjusted to the TM-derived outline. Otherwise comparison between the two data sets is not possible.

SPOT

TM scene #8 (15 Sep 1992) and SPOT scene #11 (17 Sep 1992) are used for this comparison. Both scenes share a small strip from which a test region to the south of the 'Nufenenpass' is selected, including the Gries (G), Hohsand (H), Cavagnoli (C) and Basòdino (B) glaciers which are depicted in Fig. 5.16. For 28 glaciers in this area, outlines were derived manually from SPOT (blue in Fig. 5.16) and automatically from TM (red).

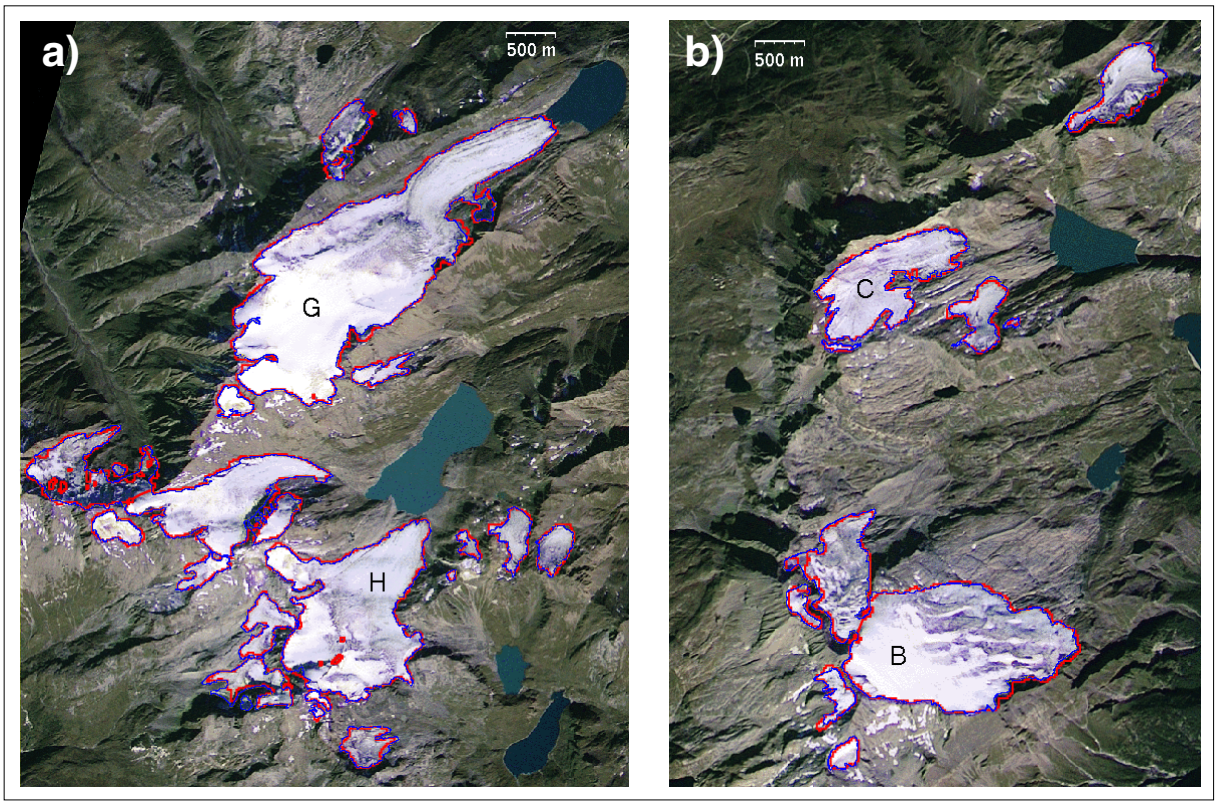

Figure 5.16: *Overlay of outlines digitized manually from SPOT (blue) and automatically from TM (red) on a fused SPOT pan / TM image as background. a) Showing Gries (G) and Hohsand glacier (H) and b) with Cavagnoli (C) and Basòdino glacier (B). SPOT data: © SPOTIMAGE.*

On average, the areas derived manually from SPOT are 1.7% smaller compared to those derived form TM (σ = 8.4%). As the value for σ is larger than obtained from the theoretical assessment (comparing 10 m and 25 m resolution), the deviation cannot be the result of the differing image scales. Moreover, the error is not from TM either, since area difference does not depend on glacier size (r=-0.03). Thus, the manual glacier delineation must be responsible for the differences, in particular the false interpretation of snow fields and rock outcrops.

IRS-1C

A subset (Mischabel test region) of IRS-1C scene #14 (20 Sep 1997) with 5 m spatial resolution is resampled to 10 m and fused with the same subset from TM scene #10 (31 Aug 1998). Manual glacier delineation is performed for about 30 glaciers. In Fig. 5.17 the overlay of glacier outlines (yellow: manually derived, red: obtained automatically from TM, black: from the digitized inventory of 1973) is shown for the tongue of the 'Findelengletscher' and some small glaciers facing north. The fused image is used as background in Fig. 5.17a and a TM 543 composite in Fig. 5.17b. Debris-covered glacier areas are not mapped with TM (white arrow), but manual glacier delineation is problematic as well, because correct interpretation of rock outcrops is difficult (black arrow). Since there was also some glacier retreat between 1997 and 1998 (in other regions), a quantitative error assessment is not carried out.

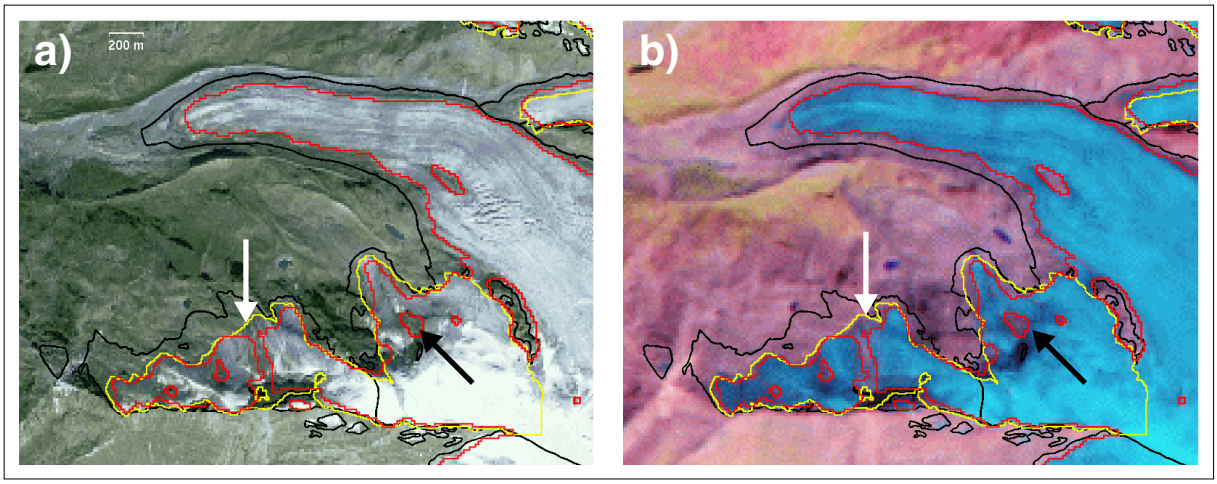

Figure 5.17: *Overlay of glacier outlines covering the lower part of the 'Findelengletscher' (Mischabel test region) from the digitized inventory in 1973 (black), from IRS-1C in 1997 (yellow) and from TM in 1998 (red). The fused TM / IRS-1C image is used as background in a) and a TM543 composite image is the background for b). The arrows indicate larger differences.*

Ikonos

Most of the glaciers in the Ikonos scene from 17 Sep 2000 (#16) cannot be used for outline delineation, because snowfields hide the glacier perimeter. At least six small glaciers within the scene are selected for manual delineation. The glacier in Fig. 5.18 is 0.23 km^2 in size and is shown together with the outlines from the digitized glacier inventory of 1973 in white, manually-derived outlines from Ikonos in blue and automatically-derived outlines from TM scene #10 in yellow. From Fig. 5.18a (overlay with Ikonos), it is obvious that debris-covered glacier areas were not (or only partly) mapped with TM (white arrows), which is also confirmed in Fig. 5.18b (overlay with TM543 composite) showing some bluish pixels outside the mapped perimeter. Apart from that, the overall correspondence with the Ikonos outline is satisfactory.

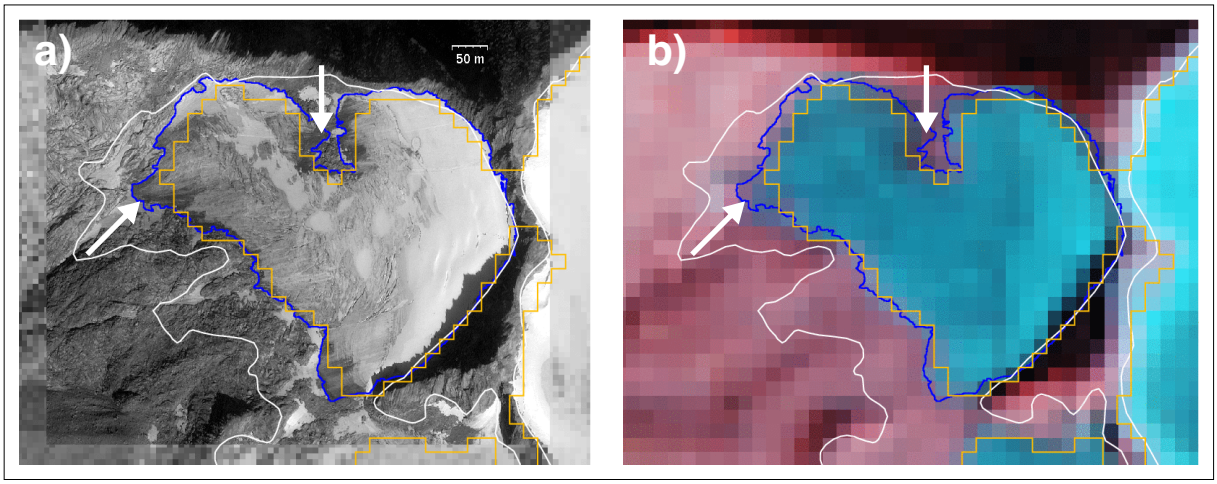

Figure 5.18: *Overlay of outlines from the digitized glacier inventory from 1973 (white), from Ikonos (blue) and from TM (yellow). a) The Ikonos image as background, and b) a TM 5, 4 and 3 (as RGB) composite image as background. Ikonos data: © SpaceImaging Europe / NPOC.*

Area values for the six selected glaciers are listed in Table 5.2 together with the relative differences in area. The average difference for the uncorrected outlines is -3.7% but with a standard deviation of 10.7%. This indicates again underestimation of TM-derived areas if no correction for debris-covered regions is applied. The outline comparisons for glaciers #2 and #3 are shown in App. 3.2-7.

Glacier	1	2	3	4	5	6
Size 1998 TM [km^2]	0.235	0.842	0.379	0.106	0.229	0.103
Size 2000 Ikonos [km^2]	0.231	0.885	0.334	0.087	0.207	0.112
Size difference [%]	-1.7	+4.9	-11.8	-17.9	-9.6	+13.8

Table 5.2: *Comparison between glacier areas derived from Ikonos and from TM.*

5.4.2. Summary of error sources

Snowfields and cast shadow

Snow fields adjacent to glaciers can hide the real glacier perimeter and will lead to large errors in glacier size. Such areas are removed by the glacier basin vector layer (see 6.3.2) if they are obvious (interactive adjustments) or glaciers are not considered if the separation is unclear. Snowfields outside of glaciers can be reduced by multi-temporal analysis (using sequential images) if they are large enough or by the median filter if they are small. Rock outcrops in cast shadow are wrongly mapped as glacier if they are surrounded by a large amount of pure snow (adjacent illumination). Corrections are applied from the digitized 1973 glacier outlines, which are transferred to the glacier basin vector layer. Only very pure glacier ice or snow is mapped correctly as glacier if located in cast shadow. The threshold for the ratio image is most sensitive in these areas. If visual inspection reveals wrong outlines, these glaciers are not considered for statistical analysis.

Debris-cover

Debris cover on a glacier is by far the largest error source. After manual editing of the semi-automatically-derived debris-covered regions improved glacier outlines result. Additional manual editing will reveal even higher accuracy. However, for smaller glaciers some pixels within the glacier perimeter might not be included and the derived glacier areas are somewhat too small. The change in area due to wrongly-classified perimeter pixels (in the ablation area), may reach 5% of the total area with values increasing as the glaciers get smaller.

Threshold and median filter

The threshold value used for glacier classification is quite robust, apart from glacier areas in cast shadow. Selection of the threshold parameter should be performed interactively to obtain best results. The relative change of glacier size due to the median filter is small (below 1%) if glaciers are larger than 0.1 km^2. For smaller glaciers the relative change can be much larger, but in such cases glaciers can be excluded from statistical analysis. Since the filter considerably reduces misclassification (noise), it is applied to all glacier maps after classification.

Column shift and resampling

The TM5 'band-to-band misregistration' is not corrected, as most small snowfields outside of glaciers are removed due to the shift. Glacier classification in cast shadow is somewhat more incorrect, but in severe cases glaciers are rejected. The resampling method used (prior to classification) influences mostly perimeter pixels and visual inspection reveals no superior method. Hence, cubic convolution is used as a compromise.

Pixel size

The synthetically-scaled glacier outlines (to larger pixel sizes) indicate little change in glacier area for pixels between 5 and 30 m on one side, unless glaciers smaller than 0.1 km^2 are compared. This enables accuracy comparisons with higher-resolution satellite data, as well as comparisons of TM-derived glacier areas with the digitized inventory data.

Accuracy in total

The accuracy of the TM-derived areas for individual glaciers or glaciers of a larger sample is difficult to estimate, since errors depend on glacier size and are rather random for glaciers with manually edited debris cover. As a rule of thumb, the accuracy of the derived areas for individual glaciers is estimated to be better than 5% for clean ice and glaciers larger than 0.1 km^2, and better than 10% for debris-covered or glaciers at least larger than 0.02 km^2 (about 30 TM-pixels). For a large sample of glaciers (more than 100) the accuracy of the derived total area should be better, as individual positive and negative deviations are summarized. Depending on the sample used (number of glaciers in total and per area class), the relative accuracy should be better than 3%.

6. GIS

6.1. Introduction

6.1.1. GIS definition and basic terms

The use of Geographic Information Systems (GIS) for spatial data handling has intensified strongly during the past decade, mainly due to increased speed and memory of computers. The GIS applications used for the SGI 2000 are covered in the books by Burrough and McDonnell (1998), Jones (1997) and Longley et al. (1998). The definitions of the term GIS are manifold, one was given by Walsh et al. (1998): "A GIS is capable of data capture, storage, management, retrieval, analysis and display." It integrates spatial and thematic data by means of geocoded data layers and associated information stored in attribute tables.

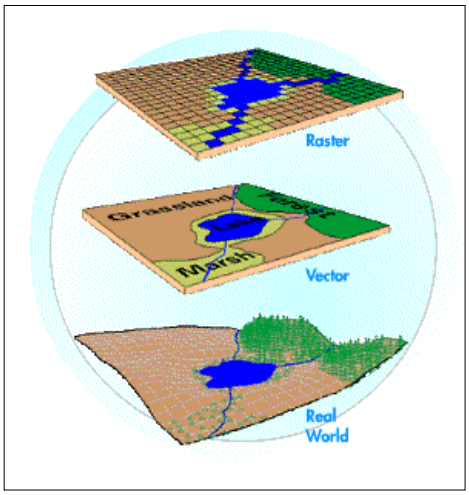

The source of each data layer can be a digitized map of a distinct theme or a classified image (e.g., from a satellite) or a scanned map (e.g., from a field survey), both of a specific theme. While the latter two denote information storage in raster format (on a cell by cell basis) with a constant grid spacing (or sample lag), the former contains only the boundary of a specific entity in vector format (cf. Fig. 6.1). While the vector format has preferences in storing discrete items (their boundaries), the raster format is better for storing continuous fields, such as elevation values of a DEM.

Figure 6.1: *Representation of real world objects in the vector and raster domain (from UniAZ, 2002).*

6.1.2. The GIS Arc/Info

While the information about the discrete x/y position of each point (*vertex*) of a vector element (*arc*) is stored in a special database that is not directly accessible for the user, the attribute information of each element (i.e., point, line, polygon) is available and can be manipulated. Within Arc/Info each polygon, for instance, has its area and perimeter, as well as an internal (unique) and user definable identification number (ID) stored in a polygon attribute table (*pat*). Manipulations of the *pat* include the extension to other fields (items) by spatial

combination (e.g. *intersect*) with another vector layer (*coverage*) holding different *pat* entries or the inclusion of external tables by a link to a specified item of the *pat* (e.g., the ID), which is common to both tables (*joinitem*). To attain full data complaisance, raster-vector conversion (and vice versa) is possible within most GIS. Queries and selections of special values of one or more items from the *pat* allows retrieval of additional information to specific questions. Hence, a GIS can be used not only as a visualization tool; the attractive display of all data is of course also possible. Table 6.1 summarizes some naming conventions of Arc/Info.

Theme	satellite imagery	glacier boundaries	label-coordinates
Source	TIF - file	digitizing	ASCII table
Type	raster	vector	vector
Arc/Info	grid or lattice	polygon coverage	point coverage

Table 6.1: *Overview of data types, sources and naming conventions in Arc/Info.*

Arc/Info program modules

The modules used are listed together below, followed by a short description:

- Arc/Info: Hybrid system with the components *Arc* to run *coverage* specific commands and all other modules and the database *Info*, which manages all spatial information (*vertex* coordinates and topology) and the entries of the attribute tables.
- AML (Arc Macro Language): Allows the storage of individual commands in a script, with access to all modules, to the system level (running UNIX commands or other programs) and the attribute tables. It is also possible to run loops to process many *coverages* with the same commands in one script.
- *arcedit*: For creation, display and editing of *coverages* (digitizing, overlay, error correction).
- *arcplot*: Creation and visualization of maps from various sources in 3D perspective views.
- *grid*: Module for processing of raster data, which have to be in grid-format.
- *tables*: Interface for export of data from attribute tables to columnar ASCII files.
- ArcView: additional ESRI software package used for visualization of spatial data (overlay of vector and raster data). Allows also database queries on attribute table items and their visualization as well as digitizing and spatial modelling.

Description of mainly-used commands

Vector - raster data conversion is performed with:

- *asciigrid*: creation of grids from data tables (e.g., DEM elevations), requires a special header for geolocation;
- *imagegrid/gridimage*: conversion of image data (tif-format) to grid format and vice versa, assigns a *grid-code* and needs a 'tfw' (tif world) file for geolocation;
- *gridpoly/polygrid*: uses the perimeter of all entities to assemble polygons, the *grid-code* is transferred to the *pat*, for later selection according to its value.

Fusion of polygon coverages with other coverages comprised of polygons, lines or points:

- *intersect*: the intersect *coverage* must have polygon topology, the other can consist of:
- polygons (e.g., glacier outlines intersected with ice divides);
- lines (e.g., cutting central flow lines with glacier boundaries of a distinct year);
- points (e.g., assigning WGI-codes or other items to individual glaciers).

Calculation of statistic parameters for specific zones (glaciers) according to a *value grid*:
- *zonalstats*: gives minimum, maximum, range, mean, median, standard deviation (σ), and some other for each zone of the *zonal grid* from the underlying *value grid*.

Landscape visualization in perspective views (draping raster or vector data over a DEM):
- *surfacedrape*: Besides other parameters, observers position, viewing direction and field of view can be selected. The resolution of the satellite image determines the resolution of the final view, independent of the DEM resolution.

Other commands:
- *reselect*: creating new coverages according to distinct selections from the attribute table;
- *joinitem*: used to append attribute tables of one *coverage* to another coverage, according to an item which is present in both data sets.

6.2. The digitized Swiss glacier inventories of 1850 and 1973

6.2.1. Previous work

The last Swiss glacier inventory was compiled from aerial photography taken in Sep 1973 (Müller et al., 1976). The interpretation of the photos was carried out by stereo-photogrammetry and the glacier boundaries were transferred to topographic maps at a scale of 1:25000. These boundaries are shown in Fig. 6.3a (black lines), together with the transient snow line (TSL) in red for part of the Weissmies test region. In September 1973 favourable conditions for glacier mapping were present (only few snowfields connected to glaciers), allowing precise determination of the glacier perimeter without obscuring snow cover. The delineation of the TSL was much more difficult, because the TSL was situated in the accumulation area of the glaciers, also showing firn from previous years with a similar albedo (Gross et al., 1976). However, the elevation of the TSL is listed in the inventory of 1973 for most glaciers, since its value quite closely resembles the ELA in that year (Müller et al., 1976).

A homogenous reconstruction of glacier outlines in 1850 was carried out by Maisch (1992) for glaciers of Grisons and surrounding mountains. Maisch used the 'Siegfried map' series showing glacier extent around 1850 and special field surveys to deduce the former glacier extent from ancient moraine ridges and other evidence. The reconstructed outlines available from about 1850 were transferred to transparent paper (black in Fig. 6.3b), together with the outlines from 1973 (blue) and additional data. Glacier parameters were obtained from analogue techniques such as planimetry.

In a first attempt at transforming glacier outlines to GIS-based vector layers, Benz (1995) digitized 1973 outlines for a certain part of southwest Switzerland. Later, the data set was extended by Wipf (1999) to all glaciers north of the Rhone River. Both authors also digitized reconstructed glacier outlines from 1850, the corresponding elevation contour-lines of 1850 and 1973, and the central flow lines for each glacier. They calculated numerous 3D glacier parameters automatically by means of AML programs from their input data sets.

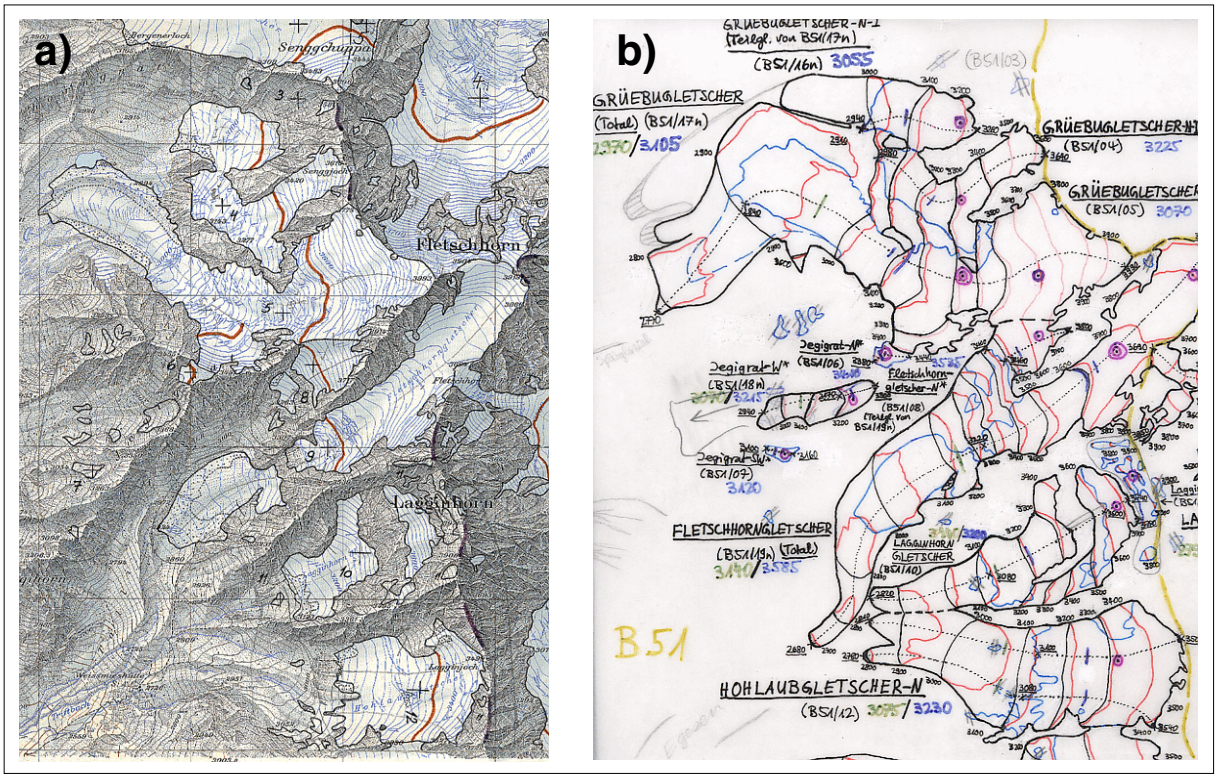

Figure 6.2: *a) Glacier inventory map for a part of the Weissmies test area, showing 1973 glacier outlines (black) and TSL (red), grid spacing is 1 km. Base map 1309 © swisstopo. b) Reconstructed glacier outlines from 1850 (black), 1973 (blue) and 100 m elevation contours (red) on tracing vellum.*

The work of Benz (1995) and Wipf (1999) was extended to all Swiss glaciers within the Swiss national science foundation project NFP31 and published by Maisch et al. (2000). This work also includes a reassessment of the inventory from Müller et al. (1976), an extended morphological classification scheme for all glaciers and their retreat characteristics, and a thorough statistical analysis of all data, their interdependencies and spatial distribution. Scenarios of future glacier development based on given climate-scenarios are also included.

6.

The reassessment of Maisch et al. (2000) encountered problems for groups of glaciers (mostly very small) with a single ID and a summarized area in the 1973 inventory of Müller et al. (1976). Moreover, glaciers that split up between 1850 and 1973 or vanished until then have to be considered individually. As a consequence, new glacier IDs were formed, glaciers were sorted into individual, total or part of a glacier, and special selections were made to account for data availability. For instance, it was not possible to reconstruct the 1850 glacier outline for each glacier of the 1973 inventory, hence the area change between 1850 and 1973 was calculated for 1640 glaciers only (from total 2244).

Glacier inventory data was also compiled for many other parts of the world from aerial photography during the 1970s and 1980s, but digital glacier outlines are not reported (IAHS, 1989). The new Austrian glacier inventory will provide such digital outlines as well as updated glacier elevation contour lines for the creation of new DEMs. Comparison with DEMs derived from 1969 contour lines will reveal glacier volume changes during the last 30 years (Würländer and Eder, 1998; Würländer and Kuhn, 2000). Useful rules for digitizing of glaciers and a general discussion of a database structure related to glacier change studies were provided by Mennis and Fountain (2001) and also for the GLIMS project (GLIMS, 2002).

6.2.2. Digitizing of glacier outlines

The inventories by Müller et al. (1976) and Maisch (1992) contain an appendix with black and white illustrations of the spatial extent of each larger glacier at a scale of approx. 1:150000 (including ice divides between connected glaciers), but the maps are available only in printed form and it is very difficult to follow glacier changes since 1973. In order to visualize and measure ongoing glacier changes more efficiently, all glacier outlines (1850, 1973 and central flow lines) are digitized, serving now as a digital base map for ice-divides and comparisons with former and future (satellite-derived) glacier geometries. The digital inventories by Benz (1995) and Wipf (1999) are used as a starting point and their digitizing rules are continued, apart from elevation contour-lines.

In short, the procedure is as follows:

- Geocoding of the 1:25000 map with the 1973 glacier outlines until the RMSE is below 5 m.
- Running an AML script with all settings (minimum *vertex* distance, tolerances, *snap* distance, name of coverage, etc.).
- Digitizing of glacier outlines: start/end with a *node* for each *arc* and a *node* at each point where an *arc* starts/ends that is shared by another glacier.
- Super-position of the tracing vellum (cf. Fig. 6.2b) with 1850 glacier extent and digitizing of outlines and flow lines.
- Saving and copying all vector layers and editing of *node errors* (open ends).

The general digitizing rules are:

- the entire map should be digitized in a single session, each glacier in a single pass;
- all boundaries from nunataks and each glacier with a label on the map is digitized;
- no generalization is done at this stage;
- no preferred direction for circulating the glacier outline;
- in the case of ambiguities (groups of glaciers, outline), digitizing is performed according to the glacier outlines on the tracing vellum;
- digitizing of glacier outlines at map borders (open ends) are completed with a node;
- central flow lines are crossed with their 1850 outlines, additional 1973 flow lines are digitized in the case of a changed geometry or a splitting of a glacier.

Digitized glacier outlines and central flow lines are displayed in Fig. 6.3 for the Mischabel test region. Digitizing of the glacier outlines from 1850 (blue in Fig. 6.3) is only done for regions outside the 1973 extent. The 1850 outlines are combined with the 1973 outline (black in Fig.6.3) to create an intersection. For larger glaciers, outlines from 1850 and 1973 can run in parallel along the glacier for a longer distance and come in contact many times. After intersection of the 1850 outline with the 1973 polygons, a large number of '*sliver polygons*' can result and careful inspection has to reveal the original outline. In addition a smaller perimeter of island polygons (rock outcrops) in 1850 requires accurate control. Central flow lines from 1850 and 1973 are depicted in red in Fig. 6.3. The digitized 1850 and 1973 glacier outlines for the entire perimeter of Switzerland are shown in two parts in App. 3.2-12 and 3.2-13.

Before creating topology (defining the neighbourhood relations of each glacier polygon), all node errors have to be removed. This is performed with ***build***, because ***clean*** has a tendency to generalize arcs. All node errors can be visualized on screen using ***editfeature (ef) node errors*** in *arcedit*. The correction process includes connection of adjacent nodes at map boundaries or as a result of undershoots (starting node has not snapped automatically to the ending node of an arc) using ***ef node*** and ***move***, and of overshoots (resulting in an intersection with an arc) using ***ef arc***, ***sel many*** and ***delete***.

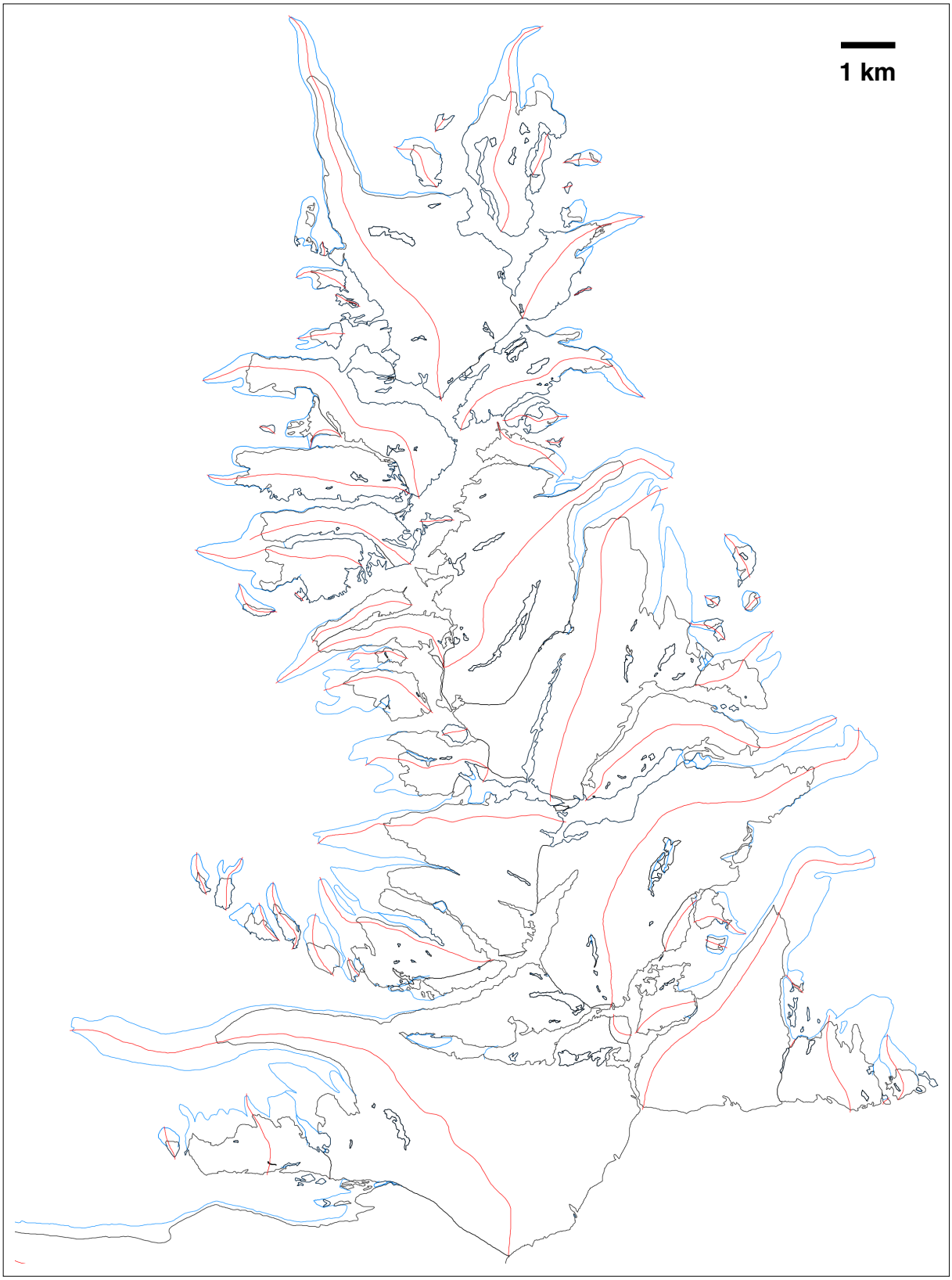

Figure 6.3: *Illustration of digitized glacier outlines from 1850 (blue) and 1973 (black) as well as central flow lines (red) for the Mischabel test region (cf. Fig. 7.2).*

6.2.3. Accuracy of glacier digitizing

The digitized glacier outlines may be incorrect for the following reasons (from largest to smallest errors): (1) wrong outlines on the original topographic maps, (2) inaccurate digitizing, (3) insufficient geocoding of the maps.

Point (1) will cause the largest deviations but (hopefully) only for very few glaciers. For the Morteratsch glacier (Upper Engadin, Grisons) such an error has been detected by chance, as the 1973 outline at the terminus has nearly the same position as in 1997, although the glacier has retreated about 300 m. In this case, a wrong transfer from or interpretation of the original 1973 aerial imagery may have caused the difference. This error has not been corrected, as length change is not obtained for this glacier and the area change is less than 0.2 km^2.

Inexact digitizing (2) can have various sources: (a) positional shifts during cross-hair cursor-tracking, (b) generalization of fine details, and (c) the number of *vertices* used for a line. As digitizing has been performed by five different persons, each with a different performance, an overall error is difficult to determine. However, a comparison of areas from about 100 glacier polygons digitized twice by one person and a second time by another person is depicted in Fig. 6.4a (see App. 3.2-15 and 3.2-16 for outlines). The average relative difference is 2.5% (σ=10%) in both cases, with most values between ±5% for polygons larger than 0.1 km^2. An example of a small glacier which is digitized four times by chance is displayed in Fig. 6.4b. The areas are (in m^2): black=13959, red=14784, green=13991, and blue=14621 with σ = 368.5 m^2 and a highest difference of 5.9%. A first comparison of glacier areas derived from digitized outlines and planimetrically reveals: in average digitized glaciers are 1.7% larger (σ=3.6%) without a dependence on glacier size (r=0.11). However, the set has been restricted to glaciers with area differences of less than ±10%, as some of the glaciers used may not be fully identical.

The least critical point (3) is geocoding of the maps prior to digitizing. Although some of the 1973 maps show a tendency to disintegrate (like small glaciers), the RMSE obtained from four control points was in general below 5 m. Somewhat less accurate (±10 m) is the geodetic control of the 1850 outlines from the tracing vellum by interactive matching. However, positioning is in general sufficient, as digital overlay of the 1850 outlines reveals (e.g., Fig. 6.3 and 7.1).

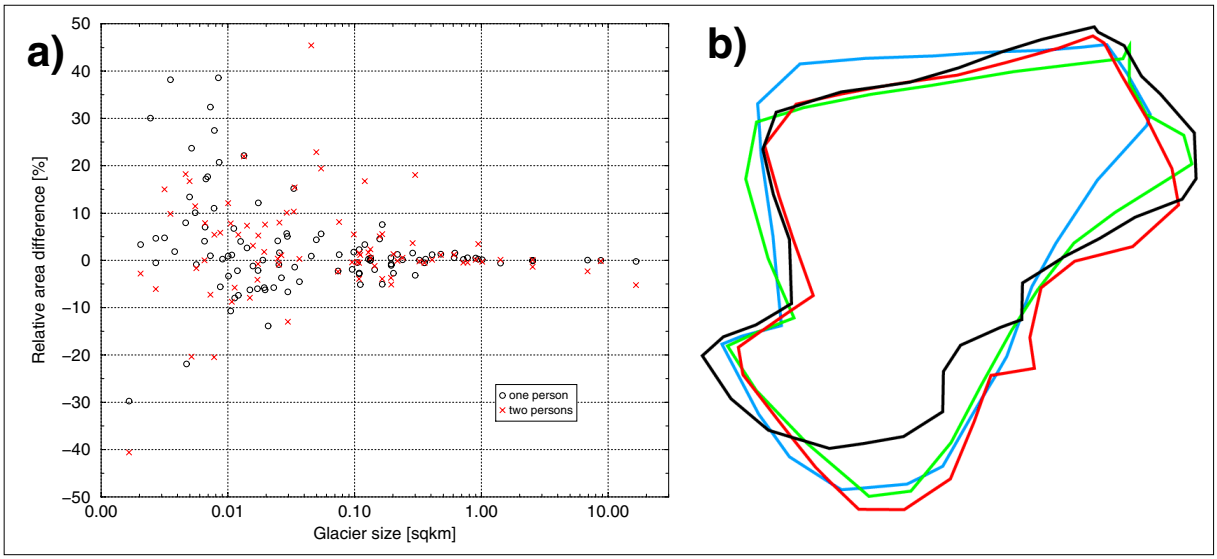

Figure 6.4: *a) Comparison of glacier areas digitized twice by one person (circles) and from a second person (crosses). b) A small glacier (0.014 km^2) digitized four times by chance (see text for areas).*

6.3. Integration of TM-derived glacier maps into the GIS

6.3.1. The glacier outline vector layer

TM-derived glacier maps are finally stored as a black ('glacier') and white ('other') images in TIF format (Fig. 6.5a). From the entire TM scene, only the part with glaciers is exported and for Arc/Info integration, coordinates of the upper left pixel corner (in units of the Swiss geodetic map projection) as well as pixel size (25 m) are stored in a separate file with the extension 'tfw' (e.g., 25.0 0.0 0.0 -25.0 545000.0 210000.0).

The conversion of the tif-image to a glacier vector layer is performed in three stupefied. 6.5):
(1) *imagegrid* name.tif gr, (2) namegr = *setnull*(gr ==1, gr) and (3) *gridpoly* namegr name.
The *setnull* command is required to assign the 'no data' flag to all areas outside and also to island polygons inside of glaciers (App. 2.2-2). In the *pat* of the glacier *coverage* (name) all polygons have an item '*grid-code*', which equals 0 for glaciers and 1 for other, depending on the assignments of the image used. As visible from Fig. 6.5, contiguous ice masses have to be divided into the individual glaciers before data retrieval makes sense. This is done by intersection with a vector layer of glacier basins (see the next paragraph).

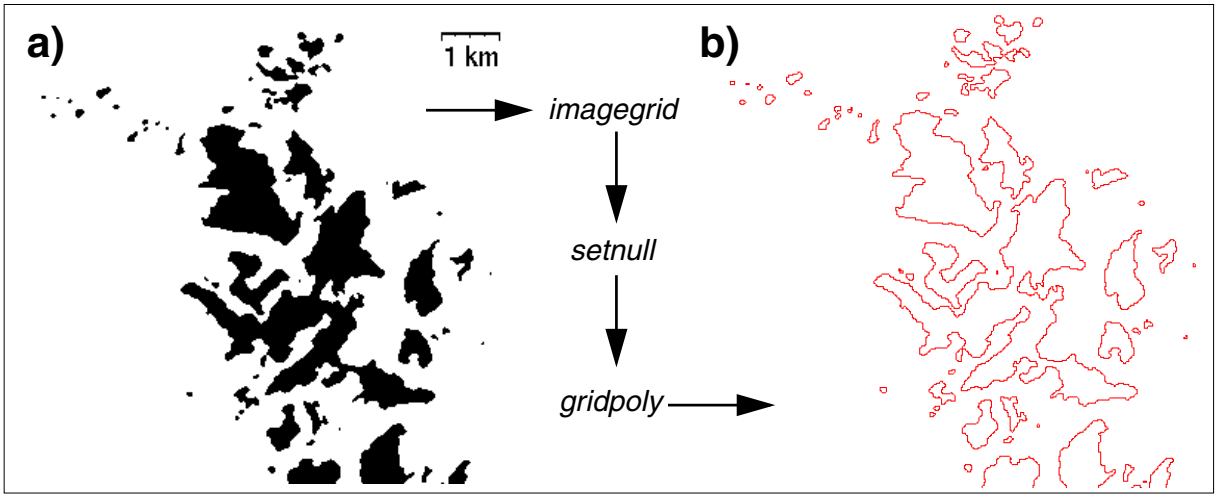

Figure 6.5: *a) Glacier map for the northern part of Weissmies test region from TM (raster image), and b) resulting vector layer showing the boundary between black and white pixels.*

6.3.2. The glacier basin vector layer

In order to separate connected glaciers in the classified TM image according to their 1973 boundaries, the ice divides between them have to be defined. This is done by on-screen digitizing of a glacier basin vector layer in *arcedit* using the digitized Swiss glacier inventory and the outlines or filled areas from the classified TM images (composite of available years) as background (Fig 6.6). In case of any ambiguities about the location of the basin outline, a sat-

ellite image is used additionally. Ice divides are transferred without modification from the digitized inventory using *ef arc, sel many* and *put* and extended to a closed polygon roughly surrounding the glacier. Isolated glaciers are also encircled by closed polygons. The thick blue lines in Fig. 6.6 represent these glacier basin polygons. They are shown together with the digitized 1973 glacier outlines (red), the final (after debris-cover correction) 1998 glacier outlines (green) and labels (yellow dots) for glaciers that have been selected for calculation of area changes. With these pre-defined glacier basins it is also possible to assign an unique ID to groups of glaciers (see 6.3.3).

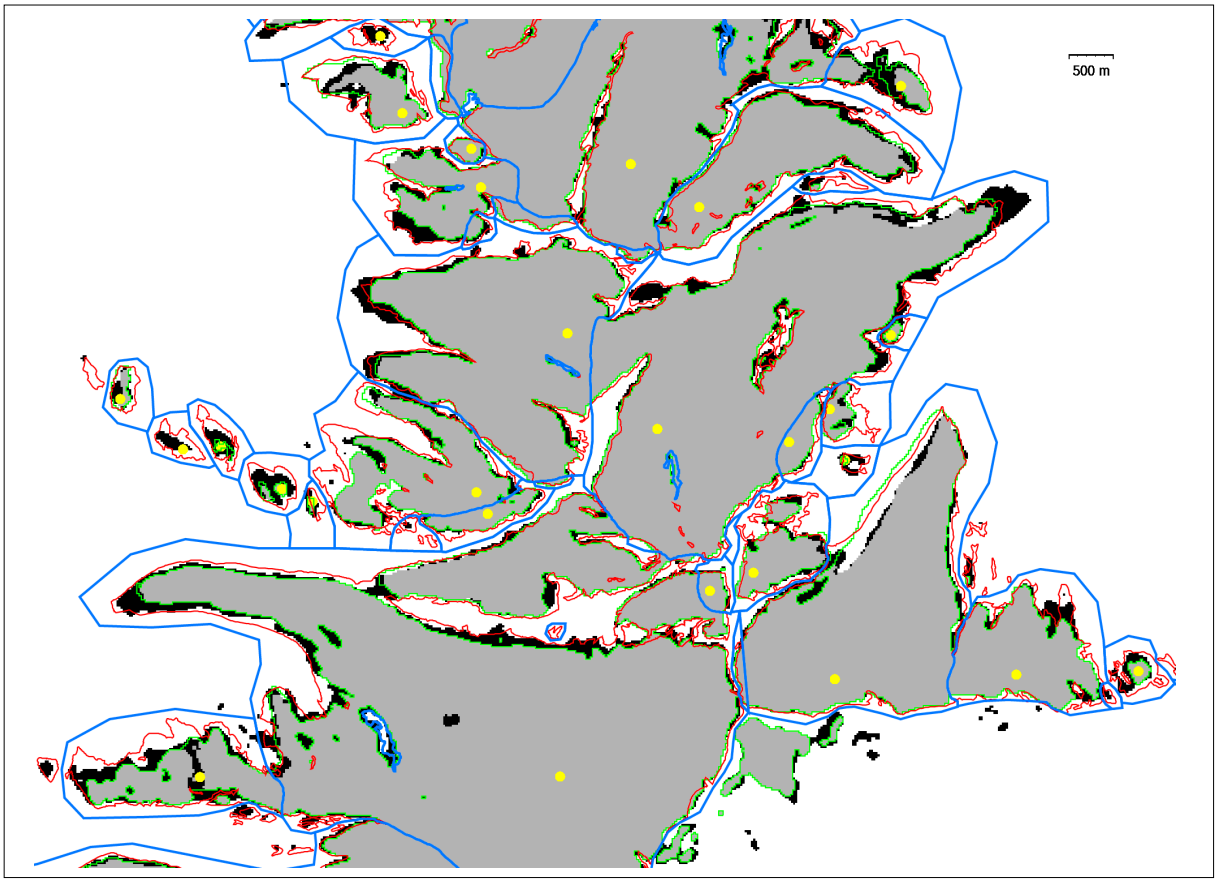

Figure 6.6: *Digitized glacier basins (blue) for the southern part of the Mischabel test region, with the digitized 1973 inventory (red), TM-derived glacier areas in 1985 (grey and black areas) and 1998 (grey areas), and final 1998 outlines (green). Yellow dots denote glaciers selected for the SGI 2000.*

The manual digitizing of glacier basins is facilitated by accurate orthorectification of the satellite images, as the same glacier basin vector layer can be used for each image. Sometimes a shift of one pixel between two images is enough to prevent separation of glaciers with the same basin. However, if differences are small enough a compromise is made for the dissection line. Otherwise (e.g., in the case of snow fields) a modified basin vector layer is used.

For quick assessments of glacier changes in small areas (about 50 by 50 km) the basin vector layer can also be created for non-geocoded images (Paul, 2002b). This is useful if DEM data or a digitized glacier inventory are not available and no further analysis (glacier parameters from DEM) is performed. The relative displacement between Landsat images from sequential years (same path and row) can be evaluated from a few control points to perform a relative image matching. Next GIS processing can be handled in the same way as for the SGI 2000.

Glacier separation with time

At this point a comment on the temporal evolution of glacier areas must be given: Glacier changes between 1850 and 1973 can be tracked from the digitized inventories and Landsat TM imagery covers the time since 1985. In both time intervals, glaciers shrank by means of retreat and partly by separation from formerly connected tributaries (larger glaciers) or disintegration (smaller glaciers). Since area change depends mainly on glacier size, it is glaciologically incorrect to track changes by using just the sum of all glacier parts.

On the other hand, disintegration seems to be a typical element of glacier behaviour in the last decades and may also intensify in the near future. As a compromise, glacier extent in 1850 is not considered as a basis for the SGI 2000 and glacier basins are defined according to their 1973 perimeter. Area changes are calculated within these basins, independent of the number or area of glacier parts within them. For efficient GIS-based data processing, information about the parent glacier of each glacier part must be available (cf. GLIMS, 2002; Mennis and Fountain, 2001). In consequence, glacier groups can have various origins: (1) they are already a part of the digitized inventory, (2) they consist of a 'total' glacier comprised of different tributaries, and (3) they originate from a single glacier through separation over time.

(1): A glacier group in the inventory of Müller et al. (1976) is comprised of a number of smaller glaciers (glacieretes, maybe snowfields) that belonged to a distinct basin or to a single (and often much larger) glacier in 1850. In the revision of Maisch et al. (2000), each glacier is treated individually and a lot of new glacier IDs were created (see Table 6.2). For the digitized inventory (1973) only the main glacier of a group (holding the ID) is digitized and possible tributaries are added according to the tracing vellum. Hence, some confusion is unavoidable and specified samples are used for area comparisons in the SGI 2000.

(2): The separation of formerly connected glacier tributaries is observed mainly between 1850 and 1973, in particular for larger valley glaciers. In the 1973 inventory from Müller et al. (1976) only total areas are given, since no comparisons with ancient extents are made. In the revision of Maisch these glaciers are treated as 'total' glaciers, while the different tributaries are catalogued as glacier parts ('Teilgletscher'). All others are listed as 'individual' glaciers (cf. Table 6.2). Only areas from total and individual glaciers are used for the SGI 2000.

(3): The disintegration of glaciers is restricted to small glaciers and is observed especially during the last two decades as a result of strongly negative mass balances (e.g., MBB, 2001). In the SGI 2000 changes in area are tracked for the sum of all glacier parts within a basin, although individual glacier behaviour becomes very different compared to a compact glacier of the same size. However, the remaining very small glacier parts can supposed to be firn fields without much movement and thus, summarized.

6.3.3. The ID vector layer

There are at least two different but complementary glacier codes for Switzerland. Both codes use the same hydrological scheme for the numbering of each glacier. While the WGI-code uses a number for the country and the continent (Hoelzle and Trindler, 1998), the code of Müller et al. (1976) does not, and letters and numbers for rivers and drainage basins are somewhat different (cf. Table 6.2). Successive numbers are given for each glacier of a hydrological basin in clockwise rotation. Maisch et al. (2000) used the numbering scheme from Müller et al. (1976), but had to introduce additional codes (further numbers and appended letters) for new

glaciers or separated glacier parts. All these codes are not usable for creation of a point *coverage* from the glaciers coordinates, since letters are not allowed as an identifier for a label. Thus, a short Fortran program was written to convert the letters into numbers (App. 2.3-2). Their position in the alphabet is used for conversion, with one digit for the first letter (A-F equals 1-6) and two digits for the second letter (b to r equals 02 to 18) of the code. If the code has no second letter, '00' is used as a place holder (see Table 6.2).

Glacier name (CH-INVGLAZ)	WGI	Müller	Maisch	SGI 2000
UNTERAARGLETSCHER (Teilgl.von A54G/50n)	4R014 4G 11	A54/G11	A54G/11	1540711
A54G/50n, Unteraargletscher (Totalgl.)	n. a.	n. a.	A54G/50n	1540750
Lauteraar-Rothörner-NE* (Teilgl. von A54G/50n)	n. a.	n. a.	A54G/52n	1540752
GROSSER ALETSCH GLETSCHER (Teilgl. von B36/49n)	4N013 36 26	B36 /26	B36/26	2360026
MORTERATSCH VADRET DA (Totalgl.)	4J143 22 3	E22 / 3	E22/03	5220003
PERS VADRET (Teilgl. von E22/03)	n. a.	n. a.	E22/11n	5220011
Morteratschgletscher (Teilgl. von E22/03)	n. a.	n. a.	E22/12n	5220012

Table 6.2: *A few examples of glacier codes used in different inventories. In the first column 'Teilgl.' means 'part of a glacier', 'Totalgl.' means 'entire glacier' and 'von' means 'of'. 'WGI' is the code used in the world glacier inventory (IAHS, 1989), 'Müller' is the code used in the Swiss glacier inventory (Müller et al., 1976), 'Maisch' is the code from the revised CH-INVGLAZ database (Maisch et al., 2000), and 'SGI 2000' is the converted number from the 'Maisch' code.*

The label-ID point *coverage* is used to assign a label to each glacier of the digitized inventory for at least three reasons: (1) To create a link to the former database CH-INVGLAZ, (2) to identify glaciers and exclude island polygons for data selection (analogue to the '*grid-code*' label for the TM-derived glacier areas), and (3) to allow attachment of items from other sources (e.g., length changes) to the attribute table of each glacier.

The point *coverage* is created from a text file (storing the ID and x/y coordinates of each label) with ***generate*** and ***input***. This *coverage* (and the *pat*) is combined with the *coverage* of the digitized inventory and also with the glacier basin *coverage* using ***intersect*** and ***joinitem*** (App. 2.2-2). Afterwards, the selection of glaciers is possible according to their hydrological basin.

Unfortunately, it is not feasible to use this concept for the SGI 2000 in practice, as glacier labels are not unique in the CH-INVGLAZ database. Most glaciers have more than one label, depending on the assignment as a 'total glacier' and 'glacier part' in 1850 or 1973. 'Total glaciers' exists in 1850 (split into 'glacier parts' in 1973) and 1973 (composed of different glacier tributaries, tongues or accumulation areas). Since the 'parent glacier' was not traced in the database, it is very difficult to decide which label belongs to which glacier.

For a first assessment of glacier change in the SGI 2000, manual labels are applied to each glacier. Special label coverages are created for each comparison between various data sets, e.g., the digitized inventory from 1973 with TM in 1998 or 1999, TM areas for 1985, 1992 and 1998 (western part of Switzerland) or 1985 and 1999 (eastern part). This four-digit label can also be used as the value item for a grid, which is generated from the 1973 glacier *coverage* (with 5 m pixel size) to calculate glacier parameters (see next paragraph).

6.4. Deriving glacier parameters

6.4.1. Methods

Obtaining glacier parameters for a larger number of glaciers by traditional methods (cartography, planimetry) is laborious, prone to errors and nearly unreproducible. The use of GIS technology at least generates reproducible results, but also offers four essential improvements: (1) Storage of 2D glacier outlines in a vector layer for tracing of geometry changes, (2) storage of corresponding glacier parameters in a relational data base, (3) combination with a DEM for retrieval of 3D glacier parameters and topographic indices, and (4) programming allows fully automatic processing of all data. A short description of the processing schemes for each parameter is given below (cf. Table 6.4).

Area and perimeter of each polygon (glacier) are calculated within Arc/Info automatically. Glacier length is computed from the central flow line, cut by the actual glacier outline (*intersect*). In order to use *zonalstats* for calculation of basic statistical values from a *value grid* (e.g., DEM) the glacier polygon *coverage* has to be converted to a *zonal grid*. Hence, the glacier ID is assigned to each glacier from the label ID *coverage* (*intersect*) and afterwards the *coverage* is converted to a 5 m cell-sized grid (*polygrid*), keeping the label ID as the zone identifier (Fig. 6.7a). A DEM-derived colour-coded eight sector aspect grid is shown in Fig. 6.7b as an example of an underlying *value grid*.

From *zonalstats* and the DEM, the minimum, maximum, range, mean and standard deviation (σ) of elevation is calculated for each glacier (Table 6.4 and App. 2.2-3). A 10 m and 100 m hypsography is computed for each glacier by additional use of *select* and a Fortran program (App. 2.2-4 and 2.3-3). Median elevation and ELA are calculated from the 10 m hypsography as the 50th and 35th percentile of the cumulated area (App. 2.3-4).

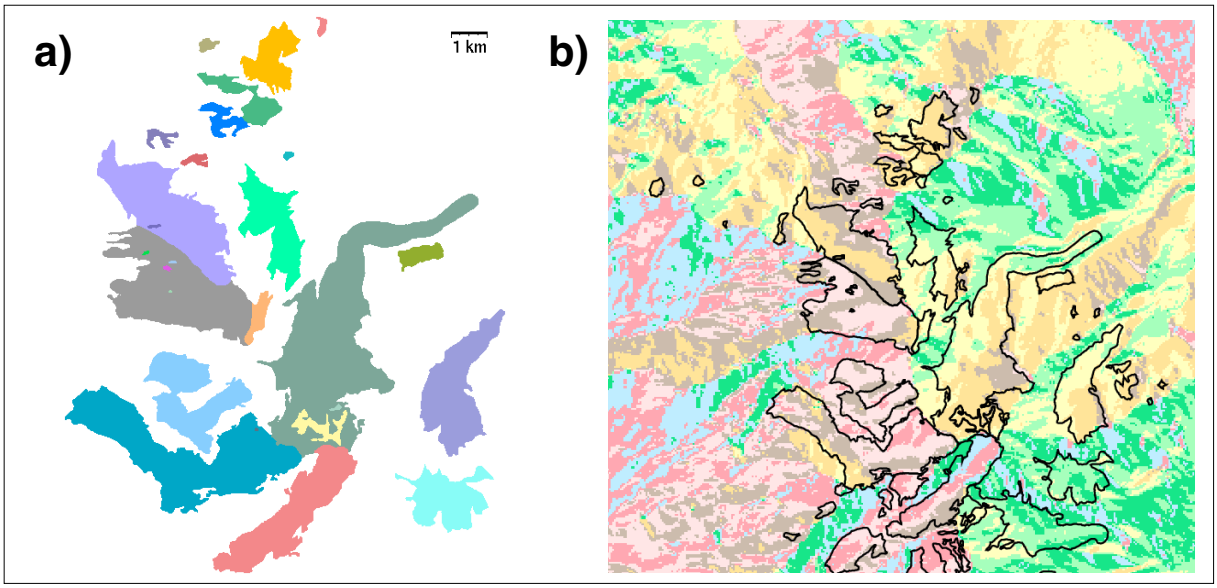

Figure 6.7: *Glacier parameters are obtained with the zonal concept (illustrated here for the northern part of the Weissmies test region). a) The zonal grid with one zone for each glacier (colour-coded) and b) a value grid (aspect sector) for the corresponding 3D parameter. DEM25 © swisstopo.*

Mean and σ of slope and sky-view factor are calculated as time-independent glacier parameters with *zonalstats* from the corresponding *value grids*. The mean potential solar radiation (psr) for June to September and cumulated cast shadow for 21 July are used as time-dependent *value grids* (cf. 3.2.2).

Mean aspect cannot be inferred directly with zonalstats from the aspect grid, as the north direction is represented by two different values (0 and 360°). Each glacier facing north and covering for example a range from 330 to 30° will have a mean aspect near 180°. As a consequence the aspect grid is separated in a sine and cosine grid, zonalstats is used to obtain the mean values and a Fortran program (App. 2.3-6) is used to get the correct mean aspect in 0-360° as well as the corresponding sector (see Table 6.3). From an aspect sector grid (derived within PCI) the percentage of glacier area in each aspect sector is calculated (App. 2.1-3).

	N	**NE**	**E**	**SE**	**SE**	**SW**	**W**	**NW**
Grid value	1	2	3	4	5	6	7	8
End of sector range [°]	22.5	67.5	112.5	157.5	202.5	247.5	292.5	337.5

Table 6.3: *Grid values used for the 8 aspect sectors and their conversion from 360°.*

It must be noted that slope and aspect are different from their equivalent in the CH-INVGLAZ database. Here they represent the mean of all slope/aspect values based on 25 m cell grids for the entire glacier. In the CH-INVGLAZ aspect (orientation) is defined as the mean aspect sector of the central flow line and slope is elevation range divided by glacier length. A comparison of the two values is given in Fig. 6.8 for a selection of 683 glaciers.

All statistical values are combined with the attribute table of the glacier *coverage* (*joinitem*) and transferred for further analysis and visualization to ASCII tables (*unload*). A summary of the calculated parameters and their sources is given in Table 6.4. The digitized 1973 inventory serves as the basis for all glacier parameters. Dependencies of changes in glacier area and length are compared to these values (see 7.3). For the 1998/99 TM-derived glacier areas only minimum elevation, elevation range and slope are calculated again from the DEM, as variations of all other parameters are comparably small (cf. 7.3.3).

Parameter	**Source**	**Format**	**Calculation**
ID	CH-INVGLAZ	ASCII	2.3-2 & 2.2-1
area, perimeter	digitized outlines	coverage	inherent
length	digitized flow lines	coverage	intersect & Fortran
minimum, maximum, mean, σ & range of elevation	DEM25L2	grid	2.2-3
median and 2:1 elevation	DEM25L2	grid	2.2-4 & 2.3-4
mean & σ of slope	Slope (curvature)	grid	2.2-3
mean & σ of sky-view factor	Sky-view (PCI)	grid	2.2-3
mean aspect (0-360 d & sector)	Aspect (sine, cosine)	grid	2.2-3 & 2.3-4
potential solar radiation	SRAD	grid	2.2-3
100 m hypsography	DEM25L2	grid	2.2-4 & 2.2-3

Table 6.4: *Summary of glacier parameters, their sources, format and calculation (numbers refer to the programs listed in the Appendix). Slope and aspect grids are derived with Arc/Infos* **curvature** *command, sky-view factor is calculated within PCI.*

6.4.2. Parameterizations

Using WGI data

The glacier parameters obtained allow calculation of further glaciological parameters using parameterization schemes. From the four basic entries of the WGI: area (A), length (L_0), minimum (H_{min}) and maximum (H_{max}) elevation, Haeberli and Hoelzle (1995) calculated a number of further parameters from physical relations. A selection of them is summarized in Table 6.5, along with the governing equations. Mean flow velocity, mass balance gradients, response and reaction times can also be calculated from these variables.

Parameter	Symbol	Equation	Remarks
vertical extent	ΔH	$H_{max} - H_{min}$	
mean altitude	H_m	$H_{min} + (\Delta H / 2)$	also used for ELA approximation
average surface slope	α	$\arctan (\Delta H / L_0)$	
mean basal shear stress	τ	$a + b \cdot \Delta H - c \cdot \Delta H^2$	1.5, if ΔH exceeds 1600 m
average depth	h_f	$\tau / (f \cdot \rho \cdot g \cdot \sin\alpha)$	taken along central flow line, f=0.8
mean thickness	h_F	$(\pi / 4) / h_f$	semi-elliptic cross-section
volume	V	$A \cdot h_F$	

Table 6.5: *Selected parameterizations for glacier inventory data as described by Haeberli and Hoelzle (1995), with ρ = ice density, g = acceleration of gravity and a, b, c = constants.*

In contrast to the approach above, vertical extent (range), mean altitude and surface slope are inferred for the SGI 2000 directly from the DEM. The comparison for mean elevation is depicted in Fig. 6.8a and for mean and average slope in Fig. 6.8b. The DEM-derived mean elevation (average from all grid cells comprising a glacier) is perhaps better suited, since maximum elevation may correspond to a singular high-reaching couloir not representative for the glacier. The same is true for slope, where the calculated value relies also on a possibly extreme maximum elevation value and also on the much more uncertain glacier length, which also explains the lower correlation between both values (0.82 instead of 0.98 for mean elevation).

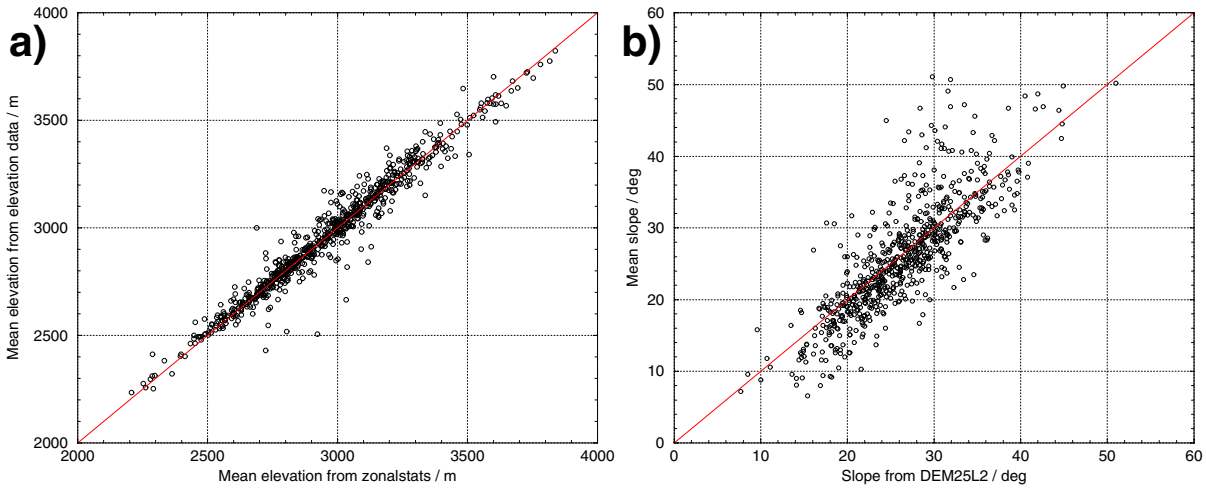

Figure 6.8: *Differences between mean altitude (a) and average surface slope (b) from zonalstats using a DEM and according to the equations given in Table 6.5. The red line is the identity.*

From the 3D glacier parameters, additional terrain properties can be calculated for each glacier, such as elevation-relief ratio (H_m-$H_{min}/\Delta H$) or catchment-related parameters (cf. Etzelmüller et al., 2001). The latter were used by Zemp (2002) in order to obtain information about the sediment balances of about 100 glaciers.

Glacier volume

Calculation of glacier volume requires a 3D representation of glacier surface and glacier bed topography. While glacier surface is maintained from a DEM, the bed topography has to be extrapolated, e.g., from radar or seismic thickness profiles measured along many transects over a glacier (e.g., Bogorodsky et al., 1985; Driedger and Kennard, 1986; Hagen and Saetrang, 1991). Some care is required in interpretation of layer and bottom returns from ground penetrating radar (Dowdeswell et al., 1984). Regression curves were derived from such (including also questionable) measurements to obtain glacier volume (e.g., Müller et al., 1976).

Glacier area is the mandatory scale factor for all volume calculations (e.g., Bahr et al., 1997), but the complexity of calculation differs. Table 6.6 provides a summary of the governing equations and their restrictions. While Maisch et al. (2000) and Müller et al. (1976) derive mean glacier thickness from a regression curve of measurements, Haeberli and Hoelzle (1995) used glacier elevation range and slope-dependent basal shear stress. The latter was also applied by Driedger and Kennard (1986), but they inferred volume of large glaciers directly from mean slope and area, as calculated for each 100 m elevation interval (cf. App. 2.2-5).

Method	Equation for Volume	Restrictions
1. Müller et al. (1976)	$A \cdot (5.2 + 15.4 \cdot A^{0.5})$	statistically derived, area: 0.5-23 km^2
2. Maisch et al. (2000)	$A \cdot (10.6 + 15.0\ A^{0.5})$	empirical relation, using all glaciers from '1.' and late glacial ice-bodies
3. Haeberli and Hoelzle (1995)	$A \cdot (\pi/4) \cdot (f \cdot \rho \cdot g \cdot \sin \alpha) / \tau$	physical relation, see Table 6.5
4. Driedger and Kennard (1986)	$3.93 \cdot A^{1.124}$	for small glaciers, statistically derived
	$\tau / (\rho \cdot g) \cdot \Sigma\ A_i / \sin \alpha_i$, and: $\tau = 2.7 \cdot 10^4 \cdot \Sigma\ (A_i / \cos \alpha_i)^{0.106}$	for large glaciers ($\tau > 1.2$), physical relation

Table 6.6: *Different methods used to calculate glacier volume, with A = glacier area, i = index (see. Table 6.5 for further symbols).*

Methods 2, 3 and 4 are applied to glacier parameters derived with 1973 outlines from the DEM25L2 and compared with each other. In Fig. 6.9 mean thickness vs. glacier size is depicted for methods 2 and 3 along with in-situ measurements from the Alps (Müller et al., 1976) and Cascades (Driedger and Kennard, 1986). Both methods yield similar results, with small glaciers somewhat thicker with method 2 and large glaciers thicker with method 3. The physical relation reveals a strong scatter, and the double-logarithmic scale confirms the non-linear relation between τ and mean slope due to the flow law (volumes are discussed in 7.3.4).

If only volume changes are of interest, other and more direct methods can be used. Some examples from high to low precision and short to longer time intervals are: (a) terrestrial photogrammetry (e.g., Finsterwalder, 1954; Finsterwalder and Rentsch, 1980), (b) DEM generation by stereo-photogrammetry from aerial photography (Kääb, 2001; Kääb and Funk, 1999), and (c) digitized contour lines from old maps and reconstruction with 3D polygonal bodies (Wipf, 1999). While (a) is suitable only for small or individual glaciers, method (b) could also be used for the SGI 2000. Using the DEM25L2 which was compiled about 10 years after the

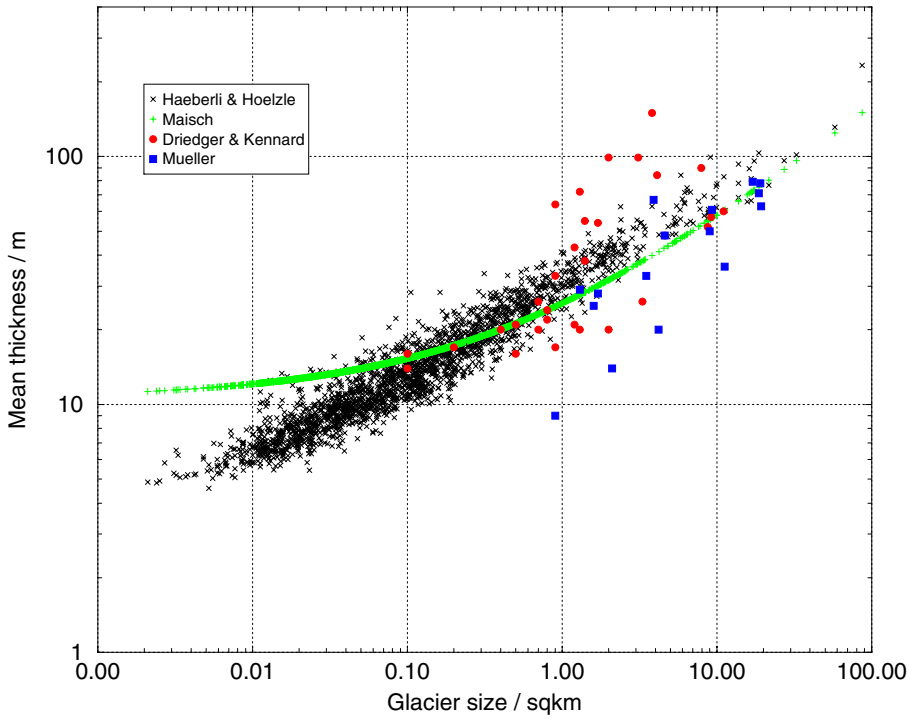

Figure 6.9: *Glacier area vs. mean glacier thickness, as obtained with different methods.*

level1 DEM25 and updated for glacier contours lines (Swisstopo, 2001), the differences between the two DEMs could be used to calculate volume changes with respect to each glacier (multiplication with the pixel area (i.e. 625 m^2) and summarizing of all pixels and each glacier). However, contour lines are only updated for the ablation areas of larger glaciers, and elevation differences due to the new interpolation algorithm are in the same order of magnitude as changes in glacier elevation. Thus, this method is not used for the SGI 2000. However, method (b) is used for the new Austrian glacier inventory, where aerial photography from 1969 and 1997 to 1999 were used for DEM generation and glacier volume change calculation (Würländer and Kuhn, 2000). Method (c) was applied to digitized elevation contour lines from 1850 and 1973 (100 m intervals) within an AML-script developed by Benz (1995), using a method of volume change reconstruction as described by Hofman (1958).

6.4.3. Accuracy of the derived 3D parameters

A comparison of DEM-derived glacier parameters with those obtained from traditional methods (e.g., planimetry) could not be achieved, since the link to the CH-INVGLAZ database has not been established yet. Possible errors may result from the following points: (1) The years of DEM acquisition (mid-1990s) are different from the year of the glacier inventory (1973). This will have its greatest effect on minimum glacier elevation. (2) Geocoding of the maps used for digitizing is, in general, better than 5 m (RMSE), while digitizing itself may reach 10 m and satellite imagery has 20 m RMSE. This shift will especially influence the accuracy of maximum elevation, if located near crests. The accuracy of the digitized central-flowlines is discussed in 7.4.3. Assuming a perfect DEM, the overall accuracy of the main derived 3D parameters is estimated to be ±50 m for all elevations and ±5° for mean slope and aspect.

6.5. Data flow

The guiding principle for the data flow concept is to perform as many calculations as possible with the fewest input data sets and minimum user interaction. The GIS is able to communicate with other software by export of ASCII data tables, but often the data has to be re-configured to a special format. This is done by small Fortran programs, acting as an interface between the GIS output and the required input format for the next step. Thus, data flow follows a general work flow between three modules (GIS, CONVersion, VISualization) and a specific data flow within each module (Fig. 6.10): (1) the GIS module for calculations within the GIS (e.g., areas of individual glaciers), (2) the CONV module for conversion and calculations with Arc/Info output tables (e.g., glacier areas of two different years converted to relative changes in area), and (3) the VIS module for creation of graphics from data files (e.g., with XMGR, App. 2.4-1). Each module consists of particular programs for individual tasks, each of which includes an input, calculation and output part. The different modules can be combined to a complete digital chain, as Arc/Info is able to run external programs (Fortran, batch jobs) by the *&system* command. The output from a program in one module acts as the input for a program in the next module (Fig 6.10a). For practical reasons (especially during development), intermediate results are stored separately (e.g., conversion of the classified TM-image to a polygon *coverage* is performed only once and used afterwards by all other programs).

The calculation of 3D glacier parameters from a specific DEM product (e.g., slope) within the GIS-module is shown schematically in Fig. 6.10b in more detail. Only three data layers are required for the input section: (A) the pre-defined glacier basins (vector layer) with assigned glacier IDs, (B) the image with the classified glacier areas from TM (tif format), and (C) the DEM or a product from it (raster grid). The calculation section consists of the following steps (numbers refer to Fig. 6.10b):

(1) A raster-vector conversion of the glacier map with *imagegrid* and *gridpoly*.
(2) Using the glacier basin *coverage* and *intersect* to obtain the individual glaciers.
(3) Conversion with *polygrid* to a *zonal grid* where each zone corresponds to a glacier.
(4) The DEM (or a product of it) is converted with *asciigrid* to a *value grid*.
(5) Combination of the *value grid* and the *zonal grid* with *zonalstats* to obtain statistic parameters for each zone (glacier) according to the *value grid*.

In the output section *unload* is used to transfer the calculated 3D parameters to a text file.

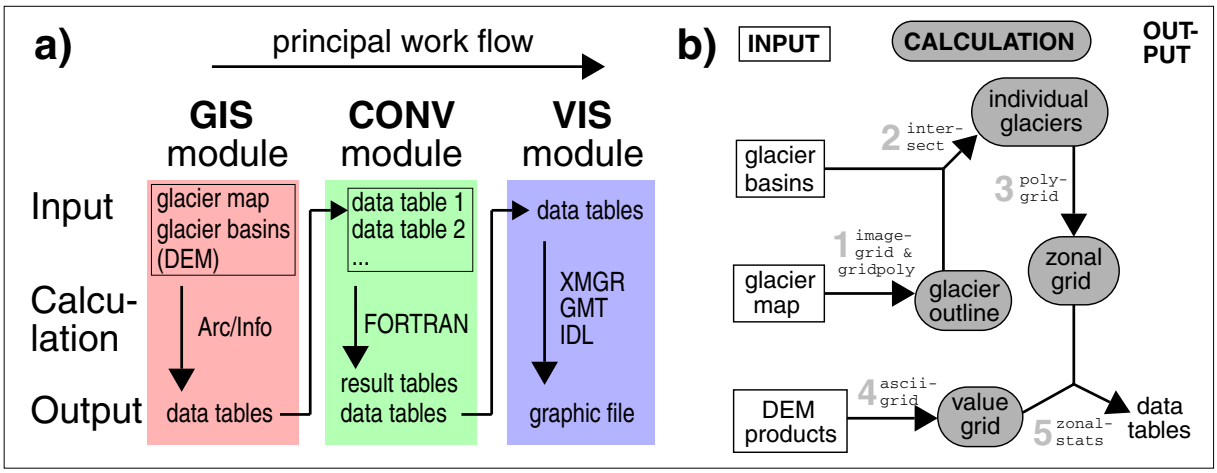

Figure 6.10: *a) General data flow between the three modules. b) Detailed processing scheme for calculation of glacier parameters from a DEM product within the GIS-module.*

Example of glacier change calculation

According to the schematic workflows given in Fig. 6.10 the calculation of glacier changes for two different years is as follows (using the `names` used in App. 2.2-2 and 2.3-5):

Pre-processing:

Satellite scenes: orthorectification (cf. 4.2), glacier classification (cf. Fig. 4.14 & App. 2.1-2), binary map (tif-format)

GIS-related: digitizing of a former glacier inventory (if available), glacier basins (polygon coverage) and glacier IDs (point coverage)

GIS module (2.2-2):

Input: glacier basins '`stanzchisl98`', glacier IDs '`lsel5_7398`', digitized 1973 glacier outlines '`gl73f98`', glacier map '`gl98.tif`'

Calculation: format conversion and intersection with basins and IDs

Output: glacier size and ID for 1998 '`gl98cc.tab`' and 1973 '`gl73f98.tab`'

CONV module (2.3-5):

Input: glacier size and ID for 1998 '`gl98cc.tab`' and 1973 '`gl73f98.tab`'

Calculation: area sums according to ID, differences and statistics

Output: tables of relative '`gldif7398.dat`' and absolute '`gldifabs7398.dat`' change in area for all glaciers and summaries for each area class for import (cf. Table 7.2) '`gldiffk7398.tab`' and further export '`gldiffk7398.dat`'.

VIS module (similar to 2.4-1):

Input: glacier size vs. relative changes in area '`gldif7398.dat`' and area class averages '`gldifflkl7398.dat`'.

Output: eps-file of glacier change (Fig. 7.8).

7. RESULTS

7.1. Digitized glacier outlines

7.1.1. Description of data sets

Four basic digitized data sets were created for the SGI 2000: (1) glacier outlines from the 1973 inventory, (2) glacier outlines from the reconstructed 1850 inventory, (3) central flow lines for 1850 and 1973, and (4) a point coverage with glacier labels, generated automatically from the glacier ID and x/y coordinates (cf. App. 2.2-1) as well as by interactive digitizing.

(1) The 1973 outlines

A copy of the 1973 glacier polygon coverage is intersected with labels (point coverage) generated from the CH-INVGLAZ database. Before intersection, many labels are shifted to a new position to be located within the respective glacier polygon. Some of these polygons receive multiple labels resulting from designation as 'total glaciers' or 'glacier parts' in the database. The assignment of a unique label from the CH-INVGLAZ database to each glacier must be performed later, as the database must be revised beforehand. Afterwards all glaciers with a label (2073 in total) are converted back from vector to raster format using a 5 m grid-cell size. This data set is used to calculate all glacier parameters (see 7.2) using the methods described in Chapter 6.

The outlines from 1973 are also used to define the glacier basins for the TM data (separation of contiguous ice masses) as well as for various overlays. The latter includes overlay with satellite imagery draped over a DEM for creation of 3D perspective views (Fig. 7.1) or without a DEM (Fig. 7.2) to visualize former glacier extent. Polygon topology is mandatory to display glaciers in ArcView according to the data in their attribute tables (cf. Fig. 7.6 and 7.7).

(2) The 1850 outlines

Glacier outlines from 1850 are partly available with polygon topology and are represented with arc-topology in all other regions. The correct intersection of 1850 outlines with 1973 polygons needs additional time and could not be entirely completed for the SGI 2000. Thus, outlines from 1850 cannot be used to derive glacier parameters. However, outlines can be used to illustrate 1850 glacier extent in 3D perspective views with *arcplot*. Two examples with glacier outlines from 1850 (red) and 1973 (blue) are shown in Fig. 7.1. Some additional examples are presented in App. 3.3. Statistical and spatial analysis of the 1850 data set is given by Maisch et al. (2000), Wipf (1999) and Benz (1995).

(3) Central flow lines from 1850 and 1973

Central flow lines of glaciers from 1850 and 1973 have been digitized for the region investigated by Benz (1995) and Wipf (1999). Within the SGI 2000 only flow lines from 1850 are digitized for the remaining part of Switzerland. The use of 1850 or even 1973 flow lines for the 1998 TM outlines is not possible without control for each glacier, because many smaller glaciers show strong changes in geometry (cf. 7.4.3). The flow lines are shifted to the place of the largest remaining ice body and corrections for the changed geometry are applied. In the case of a disappeared glacier, the flow line is deleted and glacier length is zero.

As changes in glacier length between 1973 and 1998 are calculated from the difference between the two flow lines, an additional selection is made for all glaciers with appropriate flow lines in 1973 and 1998. This selection (683 glaciers) is used in Fig. 7.5f which shows the length - mean width relationship. For these glaciers the sum of all flow line segments is calculated from an additional Fortran program according to the flow line ID. This program also calculates relative and absolute length changes as well as changes for various length classes.

(4) Glacier labels

In a first step glacier labels are assigned to each glacier according to their converted WGI code (see 6.3.3). Two problems occur: (1) The string with the code is too long for use as a grid value and (2) it is not possible to decide which of the numbers belong to the respective glacier. As a consequence, labels are assigned manually to a selection of 947 glaciers for comparison of glacier areas. For the western part of Switzerland (Landsat path 195), 721 glaciers are selected for the comparison from 1973 to 1998 (finally reduced to 713, see 7.3.1), and 226 glaciers are selected for the eastern part (path 194) for a comparison from 1973 to 1999 (see 7.3.2). The latter selection is considerably smaller, as most glaciers are located in the western part of Switzerland and many glaciers in the 1999 scene must be excluded due to adjacent snow patches. A sample of 471 glaciers (within path 195 only) is chosen for a comparison of glacier areas in 1973 - 1985 - 1992 - 1998 (see 7.3.3).

The labels are also placed within the largest of the remaining glaciers (in 1998/9) to calculate new glacier parameters only for this glacier part. The new hypsography is calculated for all glaciers within the former basin. Many of the small glaciers (around 0.1 km^2 in 1973), which have disappeared by 1998/9 or developed into small ice patches, are not considered in the selections mentioned above. This leads to a considerable decrease in glaciers by number (about 50%) but not by area (88%) compared to the inventory of Müller et al. (1976). The selection process is quite subjective and influences the value for the average relative change of glacier area in both regions (cf. Table 7.1 and 7.2).

7.1.2. Visualization with glacier outlines

As discussed above, glacier outlines from 1973 and 1850 (without polygon topology) can be used from *arcplot* as an overlay in 3D perspective views (the AML-code is given in App. 2.2-6). The examples in Fig. 7.1 illustrate the retreat of glacier tongues and the overall shrinkage between 1850 (red) and 1973 (blue). While the 3D views are more appropriate for the larger changes between 1973 and 1850, the smaller-scale glacier change between 1973 and '2000' is better depicted in 2D views (e.g., Fig. 7.2 and App. 3.2-9). In order to show the 1985-1998 change as a 2D area, the difference image is converted to grid format.

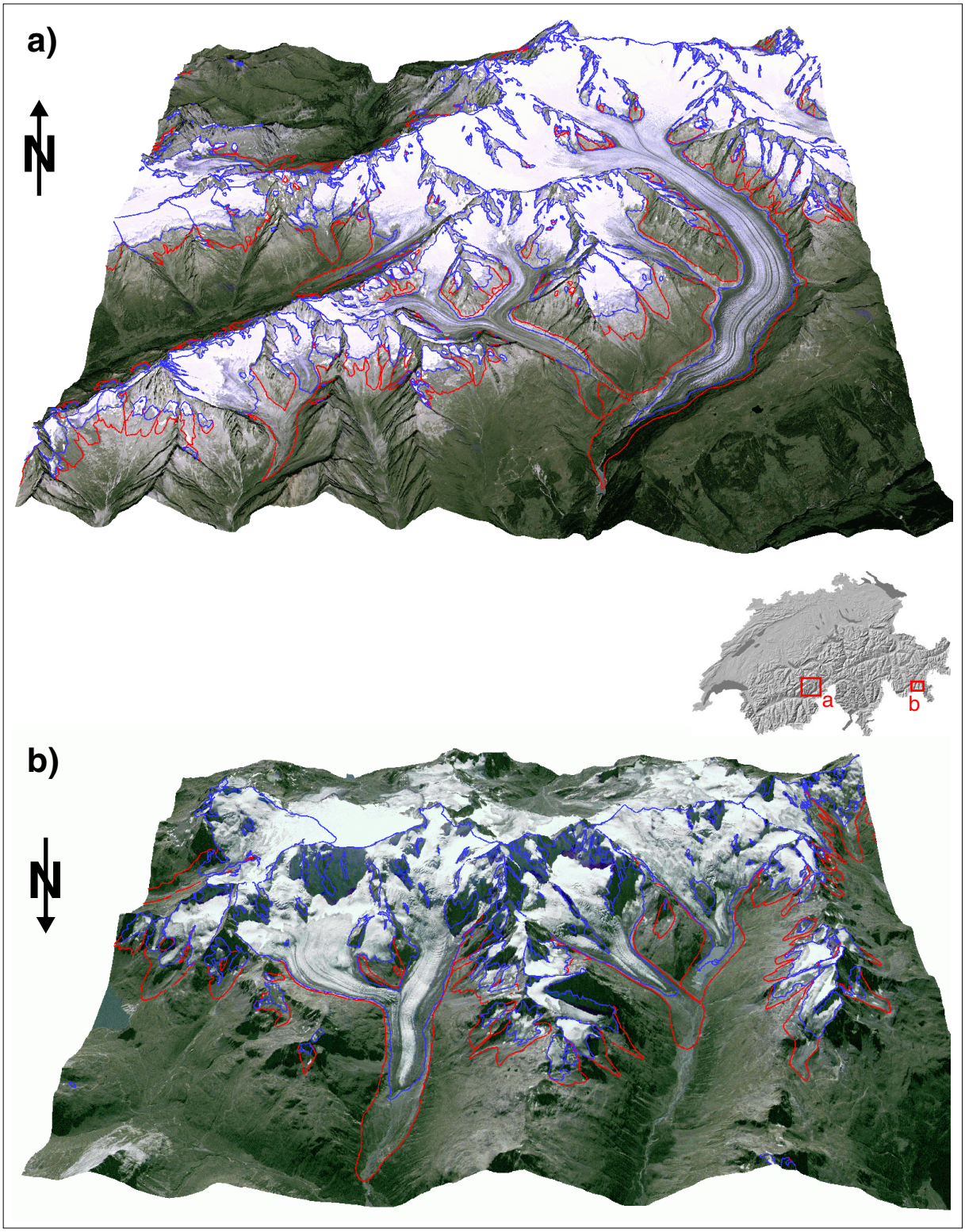

Figure 7.1: *Visualizing glacier changes with digitized glacier outlines from 1850 (red) and 1973 (blue) on fused IRS-1C / TM images that are draped over the DEM25L2. a) The Aletsch region (about 19 km wide at front side) is obtained from the fused scenes #10 and #13. b) The Bernina group of mountains (17.5 km wide at front side) uses fused scenes #5 and #15. DEM25 © swisstopo.*

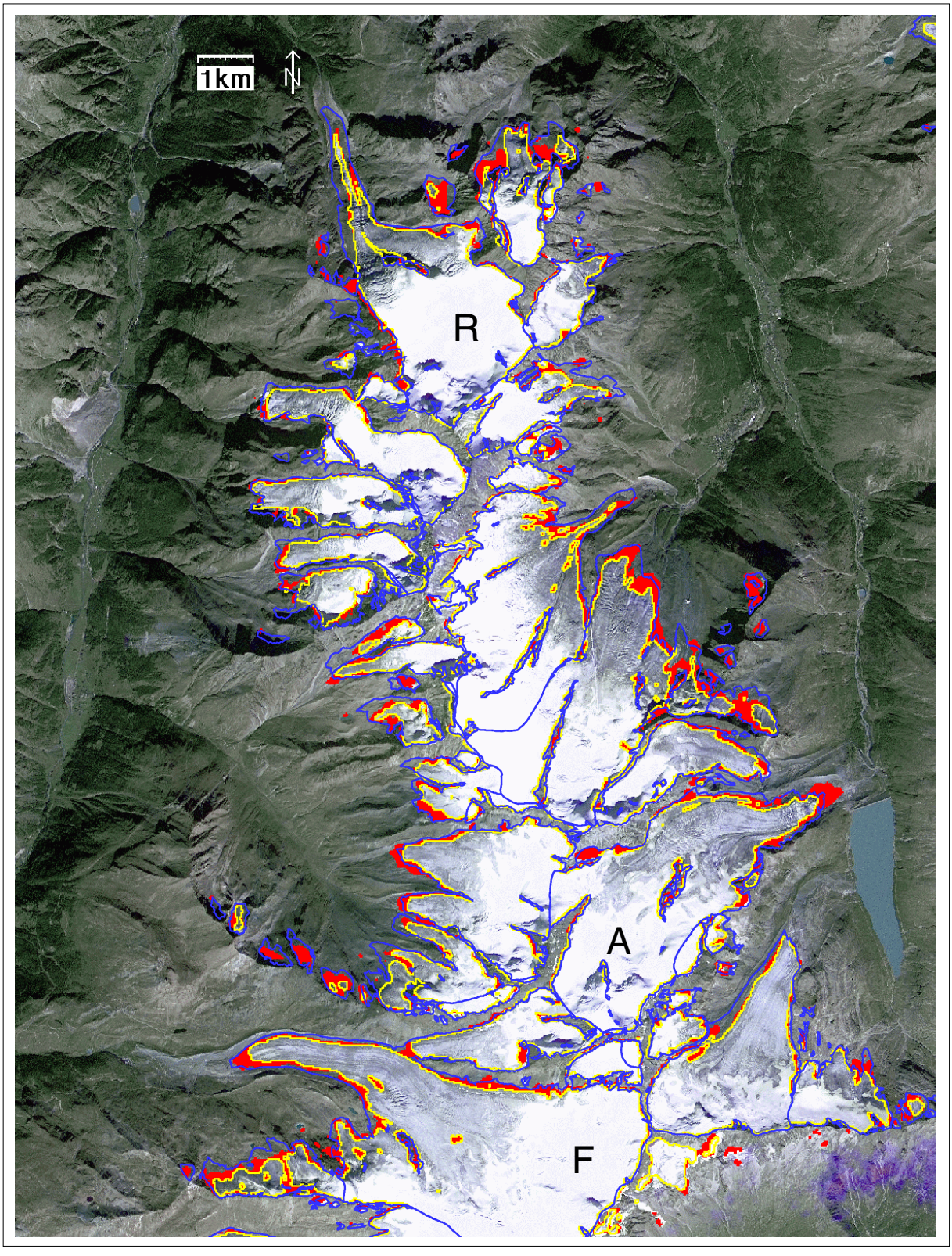

Figure 7.2: *Example of a 2D glacier change illustration for the Mischabel test region. TM-derived glacier outlines in 1998 (yellow) and area change from 1985 to 1998 (red) is shown together with outlines from the digitized 1973 inventory (blue). The background image is created from a fused IRS-1C (#14) and TM (#10) image. The purple area at bottom right is due to a cloud only present in the IRS-1C scene. Letters denote the following glaciers: F=Findelen, A=Allalin, R=Ried (cf. Fig. 6.3 and 6.6).*

7.2. 3D glacier parameters for 1973

In this paragraph some statistics of glacier parameters (based on the DEM25L2) with respect to the digitized 1973 data set are given in tabular and graphical form. A detailed hydrological and regional analysis of the 1973 inventory data is given by Maisch et al. (2000). The 3D parameters are calculated according to the description in 6.4 (see also App. 2.2-3) and linked to the original coverage with *joinitem*. Various data sets are 'unloaded' from the attribute table, and are directly imported by XMGR for visualization or, in case of histograms, summarized by a Fortran program prior to visualization.

Table 7.1 lists glacier areas and counts for all 2057 glaciers separated into 7 area classes. The part of area and count in each area class on the entire area and number is also given. In Fig. 7.3a only percentages are displayed. The corresponding values for the eight aspect sectors are given in App. 1-9. Fig. 7.3b displays the percentage on area and number for each sector.

Area class [km^2]	**0.1**	**0.5**	**1.0**	**5.0**	**10.0**	**20.0**	**100.0**	**Total**
Count	1022	673	151	157	35	14	5	2057
%	49.7	32.7	7.3	7.6	1.7	0.7	0.2	100
Area [km^2]	40.09	153.95	104.15	295.99	249.38	216.32	225.81	1285.7
%	3.1	12.0	8.1	23.0	19.4	16.8	17.6	100
Mean size [km^2]	0.04	0.23	0.69	1.89	7.13	15.45	45.16	0.63

Table 7.1: *Summary statistics for all glaciers of the digitized 1973 inventory and seven area classes. Only the largest size within each class is listed in the top row 'area class'.*

The strong asymmetry in glacier number towards smaller glaciers is also visible in Fig. 2.4 with data from the inventory of Müller et al. (1976). Here, glaciers smaller than 0.5 km^2 account for 82% of the number but only 15% of the area. If all areas from glaciers smaller than 1.0 km^2 are summarized, they account for about 23% of the entire area, similar to the other classes. The distribution of glacier number and area percentages for each exposition sector is more balanced (the blue area bar with SE aspect is dominated by 'Grosser Aletschgletscher').

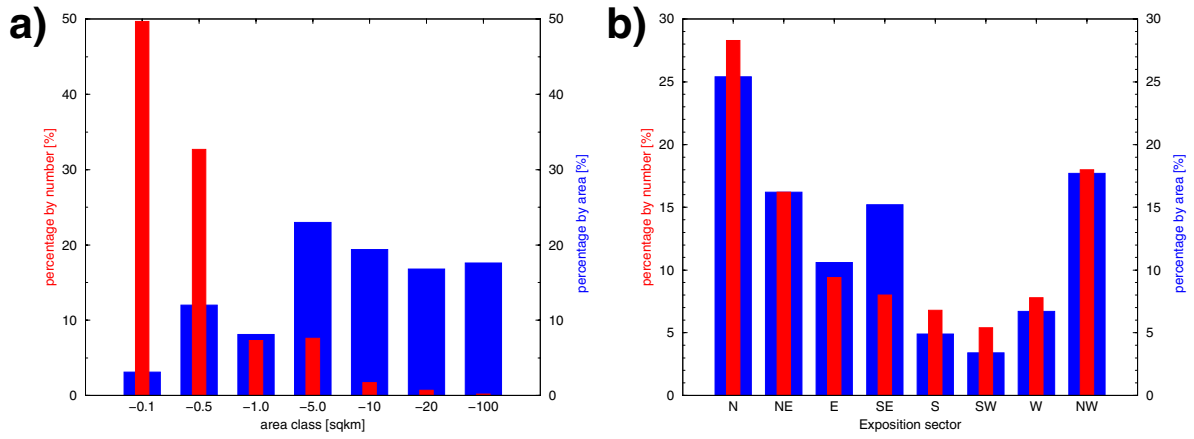

Figure 7.3: *Distribution of glaciers with area class (a) and with aspect sector (b). Red bars indicate percentage by number and blue bars percentage by area. Values are also given in Table App. 1-9.*

However, a tendency towards a larger number of glaciers with a northerly aspect is obvious. The three sectors NW, N and NE account for 63% of all glaciers by number and 59% by area.

The histograms of characteristic elevations in Fig. 7.4a-f show more or less 'Gauss-shaped' curves for each plot with exception of the elevation range (Fig. 7.4f), which is shifted to the left due to the large number of small glaciers. While minimum elevation peaks around 2700 m, maximum elevation peaks around 2900 m. Median (1:1) and 2:1 elevation (ELA) as well as mean elevation show highest frequencies around 2600-2800 m (Fig. 7.4c, d and e).

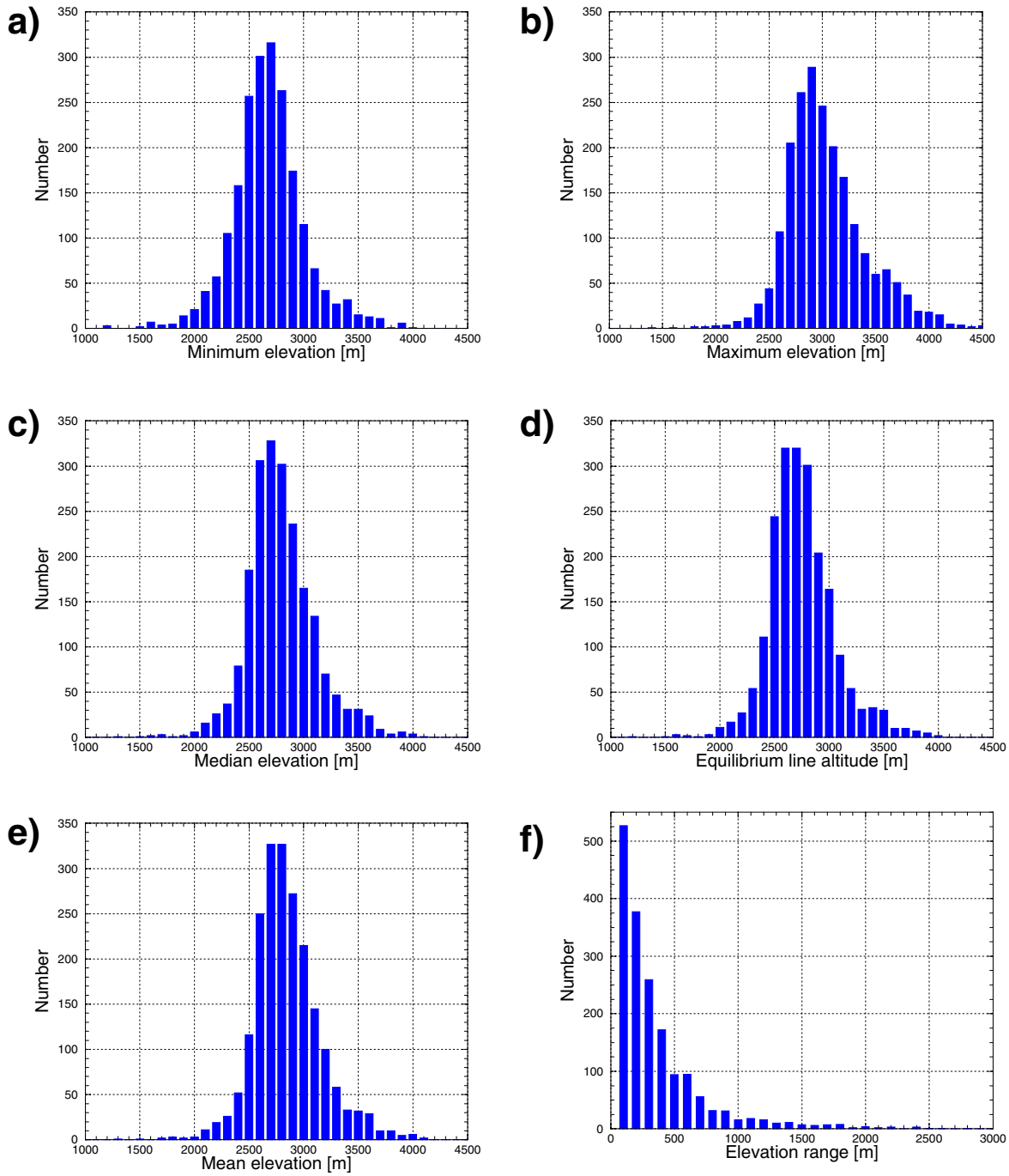

Figure 7.4: *Histograms of various elevation-based parameters derived from the digitized 1973 inventory (2057 glaciers) and the DEM25L2. DEM25 © swisstopo.*

In order to address glaciological questions, interesting parameter combinations are selected for Fig. 7.5a-f. Glacier size vs. 2:1 ELA is depicted in Fig. 7.5a, revealing no dependence of ELA on glacier size, but a very large scatter of ELA values for all glacier sizes. Glacier area vs. minimum elevation (Fig. 7.5b) shows somewhat lower minimum elevations for larger glaciers and a slightly increasing scatter towards smaller glaciers.

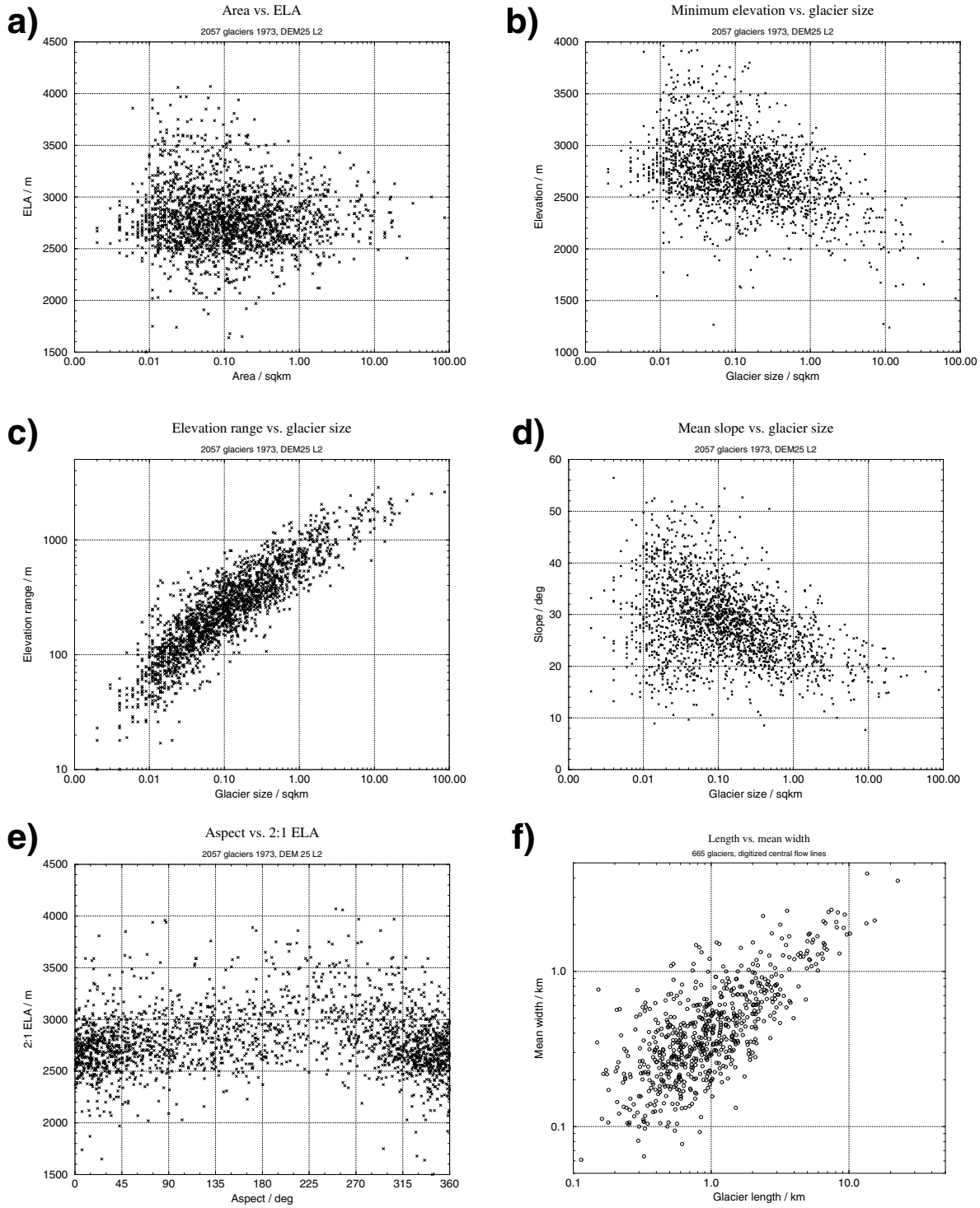

Figure 7.5: *a) - e) Scatter plots of various glacier parameters from the digitized 1973 inventory (2057 glaciers). A smaller sample is used for f). See text for discussion. DEM25 © swisstopo.*

The dependence of elevation range on glacier size is not surprising (Fig. 7.5c), but the scatter does not depend on glacier size (note double logarithmic scale). The scatter plot of mean slope vs. glacier size (Fig. 7.5d) reveals: the larger the glacier, the smaller the mean slope (cf. Fig. 7.6). Compared to Fig. 7.5b, the decrease of scatter with increasing glacier size is more pronounced. The dependence of ELA on exposition is weak with a tendency of lower ELAs for glaciers facing north (Fig. 7.5e). The figure also reveals that most glaciers have aspects between 315° and 45° (from NW to NE). For Fig. 7.5f (glacier length vs. mean width) a smaller sample is used, as glacier lengths (derived from flow lines) are only derived for the western part of Switzerland. For glaciers shorter than about 5 km, the broad scatter of mean width (size/length) is obvious (note double logarithmic scale), revealing the more individual shapes of mountain glaciers and glaciereteres (cf. Bahr, 1997b).

The colour-coded visualization of a single glacier parameter from the attribute table is possible within ArcView. The glacier areas can either be used in a coloured way (Fig. 7.6) or as a background for colour-coded dots (Fig.7.7). In Fig. 7.6 mean slope is used as the parameter for the colour, coding increase in steepness from yellow to orange to red and decreasing steepness from green to blue to purple. An explicit legend is not provided as colours are used for illustration only. Such images can be used to identify steep glaciers within a certain slope facet at a glance. A shaded DEM or a satellite image can be used as background.

With the establishment of a link to other geo-spatial data bases (e.g., mass balance data, length changes, glacier pictures, modelled permafrost distribution, etc.) the glacier outlines may become valuable to a broader community (e.g., Hurni, 2001; Sieber, 2001).

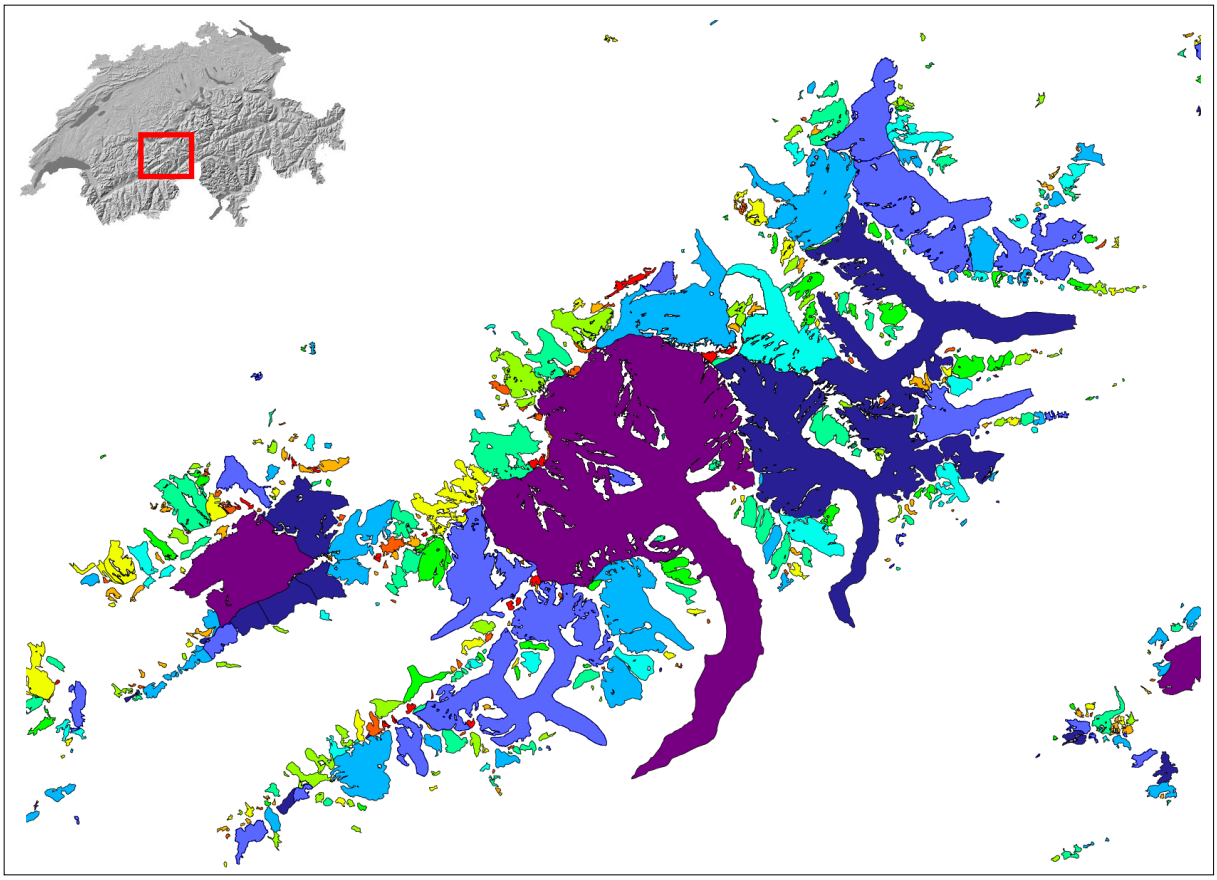

Figure 7.6: *Illustrating the glacier parameter mean slope by using colour-coded glacier areas. From high to low slope values, colours range from red, orange and yellow to green, blue and purple.*

The point coverage generated from glacier IDs can also be linked to the glacier parameter attribute table. This allows colour-coded representations of parameters with a symbol (e.g., filled circle of certain size) if the glacier area is not appropriate for expressing the parameter. As an example, Fig. 7.7 shows glacier areas as a grey background and coloured dots representing ELA from low (purple to blue), to average (green) and high (orange to red) values. In this case the regional dependence of the ELA on climate conditions (mainly precipitation) becomes evident. Glaciers at the more maritime north face of the Alps have lower ELAs (blue colours) than the more continental-type glaciers (sheltered from precipitation) in the southern part of the Valais (orange and red). Exceptions are visible in the Aletsch region, with many small glaciers situated at high altitudes or at the northeast face of the Weissmies group (arrow), where the vicinity to the Simplon pass provides enough precipitation to lower the ELA.

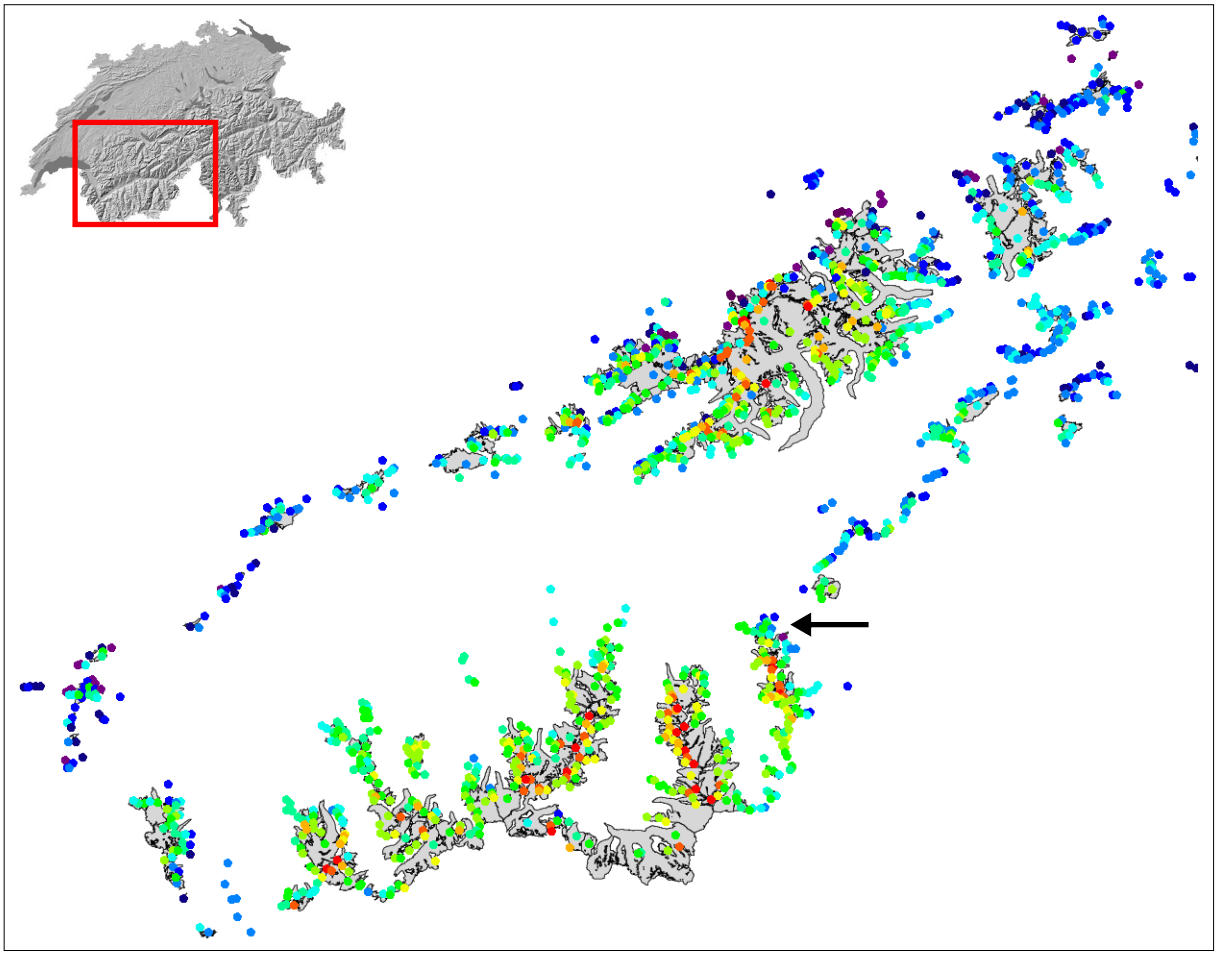

Figure 7.7: *Displaying the glacier parameter ELA by using colour-coded dots and glacier outlines as background for the western part of Switzerland. From low to high ELA values the colours range from purple, blue and cyan to green, yellow and red.*

The computation of isolines (e.g., from kriging) from parameters varying with location (such as ELA) is a third possibility for visualization. The necessary computations are beyond the scope of this thesis and are addressed together with multivariate analysis (using more than two parameters) in future studies. This includes regression and multidimensional display of glacier parameters and their changes.

7.3. Glacier change since 1973

Glacier changes are calculated for various samples as described in 7.1.1 (4). Glacier outlines in 1998 (Landsat path 195) and 1999 (path 194) are completed for debris-covered areas as far as possible using the methods described in 5.2. Some glaciers are rejected, since it is not possible to decide where the glacier boundary is, even on contrast-enhanced images. Glaciers in cast shadow with doubtful (broken) outlines are also excluded. For some small glaciers debris cover is added manually if strong deviations to the automatic classification is obvious.

Tabulated glacier areas are given with a precision of two digits and relative changes with one digit. With respect to the accuracy of the TM-derived data (better than 5% for clean ice) one digit less would indicate accuracy better. Data for glaciers smaller than 0.1 km^2 is included, but must be interpreted with care (see 5.1.3). However, their part of the entire glacier area is mostly below 1%, resulting in a very small change for the total change if a 10% area underestimation is assumed. The mean relative change in area for all glaciers depends on the largest area class considered. Some glaciers have changed their geometry by losing their tongues or splitting up into parts. Although glaciologically questionable, all parts within a basin are added in such cases in order to reveal the change with respect to the 1973 parent glacier.

7.3.1. Changes in area

Set (I): Western part of Switzerland (1973-1998, including debris correction)

Glacier areas in 1973 and 1998, their change in area, mean size and part on the entire glacier area is tabulated for 713 glaciers and seven area classes in Table 7.2 (App. 2.3-5 provides Fortran program). The relative change in glacier area for each glacier is plotted along with the average value for each area class (red) in Fig. 7.8. While mean values for each area class exhibit a dependence of relative area change on glacier size, the individual values express the strong increase in scatter with decreasing glacier size. The absolute loss of area is much higher for larger glaciers (Fig. 7.9a) but glaciers larger than 5 km^2 have increased their part of the entire glacier area by 4% (Table 7.2). This is due to the large number of glaciers smaller 1 km^2, which contribute 40% to the total area loss, although they cover only 15.5% of the 1973 area.

Area		Area [km^2]		Area change 73-98		Mean size [km^2]		% of total area	
class	Count	1973	1998	[km^2]	[%]	1973	1998	1973	1998
0.1	128	7.47	3.00	-4.47	-59.8	0.06	0.02	0.7	0.3
0.5	317	79.05	47.71	-31.34	-39.7	0.25	0.15	7.8	5.4
1.0	105	71.41	52.65	-18.76	-26.3	0.68	0.50	7.0	6.0
5.0	115	214.57	180.76	-33.80	-15.8	1.87	1.57	21.1	20.6
10.0	31	224.00	201.48	-22.52	-10.1	7.23	6.50	22.1	23.0
20.0	12	192.56	176.64	-15.92	-8.3	16.05	14.72	19.0	20.2
100.0	5	225.89	212.95	-12.95	-5.7	45.18	42.59	22.3	24.3
Total	713	1014.95	875.55	-139.41	-13.7	1.42	1.23	100	100

Table 7.2: *Summary data for glacier area change between 1973 and 1998 for the western part of Switzerland. 'Area class' is in km^2 and only the largest size within each class is listed.*

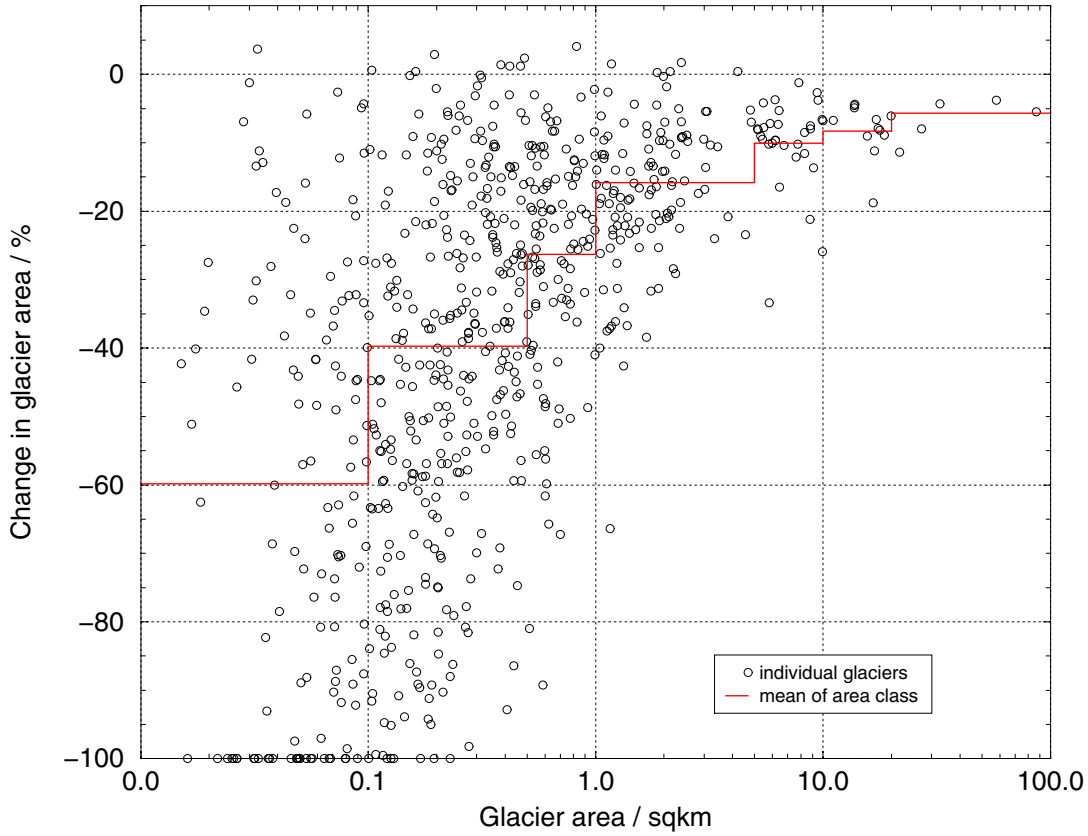

Figure 7.8: *Relative change in glacier area vs. glacier area in 1973 for the 713 glaciers of the selection 1973-1998. The average loss in each area class is shown in red.*

The mean size of all glaciers is decreasing from 1.42 to 1.23 km^2, which is still two times higher than for the 2073 glaciers (mean size 0.63 km^2). Thus, there is a bias towards larger glaciers in this selection, resulting in underestimation of the relative change in area. There is no dependence of glacier change from any of the time-independent 3D parameter variables (slope, aspect) as well as from the mean potential direct solar radiation for the months June to September (Fig. 7.9b) or from the percentage of cast shadow cover during a day.

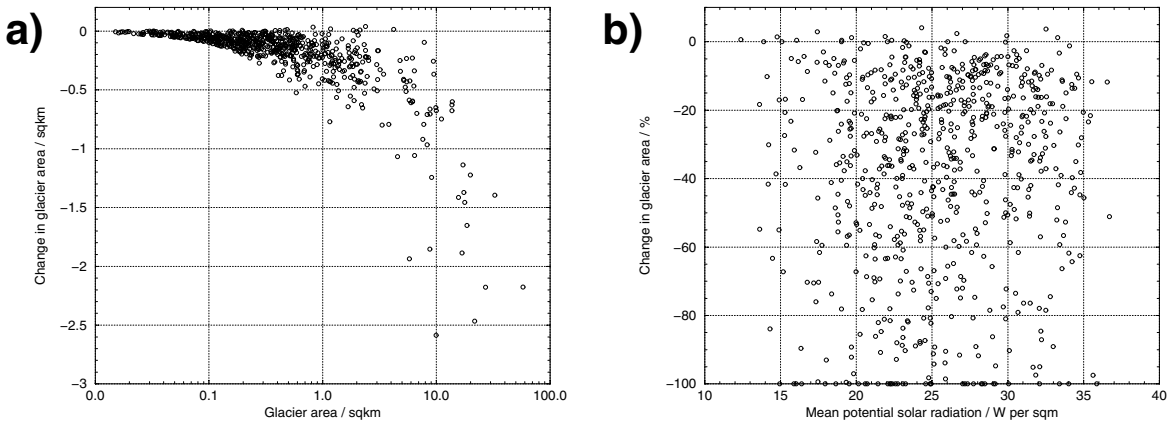

Figure 7.9: *a) Absolute change in glacier area with glacier size, and b) relative change in area vs. potential direct short-wave solar radiation.*

Set (II): Eastern part of Switzerland (1973-1999, including debris correction)

The data set for the eastern part of Switzerland is much smaller than for the western part (data are given in Table 7.3). Individual values and average losses per area class are not plotted, as this figure is similar to Fig. 7.8. Instead, an example of glacier change from 1973 (yellow) to 1999 (black) is displayed in Fig. 7.10 for the Rheinwald region, demonstrating quite clearly the differences in area change for individual glaciers (P=Paradiesglacier).

In comparison to set (I) no glacier is larger than 20 km^2, only one glacier is larger than 10 km^2, few glaciers are smaller than 0.1 km^2 and comparably more glaciers with sizes between 0.1 and 0.5 km^2 exist. The average glacier size in 1973 is now similar to the sample of the 2073 glaciers and average relative loss of area (-31%) is higher than for set (I). Glaciers smaller than 1 km^2 are responsible for 58.6% of the total area loss, although they cover only 34% of the area.

Area class	Count	Area [km^2]		Area change 73-99		Mean size [km^2]		Part of area [%]	
		1973	1999	[km^2]	[%]	1973	1999	1973	1999
0.1	36	2.58	0.56	-2.02	-78.2	0.07	0.02	1.7	0.5
0.5	131	31.65	12.56	-19.09	-60.3	0.24	0.10	20.3	11.7
1.0	26	18.21	10.86	-7.35	-40.4	0.70	0.42	11.7	10.1
5.0	26	49.64	36.29	-13.35	-26.9	1.91	1.40	31.8	33.7
10.0	5	36.72	31.10	-5.62	-15.3	7.34	6.22	23.5	28.9
20.0	1	17.41	16.20	-1.21	-6.9	17.41	16.20	11.1	15.1
Total	225	156.21	107.58	-48.63	-31.1	0.69	0.48	100	100

Table 7.3: *Summary data for glacier area change between 1973 and 1999 in the eastern part of Switzerland. 'Area class' is in km^2 and only the largest size within each class is listed.*

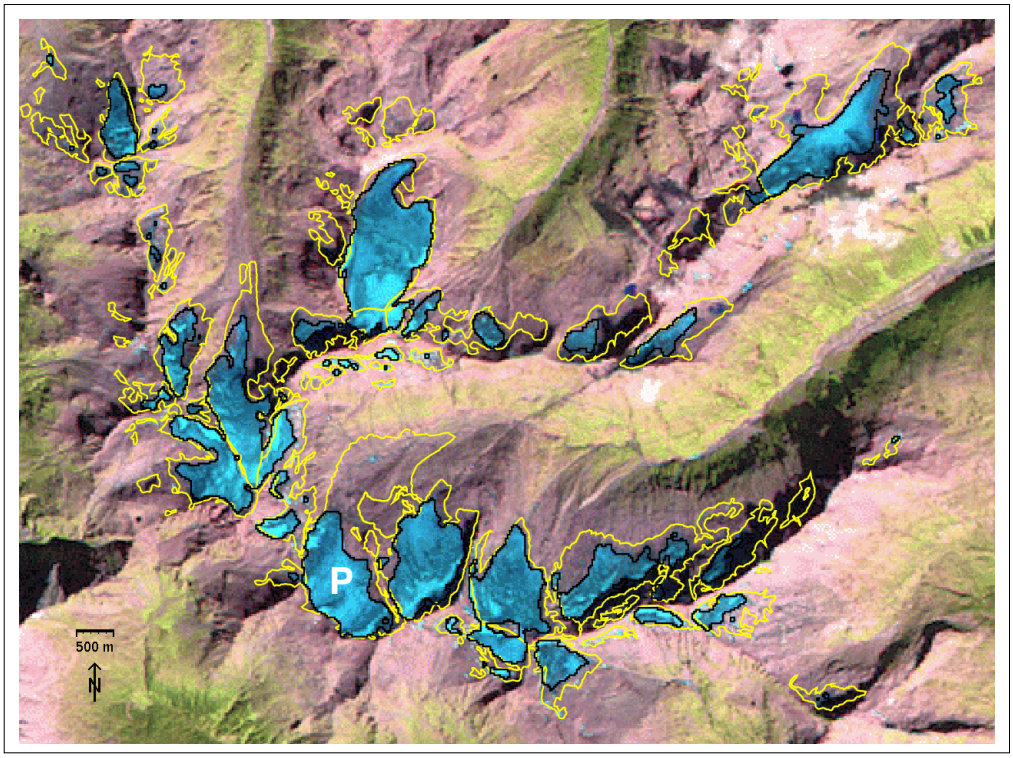

Figure 7.10: *Illustration of glacier change in the Rheinwald region (P=Paradies glacier) from 1973 (yellow) to 1999 (black) using the TM543 FCC from 1999 as background (glaciers appear light blue).*

Set (III): Western part of Switzerland (1973-1985-1992-1998, mostly debris free)

For this selection all glaciers from set (I) are evaluated again and most of the debris-covered (larger) glaciers are rejected. This increases the average loss for all 471 glaciers considered to -19.1%. Most glaciers with an advance period between 1973 and 1985 are also in the selection, as they are generally smaller than 10 km^2 and often free of larger debris. For 20 glaciers debris-covered parts are added manually in the 1985 and 1992 images. The glacier basin coverage has been edited slightly to detach some glaciers in 1985 from snowfields; some glaciers are rejected due to unclear boundaries to these snow fields.

The advance period of Alpine glaciers during the 1970s as documented from the annual length measurements (e.g., Patzelt, 1985), is also evident in Table 7.4. While the average change from 1973 to 1985 is only -1%, glaciers sized 5 - 10 km^2 even show a gain in area (+1%). Also glacier sizes in the two smaller area classes remain nearly unchanged. Glaciers smaller than 1 km^2 show a small loss in area. The average area change from 1985 to 1998 is -18.2% (with respect to the 1985 area), a value also found in previous studies (Paul, 2002b). The advance period is also depicted in Fig. 7.11a, showing relative change in glacier area between 1973 and 1985 vs. glacier size. Again, the increase in scatter towards smaller glaciers is most evident. For glaciers larger than 0.5 km^2 the increase in area does not exceed +20%. Fig. 7.11b depicts relative change in area vs. mean slope in order to verify an assumed steeper slope for glaciers with a gain of area. But as Fig. 7.11b shows, such a dependence is not obvious.

Area		Area [km^2]				Area change [km^2]			Area change [%]		
class	Count	1973	1985	1992	1998	73-85	73-92	73-98	73-85	73-92	73-98
0.1	79	4.59	4.23	2.82	1.69	-0.36	-1.78	-2.91	-7.9	-38.7	-63.2
0.5	227	56.77	53.71	42.82	34.07	-3.06	-13.96	-22.71	-5.4	-24.6	-40.0
1.0	75	51.02	50.95	43.33	37.98	-0.08	-7.70	-13.04	-0.2	-15.1	-25.6
5.0	76	135.46	134.98	122.89	112.68	-0.48	-12.57	-22.79	-0.4	-9.3	-16.8
10.0	11	78.50	79.29	75.12	71.77	+0.79	-3.38	-6.73	+1.0	-4.3	-8.6
20.0	3	49.81	49.07	47.23	46.16	-0.74	-2.58	-3.66	-1.5	-5.2	-7.3
Total	471	376.17	372.24	334.20	304.34	-3.93	-41.96	-71.82	-1.0	-11.2	-19.1

Table 7.4: *Summary data for glacier area change between 1973, 1985, 1992 and 1998 for the western part of Switzerland. 'Area class' is in km^2 and only the largest size within each class is listed.*

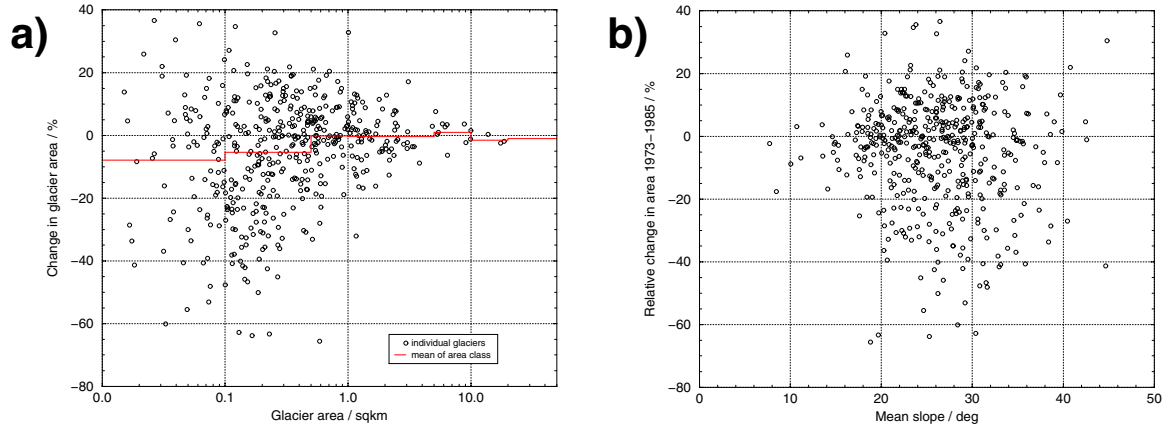

Figure 7.11: *a) Relative change in glacier area from 1973 to 1985 vs. glacier size for 471 glaciers. b) Mean slope vs. glacier change for the same sample and time period.*

In Fig. 7.12, an example with steep mountain glaciers in an advanced 1992 position located in the 'Damma group' is displayed (cf. App. 3.3-1b for location). The numbered glaciers are (1973 size in km^2): (1) *'Brunnenfirn W'* (0.86), (2) *'Brunnenfirn E'* (0.34), (3) *'Stockglacier'* (0.26) and (4) *'Flachensteinfirn'* (3.46). The image from Sep 1992 is created by a fused TM / SPOT pan image (scenes #8 and #11) as background and glacier outlines from 1973 (red), 1985 (yellow), 1992 (green) and 1998 (blue) as an overlay. Each of the four numbered glaciers are larger in 1985 and 1992 than in 1973. Glacier (1) reached its 1973 extent in 1998, glaciers (2) and (3) are somewhat smaller and (4) is in parts still larger. The very small glaciers in the lower part of Fig. 7.12 disappeared by 1998 or turned into firn fields.

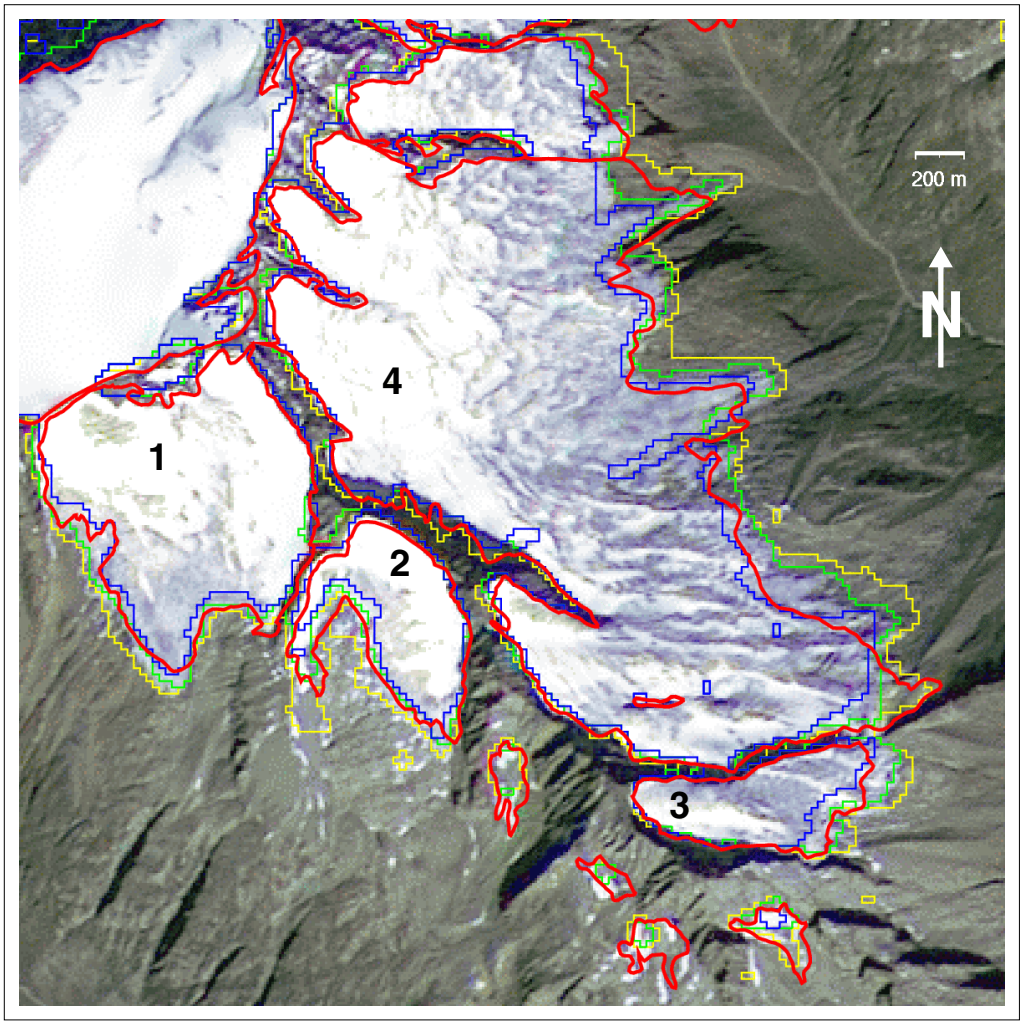

Figure 7.12: *Outlines of glaciers in the Damma group from 1973 (red), 1985 (yellow), 1992 (green) and 1998 (blue) on a fused TM / SPOT pan image as background. See text for explanation of numbers.*

The relative decrease in glacier area is somewhat greater from 1985 to 1992 than from 1992 to 1998 (Table 7.4). This is not obvious from Fig. 7.12, where individual glacier behaviour dominates the change. The four glaciers mentioned above are not within the length measurement network, and only satellite imagery (apart from aerial photography) is able to reveal such changes in a systematic way. The fact that such small-scale glacier changes during a 6- or 7-year period can be resolved with Landsat TM at this detail, indicates the possibility of implementing a five- to ten-year monitoring interval. If spatial resolution is even better (e.g., the 15 m ASTER sensor), a shorter period for control of glacier development may also be feasible.

7.3.2. Changes in length

To obtain statistical data about changes in glacier length between 1973 and 1998, 683 out of the 713 glaciers from set (I) are selected. Most of the glaciers rejected had zero length in 1998. Statistical data are summarized in Table 7.5, although the averages and totals given should not be used for climatic interpretation, as the signal from the individual response time of a glacier is erased. Relative change in glacier length vs. glacier length is given in Fig. 7.13a. While the average of the relative retreat per length class increases with decreasing glacier length, the absolute retreat for glaciers shorter than 10 km is similar. Glaciers longer than 10 km retreat twice as much, at least on average. Glaciers shorter than 5 km account for 94% of the total retreat and the part of each length class on the entire length changes slightly towards the longer glaciers (Table 7.5).

Length		Length [km]		Difference 1973 - 1998			Mean length		% of total length	
class	Count	1973	1998	[km]	%	average	1973	1998	1973	1998
0.5	156	55.13	28.30	-26.83	-48.7	-0.17	0.35	0.18	5.5	3.3
1.0	230	167.73	113.86	-53.87	-32.1	-0.23	0.73	0.50	16.8	13.4
5.0	263	505.42	443.84	-61.58	-12.2	-0.23	1.92	1.69	50.6	52.3
10.0	29	196.15	189.21	-6.95	-3.5	-0.24	6.76	6.52	19.6	22.3
50.0	5	74.98	72.81	-2.17	-2.9	-0.43	15.00	14.56	7.5	8.6
Total	683	999.42	848.02	-151.40	-15.1	-0.22	1.46	1.24	100	100

Table 7.5: *Summary data for glacier length changes between 1973 and 1998 selected from data set (I). 'Mean length' and 'Length class' is in km with only the largest length within each class being listed.*

The plot for the relative change in glacier length vs. glacier length (Fig. 7.13a) is similar to that for the area change (Fig. 7.8). The dependence is a little weaker and scatter dominates for glaciers shorter than 2 km. There is no dependence of relative or absolute change in length from further 3D parameters. Hence, a scatter plot of relative change in glacier area vs. relative change in glacier length is selected for Fig. 7.13b. As most values are above the identity line (red), the relative change in area is usually larger than the corresponding length change. This is indeed an indication that change in glacier area is not restricted to the glacier tongue and glacier monitoring from space is especially useful in revealing changes in glacier area.

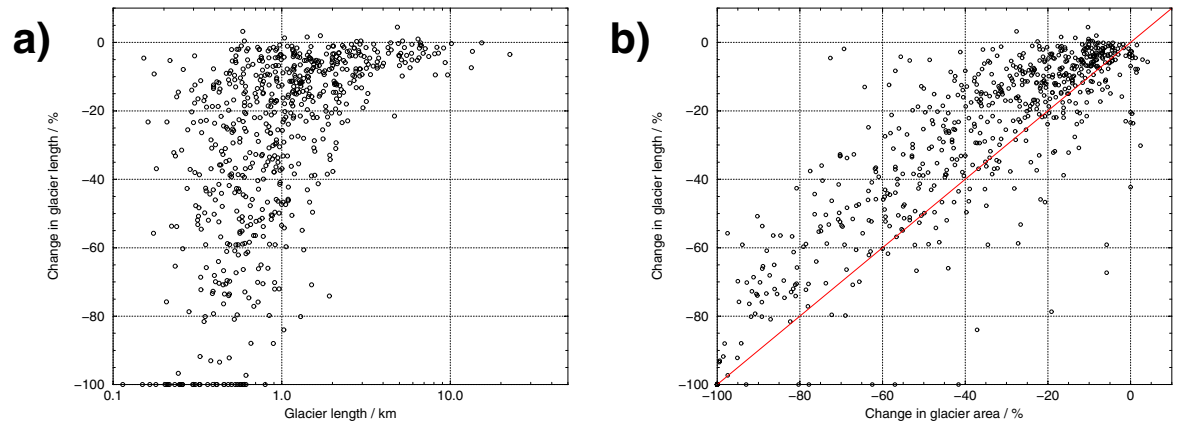

Figure 7.13: *a) Relative change in glacier length between 1973-1998 vs. glacier length for 683 glaciers. b) Relative change in area vs. relative change in length for the same glaciers and time period.*

7.3.3. Changes of 3D parameters from 1973 to 1998

Minimum elevation, elevation range and mean slope

The change of selected glacier parameters from 1973 to 1998 is derived from the DEM25L2 with the respective glacier outlines and illustrated in Fig. 7.14. While Fig. 7.14a and b are devoted to change in minimum elevation, Fig. 7.14c displays change in elevation range and Fig. 7.14d change in mean slope. The scatter plot of Fig. 7.14a exhibits a shift of minimum elevation towards higher values (points above the red identity line) with an average of +66 m and a standard deviation of 74.6 m. Some points are also below the identity line indicating that some glacier tongues in 1998 extend to lower elevations than in 1973. This is also visible in Fig. 7.14b, where the change in elevation is plotted against glacier size. At least three explanations are possible for the lower minimum elevations: (1) the glacier (or a part of its tongue) is still larger than in 1973 (cf. Fig. 7.12), (2) the outline is shifted as a result of improper orthorectification, and (3) different glacier parts are compared with each other.

In Fig. 7.14c the change in elevation range is displayed. In general there is a decreasing range covered by each glacier (circles below the identity line), but again with some exceptions (same reasons as for minimum elevation). On average, elevation range decreased by 97 m with a standard deviation of 100.5 m. Values of mean slope have increased since 1973 as most glaciers have been retreating to higher elevations with steeper topography.

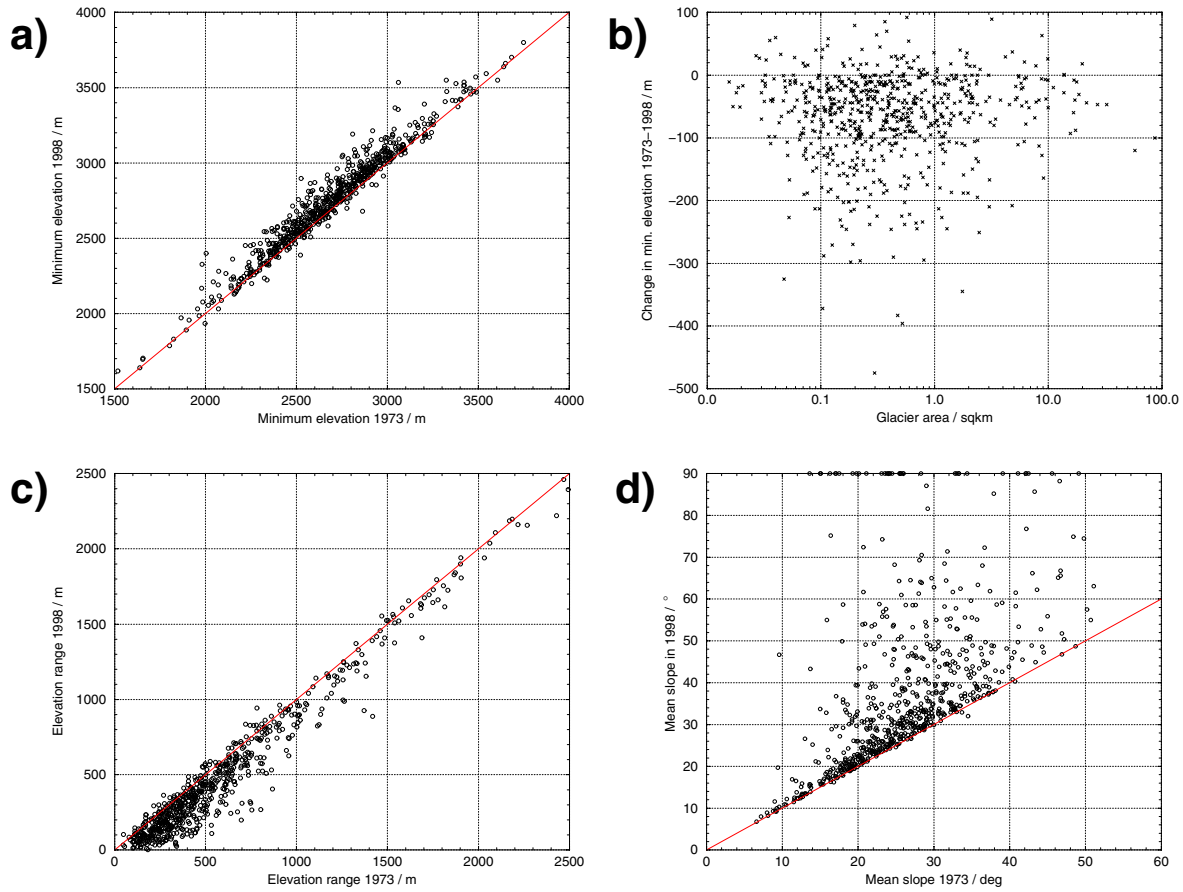

Figure 7.14: *Scatter plots of 1973 glacier parameters vs. 1998, the red line is the identity. a) Minimum elevation, c) elevation range, d) mean slope, b) change in minimum elevation vs. glacier area.*

Hypsography

For a selection of 683 glaciers (in 1973) the hypsography is calculated at 100 m intervals using an AML script and a Fortran program (App. 2.2-4 and 2.3-3). For each interval and the years 1973 (red and blue) and 1998 (blue) the area covered is plotted in Fig. 7.15. For 1998 all glaciers within a basin (defined by the former 1973 glacier extent) are summarized. The largest absolute loss of glacier area can be found in the elevation range 2700 to 3000 m. This is also the elevation range, where most of the glaciers are situated (cf. Fig. 7.4), resulting in a smaller relative change (about -20%) than for lower elevations (up to -40%). Only minimal change takes place above 3200 m. By using linear interpolation the median elevation of the area distribution is calculated as 2908 m in 1973 and 2935 m in 1998, indicating a slight shift (+27 m) of glacier distribution towards higher elevations.

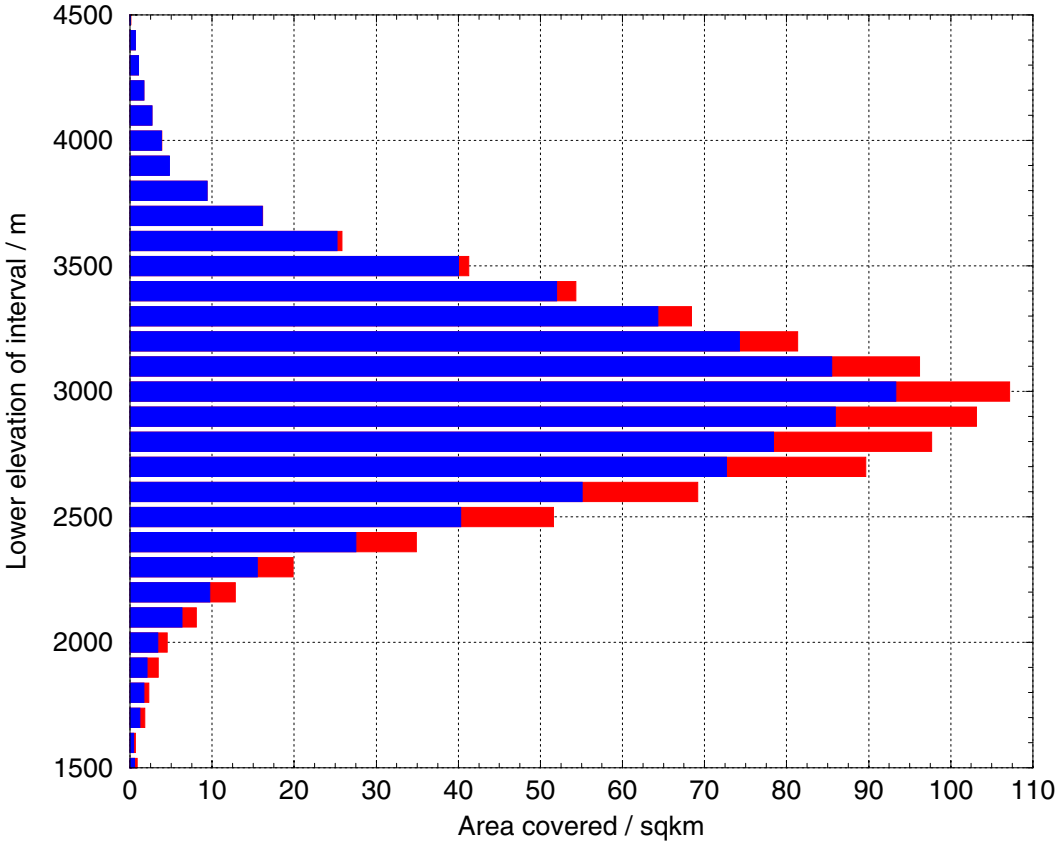

Figure 7.15: *Glacier hypsography with 100 m equidistance for 1973 (red and blue) and 1998 (blue) as derived for 683 glaciers in the western part of Switzerland from data set (I). DEM25 © swisstopo.*

7.3.4. Parameterizations

The parameterization scheme for glacier inventory data as discussed in Haeberli and Hoelzle (1995) is applied to the data obtained from DEM-derived parameters of the digitized 1973 inventory and the length changes between 1973 and 1998 as derived from the 1998 satellite image. Some of the more interesting relationships are displayed in Fig. 7.17. The gaps in Fig. 7.17c, e, and f are due to the parameterization scheme used for calculating the length of the ablation area (0.5 * L_0 for glaciers shorter than 2 km and 0.75 * L_0 for longer glaciers).

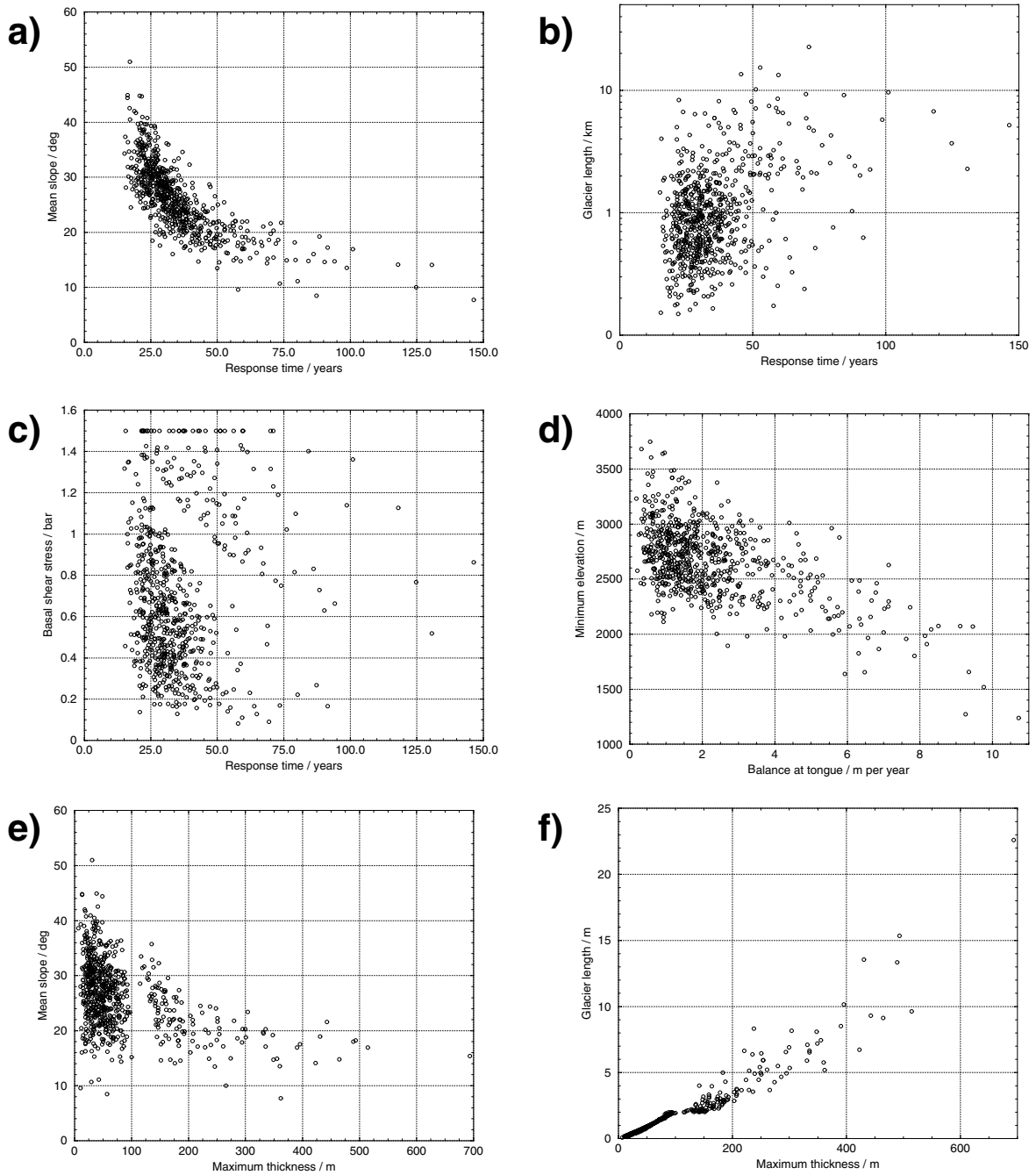

Figure 7.16: *Scatter plots derived from the parameterization scheme for glacier inventory data (Haeberli and Hoelzle, 1995) and applied to the digitized 1973 inventory data (see text for explanation). DEM25 © swisstopo.*

In order to achieve similarity with previously published figures, but in contrast to the usual display, the independent variable is shown on the x-axis (abscissa) on all graphs of Fig. 7.16. The scatter plot of response time vs. mean slope in Fig. 7.16a reveals that the steeper a glacier is, the shorter is the response time. This relation is a consequence of the physical parameterization scheme used (Haeberli and Hoelzle, 1995), which assumes a decreasing difference between ELA and terminus altitude for a decreasing slope and hence, a decreasing ablation at the terminus, resulting in increasing response times (∞ for a zero slope). Figure 7.16b

(response time vs. length) shows that response time of small glaciers (shorter than 2 km) is controlled by topography (strong scatter) and not by dynamic ice flow. However, the general trend of increasing response time (t_r) for longer glaciers is still obvious. A similar observation is evident from Fig. 7.16c (t_r vs. basal shear stress τ): For very slow-flowing glaciers (τ below 1.0), t_r is not correlated with τ, while t_r decreases with increasing τ for higher values of τ (the faster the glacier flows, the higher its basal shear stress).

In Fig. 7.16d the balance at the glacier tongue vs. minimum elevation is shown, proving that the lower a glacier tongue reaches, the higher the ablation at the tongue will be, since air temperature increases towards lower elevations. Fig. 7.16e depicts the dependence of maximum thickness on mean slope, indicating the steeper the glacier, the less thick is the ice. However, small glaciers do not conform with this statement, as they do not fit into the parameterization scheme. Finally Fig. 7.16f (maximum thickness vs. length) illustrates the increasing maximum thickness of a glacier with increasing glacier length. Although this correlation may be obvious, Fig. 7.16e also includes glaciers that deviate from the rule, making them interesting for further studies. In summary, the scatter plots indicate that small glaciers are not suitable for the parameterization scheme used and that physical relationships are reproduced adequately.

The scheme is also used for calculation of glacier volumes according to the equation given in Table 6.5 (physical relation) and using a form factor of 0.6. The form factor is used to account for the dominant glacier type in a sample and is related to the ratio of glacier half width and mean thickness (Paterson, 1994). For comparison purposes glacier volumes are also calculated using the empirical relation given by Maisch et al. (2000) with the same data set (cf. Table 6.5). The values for 718 glaciers are (in km^3): 57 (1973) and 51 (1998) with the physical relation, and 63 (1973) and 57 (1998) with the empirical relation, yielding a volume loss of 6 km^3 or -10%. The relative change in volume should be higher than the area change (-14%) as a result of additional down-wasting, but this sample holds nearly all the large glaciers with very small relative volume changes. Multiplication of the average cumulative mass balance of six Alpine glaciers (-7.2 m weq) with the half of the area sum from 1973 and 1998, yields a volume change of -6.8 km^3, agreeing quite well with the 6 km^3 calculated above. Using a form factor of 0.8 returns 43 km^3 for the 1973 volume, which is 50% less than obtained by the empirical relation, indicating the sensitivity of volume calculations to the form factor.

The parameterization of secular mass balances from changes in glacier length as described in paragraph 2.3.1 has been applied successfully to Alpine glaciers by Hoelzle et al. (2003). The same method is used here for the cumulative length changes between 1973 and 1998 and glaciers with calculated response times of 25 to 35 years. Only glaciers within the length measurement network are used, as the length changes derived automatically from central flow lines show large deviations compared to measured values (see 7.4.3). The mean mass balance for this period is calculated for each glacier by multiplication of the specific mass balance (in mm water equivalent) by the average area of 1973 and 1998. Division by the density of glacier ice (900 kg/m^3) gives glacier volume change.

The comparison with volume changes obtained from the area scaling reveals that the former are smaller by a factor of 10 to 1000. There are two reasons for this: (1) Many of the 19 glaciers considered have cumulative length changes near zero for the period 1973 to 1998 (12 have less than 100 m), resulting in extremely small volume changes. (2) Most glaciers included are rather small (9 are smaller than 2 km^2, only 6 are larger than 5 km^2), and these small glaciers do not fit into the parameterization scheme. Thus it seems that the parameterization scheme obviously gives valid results for the calculation of secular changes of comparable large glaciers. However, assuming a reaction time of about 15 years (which is half of the response time used), these small volume changes reflect the balanced period 1970 to 1985 quite well.

7.4. Discussion

7.4.1. Changes in glacier area

As with all statistical data, results have to be interpreted with care. The relative change of glacier area depends strongly on the largest area class considered. Data set (I) for the western part of Switzerland includes the five largest glaciers (all > 20 km^2) and the relative change for all glaciers is -13.7%. If glaciers > 20 km^2 are not considered, this value drops to -16.1% and down to -18.6% for all glaciers < 10 km^2. In the case of data set (II) for the eastern part of Switzerland (one glacier larger 10 km^2), the relative change is -31%, since a greater number of smaller glaciers is within the selection. This indicates that relative changes in glacier area should always be given together with the area classes used and their part on the entire area.

Assuming only small changes in glacier area between 1998 and 1999, both data sets are added, resulting in 938 glaciers with a total area of 983 km^2 in 1998/9 and a relative change in area of -16.1% (cf. Table 7.6). Interpolation of the combined relative area change per area class (column 9) to all 2057 glaciers of the basic 1973 data set (shaded columns) yields an average relative area change of -18.4% (column 10 in Table 7.6). With respect to the uncertainties of the TM-derived glacier areas (±3%), this value can be rounded to a loss of 1/5 of the 1973 area.

Area	Count		Area [km^2]		% of total area		Change 1973-1998/9		Interpol.
class	1973	1998/9	1973	1998/9	1973	1998/9	[km^2]	[%]	[km^2]
0.1	1022	164	40.1	3.56	3.1	0.4	-6.49	-64.6	-25.9
0.5	673	448	153.9	60.27	12.0	6.1	-50.43	-45.6	-70.1
1.0	151	131	104.1	63.51	8.1	6.5	-26.11	-29.1	-30.3
5.0	157	141	296.0	217.05	23.0	22.1	-47.15	-17.9	-52.8
10.0	35	36	249.4	232.58	19.4	23.7	-28.14	-10.8	-26.9
20.0	14	13	216.3	192.84	16.8	19.6	-17.13	-8.2	-17.7
100.0	5	5	225.9	212.95	17.6	21.7	-12.95	-5.7	-12.9
Total	2057	938	1285.7	982.76	100	100	-188.4	-16.1	-236.7

Table 7.6: *Summary data for the basic 1973 data set (2057 glaciers, shaded columns) and the joint 1998/9 data sets (columns 3, 5, 7-9). Interpolated change in area is given in column 10 'Interpol.' (multiplying column 4 and 9). 'Area class' is in km^2 and only the largest size within each class is listed.*

According to the annual measurements of glacier length changes (e.g., IAHS, 1998), many glaciers in the Alps advanced between 1973 and 1985 (Patzelt, 1985) and retreated or shrank in area thereafter (e.g., Böhm, 1993). The advance and retreat period can also be followed from the TM-derived area changes (Table 7.4), showing only small area changes from 1973 to 1985 (-1%). This indicates that a period of glacier advance must not be accompanied by an overall increase in glacier area, as smaller glaciers (with a different response time) may shrink during the same period, resulting in a net loss of overall glacier area. From 1973 to 1992 relative change in area was about -11.2%. Similar values were found in an earlier study with 165 glaciers of the Tyrolean Alps, Austria (-1.5% and -10.9%, respectively), but with MSS-derived glacier outlines for 1973 (Paul, 1997). Area change between 1969 and 1992 for 225 glaciers of the same region was somewhat larger (-18%), but glacier inventory data from 1969 was used for this comparison (Paul, 2002a). The relative change in area from 1992 to 1998 is comparable to

the period 1985 to 1992. This indicates that decrease in glacier area is not accelerating. Although all glaciers are controlled carefully, misinterpretation of snowfields (especially in 1985) is still possible, resulting in somewhat larger glaciers than in reality.

Glaciers smaller than 0.1 km^2 are considered after all, as they share only a small part of the entire area (less than 1%) and fit quite well to the remaining data, although their TM-derived decrease may be overestimated. If only glaciers larger than 0.1 km^2 in 1998 are considered, 258 or 36% of the 713 glaciers from data set (I) would have to be excluded (two of them are larger than 0.4 km^2 in 1973). These glaciers account for 30.7 km^2 (3%) of the entire 1973 glacier area.

The decrease in glacier size is not restricted to small glaciers and a strong scatter of area change is also evident in Fig. 7.10. While one of the larger glaciers ('Paradies') lost its tongue, others just receded or did not change at all (cf. Kuhn et al., 1985). Smaller glaciers show all variations from total disappearance, to losing half of their former area in a separate basin, to shape-conform retreat. Considering the strong variations of topography, it is obvious that there is no dependence of area change from further glacier parameters. Multivariate statistical analysis may reveal whether dependencies for more than two parameters can be found or not.

Since glacier change (area, length) depends on glacier size it must be noted again that all glacier parts of a former 1973 'parent glacier' are summarized for the following years to calculate the changes. Moreover, glaciers that share one accumulation area but develop different tongues (e.g., Stein- and Steinlimmi glacier) are not separated and glaciers with different accumulation basins and individual tongues that are in contact (e.g., Brunegg- and Turtmann glacier), are separated in most cases. Most flow divides used in the CH-INVGLAZ database are deleted if they have no visible equivalent such as rock outcrops.

7.4.2. Comparison of decadal changes

In order to compare glacier changes between 1973 and 1998/9 with the period 1850 to 1973, decadal changes are calculated for each area class. Data for 1850 and 1973 is taken from the CH-INVGLAZ database and are summarized in Table 7.7 for comparison with the other data sets, having a similar distribution of glaciers by area and number. Relative area changes are somewhat different, but show the typical characteristics: towards smaller glaciers the scatter and the average loss increases (Fig. 7.17a). While glaciers smaller than 1 km^2 account for 21.5% of the area, they cause 40% of the loss.

Area		Area [km^2]		Change 1850-1973		Mean size [km^2]		% of total area	
class	Count	1850	1973	[km^2]	[%]	1850	1973	1850	1973
0.1	297	17.27	7.68	-9.59	-55.5	0.06	0.03	1.0	0.6
0.5	715	181.29	84.39	-96.90	-53.4	0.25	0.12	10.5	6.7
1.0	249	172.51	95.25	-77.26	-44.8	0.69	0.38	10.0	7.6
5.0	253	524.38	352.71	-171.67	-32.7	2.07	1.39	30.4	28.1
10.0	26	195.53	157.73	-37.80	-19.3	7.52	6.07	11.3	12.6
20.0	18	259.87	222.67	-37.20	-14.3	14.44	12.37	15.0	17.7
100.0	9	270.50	238.20	-32.30	-11.9	30.06	26.47	15.7	19.0
Total:	1567	1621.35	1158.64	-462.71	-28.5	1.03	0.74	100	100

Table 7.7: *Summary data for glacier area change between 1850 and 1973 for all glaciers from the inventory CH-INVGLAZ. 'Area class' is in km^2 and only the largest size within each class is listed.*

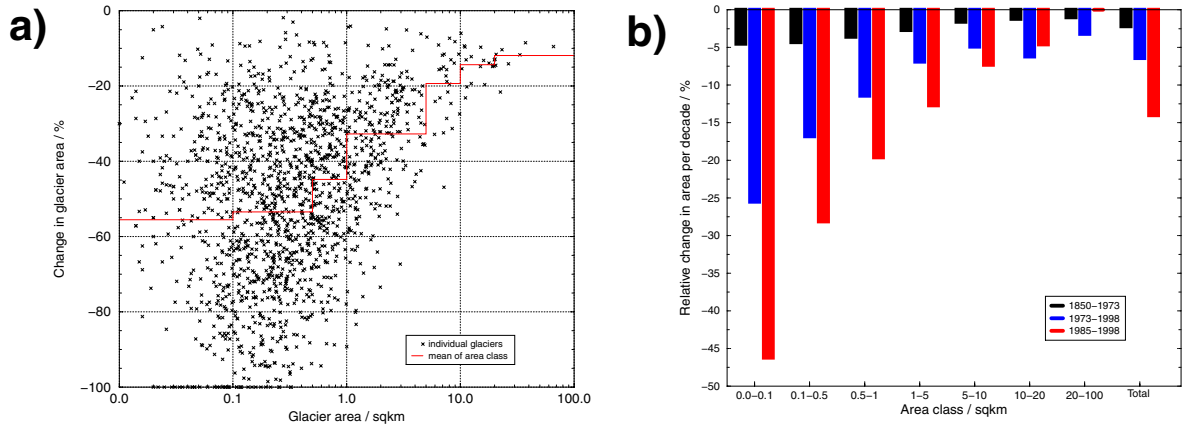

Figure 7.17: *a) Relative change in glacier area between 1850 and 1973 vs. glacier area in 1850 for 1567 glaciers of the data set CH-INVGLAZ. b) Relative change in glacier area per decade for seven area classes and three time periods.*

The average area change per decade is calculated for the time periods 1850-1973, 1973-1998/9 and 1985-1998 using the data sets CH-INVGLAZ, (I) and (II) together and (III), respectively. The data is summarized in Table 7.8 together with the number of glaciers, total area and change per decade (in km^2 and %) for each time period. The relative change per area class is also depicted in Fig. 7.17b. It must be noted that samples differ (e.g., the 1985-1998 data set is without glaciers larger than 20 km^2) and percentages of total area in each area class are not the same. This may alter the average decadal loss of area of a distinct area class by a few percent.

	1850		1850 - 1973		1973		1973 - 1998/9		1985		1985 - 1998	
Area		Area	Change / 10a			Area	Change / 10a			Area	Change / 10a	
class	count	[km^2]	[km^2]	[%]	count	[km^2]	[km^2]	[%]	count	[km^2]	[km^2]	[%]
0.1	297	17.27	-0.78	-4.5	164	10.05	-2.60	-25.9	79	4.23	-1.95	-46.2
0.5	715	181.29	-7.88	-4.3	448	110.70	-20.17	-18.2	227	53.71	-15.11	-28.1
1.0	249	172.51	-6.28	-3.6	131	89.62	-10.44	-11.6	75	50.95	-9.98	-19.6
5.0	253	524.38	-13.96	-2.7	141	264.21	-18.86	-7.1	76	134.98	-17.15	-12.7
10.0	26	195.53	-3.07	-1.6	36	260.72	-11.26	-4.3	11	79.29	-5.78	-7.3
20.0	18	259.87	-3.02	-1.2	13	209.97	-6.85	-3.3	3	49.07	-2.25	-4.6
100.0	9	270.50	-2.63	-1.0	5	225.89	-5.19	-2.3	0	0	0	0
Total	1567	1621.35	-38.30	-2.2	938	1171.16	-75.36	-6.4	471	372.24	-52.22	-14.0

Table 7.8: *Summary data for decadal glacier area change from 1850 to 1973, 1973 to 1998/9, and 1985 to 1998. 'Area class' is in km^2 and only the largest size within each class is listed.*

On the other hand, data set (II) from the eastern part of Switzerland with a much higher loss between 1973 and 1999 is not considered. Thus, the decadal loss 1985-1998/9 might even be somewhat larger. While the decadal change is relatively constant for the period 1850 to 1973 in all area classes, Fig. 7.17b clearly shows that area loss has strongly increased during the last decades, especially for smaller glaciers. This might already indicate the phase of accelerated glacier disintegration, as assumed for the next decades by Maisch et al. (2000) from model calculations. For larger glaciers the separation from formerly adjacent tributaries and the increasing size of rock outcrops will accelerate glacier decrease in the future.

7.4.3. Changes in glacier length

The comparison of satellite-derived changes in glacier length between 1973 and 1998 with in-situ measurements reveals very large differences between the two data sets. Only 20 out of 79 selected glaciers showed deviations smaller than about two TM pixels (i.e. 60 m). For all 79 glaciers, differences range from -430 to +480 m with a mean of 124 m and a standard deviation of 176 m. Visual inspection reveals the following problems (cf. Fig. 7.18):

(1) The most prominent error source results from an additional shortening of the central flow line at the highest glacier point for at least two reasons: glacier melt around the entire perimeter (small glaciers) or the use of small firnfields (couloirs) as a starting point for the central flow line (larger glaciers). While manual adjustments could help in the latter case, a more general discussion about the minimum glacier size to be considered for length change measurements is necessary to solve the former problem.

(2) Manual adjustments are applied to the 1998 flow lines as a consequence of a changed glacier geometry (nunataks, intersection with the glacier perimeter), even for larger glaciers (see Fig. 7.18). For small or disintegrating glaciers it is often very difficult to decide where to place a new central flow line, which has a different length per se.

(3) Delineation of debris-covered glacier parts (in 1998) must not coincide with the glacier terminus used in the field. Moreover, the digitized 1973 outline is possibly wrong, due to inaccurate digitizing or even misinterpretation of the original aerial photography.

(4) Field measurements of length changes are not carried out at the central flow line, but from various geodetic points in the glacier forefield. Resulting differences are even more pronounced in the case of a broad glacier terminus with various lobes.

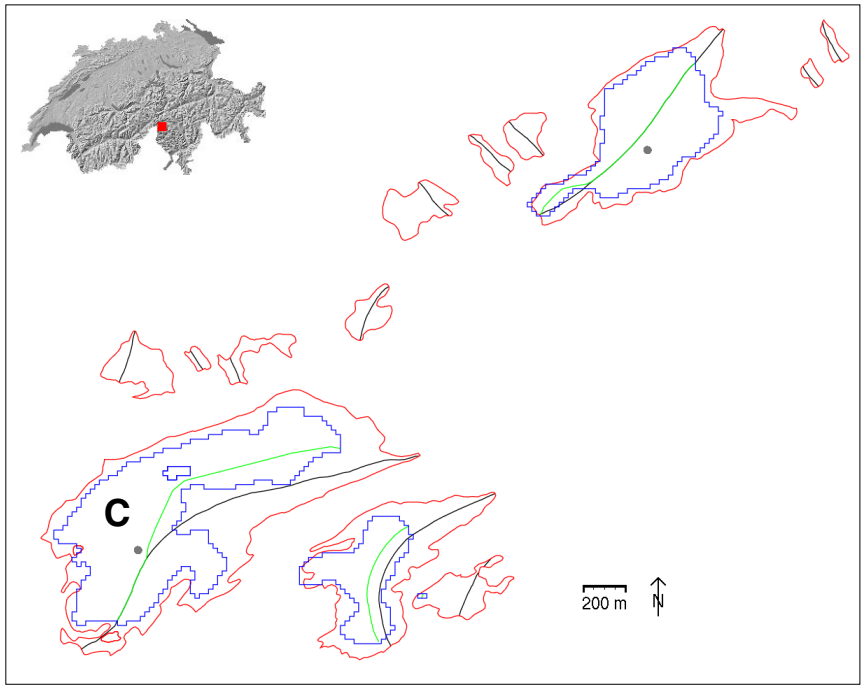

Figure 7.18: *The original 1973 central flow lines (black) have to be changed (green) in order to resemble the changed glacier geometry (perimeter in 1973 is red, in 1998 blue). The glacier group is also depicted in Fig. 5.16b (C=Cavagnoli glacier).*

In summary, the automatic GIS-based procedure used here for calculation of glacier length changes is not sufficient. While manual (on-screen) measurements of length changes are an alternative, a comparison with field measurements has to use the same geodetic control points (location and number). The required GIS integration of these points may be utilized by GPS (Global Positioning System) measurements of each point. Meanwhile the GIS-based calculation of length changes can be utilized from a set of arbitrary chosen control points in the glacier forefield to the glacier front.

7.4.4. Accumulation area ratios

Accumulation area ratios (AARs) are calculated for 167 selected glaciers from the 1985 and 1998 data set of scene 195 (western part of Switzerland). Each glacier is controlled individually for the assigned snow-covered area by comparison with contrast enhanced TM images. Glaciers with larger deviations (snow-covered areas tilted away from the sun) are not considered. For both years glacier outlines from 1973 were used for the total glacier area, as the uncertainties of the snow cover delineation (about 10 to 20%) are higher than the area change since 1973, at least for most of the glaciers investigated. Snow delineation from simple thresholds in the 1998 scene is extremely difficult as polluted firn from previous years (partly lower reflectance than bare ice) and highly reflecting bare ice areas are observed (brighter than snow). For this reason a thresholded TM3 * TM4 image is used for snow cover delineation, as both effects mentioned above are strongly reduced in TM4. The chosen threshold (20000) is a quite good compromise for most glaciers.

As both scenes are acquired near the end of the ablation period, the derived AARs can be taken as an estimation for the mass balance conditions of that year (cf. 2.1.2). The average values are: 51% for 1985 and 34% for 1998, indicating a strongly negative balance for 1998 and somewhat better (but also negative) conditions for 1985. A dependence of the AAR from glacier size could not be observed (correlation coefficient is 0.25).

8. CONCLUSIONS AND PERSPECTIVES

8.1. Conclusions

Landsat 5 TM data and a DEM are used in a GIS environment for compilation of a new Swiss glacier inventory 2000 (SGI 2000). The remote sensing and GIS methods developed may also be used in the USGS-led GLIMS project, which aims at a global glacier inventory from space.

8.1.1. Main results of glacier change analyses

Analysis of glacier change for the Swiss Alps reveals the following major findings:

- The relative loss of glacier area between 1973 and 1998/9 is 18% ±3% (about 1/5) with an assumed corresponding volume loss of about 1/4 (scaled for all glaciers).
- Relative change in area between 1985 and 1992 is similar to the period 1992 to 1998/9 with respect to the 1973 glacier size (about -10% in each period).
- The average decadal relative loss of area from 1985 to 1998 is about seven times higher than from 1850 to 1973 (but different samples are used).
- The relative change in glacier area depends somewhat on glacier size with an increasing scatter towards smaller glaciers. Other investigated 3D parameters show no correlation.
- Changes in glacier size are highly individual and only an assessment for a large number of glaciers (all size classes) gives a representative evaluation.
- The primary causes for area changes in valley and mountain glaciers are: separation from formerly connected tributaries, emerging rock outcrops, and melting along the perimeter.
- Shrinkage of small glaciers (glacieretes) is enhanced by disintegration, with an even faster melting of the smaller parts.

These observations can be interpreted as follows: The -20% reduction of glacier area since 1985 is already in the range of the -30% expected in previous studies for the year 2025 (Haeberli et al., 2002a). The change is also much faster than observed in the historical record. In particular the not monitored small glaciers contribute to the area loss, providing a good argument for intensified satellite observation. The highly variable glacier retreat characteristics (often associated with arbitrary changes in geometry) makes calculation of future glacier behaviour from numerical modelling fairly questionable, at least for the majority of all glaciers. Although changes in glacier surface elevation cannot be measured with TM, the observed changes in glacier geometry indicate a massive down-wasting since 1985 rather than a dynamic response to a changed climate. Further glacier retreat can be expected in the future, as a probable dynamic glacier reaction to the hot decade of the 1990s is still to come.

8.1.2. Results of the DIP - DEM - GIS approach

Glacier classification by means of thresholded TM4/TM5 ratio images is (1) simple, (2) robust, and (3) accurate, because (1) the method needs neither a DEM nor special image processing software and is very fast, (2) the threshold value for use is quite obvious and not very sensitive (± 0.1), and the method works also for Landsat 7 ETM+ and Terras ASTER sensor (Band 3 / Band 4), and (3) the comparison with other methods or manually derived outlines on higher-resolution satellite imagery has revealed an accuracy of better than 3% for glaciers larger than 1 km^2. The method is able to map clean glacier ice, glacier ice with sporadic (mixed pixels) or thin debris cover, clean glacier ice beneath thin cirrus clouds as well as in shadows casted by convective clouds or terrain. Misclassification occurs for vegetation and turbid water (can be corrected), and debris-covered glacier ice is not mapped (see below).

The DEM is essential for all pre-processing tasks (e.g., orthorectification of satellite images, digital terrain modelling) as well as post-processing (obtaining 3D glacier parameters, visualization of glacier changes). In order to obtain accurate glacier parameters for comparable small Alpine glaciers, the new high-precision level 2 DEM25 is used. High license costs are the major obstacle for operational use of such DEMs for glacier monitoring.

The GIS is used as the central tool for data processing and integration of various data formats (vector, raster, image), namely: (1) digitizing of glacier outlines, central flow-lines and glacier basins, (2) raster-vector conversion of TM-derived glacier maps and assignment of glacier basins and IDs, (3) calculation of 3D parameters from the DEM and storage in corresponding attribute tables, (4) 2D and 3D visual representation of glacier changes and (5) export of data tables for further computations (e.g., glacier change).

The module concept (GIS-CONV-VIS) developed can be used for operational processing of TM imagery, after basic data sets (glacier map, glacier basin vector layer, DEM) are generated. However, for practical purposes each module can also be used separately. Apart from the correct identification of individual glaciers, the correct treatment of internal polygons (nunataks) during calculations is most critical.

8.1.3. Technical problems

During data analysis the following technical problems are encountered:

- Selection of suitable TM scenes from tiny quicklooks.
  Although the new quicklooks for Landsat 7 from the USGS data server (about 250 m resolution) are well suited for a first pre-selection, snow conditions cannot be determined precisely. It would be of great advantage if it were possible to obtain particular TM4 subregions (about 200 by 200 pixels) at original resolution for a small fee.

- Availability of suitable TM scenes for glacier mapping (cloud- and snow-free):
  Since 1984 only about 2 or 3 cloud-free, end-of-ablation period scenes with appropriate snow conditions have been acquired by Landsat TM for the northwestern part of Switzerland (e.g., Silvretta, Toedi). Thus, glacier monitoring by means of optical sensors is hampered by frequent cloud cover and the remaining snowfields connected to glaciers.

- Accurate orthorectification (with an RMSE of less than a pixel) requires a lot of time:
  This is a consequence of the disturbances of the inner geometry of ESA-processed TM scenes, which do not permit the use of the same GCPs for a second scene without adjustments. Relative image matching is not used in the SGI 2000, as geocoded data sets from different sources are combined in the SGI 2000. The smaller the observed glaciers are, the better the orthorectification should be.

- Correct delineation of debris-covered ice:
  A semi-automatic method of mapping debris-covered glaciers has been developed for the SGI 2000, but the method relies on the availability of a high-quality DEM and needs manual editing in the last phase. Complete manual delineation on FCCs might provide similar results, but requires more time. On a pixel-by-pixel basis the latter is quite laborious.

8.1.4. Methodological problems

Some issues that could not be solved remain:

- Glacier identification
  A one-to-one relationship between glacier codes in the revised CH-INVGLAZ database and the digitized 1973 glacier inventory could not be established. The reason for this is the use of different glacier basins as well as a missing column in the database, responsible for tracking the parent glacier of all glacier parts assigned.

- Glacier separation
  In the SGI 2000 all glacier parts belonging to a 1973 parent glacier are summarized in the years thereafter for calculation of glacier area changes and hypsography. This is glaciologically incorrect, but the only way to include most of the glaciers in later samples. The problem is somewhat more pronounced with respect to new glacier parameters after a glacier has split into two or more parts. The part to use must be identified manually, as the GIS requires a unique code for each glacier under consideration. Moreover, the handling of glacier groups and the smallest glacier monitored should be clarified by a general discussion among experts on these issues.

- Changes in glacier length
  The automatic determination of changes in glacier length from central flow lines is not realistically possible, as glacier shortening also takes place at the highest glacier point or changes in glacier geometry (nunataks) result in divided flowlines. Length changes are difficult to compare with ground measurements because a varying number of fixed geodetic points in the glacier forefields and unknown lines of sight are used for the measurements.

Hence, the processing of the globally available old Landsat TM data sets with the efficient GIS-based methodologies available today may reveal recent glacier changes in detail. This issue could also be a goal of the GLIMS project.

8.2. Perspectives

8.2.1. Further applications of SGI 2000 data

As mentioned above, there are some issues left that could not be worked out in this thesis due to various obstacles (e.g., lack of rules for glacier basin delineation). However, most data can already be used and a large number of glaciological studies will be possible in the future.

Supplemental issues for the SGI 2000

- identification of the 'parent glacier' for each glacier in the CH-INVGLAZ database and selection of a unique code for each glacier of the digitized 1973 inventory
- creating polygon topology for the digitized 1850 glaciers by intersection with the 1973 glaciers and manual editing
- extension of the '2000' data sets to more of the disappeared glaciers after critical inspection of the 1973 data sets (outlines and database)

Possible further analysis:

- multivariate statistical analysis and visualization
- geomorphological characterization of glaciers according to their 3D parameters
- change of glacier parameters with DEM resolution and source (ASTER)
- improvement of the parameterization scheme from Haeberli and Hoelzle (1995) by using more realistic values from the set of 3D parameters (ELA, length of ablation area)

Forthcoming issues:

- improvement of snow classification on glaciers to obtain more accurate AARs
- GIS-based determination of the transient snow line elevation including a DEM
- comparing observed changes in glacier geometry with results from glacier-flow models
- relating observed climate variables with observed glacier fluctuations

8.2.2. Future global glacier monitoring (GLIMS)

Possibilities

The rather simple method used for glacier classification from satellite data (thresholded ratio images) allows rapid processing and is thus feasible for GLIMS. Automatic GIS-based data processing alone (without orthorectification and DEM information) enables quick assessments of glacier change (Paul, 2002b). However, multi-temporal change detection from sequential images is limited to regions of about 50 by 50 km with respect to the geodetic accuracy of the Landsat 5 TM raw data.

While a DEM derived from ASTER stereo bands (3N and 3B) can be used for orthorectification, the accuracy of the ASTER DEM-derived glacier parameters has to be evaluated in future studies. Support from ASTER DEMs can be expected for debris-cover delineation, especially if glaciers are much larger than Alpine glaciers and 25 m spatial resolution or 10 m vertical accuracy (RMSE) is not required (Kääb, 2002). If applied to large glaciers (area > 100 km^2), one drawback of ASTER data is the small swath covered (60 km on a side). This limitation (shared with DEMs derived from SPOT) is somewhat reduced by the comparably low price of ASTER data compared to SPOT stereo data or commercial DEMs available from national agencies. From repeated ASTER data (15 m resolution visible bands) and digital photogrammetry, calculation of glacier surface flow velocities is also possible (Kääb et al., in press), resulting in an improved understanding of glacier flow characteristics.

The capabilities of today's GIS are used in full for the GLIMS project. While database management (glacier outlines with attributes) and queries, as well as combined visualization of vector -, raster - and image data sets are used quite frequently, the GIS' computing capacity can also be utilized for GLIMS (ratio images, 3D parameters from DEM). Although an operational, work-flow-oriented processing is feasible, intermediate results should be generated for quality control (e.g., thresholds). Most time is spent on pre-processing (e.g., orthorectification, glacier basin and debris-cover delineation). The Arc/Info specific commands and procedures developed for the SGI 2000 should be transferrable to GIS software from other companies.

Limitations

Some of the limitations for satellite-derived glacier inventories are: Data availability (frequent cloud cover in high latitudes), data quality (e.g., snow cover hiding the glacier perimeter) and data pre-processing demands (e.g., orthorectification, debris cover). While accurate orthorectification is a time intensive, but at least achievable task, debris-cover delineation also requires much time, but may even fail for specific glaciers. In the case of snow or cloud cover, parts of a scene may be processed and remaining gaps filled by later scenes. Costs may be an additional limitation, for example fees for satellite data and DEM licences as well as for personnel. In comparison to a glacier inventory derived from aerial photography, the lower spatial resolution is the major drawback. However, the larger area covered and automatic multi-spectral glacier classification justify the use of satellite data.

Open questions

The technical problems mentioned above can be managed somehow, while the methodological issues may remain unsolved for some time, especially those which refer to glacier splitting with time. An example of this is, glacier tributaries that are not connected to a main glacier now, but were, perhaps, some years ago and may be again in some years. The appropriate way of assigning a unique glacier code for GIS-based processing in such cases must be clarified. However, in view of a first inventory for GLIMS, the problem is more to delineate glacier basins, especially for ice caps or ice fields, where the drainage pattern is difficult to assess. The division of glaciers with different accumulation basins that came in contact at their terminus or of many glacier lobes which originate from a single basin (in a ledge position) remain problematic.

While in the inventory of Müller et al. (1976) nearly all contributing glacier parts were added to a single glacier, the revision by Maisch et al. (2000) splits all glaciers according to (sometimes subtle) ice-flow divides, resulting in 2244 instead of 1842 glaciers. With respect to future

glacier development and GIS-based data handling a correct way of glacier identification must be defined. The calculation of glacier parameters (including lengths) is straightforward for a first inventory, but calculations become more complicated with respect to former or future inventories, because of changes in glacier geometry (rock outcrops) or glacier split (tributaries). With respect to such changes, a base year must be used to define parent glaciers.

8.2.3. Future global glacier monitoring (WGMS)

The use of satellite data for updating or generating glacier inventories has been discussed for many years (Howarth and Ommanney, 1986; Williams and Hall 1993 and 1998) and is now part of the GTOS/GCOS as Tier 5 of GHOST. Furthermore, an evolving Global Terrestrial Network for Glaciers (GTN-G) is established according to Tier 1 to 5 levels of GHOST. Its structure allows global to regional analyses of glacier changes with different intensities of measurements at various sites (Haeberli et al., 2002a). Global satellite monitoring of glaciers is now coordinated within the USGS-led GLIMS project (Kieffer et al., 2000) and possible techniques of data generation have been evaluated in this thesis. The combined use of satellite imagery and DEMs in a GIS environment is indeed a valuable method of efficient operational data processing. However, before satellite and GIS-derived glacier data can be used, new standards of data extraction and their calculation must be defined. This will be one of the major challenges for glacier monitoring in the 21. century (cf. Haeberli et al., 1998).

The primary use of satellite data will be for the creation of new and updating of former glacier inventories, as well as for monitoring of changes in glacier geometry and size. While the updating of entire national inventory data should be repeated at approximately 20 year intervals (depending on the mean size of glaciers under consideration), changes in selected smaller regions can be monitored more frequently (about 10 year intervals). For particular glaciers (hazard-related or with a characteristic behaviour) an even shorter interval (yearly) seems feasible. The exact frequency possible also depends on the availability of cloud-free scenes from the end of the ablation period and the sensor spatial resolution used.

Measurements of changes in glacier length should be continued by ground-based networks as far as possible, for a number of reasons: they have better temporal and spatial resolution, data is required for validation of satellite measurements, and the differing measurement techniques used (central-flow-line vs. multi-point) cannot be compared yet. A combined approach with yearly ground measurements and longer-term space-borne observation, covering a large number of remote and unmeasured glaciers, seems most promising.

Glacier mass balance can be estimated from space by the AAR concept or from the elevation of the transient snow line (TSL) using a DEM. If taken at the end of the balance year, AARs could indicate a regional pattern of mass balance distribution and the TSL may equal the EL. Apart from necessary improvements for robust snow classification on glaciers, some care is required for glaciers with large superimposed ice zones (refrozen meltwater). Satellite-derived ELAs will be too high in such cases. Comparisons with available field data of mass balance and ELA in that year should be used to indicate the accuracy.

In the future, detailed studies of individual glaciers with new technologies (e.g., laser scanning) and highest-resolution sensors (Ikonos) may supplement the data available from other sources. The new satellite-derived data sets could also be used to improve the assessment of global glacier area and volume as well as glacier change characteristics.

REFERENCES

ALLEN, T. R. (1998): Topographic context of glaciers and perennial snow fields, Glacier National Park, Montana, *Geomorphology*, **21** (3/4), 207-216.

AL-ROUSSAN, N., CHENG, P., PETRIE, G., TOUTIN, T., VALADAN ZOEJ, M. J. (1997): Automated DEM extraction and ortho-image generation from SPOT Level 1B imagery, *Photogrammetric Engineering and Remote Sensing*, **63** (8), 965-974.

ANDREASSEN, L. M. (1999): Comparing traditional mass balance measurements with long-term volume change extracted from topographical maps: a case study of Storbreen glacier in Jotunheimen, Norway, for the period 1940-1997, *Geografiska Annaler*, **81A** (4), 467-476.

ANIYA, M., SATO, H., NARUSE, R., SKVARCA, P. AND CASASSA, G. (1996): The use of satellite and airborne imagery to inventory outlet glaciers of the Southern Patagonia Icefield, South America, *Photogrammetric Engineering and Remote Sensing*, **62** (12), 1361-1369.

ARENDT, A. A., ECHELMEYER, K. A., HARRISON, W. D., LINGLE, C. S. AND VALENTIN, V. B. (2002): Rapid wastage of Alaska glaciers and their contribution to rising sea level, *Science*, **297**, 382-386.

BACHMANN, R. C. (1978): *Gletscher der Alpen*, Hallwag, Bern, 304 p.

BADER, S. (1990): *Die Modellierung von Nettobilanzgradienten spätglazialer Gletscher zur Herleitung der damaligen Niederschlags- und Temperaturverhältnisse - Dargestellt an ausgewählten Beispielen aus den Schweizer Alpen,* PhD Thesis, Geographisches Institut Universität Zürich, **31**, 108 p.

BAHR, D. B. (1997A): Global distribution of glacier properties: A stochastic scaling paradigm, *Water Resources Research*, **33** (7), 1669-1679.

BAHR, D. B. (1997B): Width and length scaling of glaciers, *Journal of Glaciology*, **43** (145), 557-562.

BAHR, D. B., MEIER, M. F. AND PECKHAM, S. D. (1997): The physical basis of glacier volume-area scaling, *Journal of Geophysical Research*, **102** (B9), 20355-20362.

BALTSAVIAS, E. P., FAVEY, E., BAUDER, A., BOESCH, H. AND PATERAKI, M. (2001): Digital surface modelling by airborne laser scanning and digital photogrammetry for glacier monitoring, *Photogrammetric Record*, **17** (98), 243-273.

BAYR, K. J., HALL, D. K. AND KOVALICK, W. M. (1994): Observations on glaciers in the eastern Austrian Alps using satellite data, *International Journal of Remote Sensing*, **15** (9), 1733-1742.

BELITZ, K., FRISCH, U., MAUKISCH, M., STÖTTER, J., WILHELM, F., KONETSCHNY, H., STREMPEL, K. AND ZENKE, B. (1996): Laser-Scanning ein neuartiges Verfahren zur Erstellung hochgenauer und hochauflösender digtaler Geländemodelle, *Interpraevent*, **4**, 15-25.

BENN, D. I. AND LEHMKUHL, F. (2000): Mass balance and equilibrium-line altitudes of glaciers in high-mountain environments, *Quaternary International*, **65/66**, 15-29.

BENISTON, M., HAEBERLI, W., HOELZLE, M. AND TAYLOR, A. (1997): On the potential use of glacier and permafrost observations for verification of climate models, *Annals of Glaciology*, **25**, 400-406.

BENZ, C. (1995): *Die Gletscher des Unterwallis (Hochstand 1850 - Ausdehnung heute - Schwundszenarien)*, Diploma thesis (unpublished), Geographisches Institut Universität Zürich, 181 p.

BINAGHI, E. MADELLA, A., MADELLA, P. AND RAMPINI, A. (1993): Integration of remote sensing images in a G. I. S. for the study of alpine glaciers, in: Winkler, P. (Ed.), *Remote sensing for monitoring the changing environment of Europe*, Balkema, Rotterdam, 173-178.

BINAGHI, E., MADELLA, P., MONTESANO, M. P. AND RAMPINI, A. (1997): Fuzzy contextual classification of multisource remote sensing images, *IEEE Transactions on Geoscience and Remote Sensing*, **GE-35** (2), 326-339.

BINDSCHADLER, R., DOWDESWELL, J., HALL, D. AND WINTHER, J.-G. (2001): Glaciological applications with Landsat-7 imagery: Early assessments, *Remote Sensing of Environment*, **78** (1-2), 163-179.

BISHOP, M. P., SHRODER, J. F., JR., AND WARD, L. J. (1995): SPOT multispectral analysis for producing supraglacial debris-load estimates for Batura Glacier, Pakistan, *Geocarto International*, **10** (4), 81-90.

BISHOP, M. P., SHRODER, J. F., JR., AND HICKMAN, B. L. (1999): SPOT Panchromatic imagery and neural networks for information extraction in a complex mountain environment, *Geocarto International*, **14**, 17-26.

BISHOP, M. P., KARGEL, J. S., KIEFFER, H. H., MACKINNON, D. J., RAUP, B. H. AND SHRODER, J. F., JR. (2000): Remote-sensing science and technology for studying glacier processes in high Asia, *Annals of Glaciology*, **31**, 164-170.

BÖHM, R. (1993): Kartometrische Daten der Vergletscherung der Goldberggruppe in den Hohen Tauern, *Zeitschrift für Gletscherkunde und Glazialgeologie*, **29**, 133 -152.

BOGORODSKY, V. V., BENTLEY, C. R. AND GUDMANDSEN, P. E. (1985): *Radioglaciology*, Kluwer, Dordrecht, 272 p.

BOLSTAD, P. V. AND STOWE, T. (1994): An evaluation of DEM accuracy: elevation, slope and aspect, *Photogrammetric Engineering and Remote Sensing*, **60** (11), 1327-1332.

BOURDELLES, B. AND FILY, M. (1993): Snow grain size determination from Landsat imagery, *Annals of Glaciology*, **17**, 87-92.

BRAITHWAITE, R. J. (1984): Can the mass balance of a glacier be estimated from its equilibrium-line altitude?, J*ournal of Glaciology*, **30** (106), 364-368.

R

BRAITHWAITE, R. J. (2002): Glacier mass balance: the first 50 years of international monitoring, *Progress in Physical Geography*, **26** (1), 76-95.

BRAITHWAITE, R. J. AND MÜLLER, F. (1980): On the parameterization of glacier equilibrium line altitude, *IAHS*, **126**, 263-271.

BRAUN, L. N., WEBER, M. AND SCHULZ, M. (1999): Consequences of climate change for runoff from Alpine regions, *Annals of Glaciology*, **31**, 19-25.

BRECHER, H. H. AND THOMPSON, L. G. (1993): Measurement of the retreat of Qori Kalis Glacier in the tropical Andes of Peru by terrestrial photogrammetry, *Photogrammetric Engineering and Remote Sensing*, **59** (6), 1017-1022.

BRONGE, L. B. AND BRONGE, C. (1999): Ice and snow-type classification in the Vestfold Hills, East Antarctica, using Landsat-TM data and ground radiometer measurements, *International Journal of Remote Sensing*, **20**, 225-240.

BROWN, D. G. AND BARA, T. J. (1994): Recognition and reduction of systematic error in elevation and derivative surfaces from 7 1/2-Minute DEMs, *Photogrammetric Engineering and Remote Sensing*, **63** (8), 965-974.

BURROUGH, P. A. AND MCDONNELL, R. A. (1998): *Principles of geographical information systems (2nd Ed.)*, Oxford University Press, New York, 333 p.

CANAS, A. A. D. AND BARNETT, M. E. (1985): The generation and interpretation of false-colour composite principal component images, *International Journal of Remote Sensing*, **6**, 867-881.

CAO, C. AND LAM, N. S. (1997): Understanding the scale and resolution effects in remote sensing and GIS, in: Quattrochi, D. A. and Goodchild, M. F. (Eds.), *Scale in remote sensing and GIS*, CRC Press, Lewis Publishers, Boca Raton, 57-72.

CARPER, W. J., LILLESAND, T. M. AND KIEFFER, R. W. (1990): The use of intensity-hue-saturation transformations for merging SPOT panchromatic and multispectral image data, *Photogrammetric Engineering and Remote Sensing*, **56** (4), 459-467.

CCRS (2002): Fundamentals of remote sensing (Canada Centre for remote sensing), URL: *http://www.ccrs.nrcan.gc.ca/ccrs/learn/tutorials/fundam/fundam_e.html*, access: 19 Sep 2002.

CHAVEZ, P. S., JR., SIDES, S. C. AND ANDERSON, J. A. (1991): Comparison of three different methods to merge multiresolution and multispectral data: Landsat TM and SPOT panchromatic, *Photogrammetric Engineering and Remote Sensing*, **57** (3), 295-303.

CIVCO, D. L. (1989): Topographic normalization of Landsat Thematic Mapper digital imagery, *Photogrammetric Engineering and Remote Sensing*, **55** (9), 1303-1309.

CLAGUE, J. J. AND EVANS, S. G. (1994): Formation and failure of natural dams in the Canadian Cordillera, *Geological Survey of Canada, Bulletin*, **464**, 40 p.

CLAGUE, J. J. AND EVANS, S. G. (2000): A review of catastrophic drainage of moraine-dammed lakes in British Columbia, *Quarternary Science Reviews*, **19,** 1763-1783.

R

CLICHE, G., BONN, F. AND TEILLET, P. (1985): Integration of the SPOT Pan channel into its mulispectral mode for image sharpness enhancement, *Photogrammetric Engineering and Remote Sensing*, **51**, 311-316.

CONESE, C., GILABERT, M. A., MASELLI, F. AND BOTTAI, L. (1993): Topographic normalization of TM scenes through the use of an atmospheric correction method and digital terrain models, *Photogrammetric Engineering and Remote Sensing*, **59** (12), 1745-1753.

COGLEY, J. G. AND ADAMS, W. P. (1998): Mass balance of glaciers other than ice sheets, *Journal of Glaciology*, **44** (147), 315-325.

COPLAND, L. (1998): The use of terrain analysis in the evaluation of snow cover over an alpine glacier, in: Lane, S. N., Richards, K. S. and Chandler, J. H. (Eds.): *Landform monitoring, modelling and analysis*, Wiley, New York, 385-404.

COSTA, J. E. AND SCHUSTER, R. L. (1988): The formation and failure of natural dams. *Geological Society of America Bulletin*, **100**, 1054-1068.

CRACKNELL, A. P. (1998): Synergy in remote sensing - what's in a pixel?, *International Journal of Remote Sensing*, **19** (11), 2025-2047.

CRIPPEN, R. E. (1988): The dangers of underestimating the importance of data adjustments in band ratioing, *International Journal of Remote Sensing*, **9** (4), 767-776.

DARVISHSEFAT, A. A. (1995): *Einsatz und Fusion von multisensoralen Satellitenbilddaten zur Erfassung von Waldinventuren*, Geographisches Institut Universität Zürich, Remote Sensing Series, **26**, 144 p.

DAVIS, F. W., QUATTROCHI, D. A., RIDD, M. K., LAM, N. S-N., WALSH, S. J., MICHAELSEN, J. C., FRANKLIN, J., STOW, D. A., JOHANNSEN, C. J. AND JOHNSTON, C. A. (1991): Environmental analysis using integrated GIS and remotely sensed data: Some research needs and priorities, *Photogrammetric Engineering and Remote Sensing*, **57** (6), 689-697.

DELLA VENTURA, A., RAMPINI, A., RABAGLIATI, R. AND SERANDREI-BARBERO, R. (1983): Glacier monitoring by satellite, *Il Nuovo Cimento*, C-1, **6**, 211-221.

DELLA VENTURA, A., RAMPINI, A. AND SERANDREI-BARBERO, R. (1987): Development of a satellite remote sensing technique for the study of alpine glaciers, *International Journal of Remote Sensing*, **8**, 203-215.

DING, Y. AND LIU, J. (1992): Glacier lake outburst flood disasters in China, *Annals of Glaciology*, **16**, 180-184.

DOWDESWELL, J. A., DREWERY, D. J., LIESTØL, O. AND ORHEIM, O. (1984): Radio echo-sounding of Spitsbergen glaciers: problems in interpretation of layer and bottom results, *Journal of Glaciology*, **30** (104), 16-21.

DOZIER, J. (1984): Snow reflectance from Landsat 4 Thematic Mapper, *IEEE Transactions on Geoscience and Remote Sensing*, **GE-22**, 323-328.

DOZIER, J. (1989): Spectral signature of alpine snow cover from Landsat 5 TM, *Remote Sensing of Environment*, **28**, 9-22.

R

DOZIER, J. AND FREW, J. (1981): Atmospheric corrections to satellite radiometric data over rugged terrain, *Remote Sensing of Environment*, **11**, 191-205.

DOZIER, J. AND MARKS, D. (1987): Snow mapping and classification from Landsat Thematic Mapper data, *Annals of Glaciology*, **9**, 97-103.

DOZIER, J. AND FREW, J. (1990): Rapid calculation of terrain parameters for radiation modelling from digital elevation data, *IEEE Transactions on Geoscience and Remote Sensing*, **28** (5), 963 -969.

DRIEDGER, C. L. AND KENNARD, P. M. (1986): Glacier volume estimation on Cascade volcanoes: an analysis and comparison with other methods, *Annals of Glaciology*, **8**, 59-64.

DUBAYAH, R. (1992): Estimating net solar radiation using Lansat Thematic Mapper and digital elevation data, *Water Resources Research*, **28** (9), 2469-2484.

DUBAYAH, R. AND RICH, P. (1995): Topographic solar radiation models for GIS, *International Journal of Geographic Information Systems*, **9** (4), 405-419.

DUGUAY, C. R. AND LEDREW, E. F. (1992): Estimating surface reflectance and albedo from Landsat-5 Thematic Mapper over rugged terrain, *Photogrammetric Engineering and Remote Sensing*, **58** (5), 551-558.

DYURGEROV, M. B. (2002): Glacier mass balance and regime: Data of measurements and analysis, in: Meier, M. F. and Armstrong, R. (Eds.), INSTAAR Occasional Paper, Institute of Arctic and Alpine Research, Boulder, CO, **55**, 268 p. URL: *http://instaar.colorado.edu/other/download/OP55_glaciers.pdf*, access: 16 Sep 2002.

DYURGEROV, M. B. AND MEIER, M. F. (1997A): Mass balance of mountain and subpolar glaciers: a new global assessment for 1961-1990, *Arctic and Alpine Research*, **29** (4), 379-391.

DYURGEROV, M. B. AND MEIER, M. F. (1997B): Year-to year fluctuations of global mass balance of small glaciers and their contribution to sea-level changes, *Arctic and Alpine Research*, **29** (4), 392-402.

ECHELMEYER, K. A., HARRISON, W. D., LARSEN, C. F., SAPIANO, J., MITCHELL, J. E., DEMALLIE, J., RABUS, B., ADALGEIRSDÓTTIR, G. AND SOMBARDIER, L. (1996): Airborne surface profiling of glaciers: a case-study in Alaska, *Journal of Glaciology*, **42** (142), 538-547.

EDC (2002): Land Processes Distributed Active Archive Center (LP DAAC) Products and Pricing, URL: *http://edcdaac.usgs.gov/pricing.html*, access: 11 Sep 2002.

EHLERS, M. (1991): Multisensor image fusion techniques in remote sensing, *ISPRS Journal of Photogrammetry and Remote Sensing*, **46** (1), 19-30.

EHLERS, M. AND WELCH, R. (1987): Stereocorrelation of Landsat TM images, *Photogrammetric Engineering and Remote Sensing*, **53** (9), 1231-1237.

EHLERS, M., EDWARDS, G. AND BEDARD, Y. (1989): Integration of remote sensing with geographic information systems: A necessary evolution, *Photogrammetric Engineering and Remote Sensing*, **55** (11), 1619-1627.

R

ESA (1994): *Landsat TM Products CCT Format Definition*. 15 March 1994, is/rev 3/0, ESRIN, Frascati, Italy.

ESRI (2001): Environmental Systems Research Institute Inc., ARC 8.1.

ETZELMÜLLER, B. AND SOLLID, J. L. (1997): Glacier geomorphometry - an approach for analyzing long-term glacier surface changes using grid-based digital elevation models, *Annals of Glaciology*, **24**, 135-141.

ETZELMÜLLER, B., ØDEGARD, R. S., BERTHLING, I. AND SOLLID, J. L. (2001): Terrain parameters and remote sensing data in the analysis of permafrost distribution and peri-glacial processes: Principles and examples from southern Norway, *Permafrost and Periglacial Processes*, **12**, 79-92.

EVANS, I. S. (1998): What do terrain statistics really mean?, in: Lane, S. N., Richards, K. S. and Chandler, J. H. (Eds.): *Landform monitoring, modelling and analysis*, Wiley, New York, 119-138.

FAVEY, E., GEIGER, A., GUDMUNDSSON, G. H. AND WEHR, A. (1999): Evaluating the potential of an airborne laser-scanning system for measuring volume changes of glaciers, *Geografiska Annaler*, **81A** (4), 555-561.

FIELD, O. W. (1975): *Mountain glaciers of the Northern Hemisphere - Atlas*, Cold Regions Research and Engineering Laboratory, Hanover, 49 plates.

FINSTERWALDER, R. (1954): Photogrammetry and glacier research with special reference to glacier retreat in the eastern Alps, *Journal of Glaciology*, **2** (15), 157-168.

FINSTERWALDER, R. AND RENTSCH, H. (1980): Zur Höhenänderung von Ostalpengletschern im Zeitraum 1969-1979, *Zeitschrift für Gletscherkunde und Glazialgeologie*, **16** (1), 110-115.

FISHER, P. (1997): The pixel; a snare and a delusion, *International Journal of Remote Sensing*, **18**, 679-685.

FLIRI, F. (1964): Zur Witterungsklimatologie sommerlicher Schneefälle in den Alpen, *Wetter und Leben*, **16**, 1-11.

FLORINSKY, I. V. (1998): Combined analysis of digital terrain models and remotely sensed data in landscape investigations, *Progress in Physical Geography*, **22** (1), 33-60.

FOREL, F. A. (1895): Les variations periodiques des glaciers. Discours preliminaire. *Extrait des Archives des Sciences physiques et naturelles*, **XXXIV**, 209-229.

FOX, A. J. AND NUTTAL, A.-M. (1997): Photogrammetry as a research tool for glaciology, *Photogrammetric Record*, **15** (89), 725-737.

R

GAMMA, P. (2000): *dfwalk - Ein Murgang-Simulationsprogrammzur Gefahrenzonierung*, PhD thesis (unpublished), Geographisches Institut, Universität Bern, **G66**, p.

GANGKOFNER, U. (1989): Multispectral snow classification with TM data, in: Guyenne, T.-D. and Calabresi, G. (Eds.): *Monitoring the Earth's environment*, ESA, **SP-1102**, 13-21.

GAO, J. AND LIU, Y. (2001): Applications of remote sensing, GIS and GPS in glaciology: a review, *Progress in Physical Geography*, **25** (4), 520-540.

GILABERT, M. A., CONESE, C. AND MASELLI, F. (1994): An atmospheric correction method for the automatic retrieval of surface reflectances from TM images, *International Journal of Remote Sensing*, **15** (10), 2065-2086.

GILLESPIE, A. R., KAHLE, A. B. AND WALKER, R. E. (1986): Colour enhancement of highly correlated images: 1. Decorrelation and HSI contrast stretches, *Remote Sensing of Environment*, **20**, 209-235.

GLACIERHAZARDS (2002): Web-based database and information on glacier disasters in Switzerland, URL: *http://www.glacierhazards.ch*, access: 21 Sep 2002.

GLIMS (2002): GLIMS database description, URL: *http://www.glims.org/*, access: 19 Sep 2002.

GRATTON, D. J., HOWARTH, P. J. AND MARCEAU, D. J. (1990): Combining DEM parameters with Landsat MSS and TM imagery in a GIS for mountain glacier characterization, *IEEE Transactions on Geoscience and Remote Sensing*, **GE -28** (4), 766-769.

GRATTON, D. J., HOWARTH, P. J. AND MARCEAU, D. J. (1993): Using Landsat-5 Thematic Mapper and digital elevation data to determine the net radiation field of a mountain glacier, *Remote Sensing of Environment*, **43**, 315-331.

GREGORY, J. M. AND OERLEMANS, J. (1998): Simulated future sea-level rise due to glacier melt based on regionally and seasonally resolved temperature changes, *Nature*, **391**, 474-476.

GRENFELL, T. C., PEROVICH, D. K. AND OGREN, J. A. (1981): Spectral albedos of an alpine snow pack, *Cold Regions Science and Technology*, **4**, 121-127.

GREUELL, W. (1992): Hintereisferner, Austria: mass balance reconstruction and numerical modelling of the historical length variations, *Journal of Glaciology*, **38** (129), 233-244.

GROSS, G. (1987): Der Flächenverlust der Gletscher in Östereich 1850 - 1920 - 1969, *Zeitschrift für Gletscherkunde und Glazialgeologie*, **23**, 131- 141.

GROSS, G., KERSCHNER, H. AND PATZELT, G. (1976): Methodische Untersuchungen über die Schneegrenze in alpinen Gletschergebieten, *Zeitschrift für Gletscherkunde und Glazialgeologie*, **17**, 223-251.

GROVE, J. M. (1988): *The Little Ice Age*, Methuen, London, 498 p.

GRUBER, S. (2002): personal communication.

GRUBER, D. AND KRIZ, K. (1998): DGM-Optimierung als Basis für geomorphologische Fragestellungen, *Wiener Schriften zur Geographie und Kartographie*, **11**, Wien, 76-80.

GÜNTHER, R. AND WIDLEWSKI, D. (1986): Die Korrelation verschiedener Klimaelemente mit dem Massenhaushalt alpiner und skandinavischer Gletscher, *Zeitschrift für Gletscherkunde und Glazialgeologie*, **22**, 125-147.

GUTH, P. L. (1999): Contour line 'ghosts' in USGS Level 2 DEMs, *Photogrammetric Engineering and Remote Sensing*, **65** (3), 289-296.

HAAKENSEN, N. (1986): Glacier mapping to confirm results from mass-balance measurements, *Annals of Glaciology*, **8**, 73-77.

HAEBERLI, W. (1983): Frequency and characteristics of glacier floods in the Swiss Alps. *Annals of Glaciology*, **4**, 85-90.

HAEBERLI, W. (1990): Glacier and permafrost signals of the 20th-century warming, *Annals of Glaciology*, **14**, 99-101.

HAEBERLI, W. (1991): Alpengletscher im Treibhaus Erde, *Regio Basiliensis*, **32**, 59-72.

HAEBERLI, W. (1994): Accelerated glacier and permafrost changes in the Alps, in: Beniston, M. (Ed.), *Mountain environments in changing climates*, Routledge, London, 91-107.

HAEBERLI, W. (1995): Glacier fluctuations and climatic change detection - operational elements of a worldwide monitoring strategie, *WMO - Bulletin*, **44**, 23-31.

HAEBERLI, W. (1998): Historical evolution and operational aspects of worldwide glacier monitoring, in: Haeberli, W., Hoelzle, M. and Suter, S. (Eds.), *Into the second century of worldwide glacier monitoring: prospects and strategies*, UNESCO Studies and Reports in Hydrology, **56**, 35-51.

HAEBERLI, W. AND ALEAN, J. (1985): Temperature and accumulation of high altitude firn in the Alps, *Annals of Glaciology*, **6**, 161-163.

HAEBERLI, W. AND EPIFANI, F. (1986): Mapping the distribution of buried glacier ice - an example from Lago delle Locce, Monte Rosa, Italian Alps, *Annals of Glaciology*, **8**, 78-81.

HAEBERLI, W. AND HOELZLE, M. (1995): Application for inventory data for estimating characteristics of and regional climate-change effects on mountain glaciers: a pilot study with the European Alps, *Annals of Glaciology*, **21**, 206-212.

HAEBERLI, W. AND BENISTON, M. (1998): Climate change and its impacts on glaciers and permafrost in the Alps, *Ambio*, **27** (4), 258-265.

HAEBERLI, W., MÜLLER, P., ALEAN, P. AND BÖSCH, H. (1989): Glacier changes following the little ice age - a survey of the international data basis and its perspectives, in: J. Oerlemans (Ed.), *Glacier Fluctuations and Climatic Change*, Kluwer, Dordrecht, 77-101.

R

HAEBERLI, W., HOELZLE, M. AND SUTER, S. (1998): *Into the second century of worldwide glacier monitoring: prospects and strategies*. A contribution to the International Hydrological Programme (IHP) and the Global Environment Monitoring System (GEMS), UNESCO Studies and Reports in Hydrology, **56**, 228 p.

HAEBERLI W., FRAUENFELDER, R., HOELZLE, M. AND MAISCH, M. (1999): Rates and acceleration trends of global glacier mass changes, *Geografiska Annaler*, **81A** (4), 585-591.

HAEBERLI, W., CIHLAR, J. AND BARRY, R. (2000): Glacier monitoring within the Global Climate Observing System, *Annals of Glaciology*, **31**, 241-246.

HAEBERLI, W., KÄÄB, A., VONDER MÜHLL , D. AND TEYSSEIRE, P. (2001): Prevention of outburst floods from periglacial lakes at Grubengletscher, Valais, Swiss Alps, *Journal of Glaciology*, **47** (156), 111-122.

HAEBERLI, W., MAISCH, M. AND PAUL, F. (2002A): Mountain glaciers in global climate-related observation networks, *WMO-Bulletin*, **51** (1), 18-25.

HAEBERLI, W., KÄÄB, A., PAUL, F., CHIARLE, M., MORTARA, G., MAZZA, A. AND RICHARDSON, S. (2002B): A surge-type movement at Ghiacciaio del Belvedere and a developing slope instability in the east face of Monte Rosa, Macunaga, Italian Alps. *Norsk Geografisk Tidskrift - Norwegian Journal of Geography*, **56** (2), 104-111.

HAEBERLING, C. (1998): Benutzerbedürfnisse und Anforderungen zu neuartigen Gletscherdarstellungen, *Wiener Schriften zur Geographie und Kartographie*, **11**, Wien, 81-93.

HAGEN, J. O. AND SAETRANG, A. (1991): Radio-echo soundings of sub-polar glaciers with low-frequency radar, *Polar Research*, **9** (1), 99-107.

HALL, D. K. AND MARTINEC, J. (1985): *Remote sensing of ice and snow*, Chapman & Hall, London, 189 p.

HALL, D. K., ORMSBY, J. P., BINDSCHADLER, R. A. AND SIDDALINGAIAH, H. (1987): Characterization of snow and ice zones on glaciers using Landsat Thematic Mapper data, *Annals of Glaciology*, **9**, 104-108.

HALL, D. K., CHANG, A. T. C. AND SIDDALINGAIAH, H. (1988): Reflectances of glaciers as calculated using Landsat 5 Thematic Mapper data, *Remote Sensing of Environment*, **25** (3), 311-321.

HALL, D. K., BAYR, K. J. AND KOVALICK, W. M. (1989A): Determination of glacier mass balance change using Thematic Mapper data, *Proceedings of the Eastern Snow Conference*, Lake Placid, New York, 7. - 9.6.1988, 192-196.

HALL, D. K., CHANG, A. T. C., FOSTER, J. L., BENSON, C. S. AND KOVALICK, W. M. (1989B): Comparison of in situ and Landsat derived reflectances of Alaskan glaciers, *Remote Sensing of Environment*, **28**, 493-504.

HALL, D. K., BINDSCHADLER, R. A., FOSTER, J. L., CHANG, A. T. C. AND SIDDALINGAIAH, H. (1990): Comparison of in situ and satellite derived reflectances of Forbindels Glacier, Greenland, *International Journal of Remote Sensing*, **11** (3), 493-504.

HALL, D. K., WILLIAMS, R. S. JR. AND BAYR, K. J. (1992): Glacier recession in Iceland and Austria, *EOS, Transactions of the American Geophysical Union*, **73**, 129, 135 and 141.

HALL, D. K., BENSON, C. S. AND FIELD, W. O. (1995A): Changes of glaciers in Glacier Bay, Alaska, using ground and satellite measurements, *Physical Geography*, **16** (1), 27-41.

R

HALL, D. K., RIGGS, G. A. AND SALOMONSON, V. V. (1995B): Development of methods for mapping global snow cover using Moderate Resolution Imaging Spectroradiometer (MODIS) data, *Remote Sensing of Environment*, **53**, 127-140.

HARDY, C. C. AND BURGAN, R. E. (1999): Evaluation of NDVI for monitoring moisture in three vegetation types of the western U.S., *Photogrammetric Engineering and Remote Sensing*, **65** (5), 603-610.

HEITZINGER, D. AND KAGER, H. (1999): Hochwertige Geländemodelle aus Höhenlinien durch wissensbasierte Klassifikation von Problemgebieten, *Photogrammetrie Fernerkundung Geoinformation*, **X** (1), 29-40.

HERREN, E. R., HOELZLE, M. AND MAISCH, M. (2001): *The Swiss glaciers 1997/98 and 1998/99*. Zürich, Swiss Academy of Sciences. Glaciological Comission; Federal Institute of Technology. Laboratory of Hydraulics, Hydrology and Glaciology. (Glaciological Report No. 119/120).

HOELZLE, M. AND TRINDLER, M. (1998): Data management and application, in: Haeberli, W., Hoelzle, M. and Suter, S. (Eds.), *Into the second century of worldwide glacier monitoring: prospects and strategies*, UNESCO Studies and Reports in Hydrology, **56**, 53-72.

HOELZLE, M., DISCHL, M. AND FRAUENFELDER, R. (2000): Weltweite Gletscherbeobachtung als Indikator der globalen Klimaänderung, *Vierteljahresschrift der Naturforschenden Gesellschaft in Zürich*, **145** (1), 5-12.

HOELZLE, M., HAEBERLI, W., DISCHL, M. AND PESCHKE, W. (2003): Secular glacier mass balances derived from cumulative glacier length changes, *Global and Planetary Change*, **36** (4), 77-89.

HOFMANN, W. (1958): Der Vorstoss des Nisqually-Gletschers am Mt. Rainer, USA, von 1952-1956, *Zeitschrift für Gletscherkunde und Glazialgeologie*, **4** (1/2), 47-60.

HOINKES, H. (1970): Methoden und Möglichkeiten von Massenhaushaltsstudien auf Gletschern, *Zeitschrift für Gletscherkunde und Glazialgeologie*, **6**, 37-90.

HOLBEN, B. AND JUSTICE, C. (1981): An examination of spectral band ratioing to reduce the topographic effect on remotely sensed data, *International Journal of Remote Sensing*, **2** (2), 115-133.

HOWARTH, P. AND OMMANNEY, C. S. (1986): The use of Landsat digital data for glacier inventories, *Annals of Glaciology*, **8**, 90-92.

HUBBARD, A. L., WILLIS, I., SHARP, M., MAIR, D., NIENOW, P. W., HUBBARD, B. AND BLATTER, H. (2000): Glacier-mass-balance determination by remote sensing and high-resolution modelling, *Journal of Glaciology*, **46** (154), 491-498.

HUGGEL, C. (1998): *Periglaziale Seen im Luft und Satellitenbild*, Diploma thesis (unpublished), Geographisches Institut Universität Zürich, 130 p.

HUGGEL, C., KÄÄB, A., HAEBERLI, W., TEYSSEIRE, P. AND PAUL, F. (2002): Remote sensing based assessment of hazards from glacier lake outbursts: a case study in the Swiss Alps, *Canadian Geotechnical Journal*, **39** (2), 316-330.

R

HURNI, L. (2001): The New "Atlas of Switzerland - interactive": Applications in Mountain Cartography, in: Buchroithner, M. F. (Ed.), *Proceedings of the Workshop 'High Mountain Cartography 2000' at Rudolfshütte (Austria)*, TU Dresden, 53-59.

HURNI L., KÄÄB, A. AND HAEBERLING, C. (2000): Kartographische Darstellung glazialer Phänomene. Zeitliche Entwicklung und heutiger Stand, *Salzburger Geographische Arbeiten*, **36**, 23-38.

HUTCHINSON, M. F. (1989): A new procedure for gridding elevation and stream line data with automatic removal of spurious pits, *Journal of Hydrology*, **106**, 211-232.

IAHS (1980): World glacier inventory, Proceedings of the Riederalp workshop, September 1978, *IAHS*, **126**, 352 p.

IAHS (1989): *World glacier inventory - Status 1988* (Haeberli, W., Bösch, H., Scherler, K., Østrem, G. and Wallen, C. C., Eds.), IAHS (ICSI) - UNEP - UNESCO, Nairobi, 458 p.

IAHS (1998): *Fluctuations of glaciers 1990-1995 Vol. V* (Haeberli, W., Hoelzle, M., Suter, S. and Frauenfelder, R., Eds.), IAHS (ICSI)-UNEP-UNESCO, Paris.

IPCC (2001): *Climate Change 2001: The Scientific Basis,* Contribution of Working Group I to the Third Assessment Report (Houghton, J. T., Ding, Y., Griggs, D. J., Noguer, M., van der Linden, P. J. and Xiaosu, D., Eds.), Cambridge University Press, 944 p.

ITTEN, K. I. AND MEYER, P. (1993): Geometric and radiometric correction of TM data of mountaineous forested areas, *IEEE Transactions on Geoscience and Remote Sensing*, **31** (4), 764-770.

JACOBS, J. D., SIMMS, E. L. AND SIMMS, A. (1997): Recession of the southern part of Barnes Ice Cap, Baffin Island, Canada, between 1961 and 1993, determined from digital mapping of Landsat TM, *Journal of Glaciology*, **43** (143), 98-102.

JACOBSEN, A., CARSTENSEN, A. R. AND KAMPER, J. (1993): Mapping of satellite derived surface albedo on the Midtluagkat Glacier, Eastern Greenland, using a digital elevation modell and SPOT HRV data, *Geografisk Tidsskrift*, **93**, 6-18.

JENSON, S. K. (1991): Applications of hydrologic information automatically extracted from digital elevation models, *Hydrological Processes*, **5**, 31-44.

JIA, X., RICHARDS, J. A. AND RICKEN, D. E. (1999): *Remote sensing digital image analysis: an introduction* (3rd Ed.), Springer, Berlin, 400 p.

JOHANNESSON, T., RAYMOND, C. F. AND WADDINGTON, E. D. (1989A): A simple method for determining the response time of glaciers, in: J. Oerlemans (Ed.), *Glacier Fluctuations and Climatic Change*, Kluwer, Dordrecht, 343-352.

JOHANNESSON, T., RAYMOND, C. F. AND WADDINGTON, E. D. (1989B): Time scale for adjustment of glaciers to changes in mass balance, *Journal of Glaciology*, **35** (121), 355-369.

JONES, C. B. (1997): *Geographical information systems and computer cartography*, Addison-Wesley, Harlow, 272 p.

JONES, K. H. (1998): A comparison of algorithms used to compute hill slope as a property of the DEM, *Computers and Geosciences*, **24** (4), 315-323.

JOSEPH, G. (2000): How well do we understand Earth observation electro-optical sensor parameters?, *ISPRS Journal of Photogrammetry and Remote sensing*, **55**, 9-12.

JPL (2002): ASTER spectral library, URL: *http://speclib.jpl.nasa.gov/*, access: Feb 2000.

JUSTICE, C. O., WHARTON, S. W. AND HOLBEN, B. N. (1981): Application of digital terrain data to quantify and reduce the topographic effect on Landsat data, *International Journal of Remote Sensing*, **2** (3), 213-230.

KÄÄB, A. (1996): *Photogrammetrische Analyse zur Früherkennung gletscher- und permafrostbedinger Naturgefahren im Hochgebirge*, Mitteilungen der Versuchsanstalt für Wasserbau, Hydrologie und Glaziologie (VAW), ETH Zürich, 145.

KÄÄB, A. (2000): Photogrammetry for early recognition of high mountain hazards: new techniques and applications, P*hysics and Chemistry of the Earth*, **25** (9), 765-770.

KÄÄB, A. (2001): Photogrammetric reconstruction of glacier mass-balance using a kinematic ice-flow model. A 20-year time-series on Grubengletscher, Swiss Alps, *Annals of Glaciology*, **31**, 45-52.

KÄÄB, A. (2002): Monitoring high-mountain terrain deformation from repeated air- and spaceborne optical data: examples using digital aerial imagery and ASTER data, *ISPRS Journal of Photogrammetry and Remote Sensing*, **57** (1-2), 39-52.

KÄÄB, A. AND FUNK, M. (1999): Modelling mass balance using photogrammetric and geophysical data. A pilot study at Gries glacier, Swiss Alps, *Journal of Glaciology*, **45** (151), 575-583.

KÄÄB, A. AND HAEBERLI, W. (2001): Evolution of a high-mountain thermokarst lake in the Swiss alps. *Arctic, Antarctic and Alpine Research*, **33** (4), 385-390.

KÄÄB, A., HUGGEL, C. AND PAUL, F. (2000A): Früherkennung hochalpiner Naturgefahren mittels Fernerkundung, *Interpraevent*, **1**, 49-60.

KÄÄB, A., HAEBERLI, W., HUGGEL, C. AND PAUL, F. (2000B): Glacier- and permafrost-related hazards in high mountains: Integrative assessment in the Swiss Alps based on remote sensing and geo-information systems. X Congresso Peruano de Geologia, Lima, *Volumen de Presentaciones*, CD-ROM.

KÄÄB, A., PAUL, F., MAISCH, M., HOELZLE, M. AND HAEBERLI, W. (2002): The new remote-sensing-derived Swiss glacier inventory: II. First results, *Annals of Glaciology*, **34**, 362-366.

KÄÄB, A., PAUL, F., HUGGEL, C., KIEFFER, H., KARGEL, J. AND WESSELS, R. (2003): Glacier monitoring from ASTER imagery: Accuracy and applications, EARSeL Workshop on Remote Sensing of Land Ice and Snow, Bern, 11-13 March 2002, *EARSeL eProceedings*, **2**, 43-53, CD-ROM.

R

KAUFMAN, Y. J. (1988): Atmospheric effect on spectral signature - measurements and correction, *IEEE Transactions on Geoscience and Remote Sensing*, **26** (4), 441-450.

KAUFMANN, V. AND PLOESCH, R. (2000): Reconstruction and visualization of the retreat of two small cirque glaciers in the Austrian Alps since 1850, in: Buchroithner, M. F. (Ed.), *Proceedings of the Workshop 'High Mountain Cartography 2000' at Rudolfshütte (Austria)*, TU Dresden, 239-253.

KfG (2002): Kommision für Glaziologie (Bayerische Akademie der Wissenschaften), Anaglyphen - 3D - Galerie, Alpen, URL: *http://www.lrz-muenchen.de/~a2901ad/webserver/webdata/flug99/alpen.html*, access: 11 Sep 2002.

KIEFFER, H. AND 41 OTHERS (2000): New eyes in the sky measure glaciers and ice sheets, *EOS, Transactions of the American Geophysical Union,* **81** (24), 265, 270, 271.

KLEIN, A. G. AND ISACKS, B. L. (1996): Glaciers - Tracking Change in the central Andes mountains, *Geo-World*, **9** (10), 48-52.

KLEIN, A. G. AND ISACKS, B. L. (1999): Spectral mixture analysis of Landsat thematic mapper images applied to the detection of the transient snowline on tropical Andean glaciers, *Global and Planetary Change*, **22**, 139-154.

KLEIN, A. G., SELTZER, G. O. AND ISACKS, B. L. (1999): Modern and last local glacial maximum snowlines in the central Andes of Peru, Bolivia, and Northern Chile, *Quaternary Science Reviews*, **18**, 63-84.

KNAP, W. H. (1997): *Satellite-derived and ground-based measurements of the surface albedo of glaciers*, PhD thesis, Utrecht University, Netherlands, 175 p.

KNAP, W. H., BROCK, B. W., OERLEMANS, J. AND WILLIS, I. C. (1999): Comparison of Landsat-TM derived and ground-based albedos of Haut Glacier d'Arolla, Switzerland, *International Journal of Remote Sensing*, **20** (17), 3293-3310.

KOELEMEIJER, R., OERLEMANNS, J. AND TJEMKES, S. (1993): Surface reflectance of Hintereisferner, Austria, from Landsat 5 TM imagery, *Annals of Glaciology*, **17**, 17-22.

KÖNIG, M., WINTHER, J.-G., AND ISAKSSON, E. (2001): Measuring snow and ice properties from satellite, *Reviews of Geophysics*, **39** (1), 1-27.

KRAMER, H. J. (2002): *Observation of the Earth and its environment: Survey of missions and sensors*, Springer, Berlin, 1510 p.

KRIMMEL, R. M. (1999): Analysis of difference between direct and geodetic mass balance measurements at South Cascade Glacier, Washington, *Geografiska Annaler*, **81A** (4), 653-658.

KRIMMEL, R. M. AND MEIER, M. F. (1975): Glacier applications of ERTS - 1 images, *Journal of Glaciology*, **15** (73), 391-402.

KUHN, M. (1980A): Die Reaktion der Schneegrenze auf Klimaschwankungen, *Zeitschrift für Gletscherkunde und Glazialgeologie*, **16**, 241- 254.

KUHN, M. (1980B): Climate and glaciers, *IAHS*, **131**, 3-20.

KUHN, M. (1989): The response of the equilibrium line altitude to climatic fluctuations: Theory and observations, in: Oerlemans, J. (Ed.), *Glacier fluctuations and climatic change*, Kluwer, Dordrecht, 407-417.

KUHN, M. (1993): Possible future contributions to sea level change from small glaciers, in: Warrick, R. A., Barrow, E. M. and Wigley, T. M. L. (Eds.), *Climate and sea level change observations, Projections and Implications*, Cambridge University Press, Cambridge, 134-143.

KUHN, M., MARKL, G., KASSER, G., NICHUS, U., OBLEITNER, F. AND SCHNEIDER, H. (1985): Fluctuations of climate and mass balance: Different responses of two adjacent glaciers, *Zeitschrift für Gletscherkunde und Glazialgeologie*, **21**, 409-416.

KULKARNI, A. V. (1992): Mass balance of Himalayan glaciers using AAR and ELA methods, *Journal of Glaciology*, **38** (128), 101-104.

KUMAR, L., SKIDMORE , A. K. AND KNOWLES, E. (1997): Modelling topographic radiation in a GIS environment, *International Journal of Geographical Information Science*, **11** (5), 475-497.

LANG, H. AND LIEB, G. K. (1993): *Die Gletscher Kärntens*, Naturwissenschaftlicher Verein für Kärnten, Klagenfurt, 184 p.

LI, Z., SUN, W. AND ZENG, Q. (1998): Measurements of glacier variation in the Tibetan Plateau using Landsat data, *Remote Sensing of Environment*, **63**, 258-264.

LILLESAND, T. M. AND KIEFFER, R. W. (1999): *Remote sensing and image interpretation* (4th Ed.), Wiley, New York, 736 p.

LLIBOUTRY, L., MORALES ARNAO, B., PAUTRE, A. AND SCHNEIDER, B. (1977): Glaciological problems set by the control of dangerous lakes in Cordillera Blanca, Peru. I. Historic failures of morainic dams, their causes and prevention, *Journal of Glaciology* , **18** (79), 239-254.

LONGLEY, P., GOODCHILD, M. F., MAGUIRE, D. J., RHIND, D. W. AND LOBLEY, J. (1998): *Geographic information systems and science*, Wiley, New York, 454 p.

LOUGEAY, R. (1974): Detection of buried glacial and ground ice with thermal infrared remote sensing, in: Santeford, H. S. and Smith, J. L. (Eds.), *Advanced concepts and techniques in the study of snow and ice resources*, National Academy of Sciences, Washington, D.C., 487-494.

LUNETTA, R. S., CONGALTON, R. G., FENSTERMAKER, L. K., JENSEN, J. R., MCGWIRE, K. C. AND TINNEY, L. R. (1991): Remote sensing and geographic information system data integration: Error sources and research issues, *Photogrammetric Engineering and Remote Sensing*, **57** (6), 677-687.

MAISCH, M. (1992): *Die Gletscher Graubündens. Rekonstruktion und Auswertung der Gletscher und deren Veränderungen seit dem Hochstand von 1850 im Gebiet der östlichen Schweizer Alpen (Bündnerland und angrenzende Regionen)*, Geographisches Institut der Universität Zürich, Physische Geographie, **33**, Part A: 324 p., Part B: 128 p.

MAISCH, M., WIPF, A., DENNELER, B., BATTAGLIA, J. AND BENZ, C. (2000): *Die Gletscher der Schweizer Alpen. Gletscherhochstand 1850, Aktuelle Vergletscherung, Gletscherschwund-Szenarien* (2nd Ed.), VdF Hochschulverlag, ETH Zürich, Schlussbericht NFP31, 373 p.

MARGRTEH, S. AND FUNK, M. (1999): Hazard mapping for ice and combined ice/snow avalanches - two case studies for the Swiss and Italian Alps, *Cold Regions Science and Technology*, **30**, 159-173.

MARK, D. M. (1975): Computer analysis of topography: a comparison of terrain storage methods, *Geografisker Annaler*, **57A**, 179-188.

MARKHAM, B. L. AND BARKER, J. L. (1985): Spectral characterization of the Landsat Thematic Mapper sensors, *International Journal of Remote Sensing*, **6** (5), 697-716.

MARTINEC, J. (1975): Snow-melt runoff model for streamflow forecast, *Nordic Hydrology*, **6**, 145-154.

MATHER, P. M. (1999): *Computer processing of remotely-sensed images: An introduction* (2nd Ed.), Wiley. New York, 306 p.

MBB (2001): Glacier mass balance bulletin 2001 (Haeberli, W., Frauenfelder, R. and Hoelzle, M., Eds.), IAHS (ICSI) - UNEP - UNESCO - WMO, Zürich, 94 p. (URL: *http://www.geo.unizh.ch/wgms/mbb/mbb6/MBB6.pdf*).

MEIER, M. F. (1962): Proposed definitions for glacier mass budget terms, *Journal of Glaciology*, **4** (33), 252-261.

MEIER, M. F. (1984): Contributions of small glaciers to global sea level, *Science*, **226**, 1418-1421.

MEIER, M. F. AND BAHR, D. B. (1996): Counting glaciers: use of scaling methods to estimate the number and size distribution of the glaciers of the world, in: Colbeck, S.C. (Ed.), *Glaciers, ice sheets and volcanoes: a tribute to Mark F. Meier*, CRREL Special Report 96-27, 89-94.

MEIER, E. H. AND NÜESCH, D. R. (2001): Genauigkeitsanalyse von hochauflösenden Gelände- und Oberflächenmodellen, *Photogrammetrie Fernerkundung Geoinformation*, **X** (6), 405-416.

MENNIS, J. L. AND FOUNTAIN, A. G. (2001): A spatio-temporal GIS database for monitoring Alpine glacier change, *Photogrammetric Engineering and Remote Sensing*, **67** (8), 967-975.

MERCER, J. H. (1967): *Southern hemisphere glacier atlas*, US Army Natick Laboratories, Technical Report 67-76-ES.

MOOL, P. K. (1995): Glacier lake outburst floods in Nepal, *Journal of Nepal Geological Society*, **11**, 273-280.

MOOL, P. K., BAJRACHARYA, S. R. AND JOSHI, S. P. (2001A): *Inventory of glaciers, glacial lakes and glacial lake outburst floods - Nepal*, ICIMOD, Kathmandu, Nepal, 366 p.

MOOL, P. K., WANGDA, D., BAJRACHARYA, S. R., KUNZANG, K., GURUNG, D. R. AND JOSHI, S. P. (2001B): *Inventory of glaciers, glacial lakes and glacial lake outburst floods - Bhutan*, ICIMOD, Kathmandu, Nepal, 228 p.

MOORE, I. D., GRAYSON, R. B. AND LADSON, R. B. (1991): Digital terrain modelling: A review of hydrological, geomorphological and biological applications, *Hydrological Processes*, **5**, 3-30.

MÜLLER, F. (1962): Zonation in the accumulation area of the glaciers of Axel Heiberg Island, N. W. T., Canada, *Journal of Glaciology*, **4** (33), 302-313.

MÜLLER, F., CAFLISH, T. AND MÜLLER, G. (1976): *Firn und Eis der Schweizer Alpen, Gletscherinventar*, Geographisches Institut, vdf-Verlag, ETH Zürich, **57**, 174 p.

MUNECHIKA, C. K., WARNICK, J. S., SALVAGIO, C. AND SCHOTT, J. R. (1993): Resolution enhancement of multispectral image data to improve classification accuracy, *Photogrammetric Engineering and Remote Sensing*, **59** (1), 67-72.

MURPHY, A. H. (1993): What is a good forecast? An essay on the nature of goodness in weather forecasting, *Weather Forecasting*, **8**, 281-293.

NAKAWO, M. AND RANA, B. (1999): Estimate of ablation rate of glacier ice under a supraglacial debris layer, *Geografiska Annaler*, **81A** (4), 695-701.

NAKAWO, M., RAYMOND, C. F. AND FOUNTAIN, A. (EDS.) (2000): *Debris-covered glaciers*, Proceedings of a workshop held at Seattle, Washington, USA, September 2000, IAHS, Wallingford, **264**, 288 p.

NASA (2002): Landsat 7 - Science Data user handbook, URL: *http://ltpwww.gsfc.nasa.gov/IAS/handbook/handbook_toc.html*, access: 19 Sep 2002.

NICOLUSSI, K. AND PATZELT, G. (1996): Reconstructing glacier history in Tyrol by means of tree-ring investigations, *Zeitschrift für Gletscherkunde und Glazialgeologie*, **32**, 207-215.

NOAA (2002): Operational daily snow cover analysis, URL: http://www.ssd.noaa.gov/PS/SNOW/index.html, access: 16 Sep 2002.

NPOC (2002): National point of contact, distribution of satellite imagery, former URL: *http://www.vision.ee.ethz.ch/NPOC*, access: January, 1999. Now at URL: *http://www.swisstopo.ch/de/image/sat.htm.*

NYE, J. F. (1960): The response of glaciers and ice-sheets to seasonal and climatic changes, *Proceedings of the Royal Society of London*, Series A, **256**, 559-584.

OERLEMANS, J. (1986): Glaciers as indicators of a carbon dioxide warming, *Nature*, **320**, 607-609.

OERLEMANS, J. (1988): Simulations of historic glacier variations with a simple climate - glacier model, *Journal of Glaciology*, **34** (118), 333-341.

OERLEMANS, J. (1989): On the response of valley glaciers to climatic change, in: J. Oerlemans (Ed.), *Glacier fluctuations and climatic change*, Kluwer, Dordrecht, 353-371.

OERLEMANS, J. (1994): Quantifying global warming from the retreat of glaciers, *Science*, **264**, 243-245.

R

OERLEMANS, J. (2000): Holocene glacier fluctuations: is the current rate of retreat exceptional?, *Annals of Glaciology*, **31**, 39-44.

OERLEMANS, J. AND HOOGENDORN, N. C. (1989): Mass balance gradients and climatic change, *Journal of Glaciology*, **35**, 399-405.

OMEGA (2002): Operational Monitoring system for European Glacial Areas, URL: *http://omega.utu.fi/*, access: 11 Sep 2002.

ØSTREM, G. (1975): ERTS - 1 data in glaciology - an effort to monitor glacier mass balance from satellite imagery, *Journal of Glaciology*, **15**, 403-415.

ØSTREM, G. AND HAAKENSEN, N. (1999): Map comparison or traditional mass-balance measurements: which method is better?, *Geografiska Annaler*, **81A** (4), 703-711.

ORHEIM, O. AND LUCCHITTA, B. K. (1987): Snow and ice studies by Thematic Mapper and Multispectral Scanner Landsat images, *Annals of Glaciology*, **9**, 109-118.

PARROT, J. F., LYBERIS, N., LEFAUCONNIER, B. AND MANBY, G. (1993): SPOT multispectral data and digital terrain model for the analysis of ice-snow fields on Arctic glaciers, *International Journal of Remote Sensing*, **14** (3), 425-440.

PATERSON, W. S. B. (1994): *The physics of glaciers* (3rd Ed.), Pergamon, New York, 496 p.

PATZELT, G. (1985): The period of glacier advances in the alps, 1965 to 1980, *Zeitschrift für Gletscherkunde und Glazialgeologie*, **21**, 403-407.

PAUL, F. (1995): *Fernerkundung von Gletscheränderungen in den Alpen zwischen 1973 und 1992 beobachtet mit Landsat*, Diploma thesis (unpublished), Meteorologisches Institut Universität Hamburg, **230**, 144 p.

PAUL, F. (1997): Changes of glacier area in the Austrian Alps between 1973 and 1992 derived from Landsat data, *Max-Planck-Institut für Meteorologie Report*, **242**.

PAUL, F. (2001): Evaluation of different methods for glacier mapping using Landsat TM. EARSeL Workshop on Remote Sensing of Land Ice and Snow, Dresden, 16.-17.6.2000, *EARSeL eProceedings*, **1**, 239-245, CD-ROM.

PAUL, F. (2002A): Changes in glacier area in Tyrol, Austria, between 1969 and 1992 derived from Landsat 5 TM and Austrian glacier inventory data, *International Journal of Remote Sensing*, **23** (4), 787-799.

PAUL, F. (2002B): Combined technologies allow rapid analysis of glacier changes, *EOS, Transactions, American Geophysical Union*, **83** (23), 253, 260, 261.

PAUL, F., KÄÄB, A., MAISCH, M., KELLENBERGER, T. AND HAEBERLI, W. (2002): The new remote-sensing-derived Swiss glacier inventory: I. Methods, *Annals of Glaciology*, **34**, 355-361.

PAUL, F., HUGGEL, C., KÄÄB, A. AND KELLENBERGER, T. AND MAISCH, M. (2003): Comparison of TM-derived glacier areas with higher resolution data sets. EARSeL Workshop on Remote Sensing of Land Ice and Snow, Bern, 11.-13.3.2002. *EARSeL eProceedings*, **2**, 15-21, CD-ROM.

R

PCI (1998): Digital image processing software package v. 6.3, PCI geomatics, Richmond Hill, Ontario, Canada.

PEIPE, J., REIS, P. AND RENTSCH, H. (1978): Zur Anwendung des digitalen Geländemodells in der Gletscherforschung, *Zeitschrift für Gletscherkunde und Glazialgeologie*, **14** (2), 161-172.

PELLEMANS, A. H. J. M., JORDANS, R. W. L. AND ALLEWIJN, R. (1993): Merging multispectral and panchromatic SPOT images with respect to the radiometric properties of the sensor, *Photogrammetric Engineering and Remote Sensing*, **59** (1), 81-87.

PELLIKKA, P., KAJUUTTI, K., KOSKINEN, R., JACKSON, M., STÖTTER, H., HAGGRÉN, K., LUUKKONEN, K. M., GUNERIUSSEN, T. AND SHAROV, A. (2001): Development of an operational monitoring system for glaciers - synthesis of earth observation data of the past, present and future, *Proceedings, International workshop on geo-spatial knowledge processing on natural resource management, 28-29 June 2001*, Varese, Italy, 283-288.

PIETRONIRO, A. AND LECONTE, R. (2000): A review of Canadian remote sensing applications in hydrology, 1995-1999, *Hydrological Processes*, **14**, 1641-1666.

PIKE, R. J. (1988): The geometric signature: Quantifying landslide terrain types from digital elevation models, *Mathematical Geology*, **20** (5), 491-511.

PILLEWITZER, W. (1938): Photogrammetrische Gletscherforschung, *Bildmessung und Luftbildwesen*, 66-73.

POHL, C. AND VAN GENDEREN, J. L. (1998): Multisensor image fusion in remote sensing: concepts, methods and applications, *International Journal of Remote Sensing*, **19** (5), 823-854.

PRECHTEL, N. (2001): Digitales Höhenmodell, in: Bollmann, J. and Koch, W. G. (Eds.), *Lexikon der Kartographie und Geomatik*, Band 1, Spektrum, Heidelberg, 160-162.

PROY, C., TANRE, D. AND DESCHAMPS, P. Y. (1989): Evaluation of topographic effects in remotely sensed data, *Remote Sensing of Environment*, **30**, 21-32.

QUINN, P., BEVEN, K., CHEVALLIER, P. AND PLANCHON, O. (1991): The prediction of hillslope flow paths for distributed hydrological modelling using digital terrain models, *Hydrological Processes*, **5**, 59-79.

RABUS, B., EINEDER, M., ROTH, A. AND BAMLER, R. (2003): The Shuttle radar topography mission - a new class of digital elevation models acquired by spaceborne radar, *ISPRS Journal of Photogrammetry and Remote Sensing*, **57** (4), 241-262.

REICHERT, B. K., BENGTSSON, L. AND OERLEMANS, J. (2001): Midlatitude forcing mechanisms for glacier mass balance investigated using general circulation models, *Journal of Climate*, **14**, 3767-3784.

REINHARDT, W. AND RENTSCH, H. (1986): Determination of changes in volume and elevation of glaciers using digital elevation models for the Vernagtferner, Ötztal Alps, Austria, *Annals of Glaciology*, **8**, 151-155.

R

REINWARTH, O. AND ESCHER-VETTER, H. (1999): Mass balance of Vernagtferner, Austria, from 1964/65 to 1996/97: Results for three sections and the entire glacier, *Geografiska Annaler*, **81A** (4), 743-751.

RENTSCH, H., WELSCH, W., HEIPKE, C. AND MILLER, M. M. (1990): Digital terrain models as a tool for glacier studies, *Journal of Glaciology*, **36** (124), 273-278.

REYNOLDS, J. M. (1998): High-altitude glacial lake hazard assessment and mitigation: a Himalayan perspective, in: Maund, J.G. and Eddleston, M. (Eds.), *Geohazards in Engineering Geology*, Geological Society, London, Engineering Geology Special Publications 15, 25-34.

REYNOLDS, J. M., DOLECKI, A. AND PORTOCARRERO, C. (1998): Construction of a drainage tunnel as part of glacial lake hazard mitigation at Hualcán, Cordillera Blanca, Peru, in: Maund, J. G. and Eddleston, M. (Eds.), *Geohazards in Engineering Geology*, Geological Society, London, Engineering Geology Special Publications 15, 41-48.

RICHARDS, J. A. (1994): *Remote sensing digital image analysis: an introduction* (2nd Ed.), Springer, Berlin, 340 p.

RICHARDSON, S. D. AND REYNOLDS, J. M. (2000): An overview of glacial hazards in the Himalayas, *Quaternary International*, **65/66**, 31-47.

RICHTER, E. (1892): Urkunden über die Ausbrüche des Vernagt- und Guslargletschers im 17. und 18. Jahrhundert, *Forschungen zur deutschen Landes- und Volkskunde*, **6** (4), 349-439.

RICHTER, R. (1997): Correction of atmospheric and topographic effects for high spatial resolution satellite imagery, *International Journal of Remote Sensing*, **18** (5), 1099-1111.

RICKENBACHER, M. (1998): Die digitale Modellierung des Hochgebirges im DHM25 des Bundesamtes für Landestopographie, *Wiener Schriften zur Geographie und Kartographie*, **11**, 49-55.

RÖTHLISBERGER, H. (1981): Eislawinen und Ausbrüche von Gletscherseen, in: Kaser, P. (Ed.), *Gletscher und Klima - glaciers et climat*, Jahrbuch der Schweizerischen Naturforschenden Gesellschaft, wissenschaftlicher Teil, Birkhäuser, Basel, 170-212.

ROSENTHAL, W. AND DOZIER, J. (1996): Automated mapping of montain snow cover at subpixel resolution from the Landsat Thematic Mapper, *Water Resources Research*, **32** (1), 115-130.

ROTT, H. (1976): Analyse der Schneeflächen auf Gletschern der Tiroler Zentralalpen aus Landsat Bildern, *Zeitschrift für Gletscherkunde und Glazialgeologie*, **12**, 1-28.

ROTT, H. (1994): Thematic studies in alpine areas by means of polarimetric SAR and optical imagery, *Advances in Space Research*, **14** (3), 217-226.

ROTT, H. AND MARKL, G. (1989): Improved snow and glacier monitoring by the Landsat Thematic Mapper, in: Guyenne, T.-D. and Calabresi, G. (Eds.): *Monitoring the Earth's environment*, ESA, **SP-1102**, 3-12.

ROTT, H., SCHERLER, K. E., REYNAUD, L., SERANDREI-BARBERO, R. AND ZANON, G. (1988): Glaciers of Europe - Glaciers of the Alps, in: Williams, R. S., Jr. and Ferrigno, J. G. (Eds.), *Satellite image atlas of glaciers of the world - Europe*, U.S. Geological Survey, Professional Paper, 1386-E, E1-E48.

RUNDQUIST, D. C., COLLINS, S. C., BARNES, R. B., BUSSOM, D. E., SAMSON, S. A. AND PEAKE, J. S. (1980): The use of Landsat digital information for assessing glacier inventory parameters, *IAHS*, **126**, 321-331.

SANDMEIER, S. AND ITTEN, K. I. (1997): A physically-based model to correct atmospheric and illumination effects in optical satellite data of rugged terrain, *IEEE Transactions on Geoscience and Remote Sensing*, **35** (3), 708-717.

SCHAPER, J., MARTINEC, J. AND SEIDEL, K. (1999): Distributed mapping of snow and glaciers for improved runoff modelling, *Hydrological Processes*, **13**, 2023-2031.

SCHMIDT, J. AND DIKAU, R. (1999): Extracting geomorphometric attributes and objects from digital elevation models - semantics, methods, future needs, in: Dikau, R. and Saurer, H. (Eds.), *GIS for earth surface systems*, Borntraeger, Berlin, 153-173.

SCHÖNHER, W., AUER, I. AND BÖHM, R. (2000): Climate variability and glacier reaction in the Austrian eastern Alps, *Annals of Glaciology*, **31**, 31-38.

SCHOWENGERDT, R. A. (1997): *Remote sensing - Models and methods for image processing*, Academic Press, New York, 522 p.

SERANDREI-BARBERO, R., RABAGLIATI, R., BINAGHI, E. AND RAMPINI, A. (1999): Glacial retreat in the 1980s in the Breonie, Aurine and Pusteresi groups (eastern Alps, Italy) in Landsat TM images, *Hydrological Sciences Journal*, **44** (2), 279-296.

SHETTIGARA, V. K. (1992): A generalized component substitution technique for spatial enhancement of multispectral images using a higher resolution data set, *Photogrammetric Engineering and Remote Sensing*, **58** (5), 561-567.

SHUMSKII, P. A. (1964): *Principles of structural Glaciology*, Dover, New York, 498 p.

SIDJAK, R. W. AND WHEATE, R. D. (1999): Glacier mapping of the Illecillewaet icefield, British Columbia, Canada, using Landsat TM and digital elevation data, *International Journal of Remote Sensing*, **20** (2), 273-284.

SIEBER, R. (2001): Interdisziplinarität und Multidimensionalität in thematischen Atlanten, Deutscher Kartographentag, Berchtesgaden, 331-343.

SIMONETT, D. S. (1983): The development and principles of remote sensing, in: *Manual of Remote Sensing* (2nd Ed., Vol. I) Falls Church, VA, American Society of Photogrammetry, 1-35.

SINGH, A. (1989): Digital change detection techniques using remotely sensed-data, *International Journal of Remote Sensing*, **10** (6), 989-1003.

SKIDMORE, A. K. (1989): A comparison of techniques for calculating gradient and aspect from a gridded digital elevation model, *International Journal of Geographical Information Systems*, **3** (4), 323-334.

SMALL, D., PASQUALI, P., HOLECZ, F., MEIER, E. AND NÜESCH, D. (1998): Experiences with multiresolution and multifrequency InSAR height model generation, *Proceedings of IEEE-IGARSS'98, Seattle, USA, July 6-10*, 2671-2673.

SMITH, I. N. AND BUDD, W. F. (1981): The derivation of past climate changes from observed changes of glaciers, *IAHS*, **131**, 31-52.

SPACEIMAGING (2002): Ikonos sensor characteristics. *URL: http://www.spaceimaging.com/products/ikonos/index_2.htm,* access: 19 Sep 2002.

SPOTIMAGE (2002): SPOT sensor characteristics. *URL: http://www.spotimage.fr/spot5/ensavoirplus/eng/plus_satel.html,* access: 19 Sep 2002.

SUNAR, F. AND MUSAOGLU, N. (1998): Merging multiresolution SPOT P and Landsat TM data: the effects and advantages, *International Journal of Remote Sensing*, **19** (2), 219-224.

SUTER, S., LATERNSER, M., HAEBERLI, W., HOELZLE, M. AND FRAUENFELDER, R. (2001): Cold firn and ice of high-altitude glaciers in the Alps: Measurements and distribution modelling, *Journal of Glaciology*, **47** (156), 85-96.

SWISSTOPO (2001): DHM25 - Das digitale Höhenmodell der Schweiz Level 2, Bundesamt für Landestopographie, 1-17. URL: *http://www.swisstopo.ch/de/digital/dhm25.htm,* access: 19 Sep 2002.

TARBOTON, D. G., BRAS, R. L. AND RODRIGUEZ-ITURBE, I. (1991): On the extraction of channel networks from digital elevation data, *Hydrological Processes*, **5**, 81-100.

TASCHNER, S. AND RANZI, R. (2002): Comparing the opportunities of Landsat-TM and ASTER data for monitoring a debris covered glacier in the Italian Alps within the GLIMS project, Proceedings of the *IGARSS 2002* (4), 1044-1046.

TOUTIN, T. (2002A): Three-dimensional topographic mapping with ASTER stereo data in rugged topography, *IEEE Transactions on Geoscience and Remote Sensing*, **40** (9), 2241-2247. (URL: *http://www.ccrs.nrcan.gc.ca/ccrs/rd/sci_pub/bibpdf/13119.pdf*)

TOUTIN, T. (2002B): DEM from stereo Landsat 7 data over high relief areas, *International Journal of Remote Sensing*, **23** (10), 2133-2139. (URL: *http://www.ccrs.nrcan.gc.ca/ccrs/rd/sci_pub/bibpdf/13068.pdf*)

TOUTIN, T. AND CHENG, P. (2002): A comparison of automated DEM extraction results using along-track ASTER and across-track SPOT stereo images, *Optical Engineering*, **41** (9), 2102-2106. (URL: *http://www.ccrs.nrcan.gc.ca/ccrs/rd/sci_pub/bibpdf/13217.pdf*)

TURPIN, O. C., FERGUSON, R. I. AND CLARK, C. D. (1998): The transient snowline on glaciers: Topographic controls and implications for melt productions, in: Lane, S. N., Richards, K. S. and Chandler, J. H. (Eds.): *Landform monitoring, modelling and analysis*, Wiley, New York, 363-383.

TYDAC (1999): DEM with 50 m spatial resolution from TYDAC AG (Berne, Switzerland).

R

UNEP (1992): *Glaciers and the environment*, UNEP / GEMS Environmental Library No 9, Nairobi, 24 p.

UNEP (2002): Global warming triggers glacial lakes flood threat, URL: *http://www.grida.no/inf/news/news02/news30.htm*, access: 21 Sep 2002.

UNESCO (1970): *Perennial ice and snow masses. A guide for compilation and assemblage of data for a World Glacier Inventory*, UNESCO/IAHS Technical Papers in Hydrology, 1, Zürich.

UniAZ (2002): University of Arizona, Department of Geosciences (Real world features in the GIS world), URL: *http://www.geo.arizona.edu/geos256/gis/lec4.html*, access: 16 Sep 2002.

VALLON, M. (1989): Evolution, water balance, potential hazards and control of a proglacial lake in the French Alps, *Annals of Glaciology*, **13**, 273-278.

VERMOTE, E., TANRÉ, D., DEUZÉ, J. L., HERMAN, M. AND MORCETTE, J. J. (1994): *Second simulation of the satellite signal in the solar spectrum (6S), user Guide*, NASA GSFC, Greenbelt MD, USA, 183 p.

VERMOTE, E., TANRÉ, D., DEUZÉ, J. L., HERMAN, M. AND MORCETTE, J. J. (1997): Second simulation of the satellite signal in the solar spectrum: an overview, *IEEE Transactions on Geoscience and Remote Sensing*, **35** (3), 675-686.

VOIGT, S., KOCH, M. AND BAUMGARTNER, M. F. (1999): A multichannel threshold technique for NOAA AVHRR data to monitor the extent of snow cover in the Swiss Alps, *IAHS*, **256**, 35-44.

VUICHARD, D. AND ZIMMERMAN, M. (1987): The 1985 catastrophic drainage of a moraine-dammed lake, Khumbu Himal, Nepal: cause and consequences, *Mountain Research and Development*, **7**, 91-110.

WAKONIGG, H. (1971): Gletscherverhalten und Witterung, *Zeitschrift für Gletscherkunde und Glazialgeologie*, **7**, 103-123.

WALCHER, I. (1773): Nachrichten von den Eisbergen im Tyrol, Wien.

WALDER, J. S. AND COSTA, J. E. (1996): Outburst floods from glacier-dammed lakes: the effect of mode of lake drainage on flood magnitude, *Earth Surface Processes and-Landforms*, **21**, 701-723.

WALSH, S. J., BUTLER, D. R. AND MALANSON, G. P. (1998): An overview of scale, pattern, process relationships in geomorphology: a remote sensing and GIS perspective, *Geomorphology*, **21** (3/4), 183-205.

WARREN, S. G. (1982): Optical properties of snow, *Reviews of Geophysics and Space Physics*, **20**, 67-89.

WATANABE, T. AND ROTHACHER, D. (1996): The 1994 Lugge Tsho glacial lake outburst flood, Bhutan Himalaya, *Mountain Research and Development*, **16**, 77-81.

WELCH, R. AND EHLERS, M. (1988): Cartographic feature extraction from integrated SIR-B and Landsat TM images, *International Journal of Remote Sensing*, **9** (5), 873-889.

WESSELS, R. L., KARGEL, J. S. AND KIEFFER, H. H. (2002): ASTER measurement of supraglacial lakes in the Mount Everest region of the Himalaya, *Annals of Glaciology*, **34**, 399-408.

WHALLEY, W. B. AND MARTIN, H. E. (1986): The problem of hidden ice in glacier mapping, *Annals of Glaciology*, **8**, 181-183.

WILHELM, F. (1975): *Schnee und Gletscherkunde*, Lehrbuch der Allgemeinen Geographie, Band III/3, Walter de Gruyter, Berlin, 434 p.

WILLIAMS, R. S., JR. (1983): Remote sensing of glaciers, in: Geological Applications (Williams, R. S., Jr., author-editor), *Manual of Remote Sensing* (2nd Ed., Colwell, R. N., Ed.-in chief), V. II, Interpretation and Applications (Estes, J. E. and Thorley, G. A., Eds.) Falls Church, VA, American Society of Photogrammetry, 1852-1866.

WILLIAMS, R. S., JR. (1987): Satellite remote sensing of Vatnajökull, Iceland, *Annals of Glaciology*, **9**, 119-125.

WILLIAMS, R. S., JR. AND FERRIGNO, J. G. (1988): Satellite image atlas of glaciers of the world - Europe, U.S. Geol. Survey, Professional Paper, **1386-E**, 164 p.

WILLIAMS, R. S., JR. AND FERRIGNO, J. G. (2002): Satellite image atlas of glaciers of the world, USGS Fact Sheet 133-99, URL: *http://pubs.usgs.gov/fs/fs133-99/*, access: 21 Sep 2002.

WILLIAMS, R. S., JR. AND HALL, D. K. (1993): Glaciers, in: Gurey, R. J., Foster, J. L. and Parkinson, C. L. (Eds.), *Atlas of satellite observations related to global change*, Cambridge University Press, 401-421.

WILLIAMS, R. S., JR. AND HALL, D. K. (1998): Use of remote-sensing techniques, in: Haeberli, W., Hoelzle, M., and Suter, S. (Eds.), *Into the second century of worldwide glacier monitoring: prospects and strategies*, UNESCO Publishing, 97-111.

WILLIAMS, R. S., JR., HALL, D. K. AND BENSON, C. S. (1991): Analysis of glacier facies using satellite techniques, *Journal of Glaciology*, **37**, 120-127.

WILLIAMS, R. S., JR., HALL, D. K., SIGURDSSON, O. AND CHIEN, J. Y. L. (1997): Comparison of satellite-derived with ground-based measurements of the fluctuations of the margins of Vatnajökull, Iceland, 1973-1992, *Annals of Glaciology*, **24**, 72 -80.

WILLIS, I. C., ARNOLD, N. S., SHARP, M. J., BONVIN, J.-M. AND HUBBARD, B. P. (1998): Mass balance and flow variations of Haut Glacier d'Arolla, Switzerland, calculated using digital terrain modelling techniques, in: Lane, S. N., Richards, K. S. and Chandler, J. H. (Eds.), *Landform monitoring, modelling and analysis*, Wiley, New York, 343-361.

WILSON, J. P. AND GALLANT, J. C. (2000): *Terrain analysis: Principles and applications*, Wiley, New York, 479 p.

WINTHER, J. G. (1993): Landsat TM derived and in situ summer reflectance of glaciers in Svalbard, *Polar Reserach*, **12**, 37-55.

WIPF, A. (1999): Die Gletscher der Berner, Waadtländer und nördlichen Walliser Alpen, Geographisches Institut Universität Zürich, Physische Geographie, **40**, 295 p.

WISE, S. M. (1998): The effect of GIS interpolation errors on the use of digital elevation models in Geomorphology, in: Lane, S. N., Richards, K. S. and Chandler, J. H. (Eds.): *Landform monitoring, modelling and analysis*, Wiley, New York, 385-404.

WOODCOCK, C. E. AND STRAHLER, A. H. (1987): The factor of scale in remote sensing, *Remote Sensing of Environment*, **21**, 311-332.

WÜRLÄNDER, R. AND EDER, K. (1998): Leistungsfähigkeit aktueller Photogrammetrischer Auswertemethoden zum Aufbau eines digitalen Gletscherkatasters, *Zeitschrift für Gletscherkunde und Glazialgeologie*, **34**, 167-185.

WÜRLÄNDER, R. AND KUHN, M. (2000): Zur Erfassung und Anwendung der Produkte des neuen Österrreichischen Gletscherkatasters, *Salzburger Geographische Arbeiten*, **36**, 57-67.

YOCKY, D. A. (1996): Multiresolution wavelet decomposition image merger of Landsat Thematic Mapper and SPOT panchromatic data, *Photogrammetric Engineering and Remote Sensing*, **62** (9), 1067-1074.

ZEMP, M. (2002): *GIS-basierte Modellierung der glazialen Sedimentbilanz*, Diploma thesis (unpublished), Geographisches Institut Universität Zürich, 100 p.

ZENG, Q., CAO, M., FENG, X., LIANG, F., CHEN, X. AND SHENG, W. (1983): A study of spectral reflection characteristics for snow, ice and water in the north of China, *IAHS*, **145**, 451-462.

ZEVENBERGEN, L. W. AND THORNE, C. R. (1987): Quantitative analysis of land surface topography, *Earth Surfaces and Landforms*, **12**, 47-56.

ZUO, Z. AND OERLEMANS, J. (1997): Contribution of glacier melt to sea-level rise since AD 1865: a regionally differentiated calculation, *Climate Dynamics*, **13** (12), 835-845.

APPENDIX

1. Tables:

1) Summary statistics (count and area) for all Alpine glaciers.
2) Summary statistics (count and area) for Swiss glaciers.
3) RMSE of used GCPs and CPs for each scene and threshold used for glacier classification.
4) Used parameters for atmospheric correction with PCIs RCOR2 module.
5) RMSE of used GCPs and CPs for each scene, and threshold used for glacier classification.
6) Covariance matrix for the five input channels used in PCA.
7) Eigenvectors of the covariance matrix used for PCA.
8) Eigenvalues, deviation and variance for each eigenchannel as used for PCA.
9) Count and area for each area class of the 1973 inventory sorted for aspect.

2. Programs

2.1 EASI

1) Reflectance and snow mapping from NDSI (Dozier algorithm)
2) Debris-cover mapping (including glacier classification)
   (A) debris.mod script for MODEL, (B) EASI script
3) Aspect conversion (0-360° -> 8 sectors)

2.2 AML

1) Point coverage
2) Glacier areas 1973 (inventory) and 1998 (TM)
3) Glacier parameters from DEM
4) Hypsography 100 m
5) Slope facets for individual glaciers
6) Perspective views (example Aletsch region)

2.3 Fortran

1) Removing isolated polygons (debris-mapping)
2) Conversion of WGI-code
3) Hypsography (100 m)
4) 2:1 ELA and 1:1 median elevation
5) Calculation of area changes (two years) sorted for size class
6) Conversion of mean aspect to degrees

2.4 XMGR

1) Example of batchjob for a 2D scatterplot with ACE/GR.

3. Figures

3.1 Plots

1) Scatterplot of minimum and maximum elevation vs. glacier size.

3.2 Visuals 2D

1) Left: Differences in glacier mapping using three threshold values (1.8, 1.9, and 2.0).
   Right: TM321 composite for the same region to show glacier areas in shadow.
2) Top: Worse snow conditions at 12 Sep 1999 (scene #5) for Silvretta group.
   Bottom: Favourable snow conditions in the Bernina group, located 50 km to the south.
3) Top: Bernina group at 21 Sep 1985 (scene #4), 8 days after a snow fall event.
   Bottom: Nine days later (scene #1 from 30 Sep 1985, bottom) the new snow has molten.
4) Top: Hue-component of an IHS colour-space transformation with TM bands 3, 4 and 5.
   Bottom: Mapping of vegetation free regions with a threshold of 126 (overlay with TM321).
5) Top: NDWI (TM1-TM4)/(TM1+TM4) with DOS from TM1 (scaled to 256 grey levels).
   Bottom: Mapping of lakes with a threshold of 0.45 (overlay with TM321).
6) Top: Overlay of glacier, vegetation and slope facet map for the entire test region Aletsch.
   Bottom: Combination of the glacier/debris map with the change detection map.
7) Top: Comparison of the glacier map including debris-cover with 1973 glacier outlines.
   Bottom: Comparison of debris-cover mapping with the DEM25L2 and an ASTER DEM.
8) Comparison of glacier outlines from TM, Ikonos and the digitized 1973 glacier inventory.
9) TM derived glacier change between 1985 and 1999 (Grisons).
10) TM derived glacier change between 1985 and 1999 (Bernese and Central Alps).
11) TM derived glacier change between 1985 and 1999 (ValaisAlps).
12) Digitized 1973 glacier areas and 1850 outlines for the western part of Switzerland.
13) Digitized 1973 glacier areas and 1850 outlines (for the eastern part of Switzerland.
14) The digitized glacier basin coverage used for intersection with TM-derived glacier maps.
15) Examples of glacier outlines digitized several times (Bernina group).
16) Some more examples of digitized glacier outlines.

3.3 Visuals 3D

1) Täschvalley (IRS-1C / TM fusion) and Göschener Alp (SPOT / TM fusion).
2) Steinglacier (SPOT / TM fusion) and Basòdino- / Cavagnoliglacier (SPOT / TM fusion).
3) Steinglacier and Triftglacier (Ikonos).
4) Grimsel with Aare glaciers (IRS-1C / TM fusion).
5) Valais Alps as seen from TM in 1998 with glacier outlines of 1850 and 1973.

A 1: Tables

Class	Count	%	Area	%
0.0-0.1	1971	36.4	101.23	3.3
0.1-0.5	2411	44.5	533.15	17.2
0.5-1.0	465	8.6	324.83	10.5
1-5	470	8.7	952.47	30.8
5-10	71	1.3	497.71	16.1
10-20	27	0.5	387.86	12.5
> 20	7	0.1	293.60	9.5
Total	5422	100	3090.90	100

Table 1: *Summary statistics for all Alpine glaciers. Data are taken from the digital WGMS data base with slightly different values than published in the WGI (IAHS, 1989).*

Class	Count	%	Area	%
0.0-0.1	640	35.0	29.43	2.2
0.1-0.5	826	45.2	185.47	13.8
0.5-1.0	156	8.5	108.38	8.1
1-5	152	8.3	294.80	22.0
5-10	32	1.8	223.00	16.6
10-20	16	0.9	240.10	17.9
> 20	6	0.3	260.51	19.4
Total	1828	100	1341.69	100

Class	Count	%	Area	%
0.0-0.1	0	0.0	0.00	0.0
0.1-0.5	14	11.9	4.05	0.5
0.5-1.0	14	11.9	10.03	1.3
1-5	45	38.1	102.19	13.0
5-10	24	20.3	176.01	22.5
10-20	15	12.7	228.35	29.1
> 20	6	5.1	263.19	33.6
Total	118	100	783.82	100

Table 2: *Summary statistics of Swiss glaciers according to the inventory by Müller et al. (1976) (left) and for glaciers within the Swiss length network (right).*

				GCP		CP		
Nr.	Sensor	Path-Row	Date	Count	RMSE	Count	RMSE	Threshold
1	L5 TM	193-27 (+50%)	30.9. 1985	43	30.1	-	-	2.1
2	L5 TM	193-27 (+50%)	17.9. 1992	54	28.1	-	-	2.0
3	L7 ETM+	193-27 (+50%)	13.9. 1999	42	26.0	-	-	2.1
4	L5 TM	194-27 (+60%)	21.9. 1985	76	19.3	23	23.1	2.0
5	L5 TM	194-27 (+60%)	12.9. 1999	76	23.8	23	22.7	1.9
6	L5 TM	195-28	12.9. 1985	45	26.2	-	-	-
7	L5 TM	195-27 (+70%)	28.9. 1985	86	19.2	32	20.9	1.9
8	L5 TM	195-27 (+70%)	15.9. 1992	113	19.4	39	21.4	2.1
9	L5 TM	195-27	31.8. 1998	50	16.2	14	17.8	1.9
10	L5 TM	195-28	31.8. 1998	108	18.3	26	18.7	1.9
11	SPOT Pan	55-256	17.9. 1992	20	3.8	-	-	-

Table 3: *RMS error of GCPs and CPs used for each scene. The threshold value used for glacier classification with TM4 / TM5 is also given.*

Parameter	Description	Values					
FILE	Database File Name	weissmies.pix					
AFILE	Atmospheric Correction File	tmmscogr.alt					
DBIC	Database Input Channel List	7	8	9	10	11	
SBAND	Satellite Band	1	2	3	4	5	
GNCL	Satellite Coefficient's Gain	0.727	1.385	1.102	0.885	0.126	
OFCL	Satellite Coefficient's Offset	-1.331	-2.346	-1.897	-1.942	-0.398	
DBOC	Database Output Channel List	12	13	14	15	16	
GNSC	Scale Coefficient's Gain	1	1	1	1	1	
OFSC	Scale Coefficient's Offset	0	0	0	0	0	
MASK	Area Mask (Window or Bitmap)	37	26	504	720		
DTM	DHM Channel	6					
ESCALE	Elevation Scale and Offset	1					
ILLU	Illumination Channel	2					
CAST	Cast-Shadow Channel	3					
VD	Sky-View Factor Channel	4					
VT	Terrain-View Factor Channel	5					
ZNANGLE	Solar Zenith Angle (20-70°)	46.866					
DATE	Date of the Scene (day/month/year)	12	9	1985			
ELEV	Elevation Base Height	450	600	900	1500	2500	3500
VISIBIL	Ground Visibility (km)	22	30	40	40	40	40

Table 4: *Parameters used for the atmospheric correction with PCIs RCOR2 module.*

Class	Nr.	Pixel	1	2	3	4	5	6	7	8	9	10
Snow, Sun	1	1853	95.09	0.00	4.91	0.00	0.00	0.00	0.00	0.00	0.00	0.00
Snow, Shadow	2	533	0.00	95.31	0.00	0.00	0.00	0.00	0.19	0.00	0.00	4.50
Ice	3	2530	0.79	0.00	90.16	0.04	0.00	0.00	0.00	0.00	0.00	9.01
Terrain	4	6583	0.00	0.00	0.00	98.51	0.00	1.49	0.00	0.00	0.00	0.00
Forest	5	1928	0.00	0.00	0.00	0.05	92.89	2.13	4.93	0.00	0.00	0.00
Meadow	6	959	0.00	0.00	0.00	0.00	0.52	99.48	0.00	0.00	0.00	0.00
Shadow	7	3809	0.00	1.52	0.03	0.32	6.54	0.03	91.55	0.00	0.00	0.03
Water	8	12	0.00	0.00	0.00	0.00	0.00	0.00	0.00	100.0	0.00	0.00
Frame	9	2617	0.00	0.00	0.00	0.00	0.00	0.00	0.00	0.00	100.0	0.00
Ice, Steep Slope	10	376	0.27	0.27	5.05	0.00	0.00	0.00	0.00	0.00	0.00	94.41

Table 5: *Confusion matrix of the Maximum-Likelihood classification.*

	1	2	3	4	5
1	1581.37	-	-	-	-
2	904.97	542.12	-	-	-
3	1092.57	654.58	795.42	-	-
4	519.73	344.10	415.18	560.91	-
5	-199.80	-47.77	-22.32	333.47	1269.14

Table 6: *Covariance matrix for the five input channels used in PCA.*

1	2	3	4	5
0.70572	0.41506	0.50142	0.27636	-0.04348
-0.09243	0.00319	0.02752	0.32910	0.93935
0.23297	0.06719	0.14141	-0.89988	0.33382
0.66263	-0.45566	-0.58744	0.06757	0.06028
-0.00808	0.78458	-0.61865	-0.03122	0.02561

Table 7: *Eigenvectors of the covariance matrix used for PCA.*

Eigen-channel	Eigenvalue	Deviation	%Variance
1	3105.7400	55.7292	65.40%
2	1404.8179	37.4809	29.58%
3	211.7134	14.5504	4.46%
4	25.2806	5.0280	0.53%
5	1.4108	1.1878	0.03%

Table 8: *Eigenvalues, standard deviation and variance for each eigenchannel as used for PCA.*

Size class		0.1	0.5	1.0	5.0	10.0	20.0	100.0	Total
Total	count	1022	673	151	157	35	14	5	2057
	area	40.09	153.95	104.15	295.99	249.38	216.32	225.81	1285.7
N	count	302	185	36	40	14	5	0	582
	area	11.54	42.61	23.91	76.14	94.48	77.56	0.0	326.24
NE	count	158	112	21	31	9	3	0	334
	area	6.33	24.55	15.10	56.72	60.30	44.77	0.0	207.77
E	count	90	63	18	18	3	1	1	194
	area	3.62	15.15	12.63	43.35	20.20	13.76	27.15	135.86
SE	count	68	60	18	15	0	0	3	164
	area	2.72	13.02	11.78	26.55	0.0	0.00	140.90	194.97
S	count	76	42	11	9	1	1	0	140
	area	2.77	10.22	7.78	15.12	9.52	17.44	0.0	63.03
SW	count	68	29	10	3	1	1	0	112
	area	2.43	7.12	7.01	3.99	9.96	13.77	0.0	44.28
W	count	85	51	12	9	2	2	0	161
	area	3.62	12.25	8.31	16.36	14.74	30.40	0.0	85.68
NW	count	175	131	25	32	5	1	1	326
	area	7.05	29.04	17.64	57.77	40.18	18.62	57.77	228.07

Table 9: *Count and area (in km^2) for each area class of the 1973 inventory, also sorted for aspect.*

A 2: Programs

2.1. EASI

2.1-1 Reflectance and snow mapping from NDSI (Dozier algorithm)

```
! input: DN from TM1-TM5 (%1-%5)
! outout: glacier map from NDSI (%10)
! #f=(pi*d^2)/cos(zenith angle), d=1.009528, zw=39.1777 (at 31 Aug 1998)

#f=4.1302235;

#r1=(#f/1957)*(1.331+0.727*%1);
#r2=(#f/1829)*(2.346+1.385*%2);
#r3=(#f/1557)*(1.897+1.102*%3);
#r4=(#f/1047)*(1.942+0.885*%4);
#r5=(#f/219.3)*(0.398+0.126*%5);

! * NDSI calculation *
#n=(#r2-#r5)/(#r2+#r5);

! * snow mapping *
if (#r1>0.09) and (#r5<0.2) and (#n>0.4) then
%10=0;
else
%10=255;
endif;
```

2.1-2 Debris-cover mapping (including glacier classification)

(A) debris.mod script for MODEL

```
! input: TM4 & TM5 (%9 & %10), hue345(%12),slope(%20)
! output: ice(0), debris(127), other(255) in #g (%27)

! glacier map (#g=0)
if ((%9/%10)>2.0) and (%12>126) then
#g = 0;
else
#g = 255;
endif;

! debris map (#g=127)
if (#g=255) and (%12>126) and (%20<24) and (%20 > 0) then
#g = 127;
endif;

%27 = #g;
```

(B) EASI script

```
!******************
!* debris workflow *
!******************

file="tm98.pix"
source="debris.mod”
undefval=0
report="term"
r model                  (run debris.mod script given above)
```

A

```
dbic=27
dboc=28
flsz=3,3
mask=
r fme                   (run median filter)

dbic=28
dboc=22
polv=0,127
r ipg                   (run image polygon growing)

system "\rm value.dat"

dbgeo=
dbic=22,28
numform="data"
tfile="value.dat"
r numwrit               (write values for ice, debris, other [%28] and polygon ID [%22])

system "debris.out"     (run Fortran code [see 2.3-1] for elimination of isolated polygons)

dboc=29
dbow=
tfile="debris.dat"
memsize=128
r numread               (import result from Fortran code)
```

2.1-3 Aspect conversion (0-360 deg -> 8 sectors)

```
! input: aspect in degrees (%5)
! output: aspect sector (%4)

#a = int((%5+22.5)/45.0);
%4 = (mod(#a,8))+1;
```

2.2. AML

2.2-1 Point coverage

```
generate labelch
input labelch.txt
points
q
build labelch point
tables
sel labelch.pat
alter
labelch-id
~
8
~
~
~
q
```

2.2-2 Glacier areas 1973 (inventory) and 1998 (TM)

```
imagegrid gl98.tif tmpgr
grid
gl98gr = setnull(tmpgr == 1, tmpgr)
q
gridpoly gl98gr gl98mor

intersect LSEL5_7398 STANZCHISL98 stanzint point
joinitem STANZCHISL98.pat stanzint.pat STANZCHISL98.pat STANZCHISL98#
intersect GL98MOR STANZCHISL98 gl98cc
tables
sel gl98cc.pat
res LSEL5_7398# gt 0
res GRID-CODE eq 0
unload gl98cc.tab AREA LSEL5_7398-id columnar col
q

intersect LSEL5_7398 gl73f98 gl73int point
joinitem gl73f98.pat gl73int.pat gl73f98.pat gl73f98#
tables
sel gl73f98.pat
res LSEL5_7398# gt 0
unload gl73f98.tab AREA LSEL5_7398-id columnar col
q
```

2.2-3 Glacier parameters from DEM

```
/* zonalstats calc from dem products
/* joining of slp and vd
/* calculating mean aspect, ela and median elev.

&echo &off

grid
/* SINGR = sin(DHM25L2_ASPGR div deg)
/* COSGR = cos(DHM25L2_ASPGR div deg)
gl73f98elev.stat = zonalstats(GL73F98GR, dhm12intgr, all)
gl73f98slp.stat = zonalstats(GL73F98GR, DHM25L2_SLPGR, all)
gl73f98vd.stat = zonalstats(GL73F98GR, DHM25L2_VDGR, all)
gl73f98sin.stat = zonalstats(GL73F98GR, singr, mean)
gl73f98cos.stat = zonalstats(GL73F98GR, cosgr, mean)
gl73f98psr.stat = zonalstats(GL73F98GR, sradgr, all)
q
```

A

```
/* new info-file for statistics
/* --------------------------
tables
copy gl73f98elev.stat gl73f98alle.stat

/* altering item names before joining
/* ---------------------------------
sel gl73f98slp.stat
alter
range
slp_range
~
~
~
~
mean
slp_mean
~
~
~
~
std
slp_std
~
~
~
~
~
sel gl73f98vd.stat
alter
mean
vd_mean
~
~
~
~
std
vd_std
~
~
~
~
~
q

joinitem gl73f98alle.stat gl73f98slp.stat gl73f98alle.stat value
joinitem gl73f98alle.stat gl73f98vd.stat gl73f98alle.stat value

/* deleting superfluous items and adding area in sqkm
/* -------------------------------------------------
tables
dropitem gl73f98alle.stat SUM VARIETY MAJORITY MINORITY MEDIAN
additem gl73f98alle.stat areakm2 4 10 f 3
sel gl73f98alle.stat
calc areakm2 = area / 1000000

/* calculation of mean aspect from sin and cos mean
/* -----------------------------------------------
sel gl73f98sin.stat
unload sinstat.dat value mean columnar col
sel gl73f98cos.stat
unload cosstat.dat value mean columnar col
q

&system meanasp.out

tables
define gl73f98_asp.stat
```

```
value 4 10 b
asp360_mean 4 8 f 1
aspsec_mean 4 4 I
~
sel gl73f98_asp.stat
add from degstat98.dat

/* add item areadif and import from progr. output
/* ---------------------------------------------
define areadif7398.stat
value 4 10 b
AREA_DIF7398 4 8 f 1
~
sel areadif7398.stat
add from analyse7398a.dat

/* add item area98km2 and import from progr. output
/* ------------------------------------------------
define gl73f98_area98.stat
value 4 10 b
area98km2 4 10 F 3
~
sel gl73f98_area98.stat
add from analyse7398b.dat

additem gl73f98alle.stat LSEL5_7398-ID 4 10 b
sel gl73f98alle.stat
calc LSEL5_7398-ID = value
q

joinitem gl73f98alle.stat gl73f98_asp.stat gl73f98alle.stat value
joinitem gl73f98alle.stat areadif7398.stat gl73f98alle.stat value
joinitem gl73f98alle.stat gl73f98_area98.stat gl73f98alle.stat value

/* combining info file with coverage, adding ela & median
/* ------------------------------------------------------
joinitem GL73F98SEL.pat gl73f98alle.stat GL73F98SEL.pat LSEL5_7398-ID
joinitem GL73F98SEL.pat elamedian.stat GL73F98SEL.pat GL73F98SEL-ID
```

2.2-4 Hypsography 100 m

```
/*
&echo &off

grid
&do i = 12 &to 47 &by 1
&s h1 = %i% * 100
&s h2 = ( %i% + 1 ) * 100
zone = select(dhml2intgr, [quote value gt %h1% and value <= %h2%])
hypso%i% = zonalstats(gl73f98gr, zone)
kill zone all
&end
quit

tables
&do i = 12 &to 47 &by 1
sel hypso%i%
unload hyp.tab area value %i% columnar col
erase hypso%i%
y
&end
q
```

2.2-5 Slope facets for individual glaciers

```
&echo &off

grid
&do i = 12 &to 44 &by 2
&s h1 = %i% * 100
&s h2 = ( %i% + 2 ) * 100
zonedhmgr = select(dhm12intgr, [quote value gt %h1% and value <= %h2%])
zoneglgr = GL73SELGR + setnull(isnull(zonedhmgr) == 1, 0)
zoneslp%i% = zonalstats(zoneglgr, dhm25l2_slpgr, mean)

kill zonedhmgr all
kill zoneglgr all
&end
quit

tables
&do i = 12 &to 44 &by 2
sel zoneslp%i%
unload slope.tab value area mean %i% columnar col
&end
q
```

2.2-6 Perspective views (example Aletsch region)

```
ap
display 1040
aletsch3d
mape aletschgr
pageunits cm
pagesize 29.7 21.0
surface lattice aletschgr
surfacedefaults
surfaceresolution 25
SurfaceObserver Relative 180,35,35000
SURFACEDRAPE image irs_aletsch10m.tif
SURFACEDRAPE arclines gl1850 6
SURFACEDRAPE arclines gl1973 7
q
postscript aletsch3d.gra aletsch3d.eps 1 plotparam.txt

plotparam.txt:
landscape 1
```

2.3. Fortran

2.3-1 Removing isolated polygons (debris-mapping)

```
program

C       *** reads poly-id p(i) and debris map m(i) ***
C       *** and calculates if id of ice and debris is ***
C       *** identical. YES: debris stays, NO: m(i)=190 ***

C       *** VARIABLE ***

        IMPLICIT none
        INTEGER i,m(467500),p(467500),w(500,256),mor(500)

C       *** Open files***

        OPEN (51,file='polyid.dat',status='old')
        OPEN (52,file='glaciermap.dat',status='old')
        OPEN (56,file='debris.dat')

C       *** Reading data ***

        DO 11 i=1,467500
           READ(51,*,end=11) p(i)
           READ(52,*,end=11) m(i)
           w(p(i),m(i)+1)=1
11      CONTINUE

C       *** Checking polygon-id ***

        DO 12 i=1,350
           IF (w(i,128).eq.w(i,1)) mor(i)=1
12      CONTINUE

C       *** Writing results***

        DO 13 i=1,467500
           IF(m(i).eq.127.AND.mor(p(i)).eq.0) m(i)=190
           WRITE(56,101) m(i)
13      CONTINUE

101     FORMAT(I3)

        STOP
        END
```

2.3-2 Conversion of WGI-code

```
program

C       * Conversion of WGI-Code in numberstring *
C       * separate table for code (tabcode.txt)  *

C       *** variables ***

        IMPLICIT none
        INTEGER i,j,k,pos8,xko,yko
        CHARACTER code*8,pos1*2,pos2*2,pos4*2,pos6*2
        CHARACTER let(19)*1,nr1(5)*1,nr2(19)*2

        DATA (let(k),k=1,19)/'A','B','C','D','E','F','G','H',
     &  'I','J','K','L','M','N','O','P','Q','R','S'/
        DATA (nr2(k),k=1,19)/'01','02','03','04','05','06','07',
     &  '08','09','10','11','12','13','14','15','16','17','18','19'/
        DATA (nr1(k),k=1,5)/'1','2','3','4','5'/
```

A

```
C       *** open files ***

        OPEN (52,file='invgl_code.dat', status='old')
        OPEN (51,file='invgl_coord.dat', status='old')
        OPEN (56,file='code_neu.dat')
        OPEN (57,file='code_label.dat')

C       *** conversion ***

        DO 10 i=1,3000
                READ (51,*,end=10) xko,yko
                READ (52,103,end=10) code
                pos8=0

C       -> first letter
        DO 11 j=1,5
           IF (code(1:1).eq.let(j)) THEN
           pos1=nr1(j)
           ENDIF
11      CONTINUE

C       -> first digits
        pos2=code(2:3)

C       -> position 4 = '/'
           IF (code(4:4).eq.'/') THEN
           pos4='00'
           pos6=code(5:6)
                IF (code(7:7).eq.'n') THEN
                pos8=1
                ENDIF
           ELSE

C       -> position 4 = letter
           DO 12 j=1,19
              IF (code(4:4).eq.let(j)) THEN
              pos4=nr2(j)
              ENDIF

C       *** Writing table ***

                WRITE(56,101) i,",",code,", ",pos1,pos2,pos4,pos6,
     &          ",",pos8,",",xko,",",yko
                WRITE(57,102) pos1,pos2,pos4,pos6,",",xko,",",yko
10      CONTINUE

        WRITE(57,*) 'end'

101     FORMAT(I5,A1,A9,A2,A1,3A2,A1,I2,2(A1,I8))
102     FORMAT(A1,3A2,2(A1,I8))
103     FORMAT(A8)

        STOP
        END

INPUT / OUTPUT DATA EXAMPLE:
invgl_code.dat
A10F/01
A10G/03

code_label.dat
1100601,  794800,  195400
1100703,  791900,  195200
```

2.3-3 Hypsography (100 m)

```
program

C       *** calculates 100 m hypsography according to glacier area ***
C       *** parts (area) for each glacier (nr) and each elevation ***
C       *** interval (elev) from zonalstat output (hypso100m.dat) ***

C       *** VARIABLE ***

        IMPLICIT none
        INTEGER i,j,area,nr,elev,sumarea(2200,50),sumelev(50)
        REAL f,sum
        f=1.e6

C       *** OPEN FILES ***

        OPEN (51,file='hypso100m.dat',status='old')
        OPEN (56,file='hypsogl98.dat')
        OPEN (57,file='hypsogl98abs.dat')
        OPEN (58,file='hypsogl98rel.dat')

C       *** READING DATA ***

        DO 11 i=1,4200
           READ(51,*,end=11) area,nr,elev
           sumarea(nr,elev)=area
           sumelev(elev)=sumelev(elev)+area
           sum=sum+area
11      CONTINUE

C       *** WRITING OUTPUT ***

        DO 12 i=1,731
           DO 13 j=12,47
           IF (sumarea(i,j).eq.0) GOTO 13
              WRITE(56,101) i,j*100,sumarea(i,j)
13      CONTINUE
12      CONTINUE

        DO 14 j=12,47
           WRITE(57,102) FLOAT(sumelev(j))/f,j*100
           WRITE(58,102) (FLOAT(sumelev(j))/sum)*100.,j*100
14      CONTINUE

101     FORMAT(2I6,I9)
102     FORMAT(F8.2,I6)

        STOP
        END

INPUT / OUTPUT DATA EXAMPLE:
hypso100m.dat
  13125.0000       103          12.000
   2500.0000       116          12.000
  43125.0000       103          13.000
  13125.0000       116          13.000

hypsogl98.dat
3  2500     6250
4  2700    20625
5  2400     1875
5  2500   100625
5  2600   101250
5  2700    68125
5  2800    26250
```

A

2.3-4 2:1 ELA and 1:1 median elevation

```
program

C       *** calculates 2:1 (ELA) and 1:1 (median) elevation ***
C       *** from area parts (area) within each elevation zone (elev) ***
C       *** for each glacier (nr) using zonalstat output (zone.tab) from arc/info ***

C       *** Variables ***

        IMPLICIT none
        INTEGER i,j,area,nr,zonearea(2200,470),sumelev(470)
        INTEGER sumzone(2200),gwl(2200),sumarea(2200)
        REAL elev

C       *** Open files ***

        OPEN (51,file='zone.tab',status='old')
C       OPEN (56,file='gwl.dat')
        OPEN (56,file='median.dat')

C       *** Reading data ***

        DO 11 i=1,94555
           READ(51,*,end=11) area,nr,elev
           zonearea(nr,INT(elev/10.))=area
           sumarea(nr)=sumarea(nr)+area
           sumelev(elev/10)=sumelev(elev/10)+area
11      CONTINUE
        GOTO 12

C       *** Calculation and output ***

        DO 12 i=1,2200
           DO 13 j=120,470
           sumzone(i)=sumzone(i)+zonearea(i,j)
              IF (gwl(i).eq.0) THEN
                 IF (FLOAT(sumzone(i)).gt.FLOAT(sumarea(i))/2.) THEN
                   gwl(i)=(j-1)*10
                 ENDIF
              ENDIF
13            CONTINUE

        WRITE(56,101) i,gwl(i)
12      CONTINUE

        WRITE(57,102) (FLOAT(sumelev(j))/1.e6,j*10,j=120,470)

101     FORMAT(I6,I8)
102     FORMAT(F8.3,I7)

        STOP
        END
```

3. for ELA!

2.3-5 Calculation of area changes (two years) sorted for size class

```
program

C       *** reads 2 data files (area, id) and calculates differences ***

C       *** VARIABLE ***

        IMPLICIT none
        INTEGER anz,i,j,k,b,fk(1000),fksum(7)
        REAL a,a73(1000),a98(2000),fka73(7),fka98(7),fkdif(7),f
        REAL sum73,sum98,difsum,sd,klgr(7),sumfk(3),fkdifsum,fk73sum
        DATA (klgr(k),k=1,7)/1.e5,5.e5,1.e6,5.e6,1.e7,2.e7,1.e8/
```

A

```
        f=1.e6

C       *** OPEN FILES ***

        OPEN (51,file='gl73f98.tab',status='old')
        OPEN (52,file='gl98cc.tab',status='old')
        OPEN (55,file='gldif7398.dat')
        OPEN (56,file='gldifabs7398.dat')
        OPEN (57,file='gldiffk7398.tab')
        OPEN (58,file='gldiffk7398.dat')
        OPEN (59,file='analyse7398.dat')

C       *** READ DATA ***

        DO 11 i=1,1000
           READ(51,*,end=11) a,b
           a73(b)=a73(b)+a
           sum73=sum73+a

        DO 12 j=7,1,-1
           IF (a.lt.klgr(j)) THEN
           fk(b)=j
           ENDIF
12      CONTINUE
11      CONTINUE

        DO 13 i=1,2000
           READ(52,*,end=13) a,b
           a98(b)=a98(b)+a
           sum98=sum98+a
13      CONTINUE

        sd=sum98-sum73
        difsum=(sd/sum73)*100.

C       *** COUNTING SIZE CLASSES ***

        DO 14 b=2,800
           IF(a73(b).ne.0.0) THEN
           fksum(fk(b))=fksum(fk(b))+1
           fka73(fk(b))=fka73(fk(b))+a73(b)
           fka98(fk(b))=fka98(fk(b))+a98(b)
           WRITE(55,101) a73(b)/1.e6,((a98(b)-a73(b))/a73(b))*100.
           WRITE(56,102) a73(b)/1.e6,(a98(b)-a73(b))/f
           WRITE(59,105) b,((a98(b)-a73(b))/a73(b))*100.
           ENDIF
14      CONTINUE

C       *** WRITING RESULT TABLES ***

        WRITE(57,*) 'Flkl. Anz.   Fl.73    Fl.98    Diff.    %
     &    Ø km   Ø 73    Ø 98   % 73   % 98'
        WRITE(58,*) 'Flkl.  Sumfl.  Sumdif.  % kumul.'

        DO 15 i=1,7
           anz=anz+fksum(i)
           fkdif(i)=fka98(i)-fka73(i)
           WRITE(57,103) klgr(i)/f,fksum(i),fka73(i)/f,fka98(i)/f,
     &     fkdif(i)/f,(fkdif(i)/fka73(i))*100.,fkdif(i)/(fksum(i)*f)
     &     ,fka73(i)/(fksum(i)*f),fka98(i)/(fksum(i)*f),
     &     (fka73(i)/sum73)*100.,(fka98(i)/sum98)*100.
           fkdifsum=fkdifsum+fkdif(i)
           fk73sum=fk73sum+fka73(i)
           WRITE(58,104) klgr(i)/f,fk73sum/f,fkdifsum/f,
     &     (fkdifsum/fk73sum)*100.
15      CONTINUE
```

A

```
        sumfk(1)=fkdif(1)+fkdif(2)+fkdif(3)
        sumfk(2)=fkdif(4)+fkdif(5)
        sumfk(3)=fkdif(6)+fkdif(7)

        WRITE(57,106) 'Total:',anz,sum73/f,sum98/f,sd/f,
     &  difsum,sd/(anz*f),sum73/(anz*f),sum98/(anz*f)
        WRITE(57,*)
        WRITE(57,*) 'Summarized area part on decrease in % (<1, 1-10, >10):'
        WRITE(57,*) ((sumfk(i)/sd)*100.,i=1,3)
        WRITE(58,*)
        WRITE(58,*) 'Percentage of area part on decrease'
        WRITE(58,107) (klgr(i)/f,(fkdif(i)/sd)*100.,i=1,7)
        WRITE(58,*)
        WRITE(58,*) 'Relative loss per area class'
        WRITE(58,108) (i,(fkdif(i)/fka73(i))*100.,i=1,7)

101     FORMAT(F8.4,F8.1)
102     FORMAT(F8.4,F8.3)
103     FORMAT(F5.1,I5,3F9.2,F7.1,3F8.2,2F7.1)
104     FORMAT(F5.1,2F9.2,F8.2)
105     FORMAT(I5,F8.1)
106     FORMAT(A5,I5,3F9.2,F7.1,3F8.2)
107     FORMAT(F5.1,F8.1)
108     FORMAT(I3,F8.1)

        STOP
        END
```

2.3-6 Conversion of mean aspect to degrees

```
program
C       *** reads sine and cosine data from zonalstats output ***
C       *** and calculates mean value in degrees and sector ***

C       *** VARIABLES ***

        IMPLICIT none
        INTEGER i,v,s
        REAL f,x,y,d,n,w(2100)
        f=180./(4.*ATAN(1.))

C       *** OPEN FILES ***

        OPEN (51,file='sinstat.dat',status='old')
        OPEN (52,file='cosstat.dat',status='old')
        OPEN (56,file='degstat.dat')
        OPEN (57,file='secstat.dat')

C       *** READING DATA AND WRITING OUTPUT ***

        DO 11 i=1,2057
           READ(51,*,end=11) v,x
           READ(52,*,end=11) v,y

           n=sqrt(x*x+y*y)
           d=MOD(360.+(ATAN2(x,y))*f,360.)
           s=(MOD(NINT(d/45),8))+1
           WRITE(56,101) v,d,s
           w(i)=d
C          WRITE (57,103) x/n,y/n

101     FORMAT(I5,F8.1,I3)
102     FORMAT(F7.1)
103     FORMAT(2F9.4)

        STOP
        END
```

```
INPUT / OUTPUT DATA EXAMPLE:
sinstat.dat
3    206.3840
4  -2553.9792
5    115.7823

cosstat.dat
3     86.8270
4    393.3500
5   -111.6863

degstat.dat
3    67.2  2
4   278.8  7
5   134.0  4
```

2.4. XMGR

2.4-1 Example of batchjob for 2D scatterplot with ACE/GR

```
source disk
type nxy
read "elevmima.dat"
read "elevstat.dat"
autoscale
world 0.01,1000,100,5000
g0 type logx
sets linestyle 0
s0 symbol 9
s0 symbol size 0.3
s1 symbol 10
s1 symbol size 0.3
s2 symbol 18
s2 symbol linewidth 3
s3 symbol 18
s3 symbol linewidth 3
subtitle "Minimum and maximum glacier elevations"
subtitle font 0
xaxis label "Glacier size [sqkm]"
xaxis tick major grid on
xaxis tick major linestyle 2
xaxis ticklabel prec 3
xaxis tick minor 1
xaxis tick major 1
yaxis label "Elevation [m]"
yaxis tick major grid on
yaxis tick major linestyle 2
yaxis tick minor 100
yaxis tick major 1000

INPUT DATA EXAMPLE:
elevmima.dat
   0.0254  2526  2622
   0.0178  2632  2724
   0.0418  2472  2650

elevstat.dat
0.01   2912.84  3073.56
0.10   2804.28  3205.24
0.50   2665.81  3344.65
1.00   2582.60  3608.45
5.00   2254.46  3808.68
10.0   2176.00  3947.31
20.0   1820.25  4231.75
100.0  1820.25  4231.75
```

A

A 3: Figures

3.1. Plots

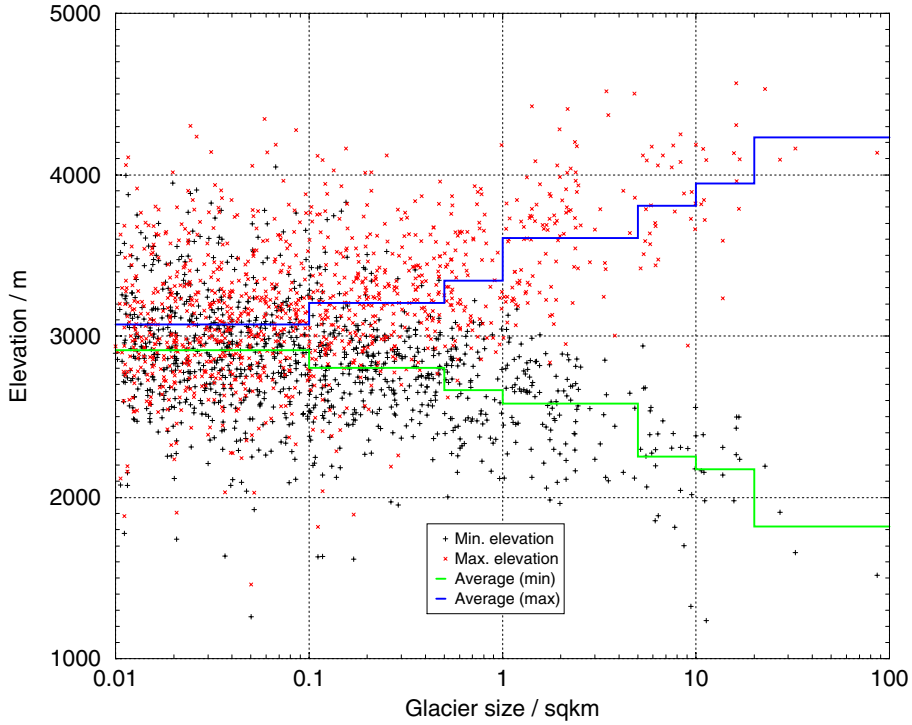

Fig. 3.1-1: *In this diagram minimum (black) and maximum (red) elevation is plotted vs. glacier size (including size class averages in green and blue, respectively). Although individual pairs are not connected, the high variability of glacier elevation range is obvious, in particular for smaller glaciers.*

3.2. Visuals 2D

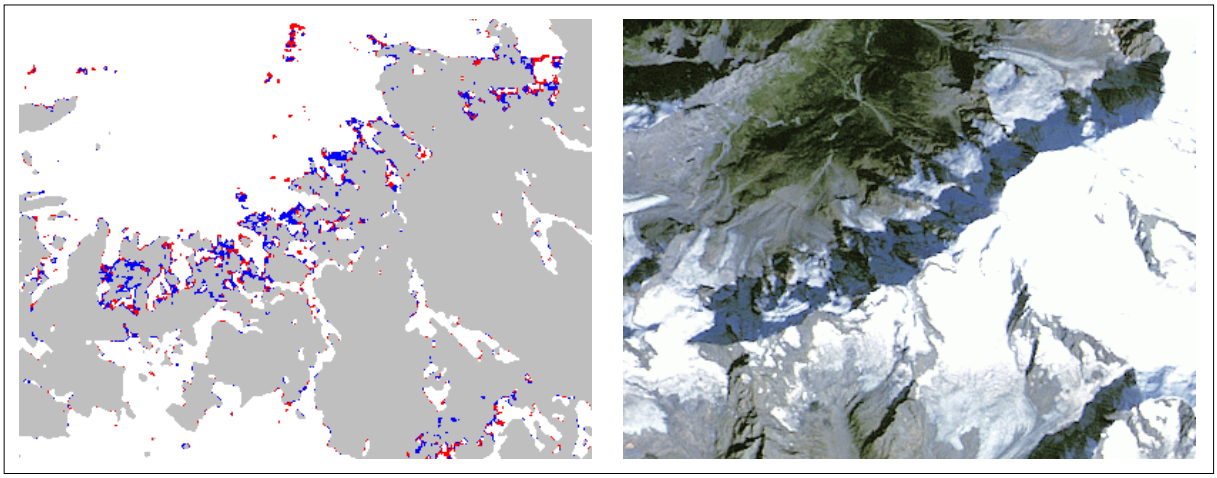

Fig. 3.2-1: *Left: Using three different threshold values for glacier mapping 2.0 (grey), 1.9 (grey and blue) and 1.8 (grey, red and blue). The classification is most sensitive to the threshold for glaciers located in cast shadow, visible on the TM321 image shown at right for comparison.*

A

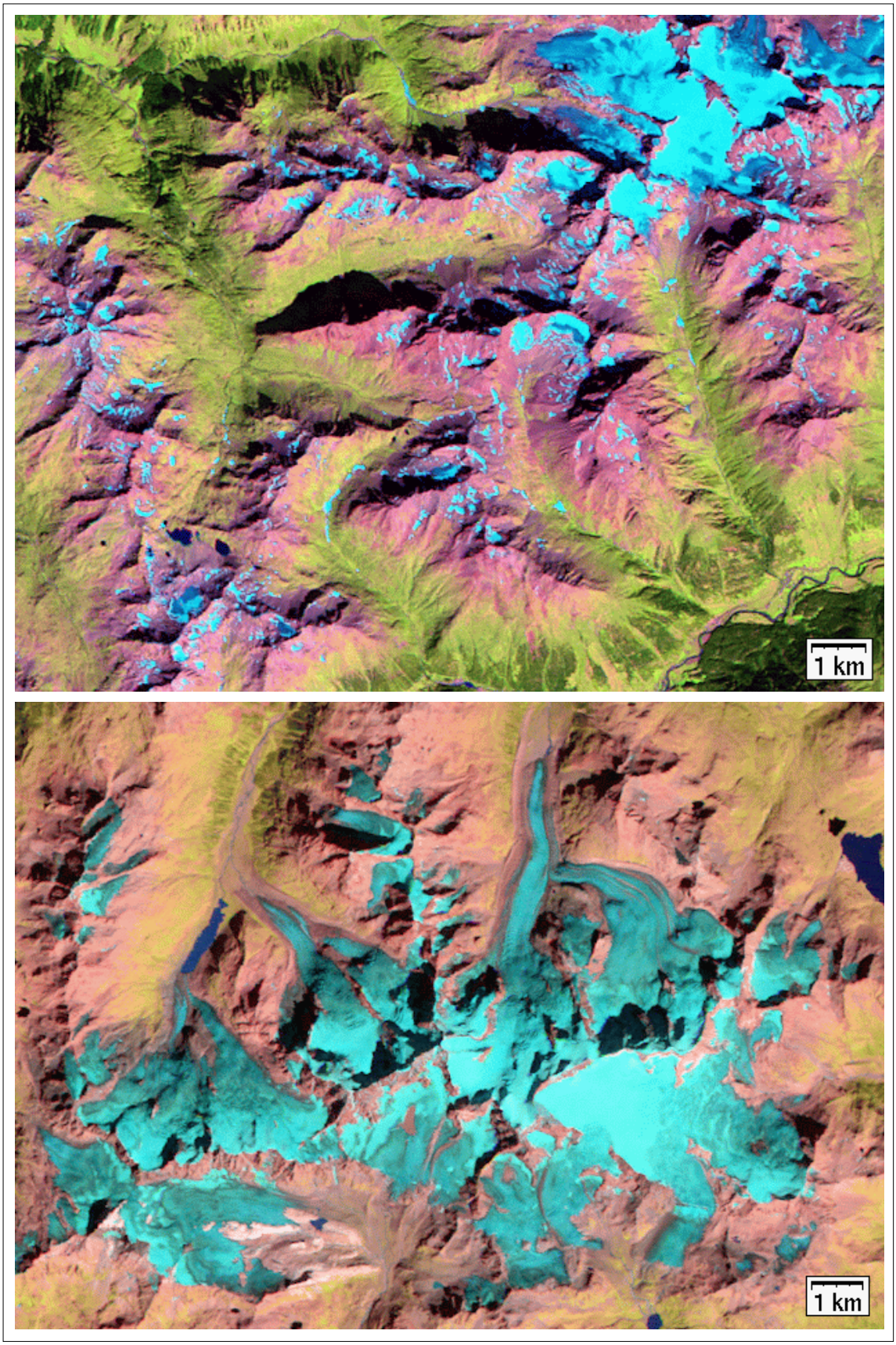

Fig. 3.2-2: *Difficult snow conditions at 12 Sep 1999 (scene #5) for Silvretta group (top) and favourable snow conditions in the Bernina group (bottom), which is located about 50 km to the south.*

A

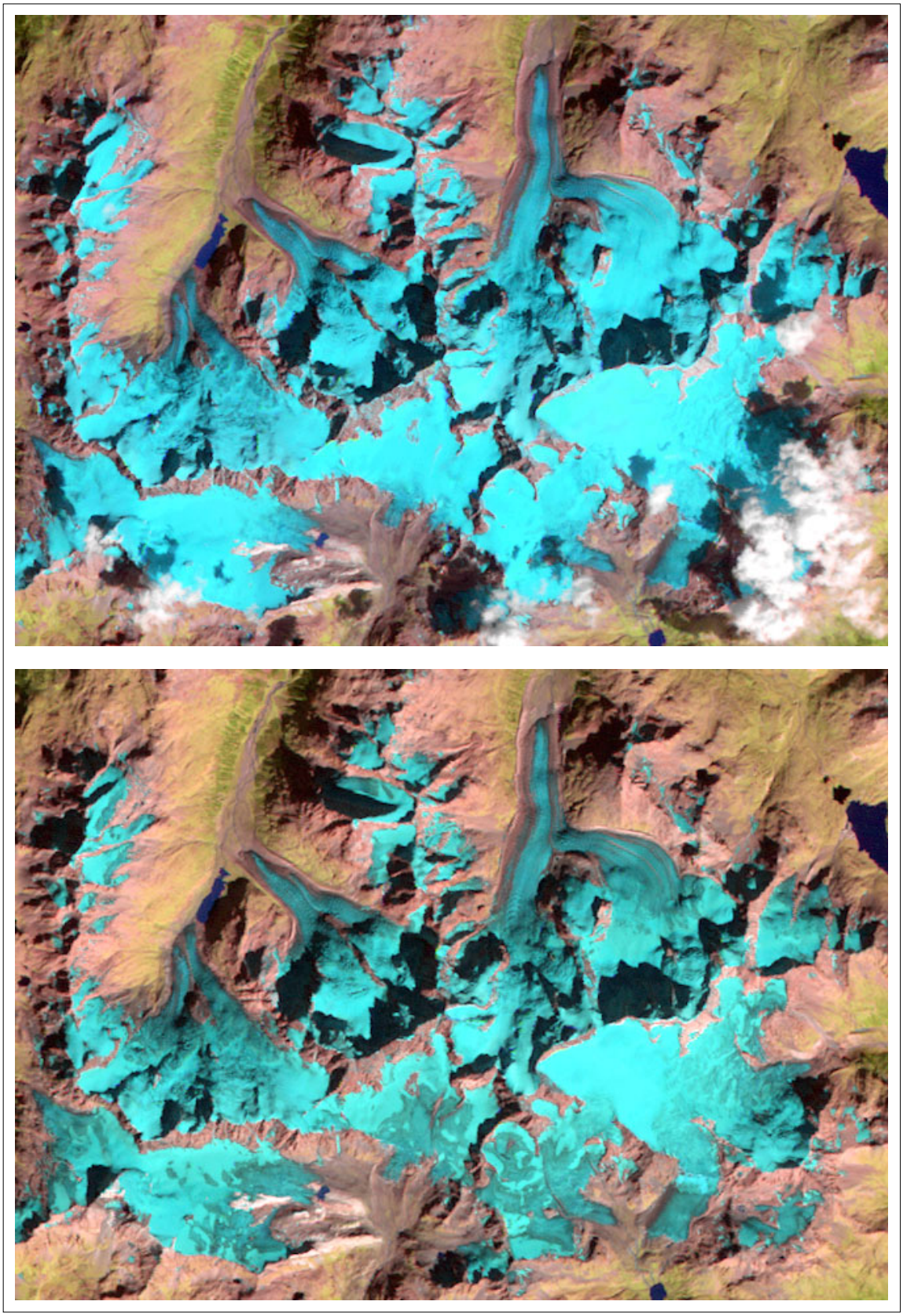

Fig. 3.2-3: *The Bernina group at 21 Sep 1985 (scene #4, top), 8 days after a snow fall event with many glaciers still completely snow-covered. Nine days later (scene #1 from 30 Sep 1985, bottom) the new snow has molten, unveiling a more complex shape of the TSL (cf. Fig. 3.2-2 for glacier retreat).*

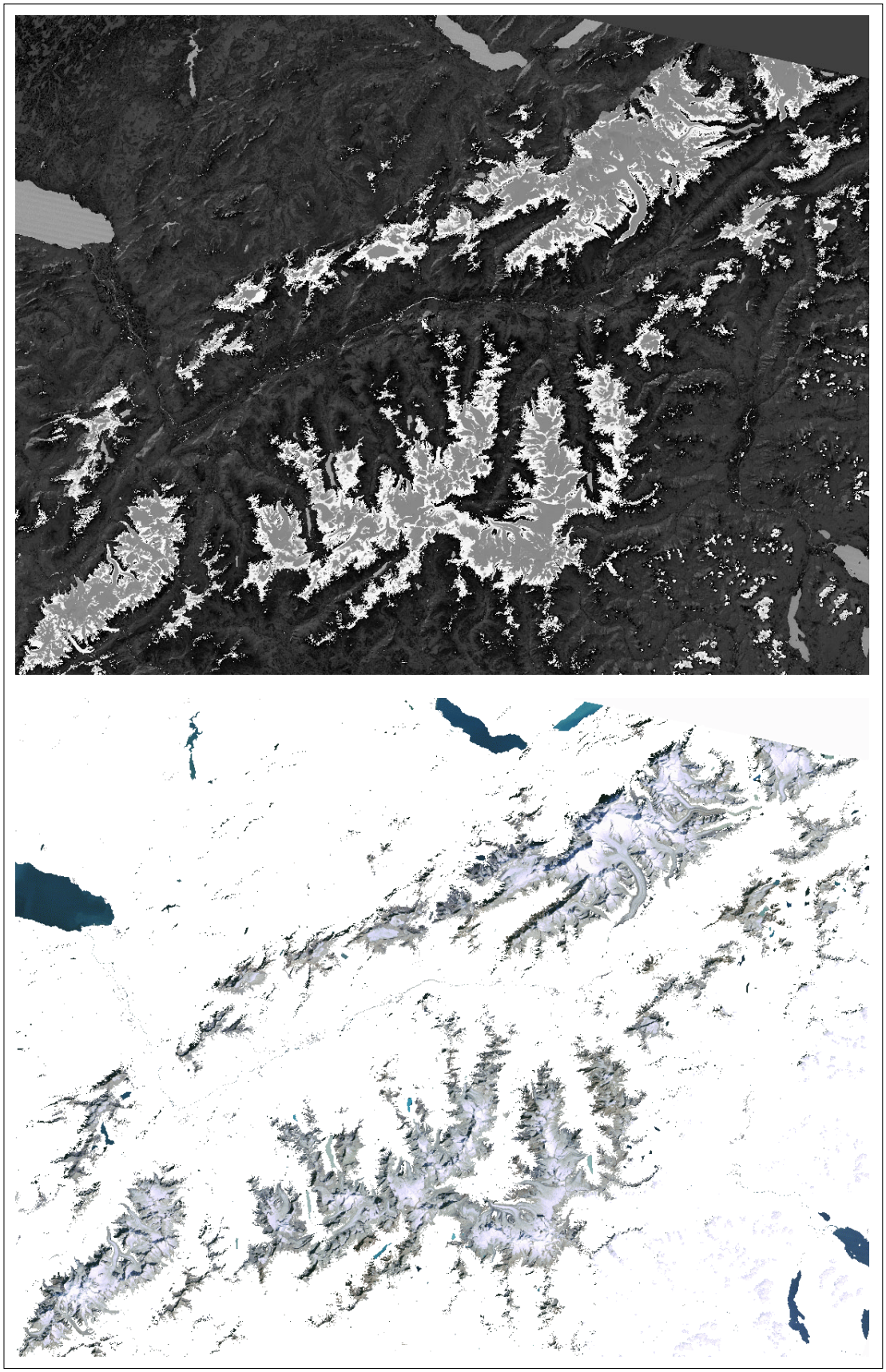

Fig. 3.2-4: *Mapping of vegetation-free regions with scene #10 using the hue-component of TM345 (top) and a threshold of 126. The obtained binary map is combined with a TM321 composite (bottom).*

A

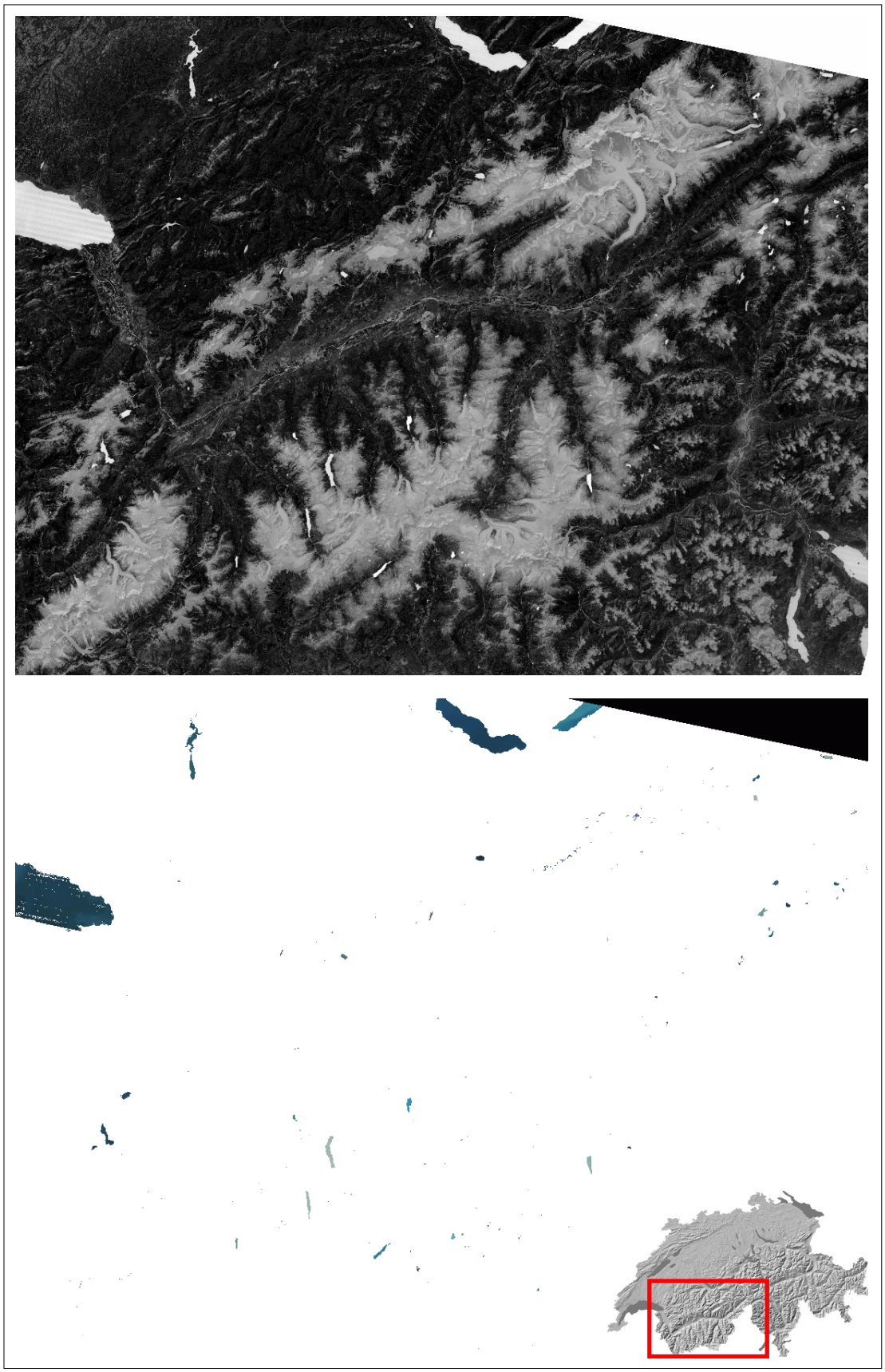

Fig. 3.2-5: *Mapping of lakes with scene #10 using the NDWI [(TM1-TM4) / (TM1+TM4)] and DOS in TM1 (top) and a threshold of 0.45. The resulting binary map is combined with TM321 (bottom).*

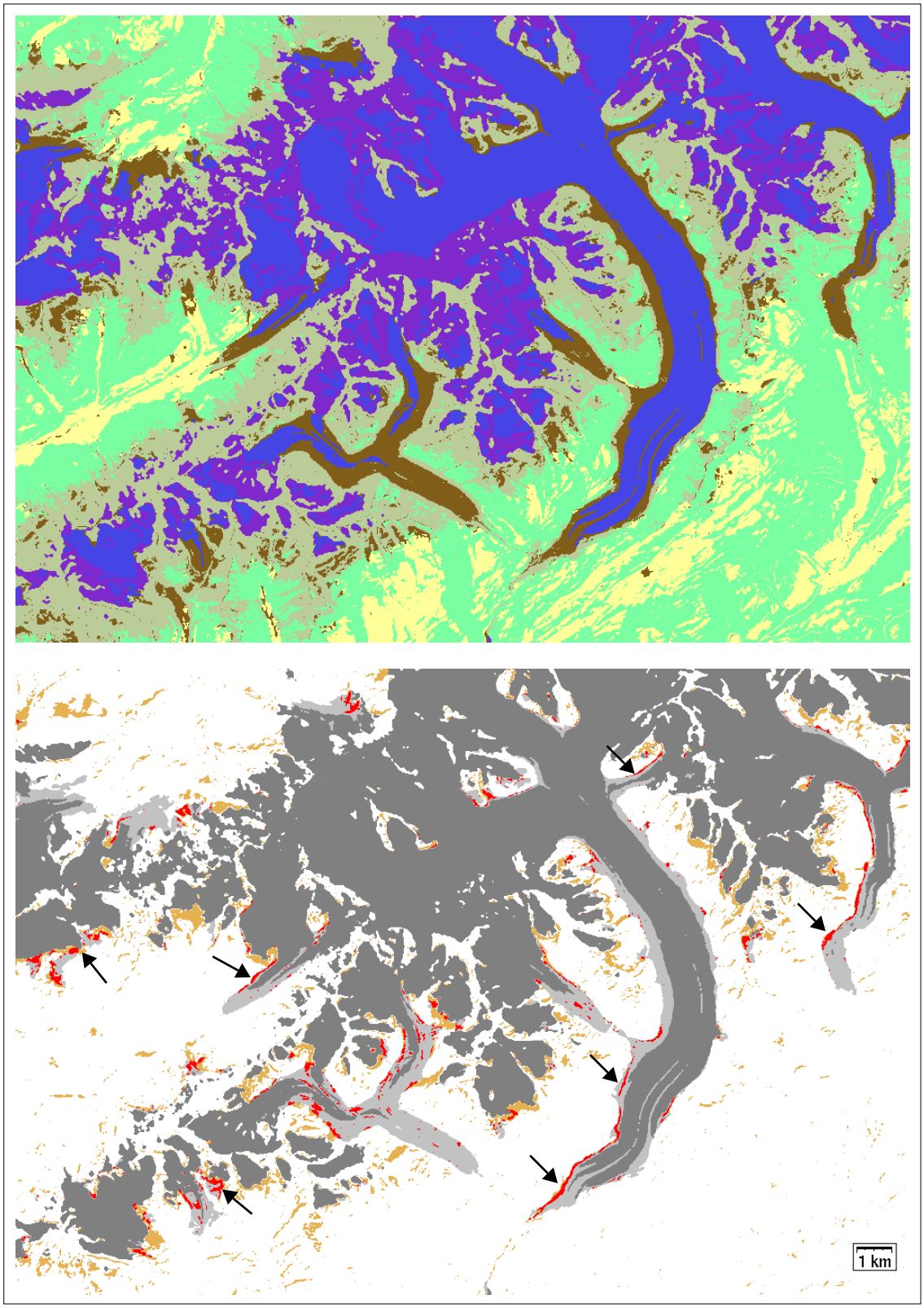

Fig. 3.2-6: *Overlay of the glacier, vegetation and slope-facet maps for the Aletsch test region at top (cf. Fig. 5.9a). With respect to slope values below/above 24°, colours are: glacier: blue/purple, vegetation: yellow/green, debris: brown/grey. At bottom the overlay of the change detection map (red and orange) with the classified ice (dark grey), debris map (grey) is shown. While the orange regions are not considered, the red areas interfere with the debris layer, indicating required adjustments (arrows).*

A

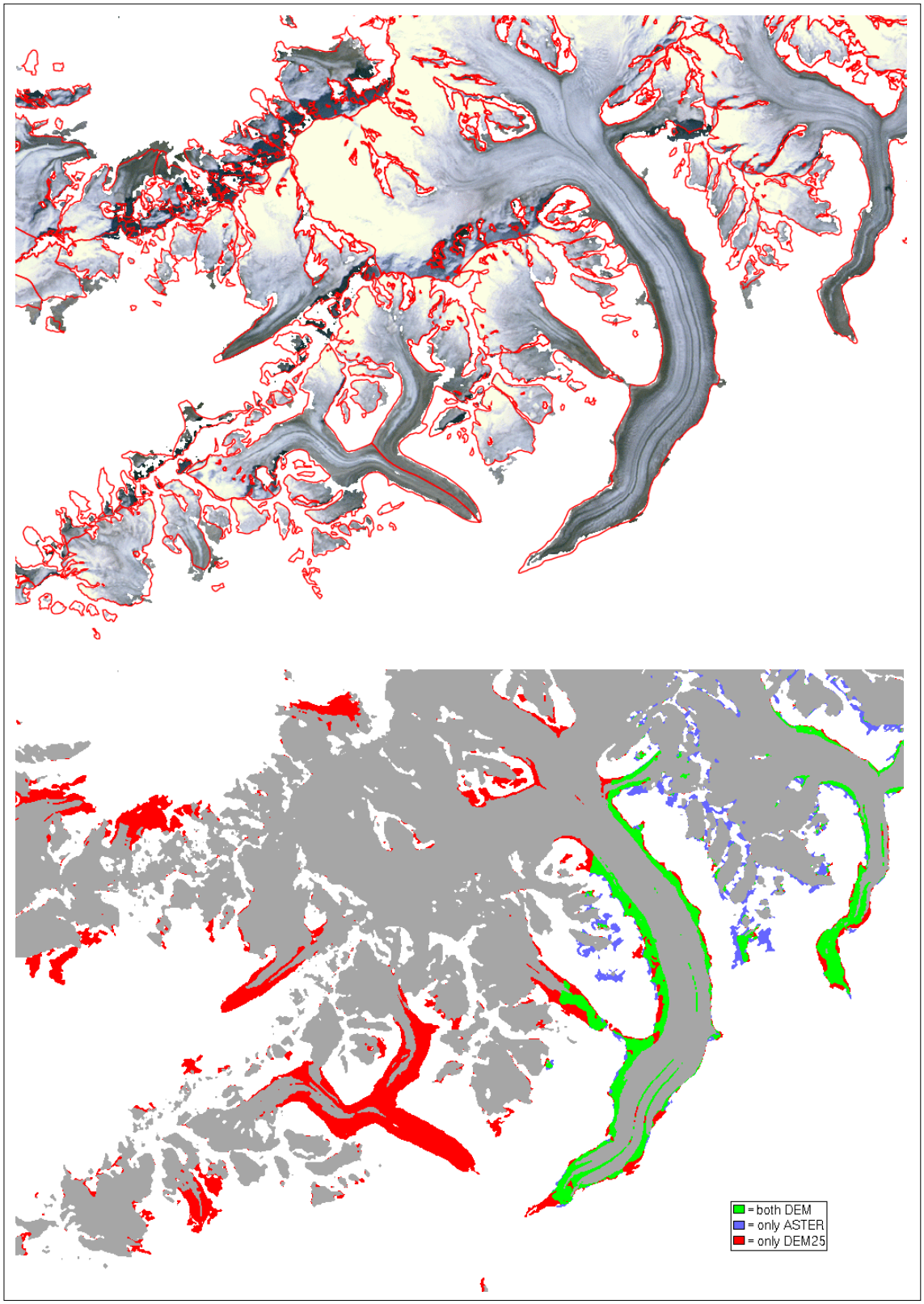

Fig. 3.2-7: *At top the overlay of the glacier map (including debris cover) with a TM321 composite and the digitized 1973 glacier outlines (red) is shown for the Aletsch test region. At bottom the comparison of the debris cover derived from the DEM25L2 is shown in red and green, and with the ASTER-derived DEM in blue and green. The ASTER scene is only available for the right part of the region.*

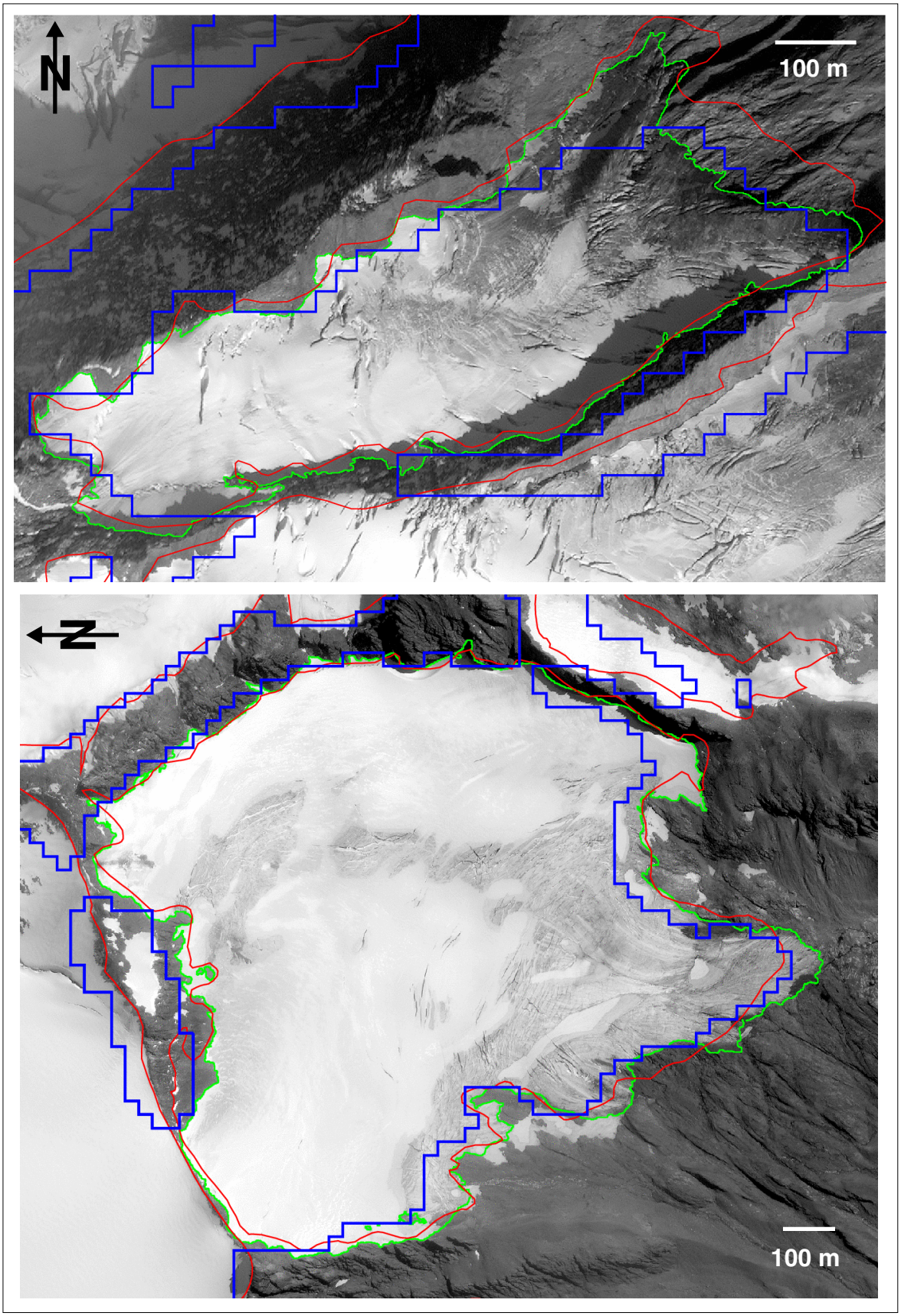

Fig. 3.2-8: *Comparison of glacier outlines derived from TM in 1998 (blue), manually from Ikonos in 2000 (green) and from the digitized 1973 glacier inventory (red). © Spaceimaging Europe / NPOC.*

A

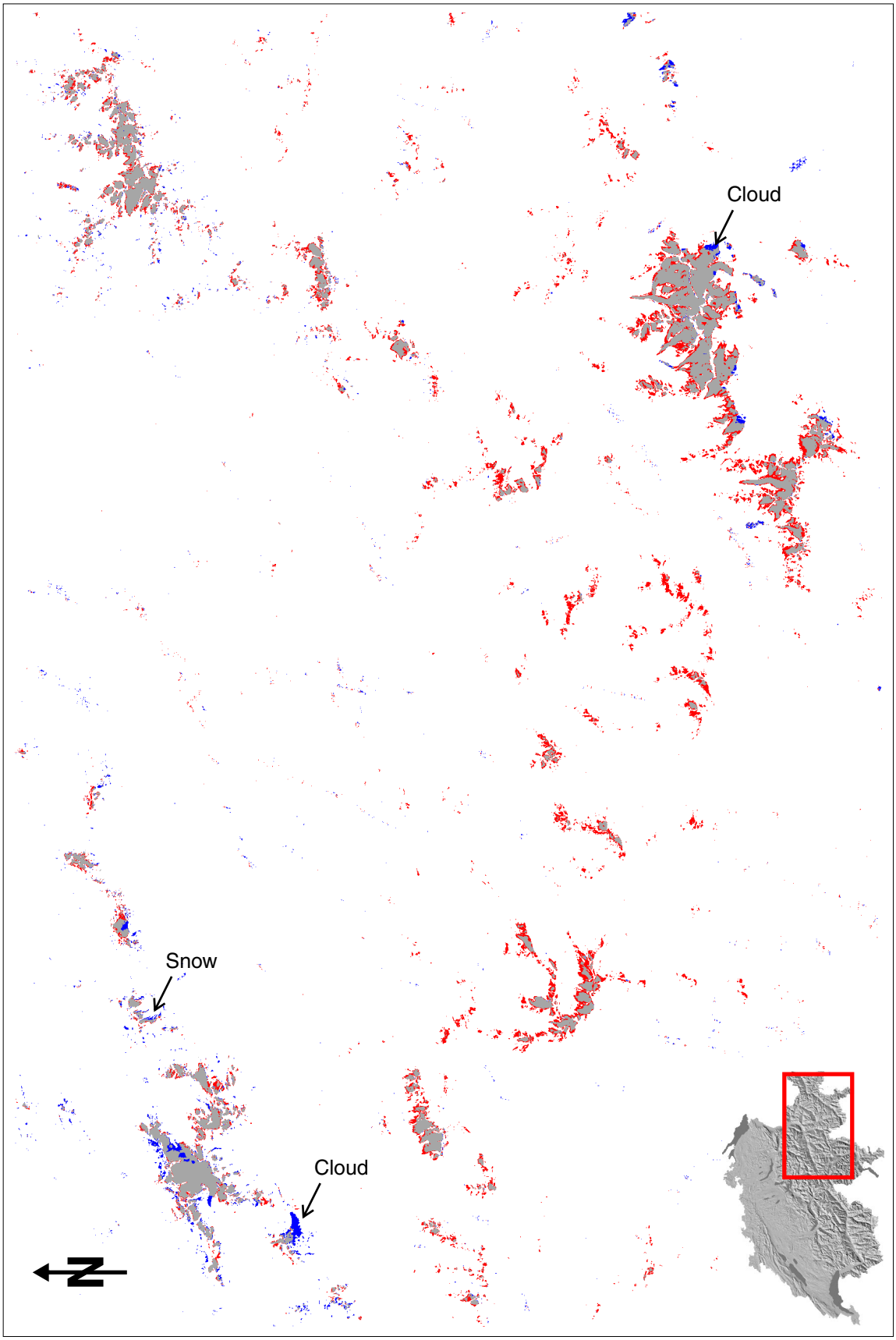

Fig. 3.2-9: *Glacier retreat in Grisons between 1985 and 1999 (red) as derived from TM raw data (at top left: Silvretta group, top right: Bernina group). Blue pixels refer to snow or cloud cover in 1999.*

A

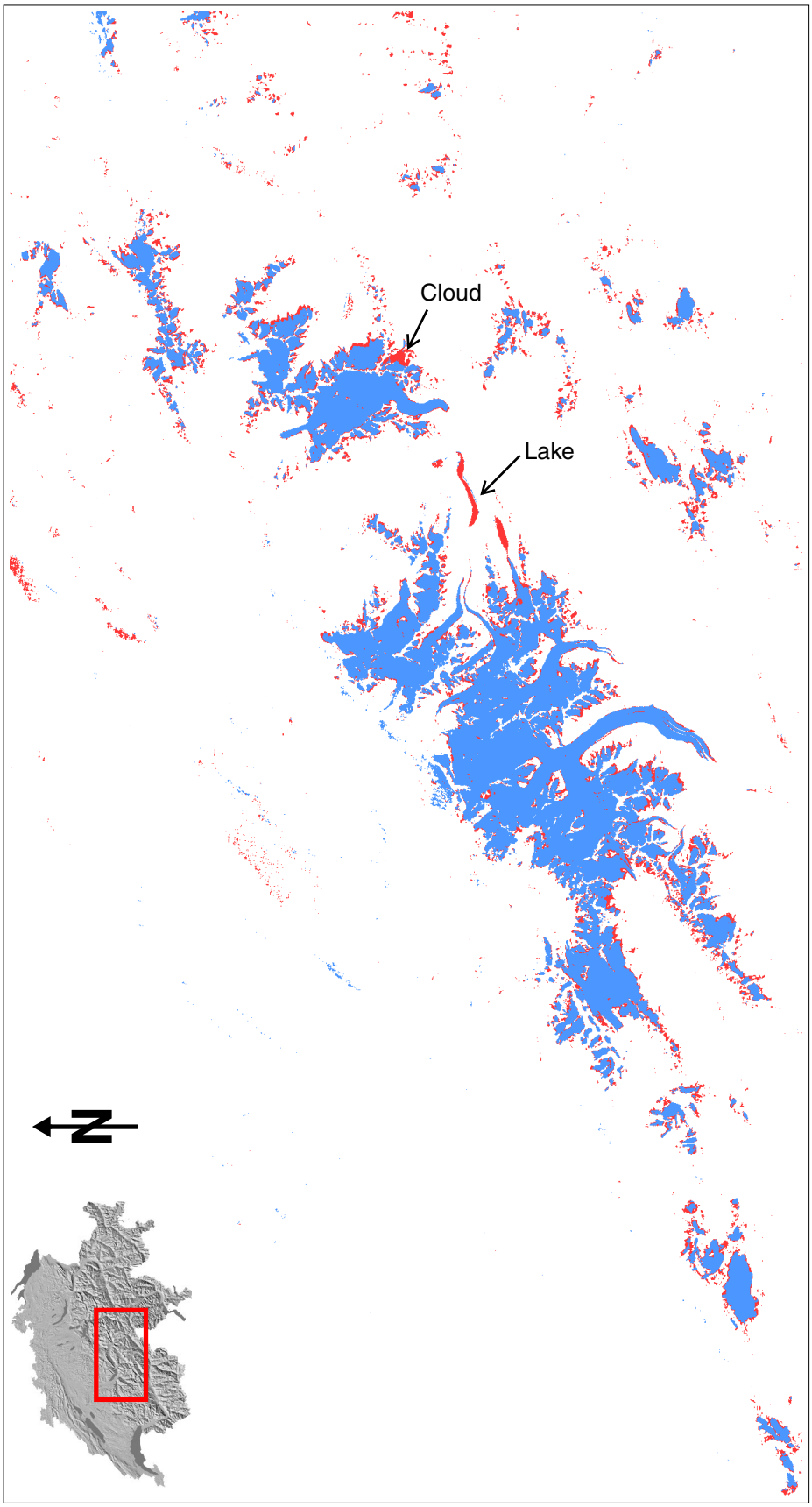

Fig. 3.2-10: *Glacier changes in the Bernese and Central Alps between 1985 and 1998 (red) as derived from TM raw data ('Grosser Aletschgletscher' in the lower centre).*

A

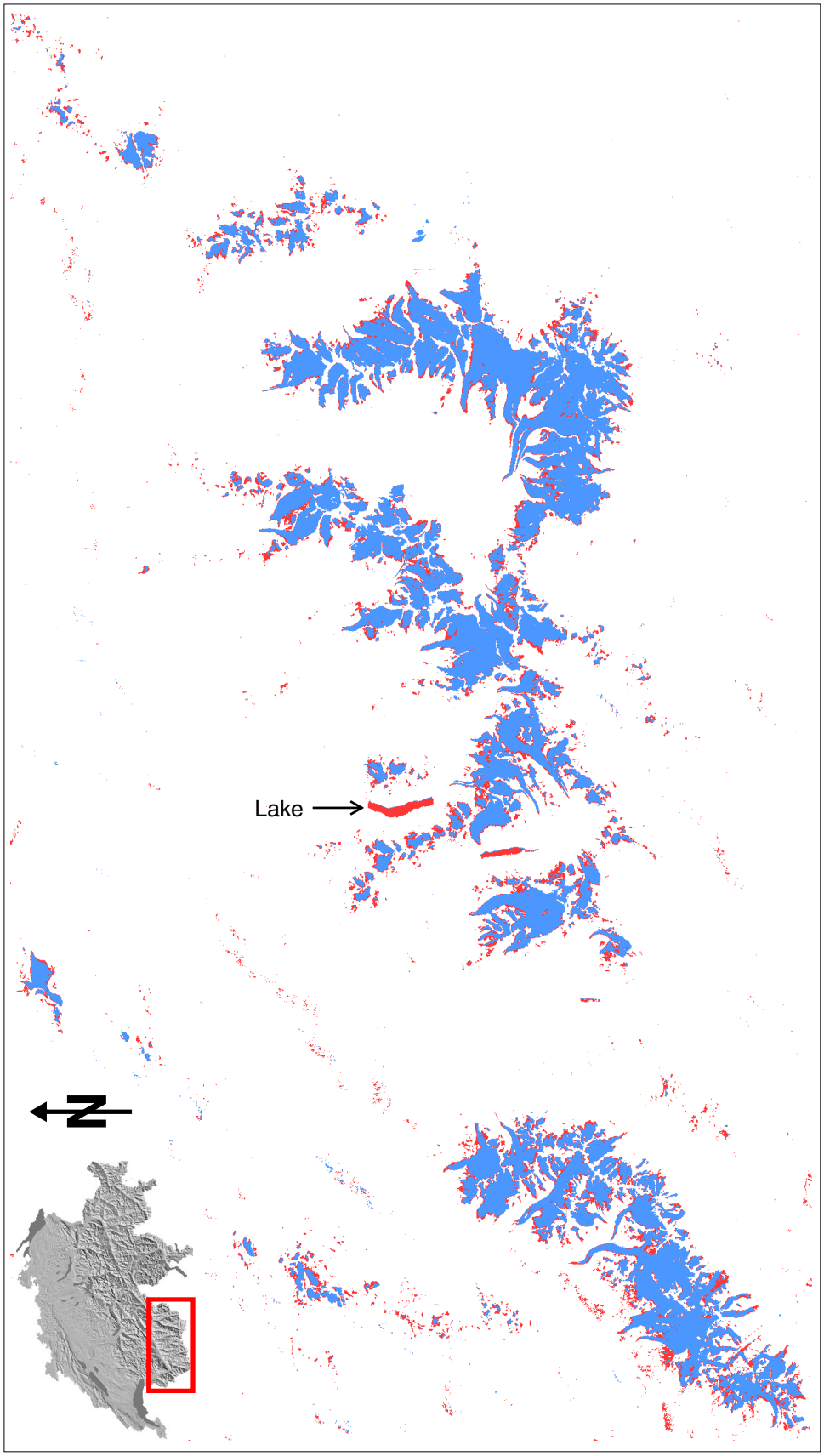

Fig. 3.2-11: *Glacier changes in the Valais Alps between 1985 and 1998 (red) as derived from TM raw data (Mont Blanc group to the lower right, Mischabel group at top centre).*

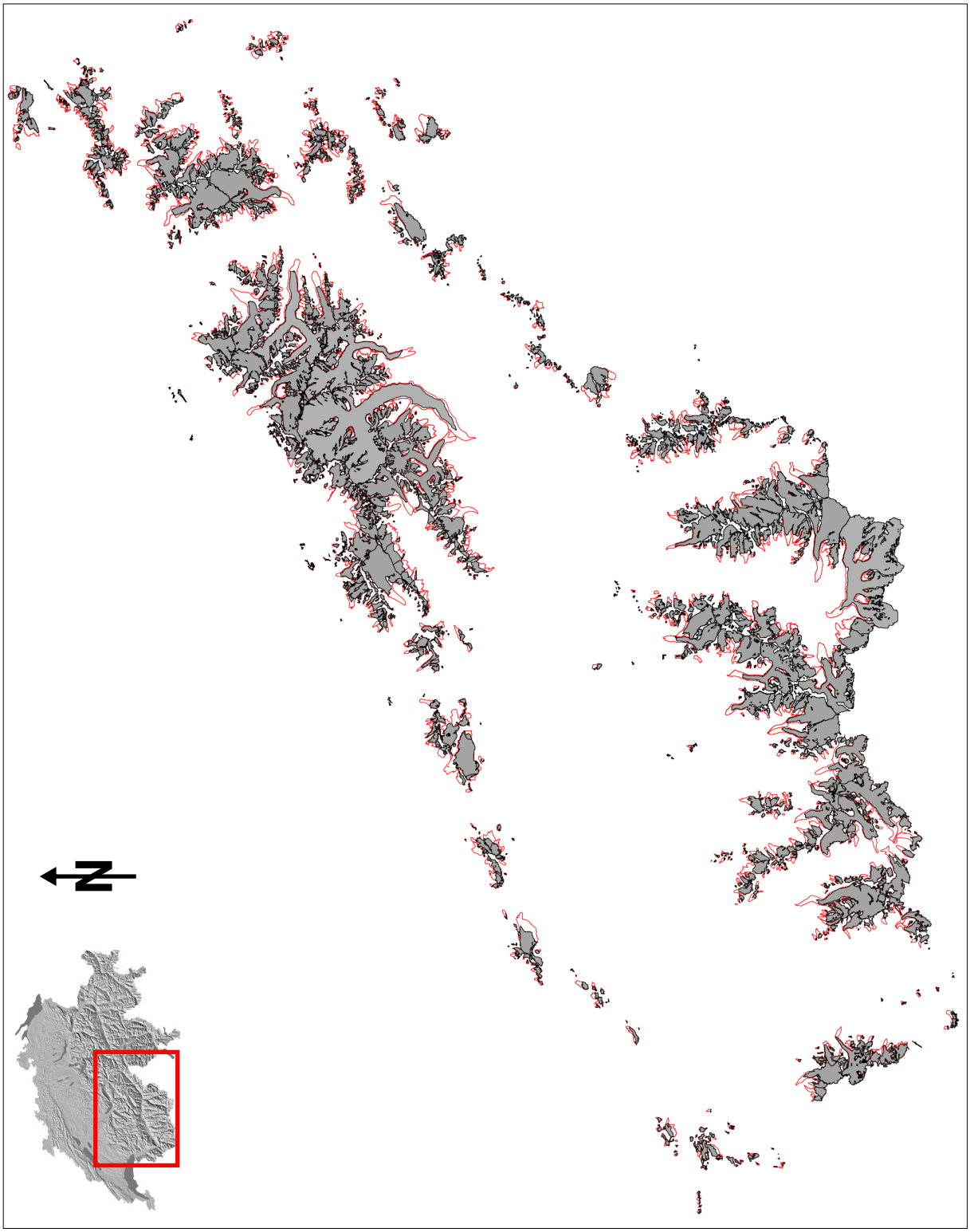

Fig. 3.2-12: *The digitized Swiss glacier inventory from 1973 (grey areas) and glacier outlines from 1850 (red) for the western part of Switzerland. See Fig. 3.2-11 for the eastern part at same scale.*

A

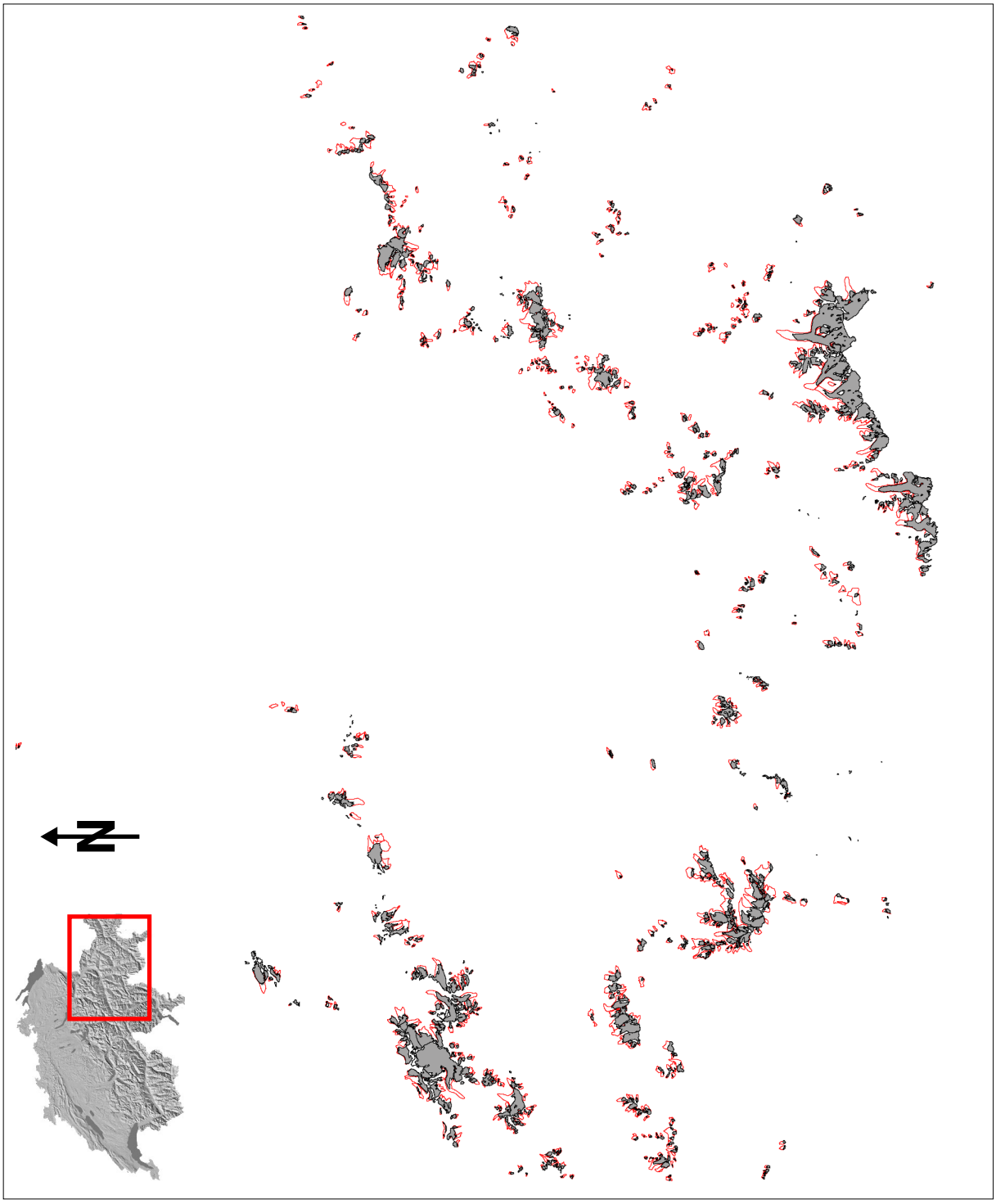

Fig. 3.2-13: *The digitized Swiss glacier inventory from 1973 (grey areas) and glacier outlines from 1850 (red) for the eastern part of Switzerland.*

Fig. 3.2-14: *The glacier basin coverage as used for intersection with TM-derived glacier maps.*

A

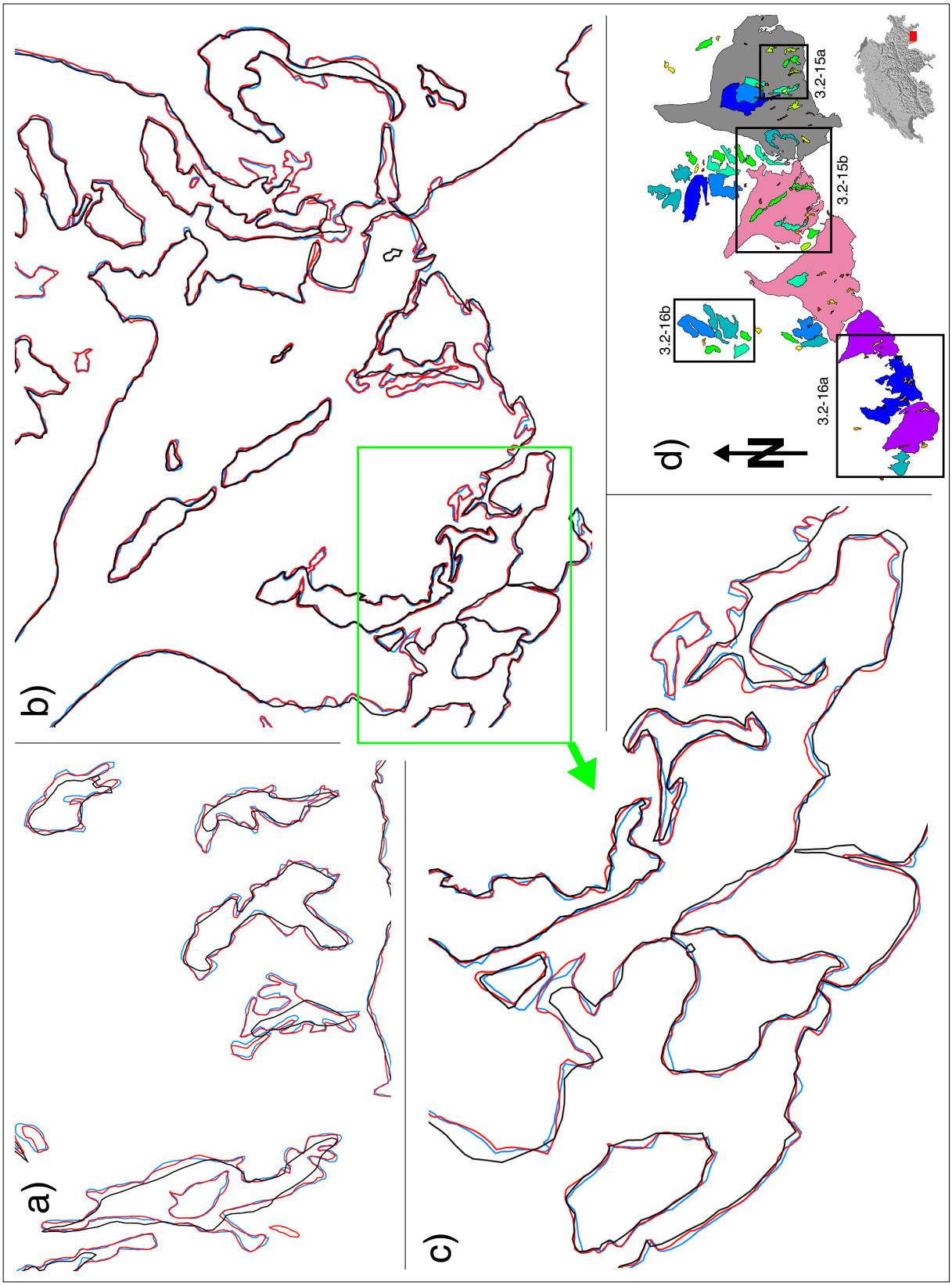

Fig. 3.2-15: *Examples of digitized glacier outlines for sub-regions of the Bernina group (see 'd)' for locations and glacier polygons used). The red and blue outlines are digitized by the same person, black outlines are digitized by another person. In particular the black lines in 'a)' exhibit differences in generalization of fine details.*

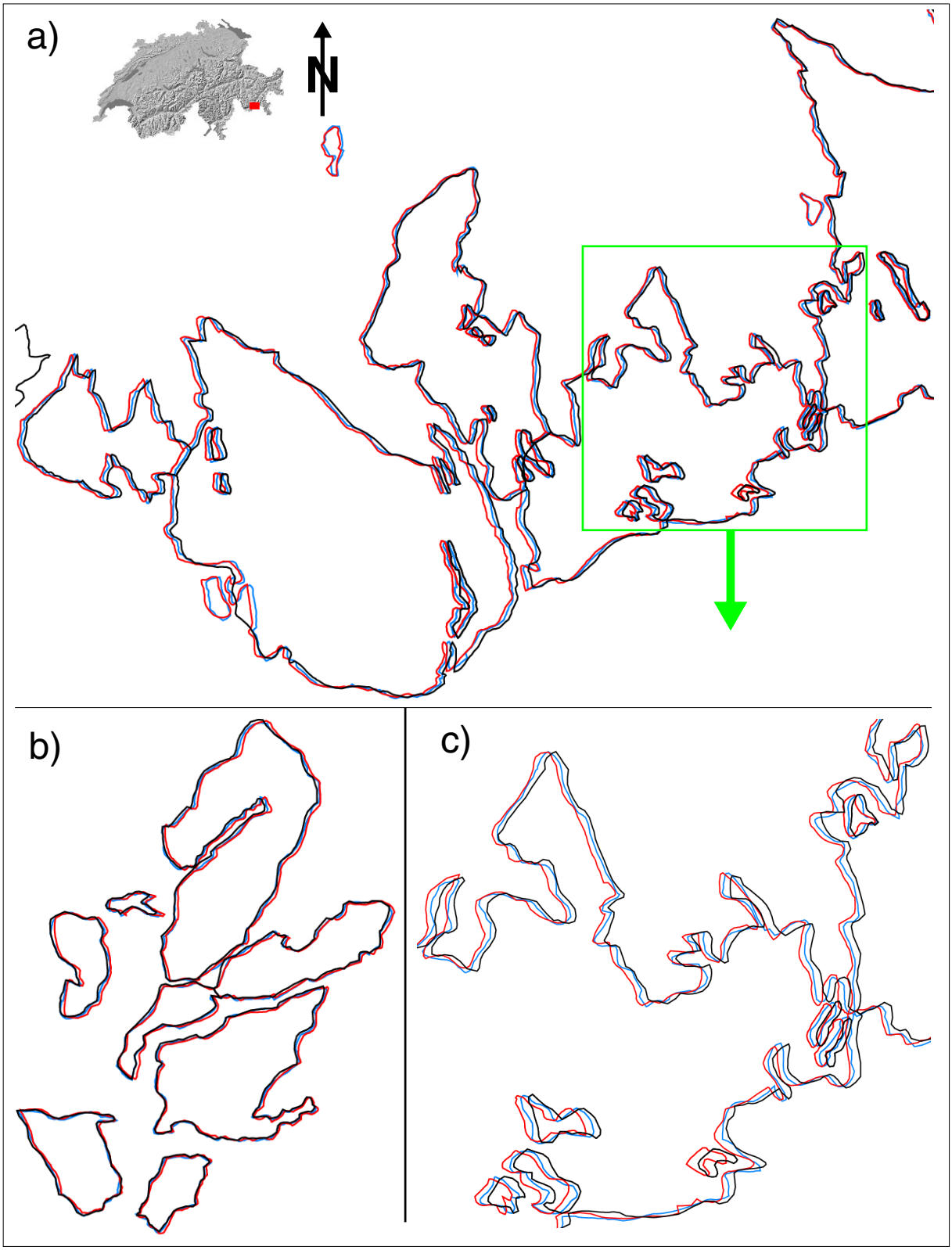

Fig. 3.2-16: *Some more examples of digitized glacier outlines for small sub-regions of the Bernina group (see 3.2-15d for locations). The red and blue outlines are digitized by the same person, black outlines are digitized by another person. The example in b) shows a very good correspondence of all three data sets, while the example in c) exhibit differences in geocoding of the base map.*

A

3.3. Visuals 3D

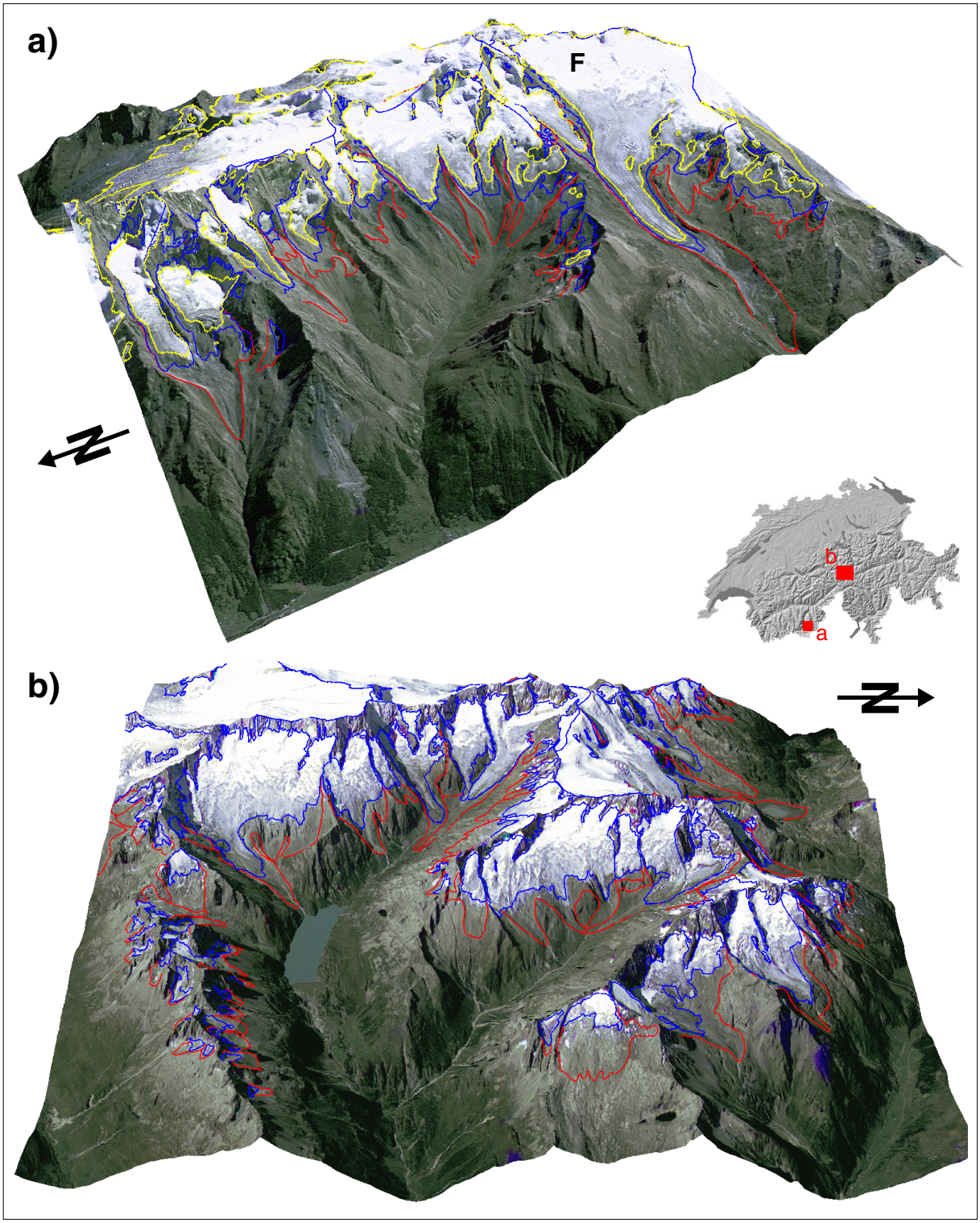

Fig. 3.3-1: *a) Täschvalley with Findelenglacier (F, 19 km^2) as seen from northwest on a fused TM / IRS-1C pan image from 1998 and 1997 with glacier outlines from 1850 (red), 1973 (blue) and 1998 (yellow). The long side of the image is 14 km. b) Göschener Alp as seen from east on a fused TM / SPOT pan image from 15 / 17 Sep 1992 (front side of the image is 14.5 km wide). Glacier outlines from 1850 (red) and 1973 (blue) are superimposed. While some of the glaciers partly are still larger than in 1973 others have vanished completely (a subsection is shown in 2D in Fig. 7.12). DEM25 © swisstopo.*

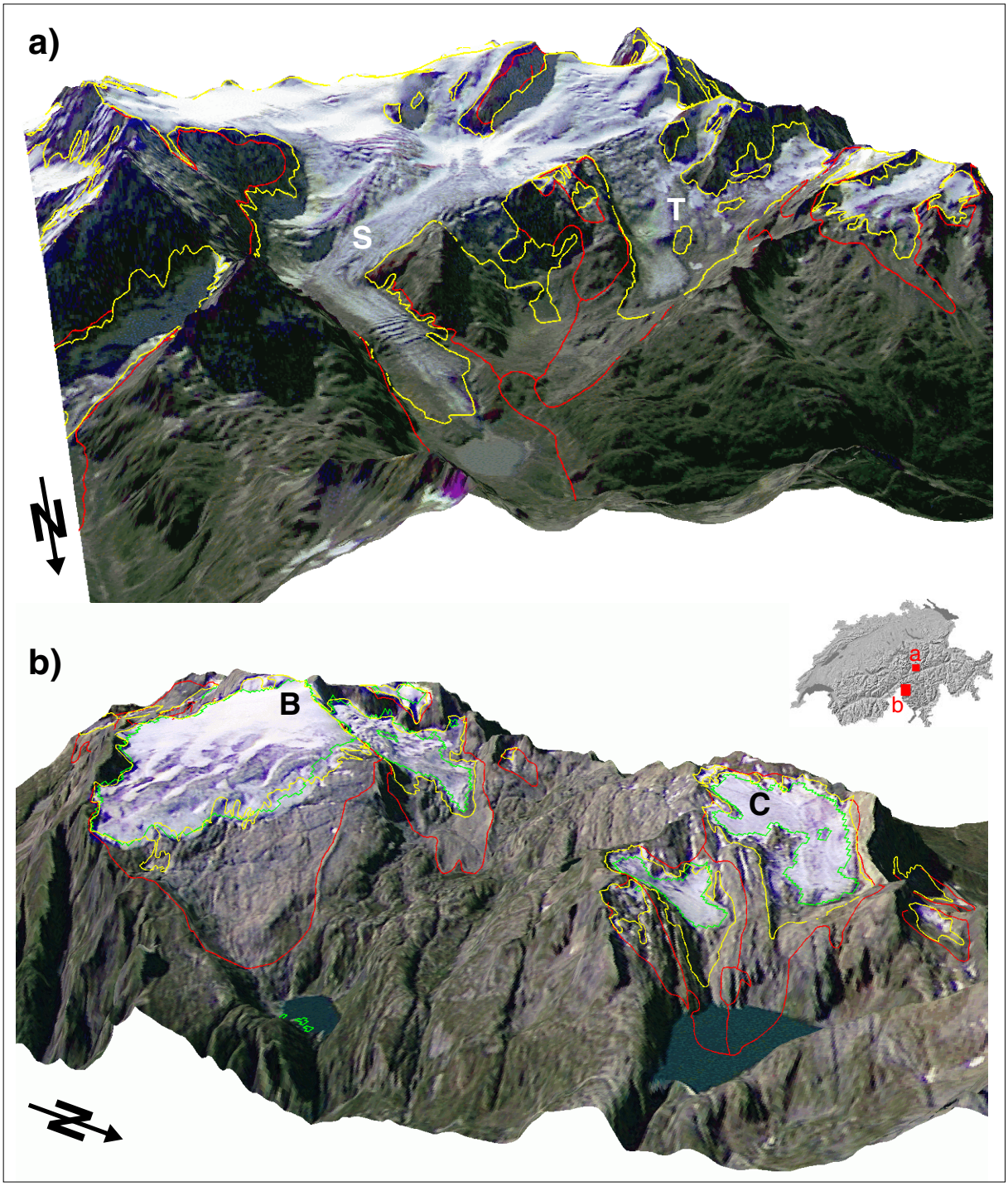

Fig. 3.3-2: *a) Steinglacier (about 8 km^2) as seen from north on a fused TM / SPOT pan image from 15 / 17 Sep 1992 with glacier outlines from 1850 (red) and 1973 (yellow). The main terminus of Steinglacier (S) is still in contact with a pro-glacial lake and about 190 m longer than in 1973, while his second tongue (T) has receded. In the SGI 2000 the entire glacier system is treated as one glacier, since ice flow divides are difficult to determine. b) Basòdinoglacier (B, 2.3 km^2) and Cavagnoliglacier (C, 1.3 km^2) as seen from northeast with the same fused TM / Spot pan image and glacier outlines as above. Additionally TM-derived 1998 outlines are superimposed in green. While Basòdinoglacier is in part still larger than in 1973, the glacier to its right shows only little change from 1973 to 1998. Despite the similar topographic setting, Cavagnoliglacier and his left neighbours in particular shrunk significantly or even vanished until 1998 (cf. Fig. 5.16b for a 2D image). DEM25 © swisstopo.*

A

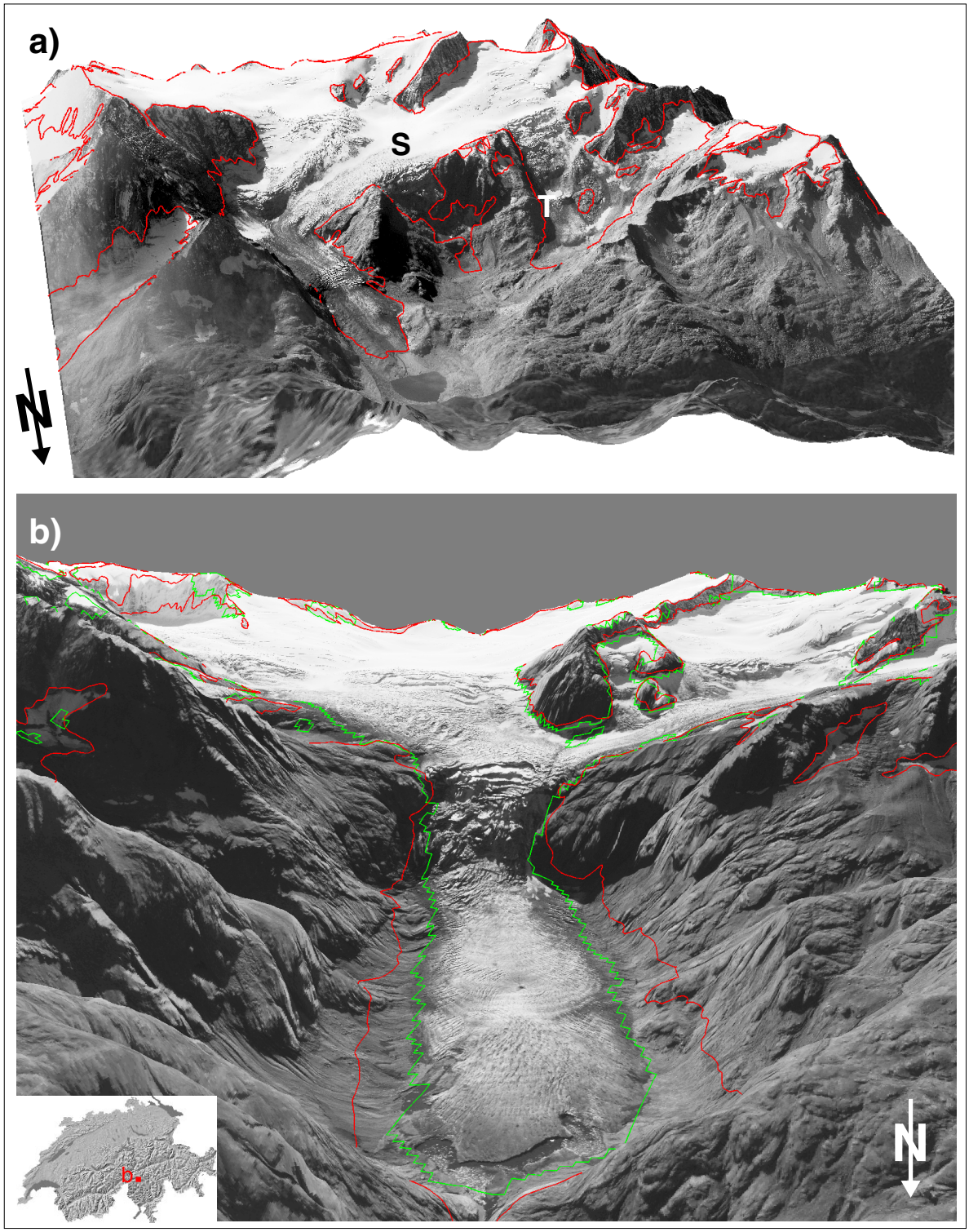

Fig. 3.3-3: *a) Steinglacier (S) as seen from north with Ikonos on 17 Sep 2000 in a perspective view using the DEM25L2 and depicting 1973 glacier outlines in red (cf. Fig. 3.3-2). The SPOT pan image from 17 Sep 1992 is used to fill the foreground. While Steinglacier is in part still longer than in 1973, Steinlimmiglacier (T) has receded strongly. b) The same Ikonos scene is used to visualize the dramatic down-wasting of the approximately 400 m wide Triftglacier (17 km^2) tongue within 25 years, by depicting 1998 glacier outlines in green. The pro-glacial lake has expanded rapidly since 2000, leading to a possible floating of the tongue (cf. Fig. 2.5d). Ikonos data: ©Spaceimaging Europe / NPOC. DEM25 © swisstopo.*

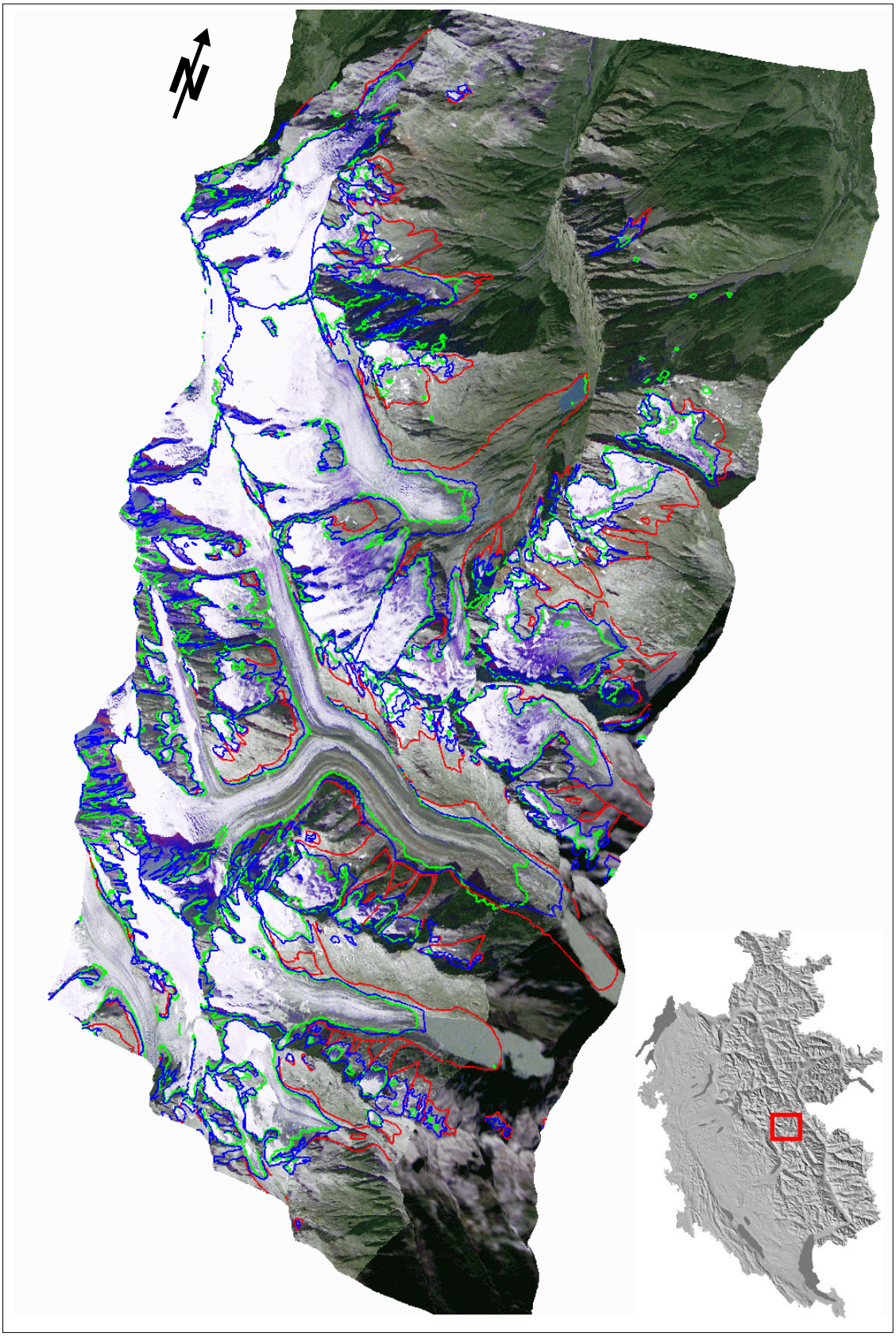

Fig. 3.3-4: *Grimsel as seen from east on a fused TM / IRS-1C image (from 1998 / 1997), showing glacier outlines from 1850 (blue), 1973 (red) and 1998 (green). IRS-1C data is not available for the dark strip in the foreground and is replaced by TM data. The long side has 20 km. DEM25 © swisstopo.*

A

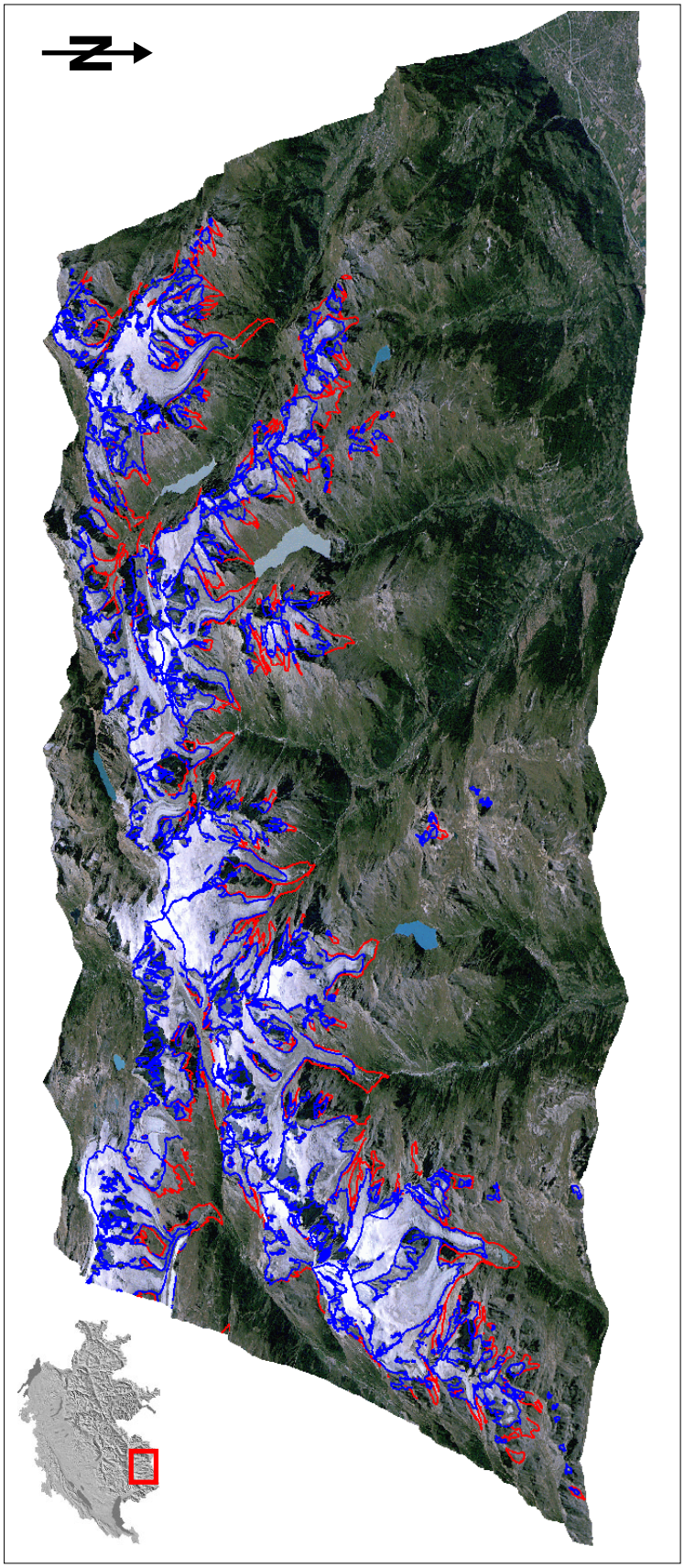

Fig. 3.3-5: *Overview of Valais Alps in a perspective view with a TM scene from 1998 and glacier outlines from 1850 (red) and 1973 (blue) on the DEM25L2. The long side has 45 km. DEM25 © swisstopo.*

A 4: Software

Overview
The entire SGI2000 was performed in a UNIX environment on SUN workstations using the software described below (PD=Public Domain):

FrameMaker:	Desktop publishing program from Adobe (v5.5.6)
Netscape:	Internet browser (v4.75)
Fortran 77:	Scientific programming language
PCI:	Digital image processing software from PCI-geomatics (v6.3)
Arc/Info:	GIS for spatial data handling and manipulation from ESRI (v8.0)
ArcView:	GIS for simultaneous visualization of vector and raster data from ESRI (v3.2)
XMGR:	PD data visualisation tool from ACE/gr (v4.1.2)
ImageMagick:	PD image manipulation and format conversion software package (v4.2.1)
XView:	PD tool for image enhancement and format conversion (v3.10a)
XPAINT:	PD image manipulation tool (v2.4.7)

Comments
The thesis is written with **FrameMaker** using the eleven point Palatino font for the main text. The internet browser **Netscape** is used for selection of satellite images (quicklook browsers from EURIMAGE, the EROS Data centre, SPOT image and the NPOC), to maintain a homepage of the SGI 2000 (http://www.geo.unizh.ch/~fpaul/SGI2000) and the GLIMS project (http://www.geo. unizh.ch/~kaeaeb/GLIMS) as well as for some of the illustrations used and references cited in the text. **Fortran77** programs are used for various calculations, data conversions and formatted output.

The commercial **PCI**-geomatics software package is used for processing of satellite imagery. Especially *image works* (visualisation and classification), *gcpworks* (gcp collection), *Xpace* (interactive processing) and *EASI* (script-based processing) is used. **Arc/Info** is utilized for all GIS based processing, including digitizing and editing (*arcedit*), raster - vector conversion and data selections (*arc*), 3D visualizations (*arcplot*), calculations with raster data (*grid*) and input/output of results (*tables*). *AML* scripts are used for automatic processing of work flows and 3D vector/raster overlays. **Arcview** is used for data analysis and 2D overlays. The scatter plots are created with **XMGR**, which is able to operate in an automatic batch mode.

Various software tools from the public domain are used for interactive editing of imagery. This includes **ImageMagick** for interactive contrast enhancement (*display*), file format conversion and image cropping (*convert*) as well as creation of RGB images (*combine*). **Xview** is mainly used for interactive contrast enhancement/pseudo colouring and generation of postscript output. Scales and legends as well as delineation of debris-covered regions on glaciers is performed with **Xpaint**. Other software frequently applied includes *ghostscript* (eps to tif conversion), *Imagetool* (postscript visualization) and *UNIX* shell scripts (file conversions).

For the following Figures the DEM25 from Swisstopo is used:
3.1, 3.2, 3.5, 3.6, 3.7, 4.11, 5.7, 5.8, 6.7, 7.1, 7.4, 7.5, 7.15, 7.16 and App. 3.3-1 to 3.3-5.
The DEM25 is reproduced by permission of the Swiss Federal Office of Topography (BA024887).

A

Acknowledgements

This work is made possible by a generous grant from the Swiss National Science Foundation (contract 21-54073.98). Many persons that give valuable support are not mentioned below, also their help was greatly appreciated!

First of all I want to express my gratitude to Andi Kääb for his outstanding proposal, for always encouraging me with constructive comments, for his helpful answers to my numerous questions and his engagement to keep the red line and the time.

I am also grateful to Wilfried Haeberli for the friendly welcome in the Department of Geography and the opportunity to perform this work at the University of Zurich as well as for his many stimulating suggestions.

I am indebted to Max Maisch for providing me his glacier inventory data in any combination, his precise digitizing of glacier outlines and the fruitful discussions on all kinds of topics.

I also appreciate the support of Tobias Kellenberger in using the digital image processing software PCI, in particular the atmospheric correction and orthorectification process.

Furthermore, I want to give special thanks to Andi Bachmann for his invaluable help in using Arc/Info and all its little tricks, our UNIX system administrator Othmar Wigger for his unselfish support and solutions for all my hard- and software questions, Andreas Wipf for his introduction to Arc/Info and the digitizing procedure, as well as for his accurate digitizing of the main parts of the Swiss glacier inventories and Christof Benz for his support in using Arc/Info and the valuable discussions on GIS related problems.

Thanks are extended to Jean-Pierre Perret, Jesko Schaper and Klaus Seidel from the NPOC for their help in selection and ordering of satellite imagery and Catherine Marion from Swisstopo for her support in obtaining the DEM25. Further DEM and GCP data are kindly provided by Philippe Meuret, Urs Frei and Erich Meier from the RSL and MeteoSwiss contributes visibility data for atmospheric correction.

Moreover, I appreciate the help of Michaela Honegger on administrative issues, Dani Wirz, Peti Schmid and Guido Dorigo on technical hard- and software support and I wish to thank Susan Braun-Clarke for her careful proof reading.

Last but not least I would like to thank all colleagues from the Physical Geography Department for the pleasant atmosphere and all the delicious 'Guetzli', in particular Regula Frauenfelder, Stephan Gruber, Susanne Hanson, Martin Hoelzle, Christian Huggel, Catherine Stocker-Mittaz and Sonja Oswald from the Glaciology and Geomorphodynamics Group.

And I will not forget to thank Christine Rothenbühler for accommodation, Christian Klepp for our joint excursions to numerous Alpine glaciers and Sabina Dürrenberger for her accurate final editing. At the end, I wish to say a heartily 'Danke' to my mother for her hospitable support, which enables me to write this thesis in Zurich.

Abbreviations and acronyms

2D, 3D:	2 dimensional, 3 dimensional
AAR:	Accumulation Area Ratio
AML:	Arc Macro Language
ASTER:	Advanced Spaceborne Thermal Emission and reflection Radiometer
BI:	Bilinear Interpolation
CC:	Cubic Convolution
CH-INVGLAZ:	Revised database of the Swiss glacier inventory 1850/1973
CP:	Check Point
DEM:	Digital Elevation Model
DIP:	Digital Image Processing
DOS:	Dark Object Subtraction
DN:	Digital Number
DSM:	Digital Surface Model
DTM:	Digital Terrain Model
ELA:	Equilibrium Line Altitude
EOSAT:	Earth Observation Satellite Agency
ERS 1/2:	European Radar Satellite 1/2
ESA:	European Space Agency
ESRI:	Environmental Systems Research Institute
ETM+:	Enhanced Thematic Mapper Plus
FCC:	False Colour Composite
GCOS:	Global Climate Observing System
GCP:	Ground Control Point
GCM:	Global Circulation Model
GHOST:	Global Hierarchical Observing Strategy
GIS:	Geographic Information System
GLIMS:	Global Land Ice Measurements from Space
GLOF:	Glacier Lake Outburst Flood
GPS:	Global Positoning System
GTOS:	Global Terrestrial Observing System
GTN-G:	Global Terrestrial Network - Glaciers
HRV:	High Resolution Visible
IAHS:	International Association of Hydrological Sciences
ID:	IDentification number
IFOV:	Instantaneous Field Of View
IHS:	Intensity-Hue-Saturation
IPCC:	Intergovernmental Panel on Climate Change
IRS:	Indian Remote sensing Satellite
ISODATA:	Iterative Self Organizing DATa Analysis
LIA:	Little Ice Age
MBB:	Mass Balance Bulletin
MIR:	Middle InfraRed
MLC:	Maximum-Likelihood Classification
MODIS:	MODerate resolution Imaging Spectroradiometer
MSS:	Multi-Spectral Scanner
NASA:	National Aeronautics and Space Administration
NDSI:	Normalized Difference Snow Index
NDVI:	Normalized Difference Vegetation Index
NDWI:	Normalized Difference Water Index
NIR:	Near InfraRed
NN:	Nearest Neighbour
NPOC:	National Point Of Contact
NSIDC:	National Snow and Ice Data Center
OMEGA:	Operational Monitoring of European Glacial Areas
Pan:	Panchromatic
PC:	Principal Component
PCA:	Principal Component Analysis
RGB:	Red Green Blue
RMSE:	Root Mean Square Error
RSL:	Remote Sensing Laboratories
SAR:	Synthetic Aperture Radar
SCA:	Snow Covered Area
SGI 2000:	Swiss Glacier Inventory 2000
SIZ:	Superimposed Ice Zone
SPOT:	Système pour l'Observation de la Terre
TM:	Thematic Mapper
TSL:	Transient Snow Line
UNEP:	United Nations Environmental Program
USGS:	United States Geological Survey
VIS:	Visible
WEQ:	Water EQuivalent
WGI:	World Glacier Inventory
WGMS:	World Glacier Monitoring Service
XS:	Multi-Spectral